OFFICE OF ADVANCED RESEARCH AND TECHNOLOGY
SPACE VEHICLES DIVISION

56519

PROCEEDINGS OF SECOND CONFERENCE ON

SOLAR SIMULATION RESEARCH

APRIL 7–8, 1964

NASA HEADQUARTERS

WASHINGTON, D.C.

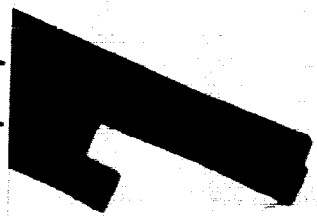

Table of Contents

ATTENDEES FOR SOLAR SIMULATION CONFERENCE

April 7 & 8, 1964

GODDARD SPACE FLIGHT CENTER

Norman Ackerman
Edward Powers
John Rogers
Robert E. Bernier
Milton Schach
John C. Flemming
Archie Cunningham
M.P. Thekaekara
Henry Maurer
Charles Duncan
Raymond Kruger
A. Retzler
Nelson Hyman
Robert Kidwell
N.P. Zylich
D.C. Kennard

AMES RESEARCH CENTER

Donald Anderson
John Arvesen
James Wortman

MARSHALL SPACE FLIGHT CENTER

Bill J. Duncan
Al Krupnick
Gene E. Comer
Werner H. Sieber
J.O. Ballance

LANGLEY RESEARCH CENTER

Ed Kersey
Victor L. Vaughan, Jr.
Dewey E. Wornom
Gilbert A. Haynes

MANNED SPACECRAFT CENTER

J.A. Muller
H. Kurt Strass

JET PROPULSION LABORATORY

Elmer Christensen
Michael Kahn
Norman Riise
Roger Barnett
Ralph Bartera
John W. Lucas
Donald W. Lewis

LEWIS RESEARCH CENTER

Gary Goldman
John L. Pollack
Herman Mark

NASA HEADQUARTERS

Bernard Leefer
W.A. Menzel
Arthur Reetz
Conrad P. Mook
Warren Keller

NORTH EASTERN OFFICE

John C. Loria

Space Vehicles Division
Office of Advanced Research and Technology
NASA Headquarters
Washington, D. C.

SOLAR SIMULATION RESEARCH AND TECHNOLOGY

Agenda f Review and Planning Conference - April 7-8, 1964) to be held in RT Conference Room 6032, Federal Office Building 10B.

Tuesday, April 7, 1964

9:00 Introduction and Welcome

9:15 JPL Spacecraft Testing in Space Simulators - E. M. Christensen and M. E. Kahn - JPL

10:15 BREAK

10:30 Status and Future Requirements in Solar Simulation at MSC - Joseph Muller - MSC

11:00 Status of Development of JPL Solar Simulator, Type A - Ralph Bartera and Roger Barnett - JPL

12:00 LUNCH

1:15-4:45 Tour of Radiometry Laboratories of National Bureau of Standards. The tour will include a discussion of "Ideas and Problems in Solar Simulator Radiometry" with Dr. Henry Kostkowski of NBS serving as moderator, as well as a tour of working areas. (Chartered bus will depart FOB 10-B 1:15 p.m. for National Bureau of Standards returning to vicinity of Statler Hotel, 16th & K. Streets, N.W., at approximately 4:45 p.m.)

Wednesday, April 8, 1964

9:00	Performance Characteristics of the Ames 10-Solar Constant Solar Radiation Simulator - Donald L. Anderson - Ames Research Center
9:30	Status of Solar Simulation at Lewis Research Center - John Pollack - Lewis Research Center
10:00	Spectral Measurements on Lewis Carbon Arc Solar Simulator - Gary Goldman - Lewis Research Center
10:30	BREAK
10:45	Spectral Radiance Measurements on High Intensity Light Sources - John Flemming and Charles Duncan - Goddard Space Flight Center
11:15	Simulation of Albedo and Earth Emitted Radiation - John Rogers - Goddard Space Flight Center
11:45	Progress Report on Plasmadyne Contract NASw-858, "Basic Studies on Vortex Stabilized Radiation Sources for Improved Solar Simulation"- Conrad P. Mook - NASA Headquarters
12:15	LUNCH
1:15	The Solar Constant and Spectral Distribution of Solar Radiant Flux - M. P. Thekaekara - Goddard Space Flight Center
1:45	Solar Simulation Testing of an Earth Satellite at Goddard - R. E. Bernier, R. H. Hoffman, A. R. Timmins and E. I. Powers - Goddard Space Flight Center
2:45	Development and Performance of the JPL Glass-Lined Metal Reflectors for the Solar Simulation System in the 25-Foot Space Simulator - H. N. Riise - Jet Propulsion Laboratory
3:00	BREAK
3:15	Round Table Discussion - Moderator - Conrad P. Mook

CONFERENCE NOTES

The second of what is hoped will be a series of annual NASA conferences on Solar Simulation Research and Development was held in Washington, D. C., on April 7-8, 1964. The first such meeting took place February 27-28, 1963, the proceedings of which have been issued as a similar NASA internal document.

The subjects most actively discussed informally at the 1964 meeting included progress reports on solar simulators which have been completed or are planned or under construction. Need for radiometric standards and the possible need for further solar data were also discussed.

The present document contains the presentations made by individuals representing the various NASA centers and describe overall progress made during the year since the last meeting. The presentations made by Michael Kahn and Elmer Christensen of JPL are reproduced as individual reports. The paper by John Rogers of GSFC was not submitted for inclusion herein.

The presentations made by staff members of the National Bureau of Standards are not included herein. The speakers who addressed the meeting at the Bureau were Dr. Henry J. Kostkowski, Mr. Ralph Stair, Mr. William Schneider, and Mr. C. R. Yokely. The visit to the Bureau on the afternoon of April 7 included inspection of a high accuracy spectroradiometer and a high pressure arc source plus a tour of the Radiometry Laboratory. The developments discussed at NBS were the outcome of two NASA-NBS contracts which became activated on January 1, 1964, in the Metrology Division and the Heat Division.

Time was not available for a review of the Plasmadyne contract as mentioned in the agenda. Quarterly reports on this contract (NASw-858) are being furnished to those interested. It is expected that the final report on the contract will receive wide distribution.

A suggestion made by Mr. Henry Maurer of GSFC was approved by the conferees, namely that a monthly newsletter on solar simulation developments be initiated by NASA Headquarters. Such a newsletter has been initiated and is expected to continue as a monthly publication indefinitely.

C. P. Mook
NASA Headquarters (Code RV-1)
Washington, D. C.

SPECTRAL MEASUREMENTS BY THE FILTER METHOD ON LEWI

CARBON ARC SOLAR SIMULATORS

by Gary C. Goldman

Lewis Research Center

INTRODUCTION

There exists a problem in the measuring of the spectral irradiance of solar simulators. This difficulty has manifested intself in both monochromator and filter measurements. This report is the discussion of the measurements by Eppley Laboratory on the Lewis carbon arc solar simulators, the further analysis of the method of filter radiometry made by Lewis personnel, and the comparison with the monochromator measurements.

Previously when the filter technique was used it was assumed that the a priori knowledge of the source's spectral characteristics must be known. In this report it will be shown that for a carbon arc source a knowledge of the source is not required after the filters have been properly chosen.

THE EPPLEY REPORT

In June of 1963, Eppley Laboratory, under contract to Lewis, sent representatives to Cleveland to measure the spectral distribution of three operational carbon arc solar simulators using the filter method and their prototype Mark IV filter radiometer. Measurements were made on air on the two smaller systems and in air, vacuum, and vacuum and cold walls on the 30-inch-diameter system. The air measurements were repeated for reproducibility. The results was essentially six sets of narrow band filter data supplemented by four sets of broad band data.

The final report, dated November 5, 1963, averaged all the narrow band data together. Figure 1 is the resultant continuous curve taken from the report of all the narrow band data versus the extraterrestial sun curve.

Because this curve was an average of three different systems under many different conditions, because there was an abundance of narrow band data available, and because we were to receive a similar instrument for filter measurements, we began to analyze the mathematics of filter radiometry.

After an analysis of Eppley's method, which follows immediately, we developed what we feel are more rigorous treatments to the filter data that will be presented later.

THE EPPLEY METHOD

Using the filter method to obtained spectral measurements, one essentially has a total thermopile detector. When the detector is covered with various filters the energy within a given bandwidth is then isolated. If this method is repeated throughout the spectrum with the available filters, the energy within all the small segments making up the total spectrum can be found.

If the transmission of each filter is known, as in figure 2, where $\tau(\lambda)$ is the transmission of the filter, λ is the wavelength, and λ_1 and λ_2 are the bandpass limits of the filter, the center wavelength λ_0 or the center of gravity of the transmission curve can then be found by

$$\lambda_0 = \frac{\int_0^\infty \tau(\lambda)\lambda\, d\lambda}{\int_0^\infty \tau(\lambda)d\lambda}$$

A more suitable form for machine computation can be made by breaking up $\tau(\lambda)$ into small increments $\Delta\lambda$ and by summing:

$$\lambda_0 = \frac{\sum_{N=1}^{L} \lambda_N \tau_N \Delta\lambda_N}{\sum_{N=1}^{L} \tau_N \Delta\lambda_N}$$

If all the $\Delta\lambda_N$'s are equal and the appropriate $\tau(\lambda)$ is used for each filter, λ_{OF} is calculated by

$$\lambda_{OF} = \frac{\sum_{N=1}^{L} \lambda_{NF} \tau_{NF}}{\sum_{N=1}^{L} \tau_{NF}}$$

where λ_{OF} is the center wavelength for the F^{th} filter and L is the number of increments within the transmission curve for the filter. This result is similar to the reference wavelength discussed in Eppley's report.

To compute the spectral irradiance of the source at the target plane the report indicates that prior knowledge of the spectral distribution of the bare source is required and that the distribution be a reasonably

smooth curve. It was further stated that the carbon arc satisfies these conditions. A quantity is defined that, when applied to the data, will indicate the energy that would fall on the detector within the bandpass limits λ_1 and λ_2 if the filter were not in place. This quantity is given by

$$F = \frac{\int_0^\infty J(\lambda)S(\lambda)d\lambda}{\int_0^\infty J(\lambda)\tau(\lambda)S(\lambda)d\lambda}$$

where $J(\lambda)$ is the assumed spectral irradiance curve (usually taken from monochromator data of the bare source), $S(\lambda)$ is the sensitivity of the detector (in this case a constant over the limits involved), $\tau(\lambda)$ is the transmission of the filter in question, and F is the filter factor, which is approximately equal to the reciprocal of the transmission of the equivalent square filter. The denominator of the fraction is the measured voltage output of the detector. When the previous expression for F is rewritten, it is found that

$$F_F = \frac{S\int_{\lambda_1}^{\lambda_2} J(\lambda)d\lambda}{S\int_{\lambda_1}^{\lambda_2} J(\lambda)\tau(\lambda)d\lambda} \qquad (1)$$

or

$$F_F = \frac{S\int_{\lambda_1}^{\lambda_2} J(\lambda)d\lambda}{V_F}$$

where V_F is the voltage output of the detector with the $F^{\underline{th}}$ filter is in place, λ_1 and λ_2 are the band pass limits of the filter, and F_F is the filter factor for the $F^{\underline{th}}$ filter.

The average energy to the detector within the limits λ_1 and λ_2, if the filter were not present, is given by

$$\bar{J} = \frac{\int_{\lambda_1}^{\lambda_2} J(\lambda)d\lambda}{\lambda_2 - \lambda_1} \qquad (2)$$

where $J(\lambda)$ is the spectral irradiance of the source at the target plane, λ_1 and λ_2 are the band pass limits, and $\lambda_2 - \lambda_1$ is the bandwidth. If equation (1) is solved for the integral and the result substituted into equation (2), the new expression for $\bar{J}$ is

$$\bar{J} = \frac{FV}{S(\lambda_2 - \lambda_1)}$$

If the bandwidths are normalized to 50 millimicrons, the average irradiance at the target plane within the given bandwidth limits is then

$$\bar{J}_F = \frac{F_F V_F}{S}\left(\frac{50}{\lambda_2 - \lambda_1}\right)$$

This process is repeated for all F filters, and the report lists twelve values of $\bar{J}_F$ corresponding to twelve values of λ_{OF} through which a smooth continuous curve is drawn to indicate the approximate spectral distribution of the source.

To calculate this spectrum the contractor chose values of $J(\lambda)$ from the curves published by the National Carbon Company indicating the spectral distribution from a "High Intensity" electrode. Since the three systems at Lewis use "Ultrex" electrodes with a significantly different source distribution, we recalculated the spectrums using the new values of $J(\lambda)$ published for the "Ultrex" electrode. The final results did not change.

MODIFIED EPPLEY METHOD

The altering of assumed irradiance curves leading to no change in the results led us to the conclusion that once the filters were judiciously chosen based on prior knowledge of a smooth carbon arc spectrum, the calculated results were relatively insensitive to the chosen spectral irradiance curve. Continuing along this line of reasoning it was found that any continuous curve, straight line, or segmented line curve will serve quite well as the chosen $J(\lambda)$. The filter factor F_F and the average irradiance within the given bandwidth of the filter $\bar{J}_F$ were calculated and a linear interpolation between all twelve points resulted in a segmented line curve. With this new $J(\lambda)$ new values of $\bar{J}_F$ and F_F

were again calculated and with these twelve new points a new $J(\lambda)$ was calculated. When the iterative method and the available computer were used, it was observed that the results converged rapidly, and the spectrum calculated using this method is very close to that calculated using the method indicated in the Eppley report. This shows it is possible to calculate the spectral irradiance produced by a carbon arc or any smooth source using filter measurements and having no prior knowledge of the spectral radiance of the bare source.

NONFILTER FACTOR METHOD

Another method of calculating spectral irradiance using the same raw data was developed at Lewis. This method uses no filter factors or bandwidth limits. In its use we assume a spectrum and by an iterative process alter the assumed spectrum to match the measured data. To use this method the measured data must be available and related by the expression

$$V_{FM} = \int_0^\infty S(\lambda)\tau_F(\lambda)J(\lambda)d\lambda$$

where V_{FM} is the measured voltage output from the detector with a filter in place, $S(\lambda)$ is the sensitivity (a measured constant), $\tau_F(\lambda)$ is the measured transmission of the filter, and $J(\lambda)$ is the spectral irradiance at the target plane we are trying to measure. Again one assumes <u>any</u> set of F number points (F corresponds to the number of filters) and a value of irradiance is chosen for each value of λ_{OF}. Then if a linear interpolation is performed between the points, a segmented line curve of irradiance $J_A(\lambda)$ is developed, which may also be a straight line as shown in figure 3. Using this assumed irradiance curve calculate

$$V_{FA} = \int_0^\infty J_A(\lambda)\tau_F(\lambda)S(\lambda)d\lambda$$

or

$$V_{FA} = S\sum_{N=1}^{L} J_{AN}\tau_{FN}\Delta\lambda_{FN}$$

where V_{FA} is the voltage, with the $F^{\underline{th}}$ filter in place, calculated using the assumed irradiance curve $J_A(\lambda)$, L is the number of increments, and $\Delta\lambda_{FN}$ is the width of each increment. Now calculate the ratio

$$\frac{V_{FA}}{V_{FM}} = R_F$$

and if R_F is less than one raise V_{FA}, if R_F is greater than one lower V_{FA}, and, finally, if R_F is equal to one keep V_{FA} unchanged. Due to the overlapping of filters a change in V_{FA} affects V_{FA+1}, so again an iterative process is called for. This method converges to the same results regardless of the initial assumed irradiance curve.

RESULTS AND CONCLUSION

Figure 4 is a chart showing a comparison among the three methods of filter calculations. Figure 5 is a plot of irradiance versus wavelength of a carbon arc simulator using three different methods of calculations. All three of these methods agree very closely with each other indicating after the filters have been chosen for a continuous source there is no need for prior knowledge of the source or to arbitrarily choose correct band pass limits.

FUTURE WORK

Figure 6 is a plot of the irradiance of a carbon arc solar simulator as a function of wavelength using one of the filter methods and an equally normalized monochromator measurement. Also on Figure 6 is the normalized Johnson extraterrestrial sun curve. The discrepancy between the two methods of measuring spectral irradiance on the same system is under continuing investigation at Lewis. One member of the staff is concentrating on a theoretical approach to predict the uncertainty in filter measurements, others are working in the problem areas associated with the monochromator measurement.

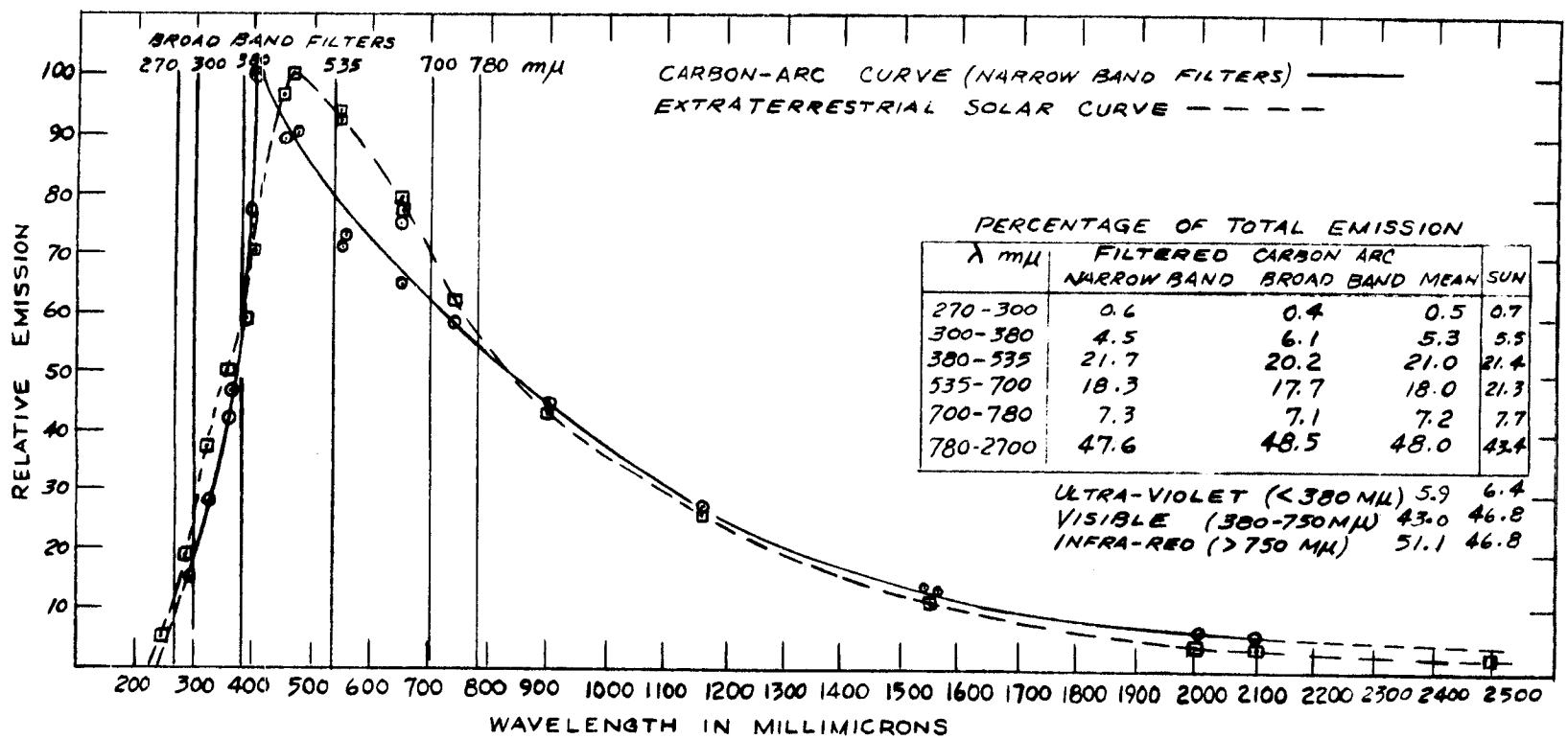

PERCENTAGE OF TOTAL EMISSION

λ mμ	FILTERED CARBON ARC NARROW BAND	BROAD BAND	MEAN	SUN
270-300	0.6	0.4	0.5	0.7
300-380	4.5	6.1	5.3	5.5
380-535	21.7	20.2	21.0	21.4
535-700	18.3	17.7	18.0	21.3
700-780	7.3	7.1	7.2	7.7
780-2700	47.6	48.5	48.0	43.4
ULTRA-VIOLET (<380 Mμ)	5.9			6.4
VISIBLE (380-750 Mμ)	43.0			46.8
INFRA-RED (>750 Mμ)	51.1			46.8

COMPARISON BETWEEN N.A.S.A. CLEVELAND CARBON-ARC SOURCES AND THE EXTRATERRESTRIAL SUN

FIGURE 1. CURVE OF CARBON ARC AS APPEARED IN THE EPPLEY REPORT.

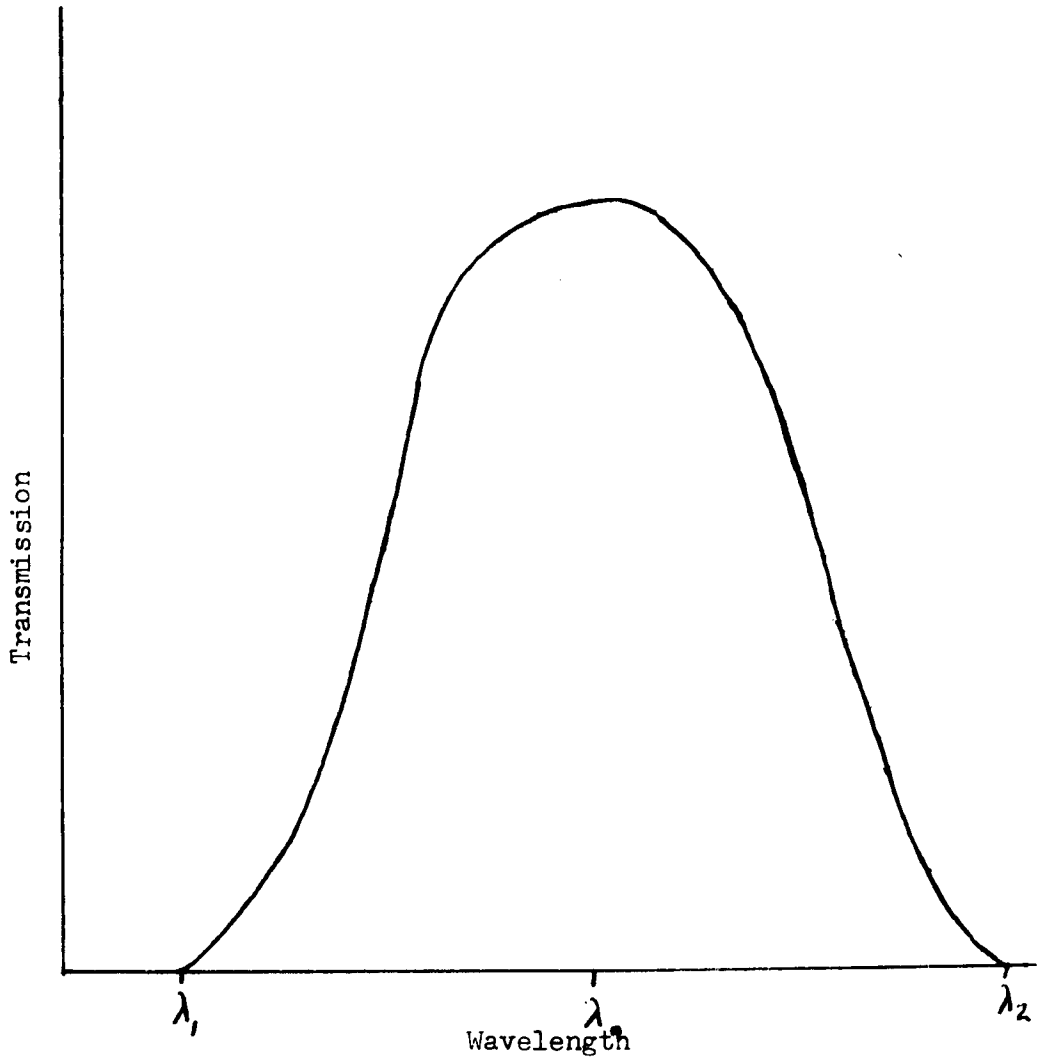

Figure 2. TRANSMISSION OF TYPICAL FILTER AS A FUNCTION OF WAVELENGTH

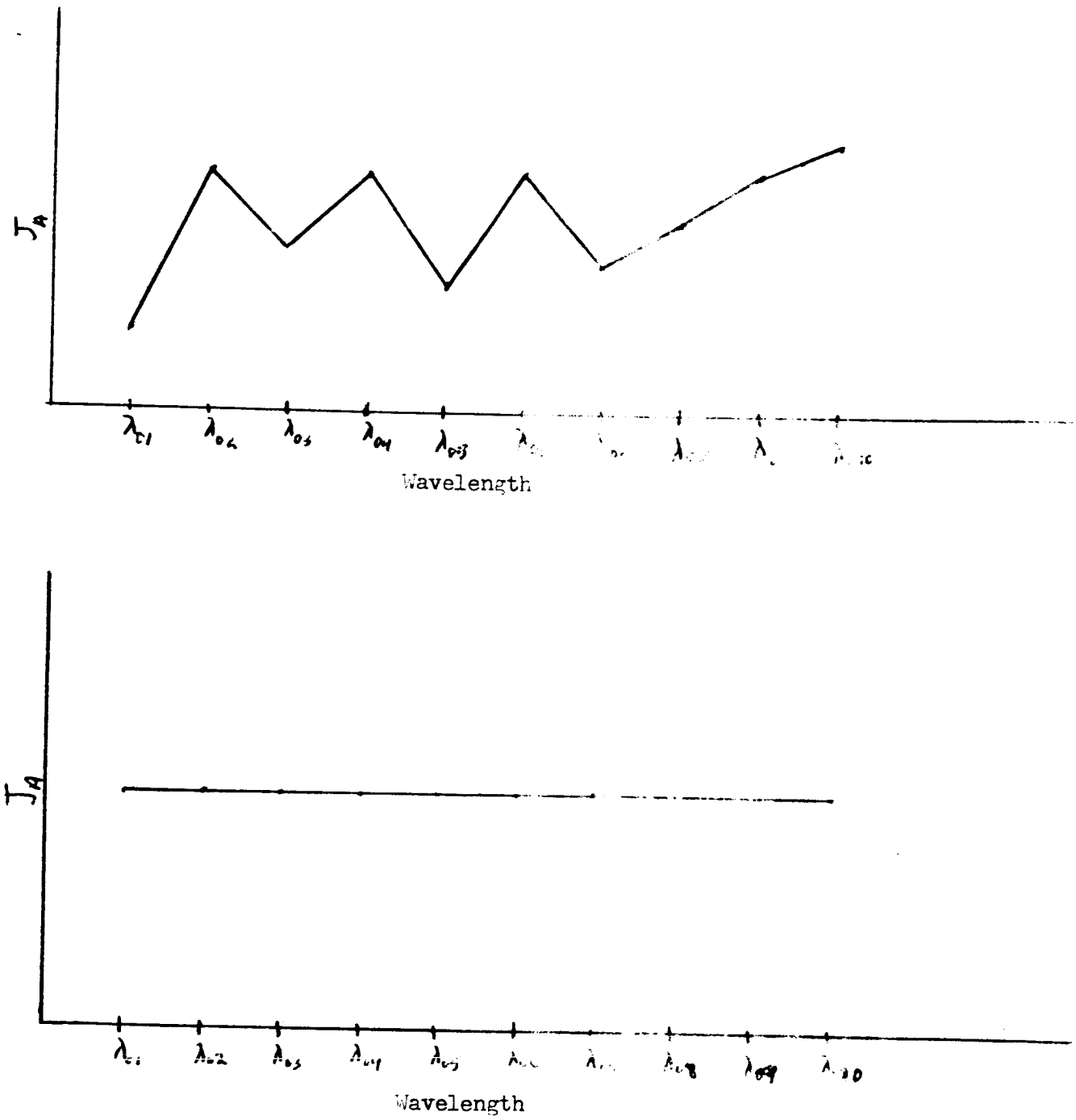

Figure 3. POSSIBLE ASSUMED IRRADIANCE CURVES J_A, AS A FUNCTION OF WAVELENGTH

	Non-filter Factor Method	Modified Eppley Method	Eppley Method
λ_0	$= \frac{\sum_{N=1}^{L} \tau_N \lambda_N}{\sum_{N=1}^{L} \tau_N}$	$= \frac{\sum_{N=1}^{L} \tau_N \lambda_N}{\sum_{N=1}^{L} \tau_N}$	Approximated
Assumed spectral distribution	Any segmented line	Any segmented line	Monochromator data of bare source
Filter factor	None	$= \frac{\sum_{N=1}^{L} J_N}{\sum_{N=1}^{L} J_N \tau_N}$	$= \frac{\sum_{N=1}^{L} J_N}{\sum_{N=1}^{L} J_N \tau_N}$
Bandpass limits	Not needed	0% trans.	1% trans.
Number of calculations	Iterative	Iterative	One
Agreement with data	Exact	Approximated	Approximated

Figure 4. COMPARISON CHART SHOWING DIFFERENCES IN TECHNIQUES OF EVALUATING FILTER DATA

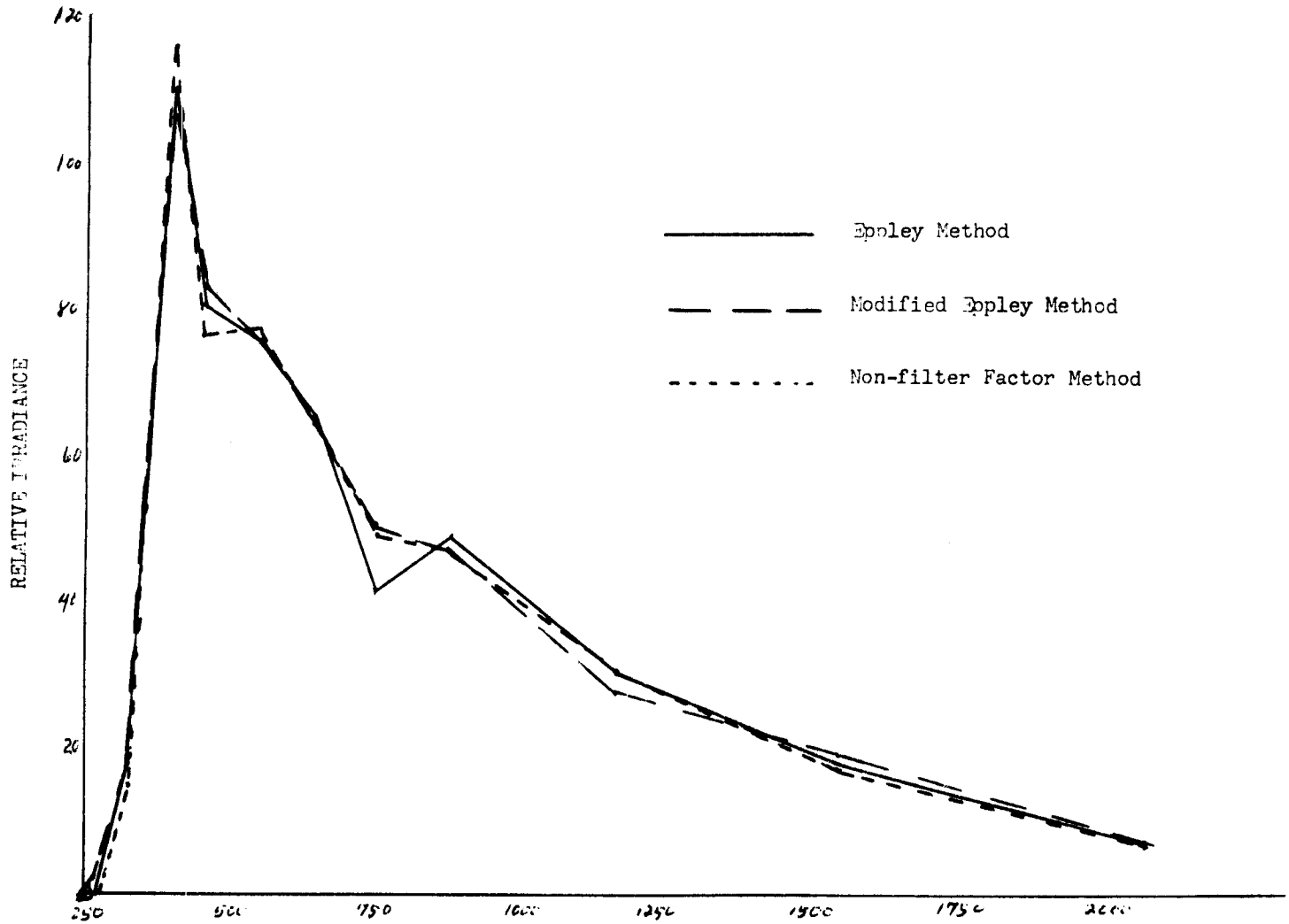

Wavelength (millimicrons)

Figure 5. RELATIVE IRRADIANCE OF IRL SOLAR SIMULATOR AS MEASURED BY FILTER METHODS

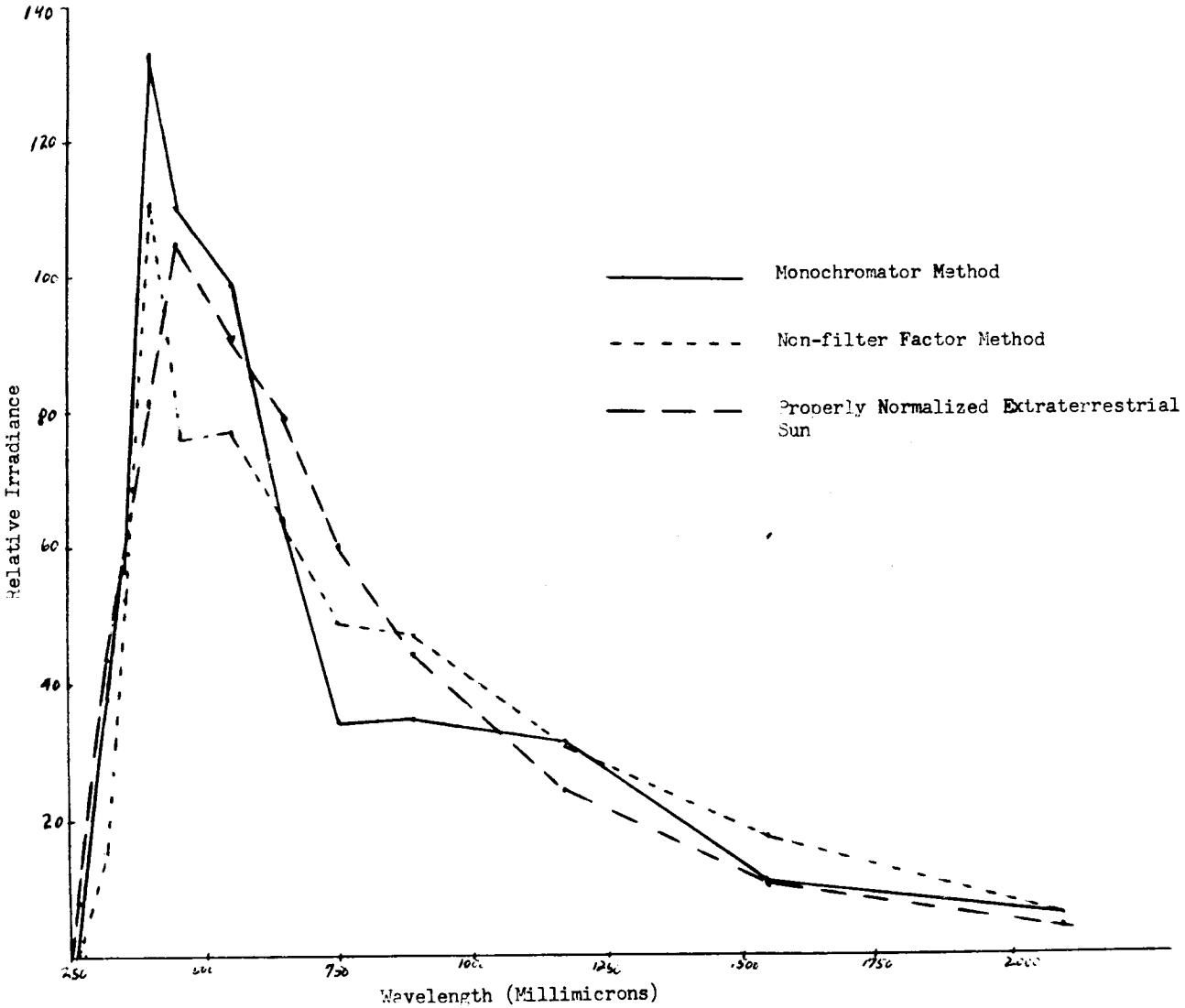

Figure 6. RELATIVE IRRADIANCE OF IRL SOLAR SIMULATOR AS MEASURED BY FILTER AND MONOCHROMATOR VS SUN

Spectral Measurements on High Intensity Light Sources

by

John C. Flemming & Charles H. Duncan
NASA Goddard Space Flight Center
Greenbelt, Maryland

Dupe of X64-34134

ABSTRACT

Measurements of the spectral distributions of a xenon, mercury-xenon, and carbon arc have been accomplished. The carbon arc and xenon arc have spectral distributions most similar to air mass zero solar irradiance. The absorptivities of gold, silver, and aluminum have been calculated using the measured spectral distributions. The per cent variations from the solar absorptivities of these materials vary from -3% to +26% for the xenon arc; -26% to +11% for the carbon arc; and, -8% to +77% for the mercury-xenon arc.

Introduction

The Solar Simulation Group of the Thermal Systems Branch has developed and calibrated an instrumentation for measuring the spectral characteristics of any light source. The calibration of the instrument was accomplished by using a strip-filament tungsten lamp calibrated by the National Bureau of Standards. The uncertainty of the calibration of this lamp varies from 3 per cent in the infra-red to 8 per cent in the ultraviolet(1). This instrumentation uses a Leiss double monochromator as the dispersing element and has been previously described(2). The instrumentation and techniques of data acquisition have been developed to a point which allows repeatability of results to 1 per cent or less on measurements of light sources comparable to the standard lamp. The instrumentation has been used to calibrate one N.B.S. standard lamp in terms of another N.B.S. standard lamp. The results obtained were in agreement to the N.B.S values within 1%.

In measurements of the spectral distributions of campact arc sources and carbon arcs, complications are encountered which are not present in tungsten strip filament lamps. The complications are: the non-uniformity of the source, the instability of the source, and the extremely

high spectral radiances of the source. The micro brightness contours of a xenon[3] and mercury-xenon[4] source vary by a factor of 3 to 4 between the cathode of the lamp and a point 1.0 mm. removed from the cathode toward the anode. The stability of these micro brightness contours in time has been studied qualitatively, and variations are evident which will produce significant errors if the position of the arc focused on the entrance slit of the monochromator is not held to tolerances of 1/10 mm. or less. To accomplish this repositioning of the instrumentation repeatedly is very difficult, if not impossible. The spectral radiances produced by these lamps are as much as 6 orders of magnitude greater than the spectral radiances produced by the standard lamp. This introduces large scaling factors which can become a source of uncertainty.

All the preceding discussion related to absolute spectral radiance measurements. If the primary interest in a source is the spectral distribution only, then a relative spectral energy determination will suffice. Relative energy determinations are not as strongly dependent upon variation in arc characteristics because the source can be focused at a convenient position in the optical train which does not have to be the entrance slit of the monochromator. This minimizes the arc fluctuations described above. Also, the extreme differences in spectral radiances between the standard and the unknown source can be reduced by neutral filters whose transmission characteristics do

not have to be known.

The collection of energy[1] incident to the entrance slit of the monochromator can also be varied by an aperature which changes the effective f/no of the entrance optics. In this manner, scans of individual spectral regions can be accomplished and then normalized to yield a complete spectral distribution curve.

Experimental Procedure

Two methods of illumination of the entrance slit of the monochromator have been used. These are diagrammed in Figure 1. In Method A, radiation from the lamp is introduced onto a block of magnesium oxide by means of a front-surfaced aluminum mirror. The MgO block is then focused onto the entrance slit of the monochromator by means of a spherical mirror and turning flat. Corrections for the reflectivity of MgO and the other optical elements have been made in the data presented. In method B, radiation from the lamp is focused at a point about nine inches ahead of the entrance slit in the optical train. This is accomplished by the optical components shown. This allows divergent illumination to be incident upon the slit of the monochromator. This means that the radiation has a different optical path

through the instrument than it does when an image is formed at the slit. This also means that a different area of the detector will be illuminated than that when the calibration was performed. This introduces no errors which are wave length selective according to a recent paper[5].

The detectors used in obtaining this data were: (1) 1P-28 photomultiplier, (2) 9592B photomultiplier, (3) 7102 photomultiplier, and (4) lead sulfide cell. The bandwidth of radiation passed by the instrument varied from 5A in the ultraviolet to 250A in the infra-red.

The data is recorded on a strip-chart recorder at present and about 500 points between 250 nm and 2500 nm are reduced. This is a very slow and tedious procedure and a procurement request has been initiated to provide a digital output from the Leiss which can be processed by a computer. A program has been written to process the data and compute spectral radiances; and, absorptivities of selected materials based on the spectral distribution measured.

Spectral Distribution Measurements

Spectral measurements have been obtained for an Osram XBO 1600 watt xenon lamp, an Hanovia 929B1 2500 watt mercury-xenon lamp, and a Genarco ME4 CWM carbon arc.

Figure 2 shows the spectral distribution obtained from the Osram lamp operated at 2500 watts using Method A of illumination shown in Figure 1 and described above. Figure 3 shows the spectral distribution of the same lamp operated at the same wattage but using Method B of illumination as described above.

Figures 4 and 5 show the spectral distribution obtained from the Hanovia lamp operated at 2500 watts. The method of illumination used was A and B respectively.

Figure 6 shows the spectral distribution of the Genarco carbon arc operated at 185 amperes. The method of illumination used was B. Carbons used were Lorraine Orlux.

Figure 7 is a plot of Johnson's data[6] plotted in a similar manner as the data above.

Figures 8, 9, and 10 are plots of the above data presented in a different manner. The per cent of the total energy per 10 nm bandwidth between 250 nm and 2500 nm is plotted against wavelength. Each of the above measurements using illumination method B is shown. A plot of Johnson's data is shown on each curve for comparison purposes. The

areas under the curves are the same for each figure for both the solar irradiance and the respective lamp. An inspection of these three figures shows that the source most similar to the air-mass zero solar irradiance is the carbon arc with xenon next and mercury-xenon last. The carbon arc is deficient in the ultraviolet and part of the infrared; the xenon is deficient in the visible and infrared except for the strong excess between 800 and 1000 nm; the mercury-xenon is deficient in the visible except for the strong emission lines of mercury around 420 nm and 580 nm. If a filter were manufactured which would eliminate the excess energy of xenon betwen 800 nm and 1000 nm, then xenon would approach or surpass the carbon arc in suitability of spectral characteristics.

The data presented in Figures 8, 9, and 10 have been used to calculate the absorptivities of gold, aluminum, and silver. The spectral band widths used for these calculations were: 20 nm from 250 nm through 600 nm; 50 nm from 600 nm through 1000 nm; and 100 nm from 1000 nm through 2600 nm. The values for the reflectivities of the materials were obtained from the American Institute of Physics Handbook for 1957, Table 6K-4. The values for air-mass zero solar irradiance are from Johnson [6] and were used to calculate the solar absorptivities.

The results of these calculations are:

Source	Gold	Silver	Aluminum
Solar	19.2%	4.9%	7.9%
Xenon	18.7%	6.2%	8.4%
Hg-Xe	19.7%	8.7%	7.3%
Carbon Arc	21.3%	3.6%	7.7%

The deviations of absorptivity of each material from the solar absorptivity is summarized below:

Source	Deviation from Solar Absorptivity		
	Gold	Silver	Aluminum
Xenon	-2.6%	+26,3%	+6.2%
Hg-Xe	+2.7%	+77.1%	-7.7%
Carbon Arc	+11%	-26.5%	-2.6%

A study of this table reveals that for these three materials, the carbon arc and xenon will yield about the same absolute errors. It also shows that Hg-Xe is quite suitable if materials such as gold and aluminum are used. However, if silver is used, a much larger error will result with the mercury-xenon lamp. This points to the result that for thermal balance studies, the materials used can be strongly affected by the spectral characteristics of the simulation. So long as materials with uniform spectral absorptivities are used, the spectral characteristics of the source are of minor importance but when a material has a strong change in absorptivity with wavelength the spectral distribution of the simulator becomes

quite important. These values of absorptivities are based on the data shown in Figures 8, 9, and 10 and are probably accurate to ±10% for sources of these types in general. It should be restated that the absorptivities discussed above relate only to the source and do not take into account the effects of any optical system which will be present in a simulator. The effect of adding an optical system is, in general, to attenuate the shorter wavelengths more than the longer.

References

1. Stair, Johnson, Halback; "Standard of Spectral Radiance for the Region of 0.25 to 2.6 microns"; J. of Res. NBS, Vol. 64A, No. 4., July-August 1960.

2. Flemming, Hobbs; "Calibration of the Leiss Instrumentation"; Conference on Solar Simulation Research and Technology, 1963.

3. Macbeth Sales Corporation; "Technitalk"; L-8, 4-62.

4. Hanovia Lamp Division; "Hanovia Compact Arc Lamps"

5. Stair, Schneider, Jackson; "A New Standard of Spectral Irradiance"; J. App. Opts.; Vol II, No. 5, Nov. 1963.

6. Johnson; "The Solar Constant"; J. of Met.; Vol. XI, No. 6, Dec. 1954.

Appendix

Operational Experience with Genarco Model ME4 CWM Automatic Reloading Carbon Arc

A Genarco carbon arc with an automatic reloading device has been operated for approximately sixty hours. The reloading mechanism is essentially a plunger which drives a female carbon onto a tapered male carbon. The joint holds together by friction, both male and female having been machined to fit very snugly. A disadvantage to this method is that each carbon has to be custom fitted in the sequence since no two are exactly the same. Another disadvantage is the fact that the alignment necessary between the carbons to be joined is very critical. In operation, about one of every three joinings is not accomplished because of misalignment of the two carbons. In some cases, the joining can be accomplished manually without shutdown of the arc and in some others fracture of the female carbon results which requires shutdown of the arc for correction. There is no mechanism for joining the negative carbons, the solution for long operation periods being the use of long negative carbons of the order of four feet in length. The stability of the arc has been measured using an Eppley normal incidence pyrheliometer. Variations averaged about five per cent. When a joining of the carbons was accomplished, a short term excess of about 15-25 per cent was noted which fell back to the normal level within one or two minutes. This is caused

by slippage of the positive carbon in the feed mechanism due to the plunger action of the reloading mechanism. When a joint burns through, the variation is within the five per cent quoted above.

METHOD "A"

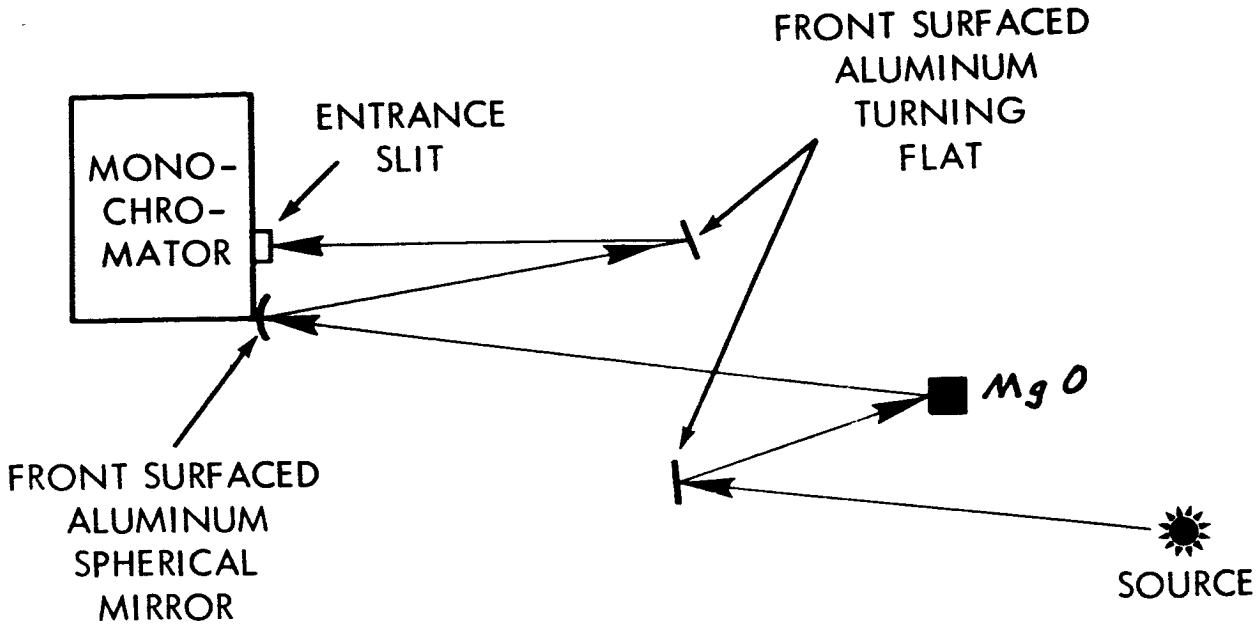

METHOD "B"

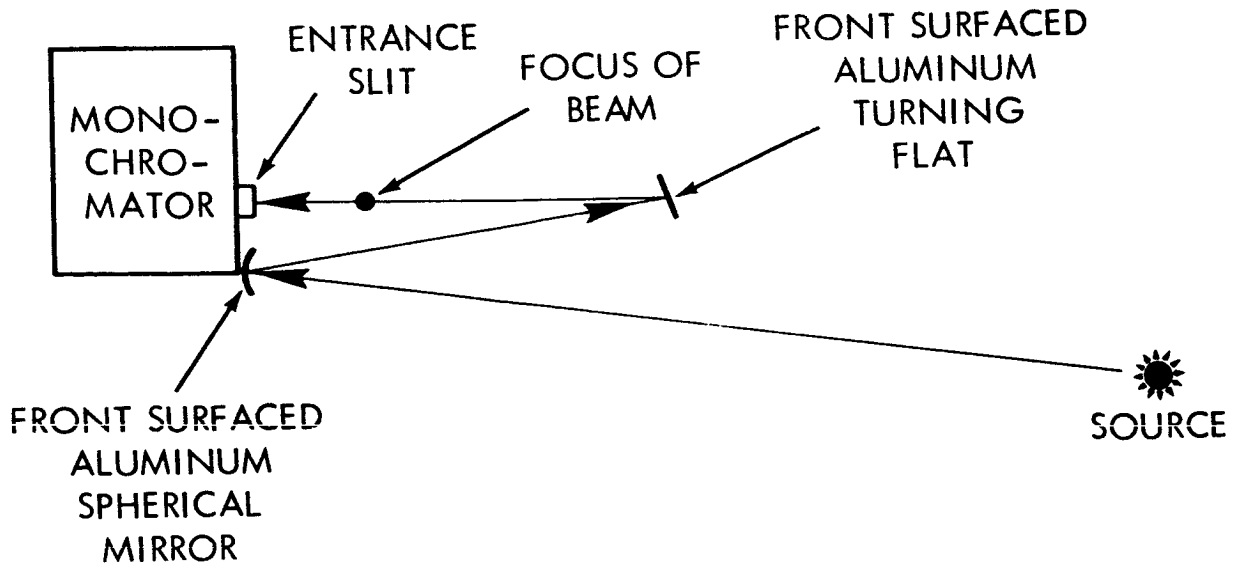

Fig. 1 - Optical Diagram

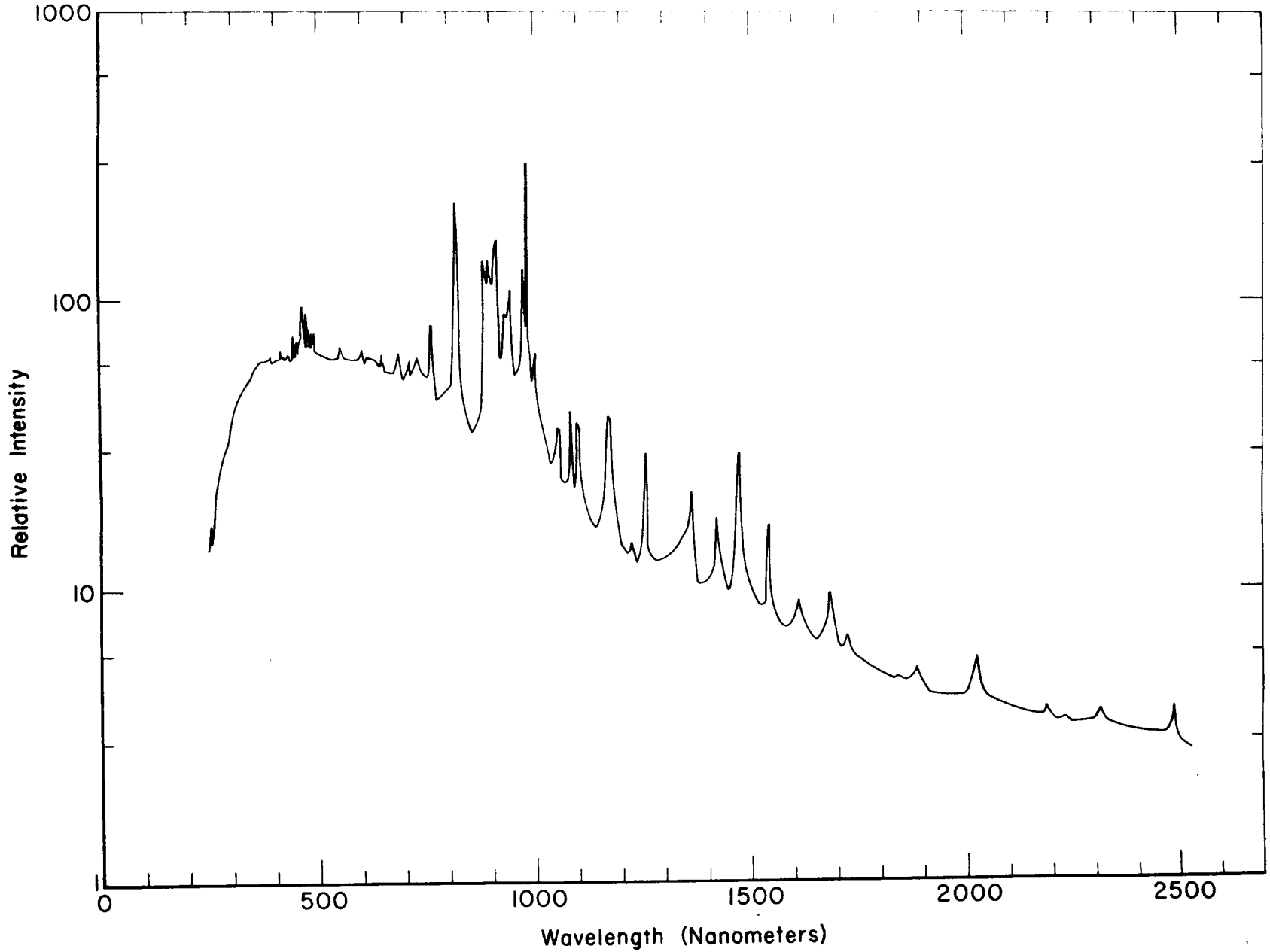

Figure 2. - Spectral Distribution of Xenon Lamp Operated at 2500 Watts, Illumination Method "A".

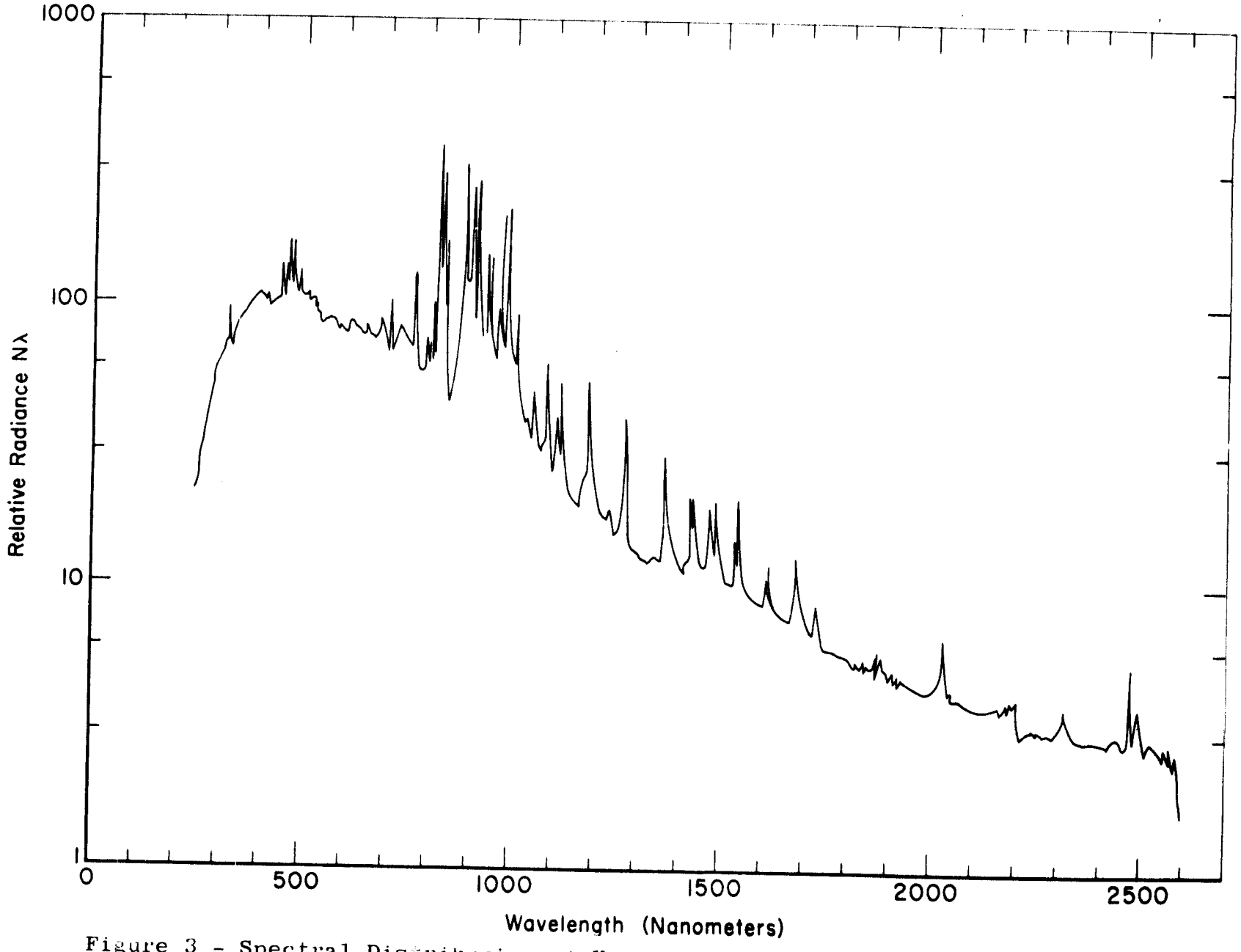

Figure 3 - Spectral Distribution of Xenon Lamp Operated at 2500 Watts, Illumination Method "B".

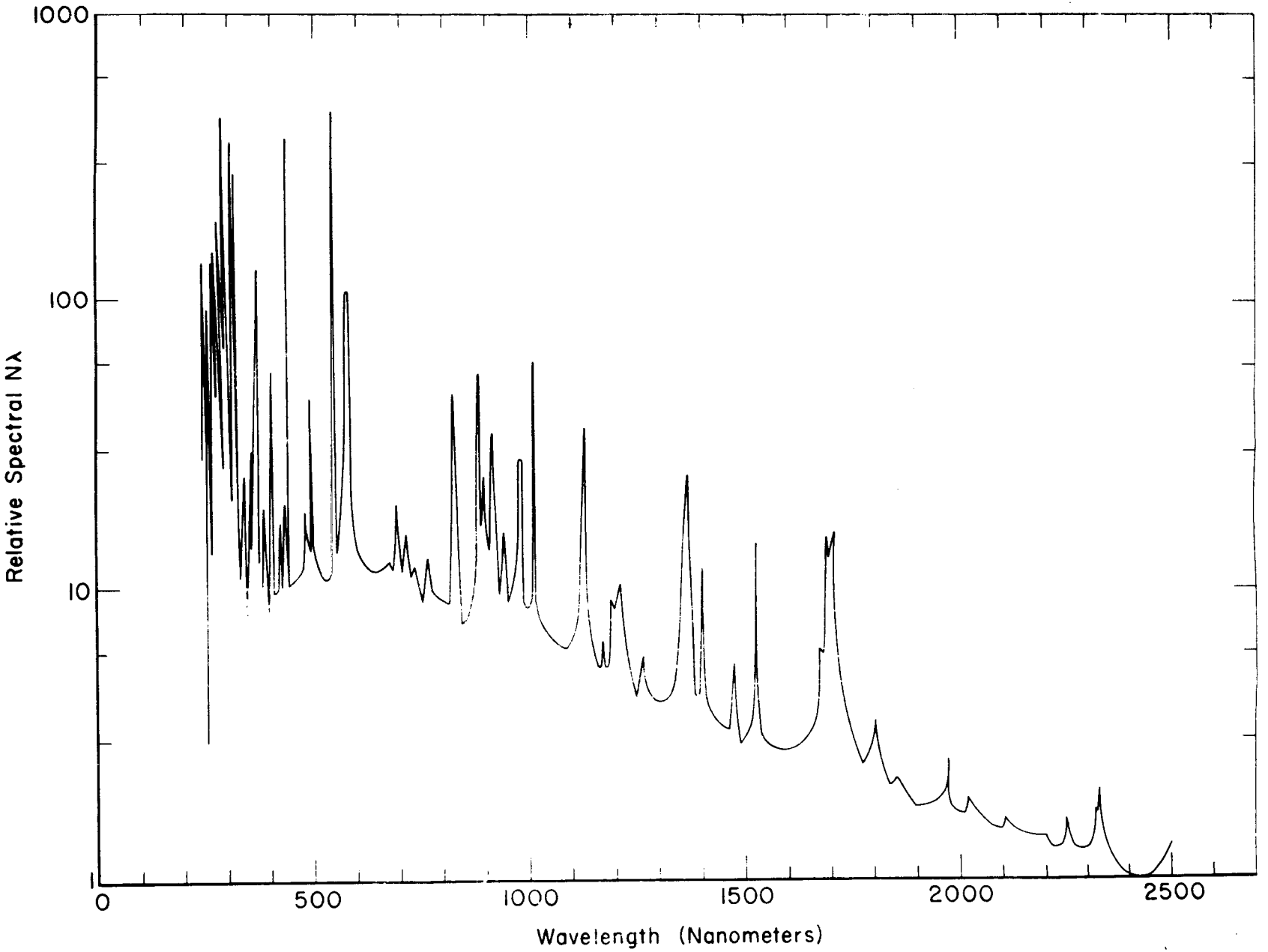

Figure 4 - Spectral Distribution of Mercury-Xenon Lamp Operated at 2500 Watts, Illumination Method "A".

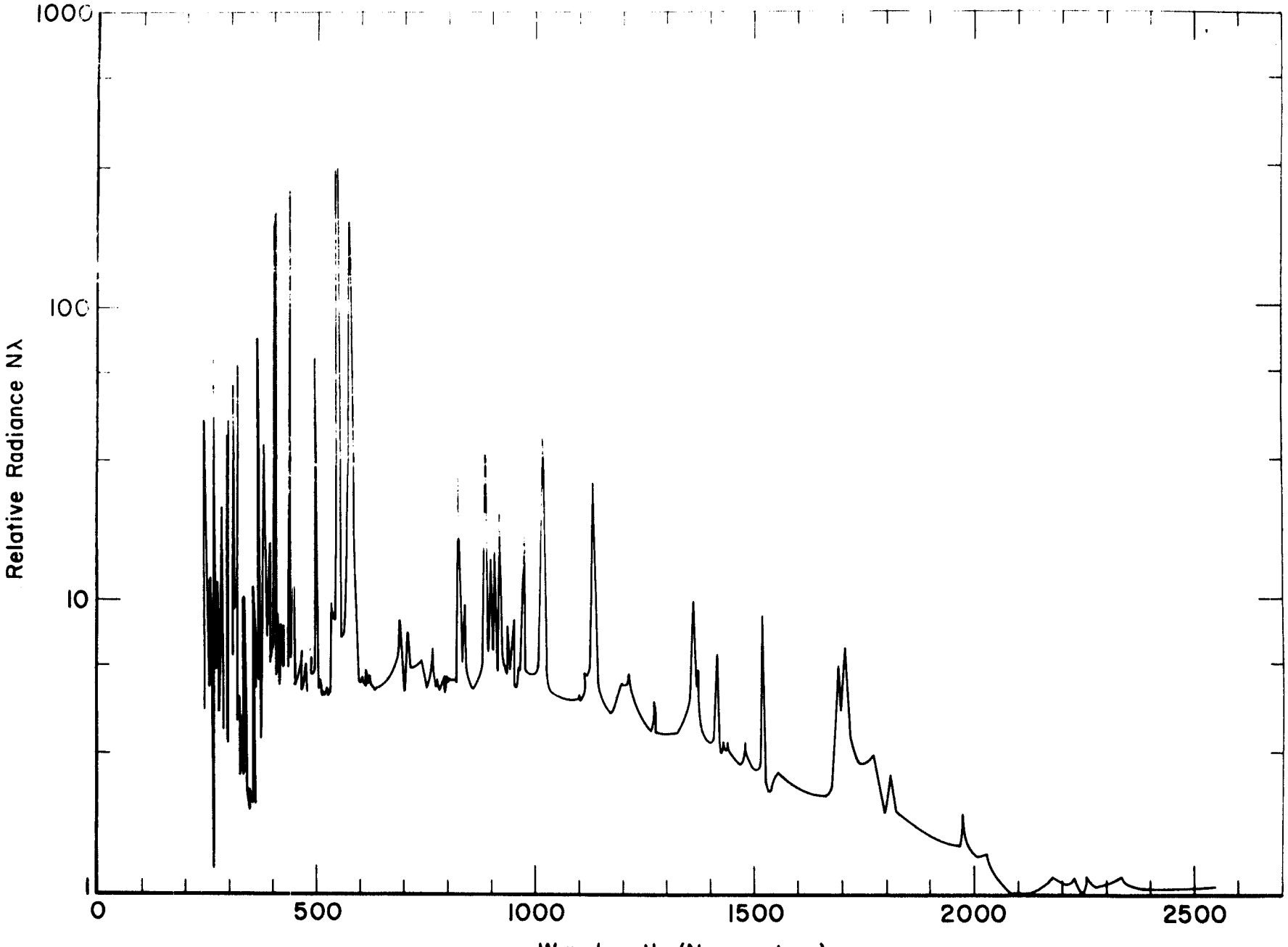

Figure 5 - Spectral Distribution of Mercury-Xenon Lamp Operated at 2500 Watts, Illumination Method "B".

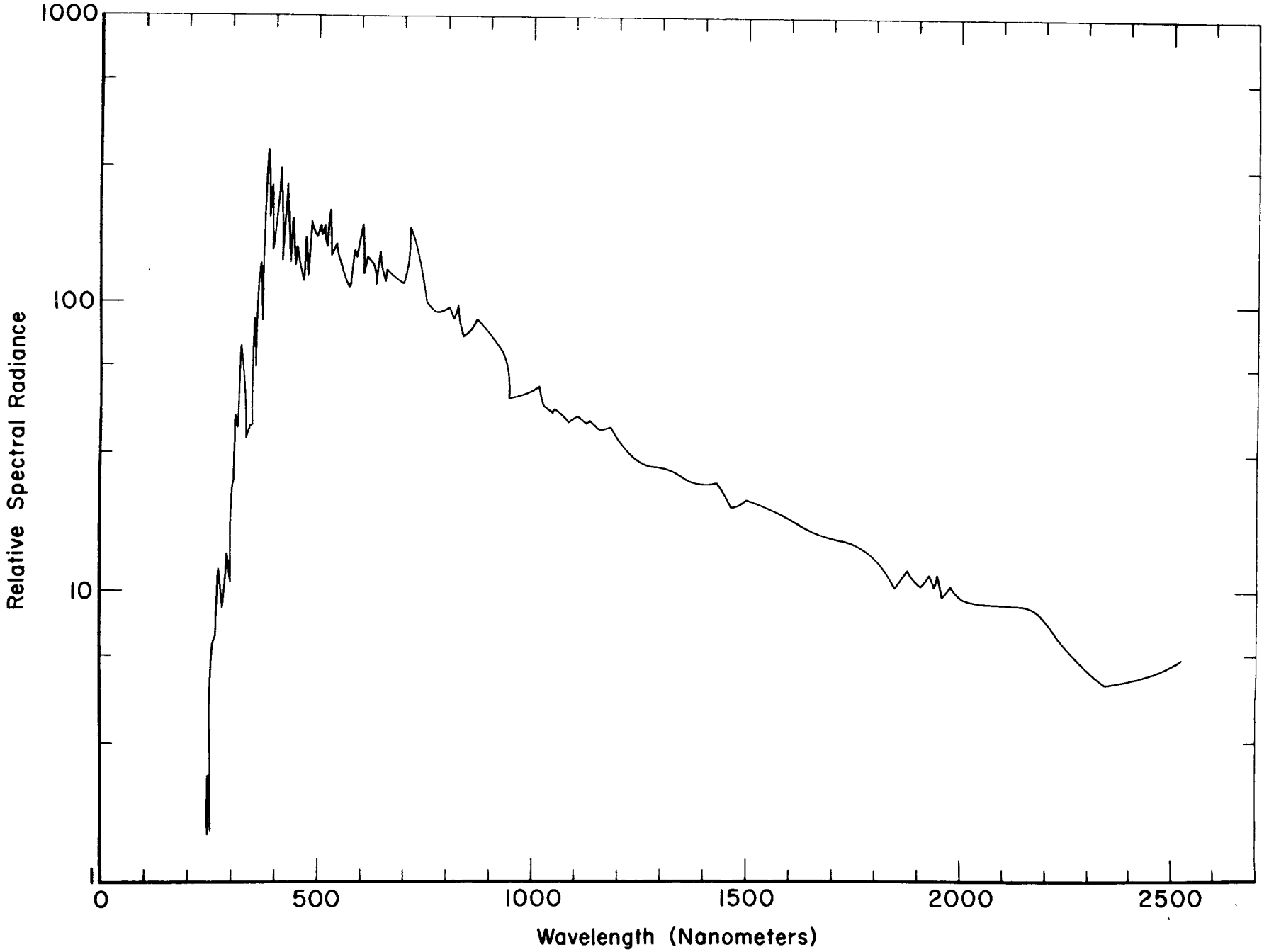

Figure 6 - Spectral Distribution of Carbon Arc Operated at 10,000 Watts, Illumination Method "B".

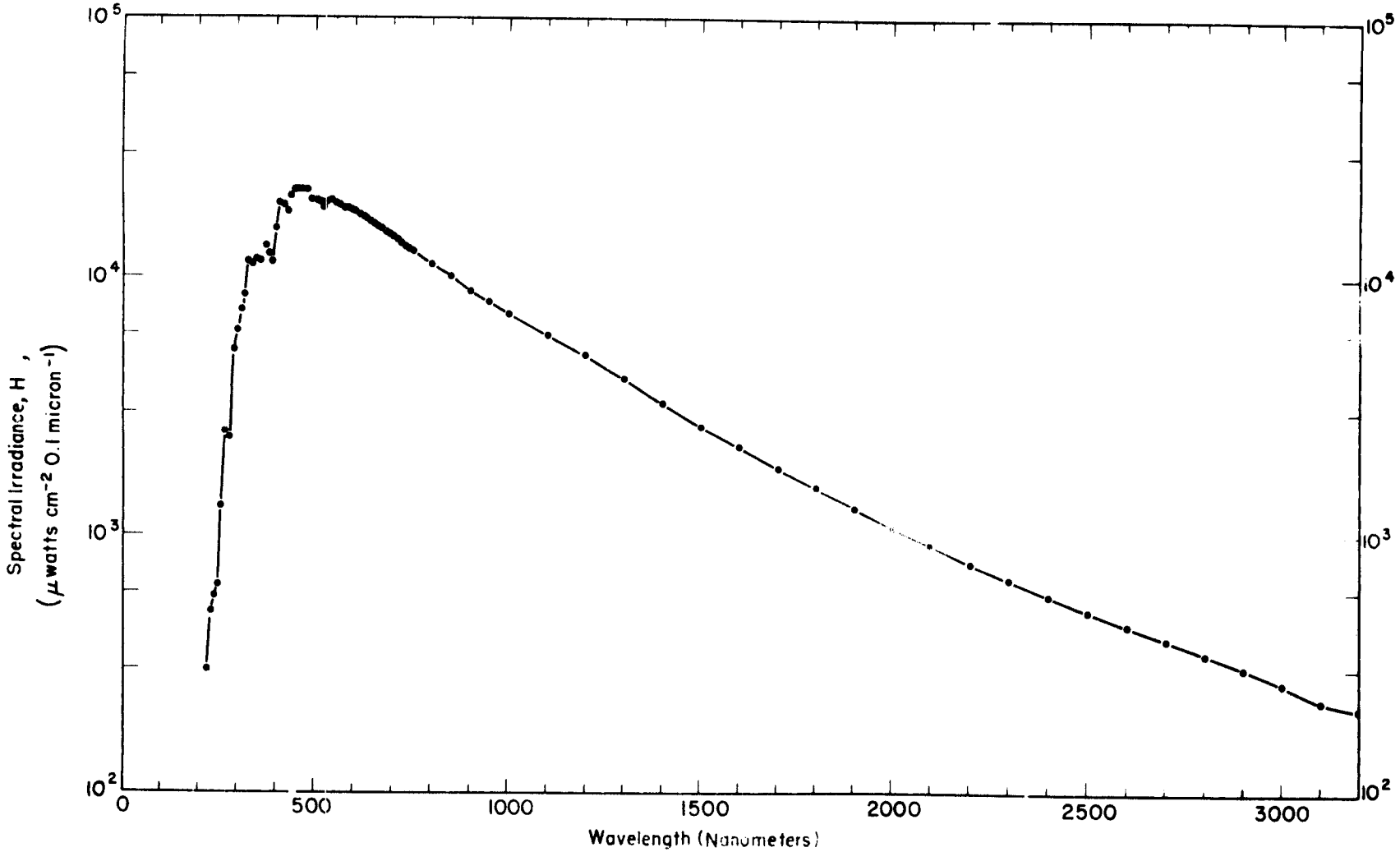

Figure 7 - Air Mass Zero Solar Irradiance (Johnson)

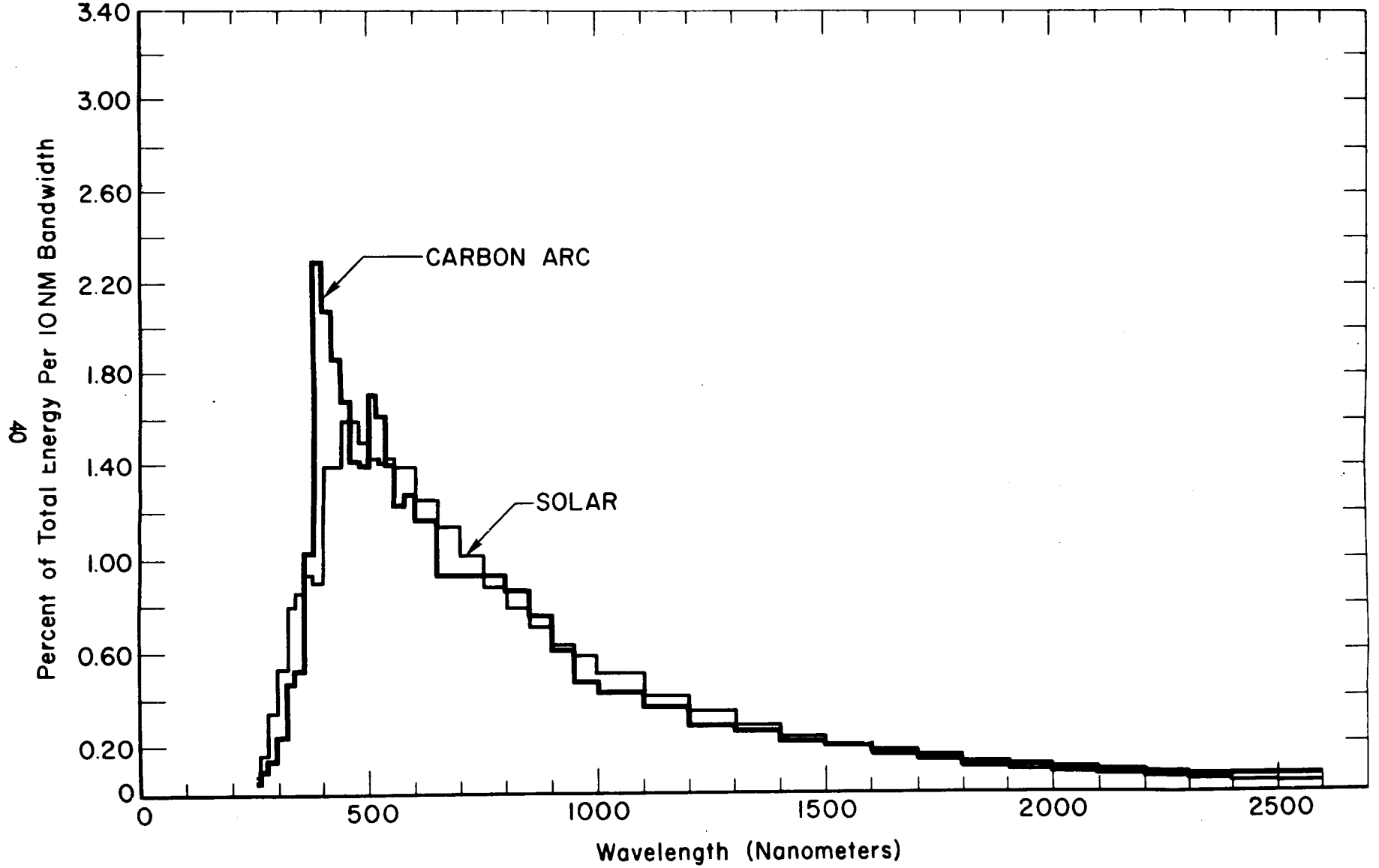

Figure 8 - Comparison of Carbon Arc Spectrum with Solar.

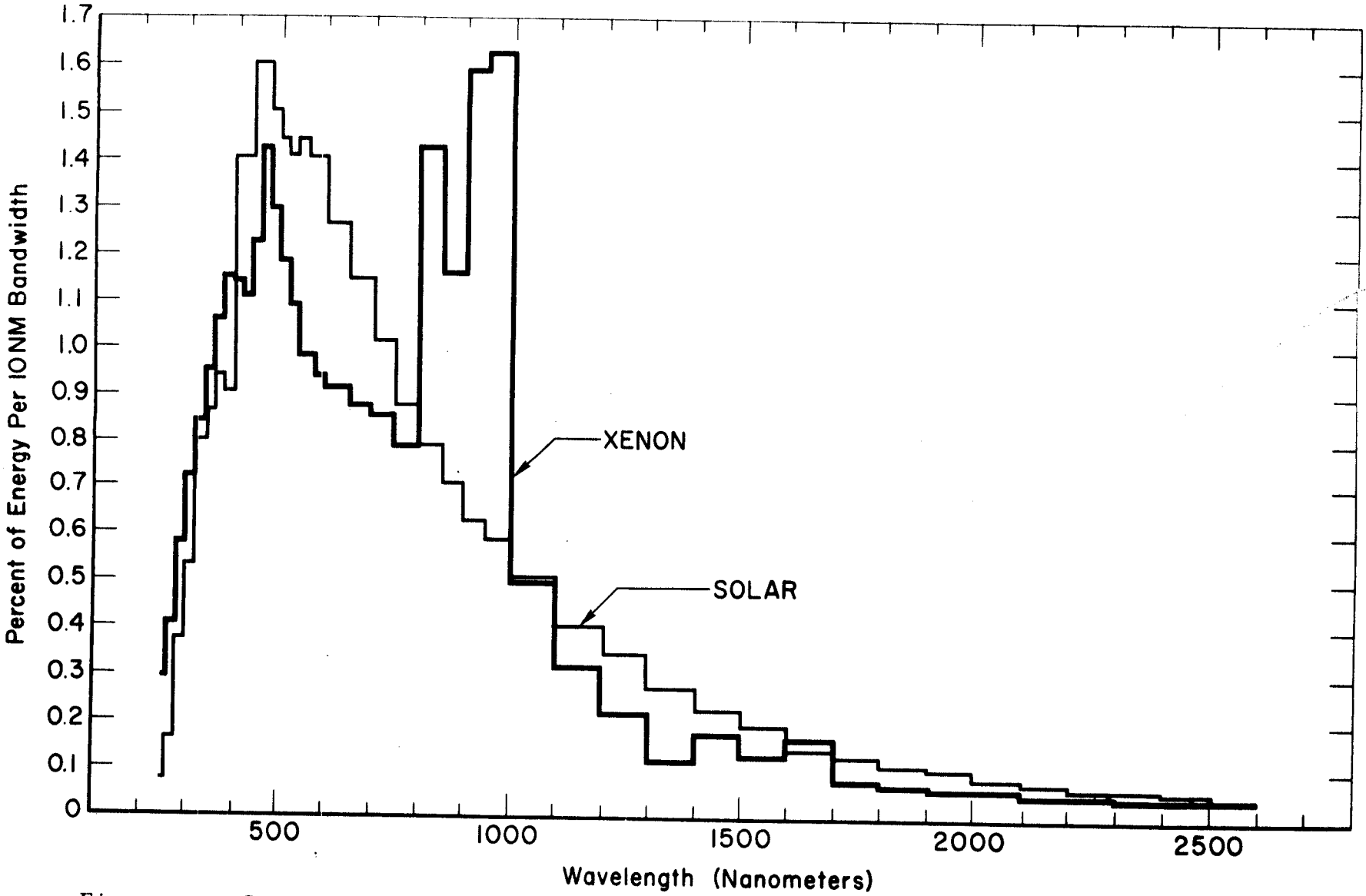

Figure 3 - Comparison of Xenon Spectrum with Solar.

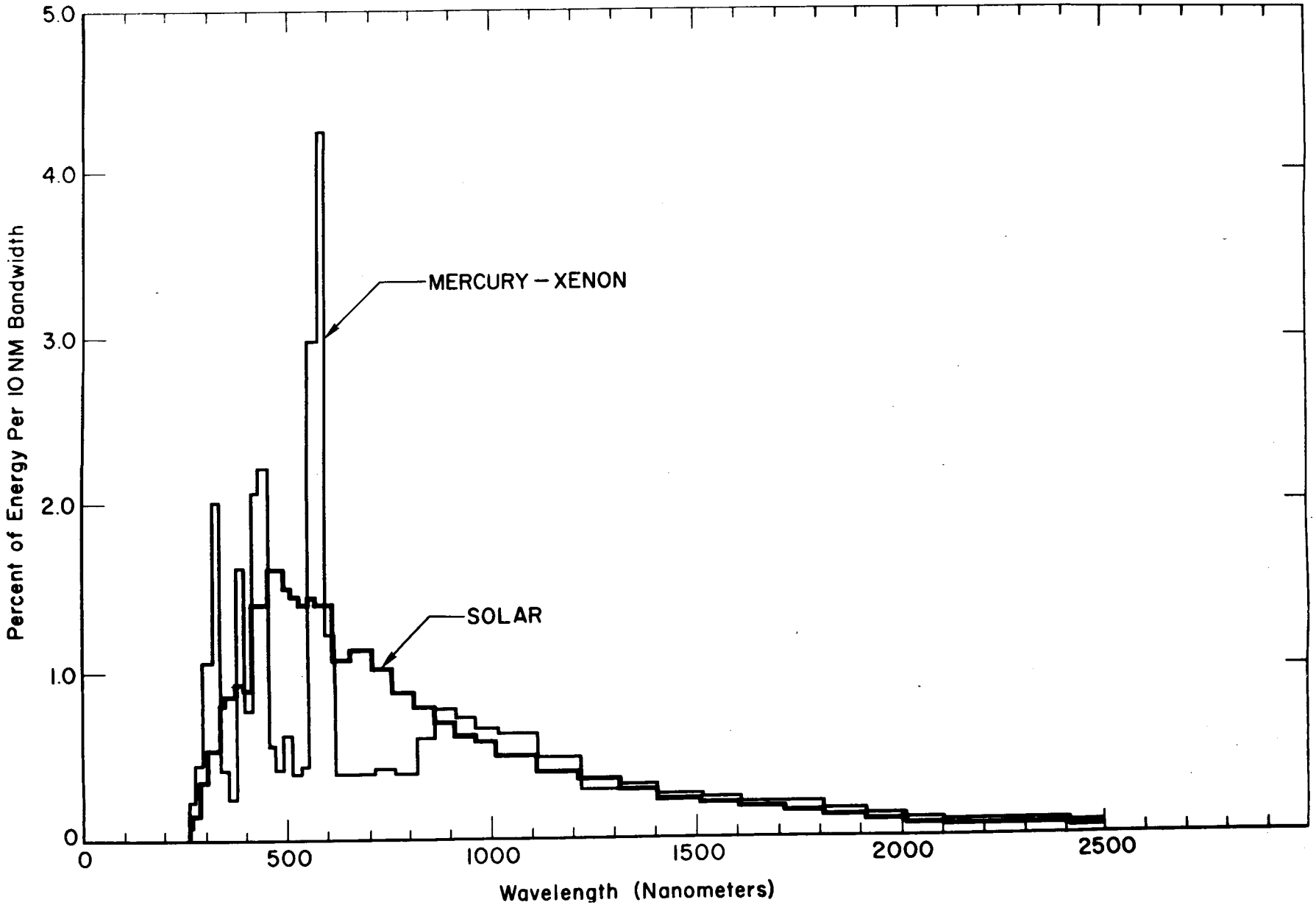

Figure 10 - Comparison of Mercury-Xenon Spectrum with Solar.

THE SOLAR CONSTANT AND SPECTRAL DISTRIBUTION OF SOLAR RADIANT FLUX

Matthew P. Thekaekara
Goddard Space Flight Center, Greenbelt, Maryland

ABSTRACT

A survey has been made of the data currently available on the solar constant and the spectral distribution of the solar radiant flux. The relevant theoretical considerations on radiation, solar physics, scales of radiometry and thermal balance of spacecraft have been briefly discussed. A detailed review has been attempted of the data taken by the Smithsonian Institution, the National Bureau of Standards and the Naval Research Laboratory, of the methods of data analysis and the many revisions of the results. The survey shows that the results from different sources have wide discrepancies, that no new experimental data have been taken in recent years, and that the conventional technique of extrapolation to zero air mass leaves large uncertainties. The feasibility of further measurements and of a new method of approach has been discussed in the light of the results of this survey.

I. INTRODUCTION

The solar constant and the spectral distribution of the solar radiant flux are of considerable importance in many areas of physics and engineering. In geophysics and meteorology, in studies of the upper atmosphere and of the thermal balance of the earth, in the investigation of solar phenomena and in many areas of illuminating engineering, the radiant energy received from the sun is a significant parameter. In recent years the topic has received a great deal of attention because of its bearing on the thermal balance of spacecraft.

In spite of the widespread interest in the subject and its importance in many areas of scientific research, no new experimental data have been collected in recent years. It is generally assumed that the best value of the solar constant available at present is 2.00 cal. cm^{-2} min^{-1}. This value was deduced by Francis S. Johnson at the Naval Research Laboratory, Washington, D. C. in 1954[1]. It is based on revisions of data which had been collected for over 30 years by the Smithsonian Institution, later data collected by Dunkelman and Scolnik[2] in 1951, and a reevaluation of the correction factors for the infrared and ultraviolet regions of the spectrum.

It is interesting to observe that the solar constant has frequently been revised, and each new revision has increased its value. Parry Moon[3] in 1940 published a detailed analysis of the data of the Smithsonian Institution and arrived at the value 1.896 cal. cm^{-2} min^{-1}. A revision in 1952 by Aldrich and Hoover[4] raised the value to 1.934 cal. cm^{-2} min^{-1}. C. W. Allen[5], in 1955 gave a value, 1.97± .01 cal. cm^{-2} min^{-1} and Francis S. Johnson's value, as stated earlier, was 2.00± .004 cal. cm^{-2} min^{-1}. An independent set of measurements was made by Ralph Stair and Russell G. Johnston[6] at an altitude of 9200 feet; they published in 1956 a still higher value, 2.05 cal. cm^{-2} min^{-1}.

The discrepancies between different investigators are even greater for the published data on the spectral distribution of the radiant flux. Some of the more reliable data have been collated and published by P. R. Gast[7] in the "Handbook of

Geophysics", where he makes the following observation: "As an example of a more important uncertainty, in the ultraviolet region (300 to 359 mμ), the discrepancy between various observations is about 10 per cent, and there have been reported[8] variant observations as large as 40 per cent which can be neither ignored nor explained."

In this paper an attempt will be made to present the relevant theoretical considerations and to collect together and evaluate the available information on the solar constant and the solar spectral radiant flux. The feasibility of further measurements will be studied in the light of existing data.

II. THEORETICAL CONSIDERATIONS

1. Terminology and Laws of Radiation

There is no uniformity in the literature concerning the terms and symbols used for the physical quantities involved in the statement of radiation laws. In recent years many authors have shown a preference for "The American Standards Nomenclature for Radiometry", ASA Z 58.1.1 - 1953[9], which was proposed by the American Standards Association Sectional Committee, Z - 58. This Committee had been sponsored by the Optical Society of America and the proposed nomenclature was approved on February 27, 1953. This nomenclature will be followed here.

Radiant energy density or radiant density, u, at a given point in space is the energy per unit volume in the vicinity of that point.

The radiant flux, P, through a given surface is the radiant energy which crosses unit area in unit time.

The radiant emittance (or flux density), W, of a radiating surface at a given point is the radiant energy emitted per unit area in the vicinity of that point per unit time.

The radiance, N, of a radiating surface at a given point in a given direction is the radiant energy emitted per unit

area, per unit solid angle in that point, per unit time.

Related quantities are radiant reflectance, ρ, transmittance, τ, and absorptance, α, which are the ratios of energy reflected, transmitted and absorbed, respectively, to the energy incident.

Emissivity, of a given surface ϵ, is the ratio of the radiant emittance of the surface to that of a blackbody surface at the same temperature.

The solar constant is the radiant flux due to the sun which crosses unit area exposed normally to the sun's rays at the average distance of the earth from the sun.

The above quantities refer to the energy radiated at all frequencies or in the entire wavelength range. The corresponding spectral quantities are denoted by adding the subscript λ, for wavelength, or ν, for frequency, to the respective symbol.

The spectral radiant flux P_λ, for example, is related to the radiant flux P by the equation $P = \int_0^\infty P_\lambda \, d\lambda$.

Certain simple relations hold between the quantities P, W, u, and N, if the radiating surface is perfectly diffuse, that is, if it has a constant radiance in all directions. These relations are:

$W = \pi \Omega_0 N$, where Ω_0 is one steradian;

$u = \frac{4\pi\Omega_0 N}{c}$, where c is the velocity of light; and

$W = \frac{cu}{4}$.

For collimated radiation, $P = cu$. The Planck's law gives the spectral radiant density in terms of the temperature, as

$$u_\lambda = \frac{8\pi hc}{\lambda^5 (e^{hc/\lambda kT} - 1)} \quad . \qquad (1)$$

The Stefan - Boltzman law gives the radiant emittance of a blackbody surface as $W = \sigma T^4$, where $\sigma = \frac{2}{15} \frac{\pi^5 k^4}{c^2 h^3}$. (2)

This may be derived from Planck's law by integrating the right hand side of equation (1).

From Planck's law may also be derived, by differentiating the right hand side and equating it to zero, the Wien displacement law which states that the wavelength at which the spectral distribution of the radiant emittance of a blackbody is maximum varies inversely as the temperature. $\lambda_{max.} T$ is a constant, equal to 0.289776 cm degree K.

The above equations of a blackbody radiation are applicable to the solar radiant flux though only to a first order of approximation. If the effective temperature of the sun's radiating surface and the area of the radiating surface are accurately known, both the solar constant and the spectral solar radiant flux can be determined from purely theoretical considerations. But these quantities do not permit a precise definition, nor can they be determined experimentally with sufficient accuracy.

The different parts of the sun which are responsible for the energy received from the sun are distinguished as the photosphere, the reversing layer, the chromosphere and the corona. The photosphere is the sun's surface directly visible in a telescope or a darkened glass. The opacity of the gases in this layer increases rapidly with depth, and hence prevents us from seeing farther into the sun. Even with the best of telescopes the edge of the photosphere at the circumference of the solar disc appears very sharp; hence we conclude that the transition from maximum brightness to total opacity occurs within a relatively short distance of about 50 km. This explains the close similarity of the solar spectrum to that of blackbody radiation.

The reversing layer and the chromosphere together form the atmosphere of the sun. They consist of luminous but very transparent gases. The reversing layer extends to a few hundred miles and the chromosphere to a height of several hundred miles. The chromosphere, consisting mainly of hydrogen and helium, is a partial absorber of solar radiation,

but its effect is small compared to the more dense reversing layer. The reversing layer contains vapours of almost all the familiar elements of the earth's crust. The strong absorption of energy by the reversing layer is mainly responsible for the departure of the spectral radiant flux of the sun from that of a blackbody.

The corona may be considered the extreme fringes of the solar atmosphere. The luminous part of the corona, as seen during a total eclipse, extends to a height of several solar radii. But recent experiments with space probes have shown that the corona has no distinct outer boundary, and that even the earth's orbit is enclosed within a tenuous coronal region. Hence the attenuation of energy in the sun-earth distance is greater than in the more rarefied regions of interstellar or intergalactic space.

There are several other factors which affect the total and spectral radiant flux of the sun. Among these are the sunspots which have a periodicity of eleven years, the faculae and the prominences which are relatively unpredictable, and the more permanent inhomogeneities of the photosphere. Thus we conclude that many complex radiative processes of emission and absorption combine to make the energy received at the average distance of the earth to be significantly different from that of blackbody radiation.

2. Solar Simulation and Thermal Balance of Spacecraft

In the area of solar simulation and thermal balance of spacecraft, the above theoretical considerations of blackbody radiation laws and solar radiant flux are of great importance. A question of special significance is the degree of error and inaccuracy in the predicted equilibrium temperatures of satellites, caused by errors in the assumed values of the solar constant and the solar spectral radiant flux. A complete discussion of this problem in any actual case involves many, highly complex and variable parameters. Among these parameters are the planet radiation of the earth, the reflected solar radiation from the earth, cloud cover and meteorological conditions, relative duration of the satellite inside and outside the earth's shadow, the ellipticity of the satellite orbit round the earth, the ellipticity of the earth's

orbit round the sun, the external geometry of the satellite, the internal transfer of heat between satellite components, and the properties of the exposed surface of the satellite as regards absorption of radiation and its reemission.

In our discussion of the problem we shall ignore the radiation from the earth. It is also permissible to treat many of the other parameters as a constant, independent of the solar radiant flux. For the sake of mathematical simplicity we shall consider first the case of a flat disc and that of a sphere, and extend the conclusions to a few other more general cases.

Let A be the surface area of the disc, and let the thickness of the disc be negligibly small compared to A. Let the disc be coated with an ideal black paint. Hence the surface is a perfect absorber and emitter, so that the radiant emittance is given by the Stefan - Boltzman law, equation (2) and all the solar energy incident on the surface is absorbed by it. If the exposed area is normal to the solar radiant flux, the energy absorbed is PA, where P is the solar radiant flux. The energy radiated by the body is

$$2 A \sigma (T^4 - T'^4)$$

where T is the temperature of disc and T' is the ambient temperature. Since T and T' are respectively of the order of 300° K and 4° K, T'^4 is about 10^{-7} times T^4, and is negligible in comparison to T^4. Let T be the equilibrium temperature. Since the heat absorbed is equal to the heat radiated,

$$2 A \sigma T^4 = PA ;$$

$$\text{i.e.,} \quad T^4 = \frac{1}{2\sigma} P. \tag{3}$$

Differentiating both sides,

$$4 T^3 dT = \frac{1}{2\sigma} dP. \tag{4}$$

Dividing equation (4) by equation (3),

$$dT/T = 1/4(dP/P). \tag{5}$$

Hence for a perfectly flat disc, the percentage error in the predicted value of equilibrium temperature, on the Kelvin scale, is one-fourth the percentage error in the assumed value of the solar constant.

It may readily be shown that equation (5) is independent of the geometrical shape of the body, and holds true for all cases of a perfectly black surface, with no internal heat sources or heat sinks.

If the body is spherical of radius R, the effective absorbing area is the area of cross-section πR^2, and is one-fourth the total emitting area. Hence equation (3) should be changed to $T^4 = (1/4\sigma)P$; the equation (5) is unchanged. For a cube having one of its six surfaces normal to the solar radiation, the equation of thermal balance corresponding to equation (3) is $T^4 = (1/6\sigma)P$. For a spinning body of arbitrary shape, the only term that needs modification is the area of the absorbing surface, which is the time average of the area of cross-section normal to incident radiation.

The above results may be illustrated by a few numerical examples. The Stefan - Boltzmann constant, σ, is 5.6693×10^{-5} erg cm^{-2} s^{-1} $(°K)^{-4}$, the solar constant, P, is assumed to be 0.1395×10^7 erg cm^{-2} s^{-1}. Substitution of these values in equation (3) gives the equilibrium temperature of a disc to be 331.1°K or 60.1°C. An increase of ten per cent in the assumed value of the solar constant would increase the predicted equilibrium temperature to 68.1°C, and a decrease of ten per cent would lower the predicted value to 51.4°C.

For a spherical body, the ratio of the absorbing area to the emitting area is half that of a flat disc, and the equilibrium temperatures are lower. The predicted values are 7°C, 13.4°C and -0.2°C respectively for assumed solar constant 0.1395, 0.1535 and 0.1256 watts cm^{-2}.

Actually the surfaces of satellites are not perfect absorbers or emitters, and hence it is necessary to introduce the expressions for absorptance and emissivity into the equations of thermal equilibrium. Both absorptance and

emissivity are to be distinguished as total and monochromatic. The relations between the different quantities can be best expressed by the following equations:

If $P'_\lambda \, d\lambda$ is the energy incident in the wavelength range λ to $\lambda + d\lambda$, the energy absorbed in the same range is $P'_\lambda \alpha_\lambda d\lambda$. (The prime indicates that the radiant flux has a spectral distribution different from that of a blackbody). The total energy absorbed is $\int_0^\infty P'_\lambda \alpha_\lambda d\lambda$, and the total incident energy is $\int_0^\infty P_\lambda \, d\lambda$. The ratio of the two integrals is the total absorptance α. The definition of the absorptance of a surface is thus necessarily with reference to a specific spectral distribution of the incident radiant flux. In particular, solar absorptance values differ according as one considers the absorptance at sea level or for zero air mass and according as one or another of the accepted solar spectral radiation functions is used for performing the integration. Solar absorptance is determined either by exposing specimens to sunlight and measuring the energy absorbed or by calculating the value from known functions of α_λ and P'_λ.

The radiant emittance from a non-blackbody surface is given in terms of that from a blackbody surface at the same temperature by the equation

$$W' = \int_0^\infty W'_\lambda \, d\lambda = \int_0^\infty \varepsilon_\lambda W_\lambda \, d\lambda = \varepsilon \int_0^\infty W_\lambda \, d\lambda = \varepsilon W. \tag{6}$$

ε and ε_λ are respectively the total emissivity and the spectral emissivity.

The equation for temperature equilibrium for a body which is not a perfect absorber or emitter is

$$\varepsilon A_\varepsilon \sigma T^4 = \alpha A_\alpha P'. \tag{7}$$

A_ε and A_α are respectively the areas of the emitting surface and the absorbing surface.

The equilibrium temperature depends not only on the ratio A_α / A_ε as discussed earlier, but also on the ratio α/ε. For numerical examples, we might consider two extreme cases of α/ε equals16 or 1/16. These numbers are respectively 2^4 and 2^{-4}. The corresponding equilibrium temperatures of a flat disc are respectively 666.2°K and 166.6°K. In actual cases α/ε does not vary over such wide ranges. For white paint, representative values are $\alpha = 0.22$; $\varepsilon = 0.88$; for evaporated gold, $\alpha = 0.07$; $\varepsilon = 0.02$. It is important to note that the temperatures with reference to which are measured the two ratios α and ε, are very different. The emissivity refers to the actual temperature of the satellite. The definition of α assumes the spectral energy distribution of a body at a relatively high temperature, 6000°K.

In so far as the calculation of α is dependent on the assumptions regarding the solar constant and the solar spectral radiant flux, the degree of error in these values causes a corresponding error in the predicted values of the equilibrium temperature. However, this is a second order effect since α is the ratio of the two integrals,

$$\int_0^\infty P'_\lambda \alpha_\lambda \, d\lambda \quad \text{and} \quad \int_0^\infty P'_\lambda \, d\lambda .$$

This becomes significant only in cases where α_λ is very highly wavelength dependent, as may well happen with specially prepared surfaces of very thin multilayer coatings. Reference may be made in this connection to the extensive studies made by the Armour Research Foundation (WADC Technical Report, May 1957) on solar absorptances at sea level and for zero air mass of a large number of standard aircraft materials. These data have been cited in a review of literature entitled "Thermal Radiation Properties Survey," by G. G. Gubareff, J. E. Janssen and R. H. Torborg, published in 1960 by Honeywell Research Center, Minneapolis, Minnesota[10]. Over 70 different types of surfaces have been examined, mostly metal surfaces with different grades of polishing, and a few surfaces of graphite and plastic laminate. The difference between α at sea level and α above the atmosphere is of the order of one or two per cent for surfaces having α greater than 0.4. Large percentage differences of 5 to 35 per cent occur in

cases where α is small, as for example copper, aluminum and magnesium alloys. For copper and magnesium alloys the absorptance at sea level is lower than that above the atmosphere and for aluminum it is higher. The uncertainities in our current knowledge of the solar spectral radiant flux are the greatest in the wavelength range below 3600 A, and unfortunately this is also the range where the spectral absorptance of most satellite coatings are highly wavelength dependent. As stated earlier the percentage error in the predicted temperature in degrees Kelvin is one fourth the corresponding percentage error in the assumed values of α or P. The errors are cumulative.

Given the large variety of the external shape and the surface coating of spacecraft, it is not possible to draw any more specific conclusions about the degree of error in predicted equilibrium temperatures. Those engaged in pre-launch testing in solar simulators and in theoretical computations of predicted temperatures should have at hand the values,as accurate as possible, of the solar constant and the solar spectral radiant flux. And more importantly they should have an estimate of the possible errors in the accepted values of these quantities.

3. Standard Scales of Radiation Measurement

One of the major problems in all measurement of energy is the standard scale with reference to which the energy measurements are reported. Internationally accepted standards exist for fundamental units like length and mass and for many of the derived units like ampere and volt. As for total radiant flux and spectral radiant flux, different countries use different standards, and intercomparisons between them show that they differ among each other by one or two per cent.

For the sake of clarity the question of a standard may be put thus: when can one say that a certain length is one meter, that a certain current is one ampere or that a certain radiant flux is one watt per cm^2? The answer about the meter

and the ampere are given unambiguously, with a high degree of accuracy, and is accepted by international commissions. The meter is defined in terms of a spectral line of krypton, and the ampere in terms of the amount of silver deposited by a standard cell. There is no such internationally accepted standard for energy.

A secondary standard of spectral radiant energy most widely used in the U.S. is the tungsten ribbon lamp operated at a specified current[11]. The calibration table supplied along with the lamp gives the spectral radiance of the incandescent ribbon at a large number of wavelengths. The physical quantity which is measured in the process of calibration is the color temperature of the ribbon at one or more wavelengths. The color temperature is determined with reference to a blackbody of known temperature. From known values of the emissivity of tungsten, transmission coefficient of the envelope of the lamp and blackbody radiation functions, it is possible to calculate the spectral radiance from the color temperature. Relatively large errors may be introduced into the calculations because of the poor accuracy with which the emissivity of tungsten and the color temperature are determined. The calibration tables of the tungsten standard ribbon lamps do not claim an accuracy better than 5 per cent. This may perhaps be a conservative estimate. No attempt has been made to establish an international standard for spectral radiance.

The situation is slightly better for total radiant flux[12]. The standard in this case is not a source of radiant flux but an instrument for measuring radiant flux. In other words, a standard scale of radiant flux is established giving the incident energy (in watts per cm^2) in terms of a more readily measurable physical quantity, temperature (in degrees C) or current (in amperes) generated in a given instrument. Most of this work of standardization has been done in connection with the measurement of solar energy, and the instrument is the pyrheliometer.

In meteorological institutes measurements of total radiant

flux are usually standardized with reference to one or the other of two standard scales. For the sake of brevity we shall refer to them as the Smithsonian scale and the Ångström scale. Both scales have been periodically revised and considerable work has been done in comparing them with each other and with other independent radiation scales. A brief description of the instruments and the standardization procedures will help clarify some of the confusion concerning radiation measurement and will show the degree of error in such measurement.

The Smithsonian scale is defined with the aid of the Abbot silver disc pyrheliometer. A silver disc is exposed to solar radiation and the rise in temperature of the disc is measured. To convert the temperature rise in °C to energy in watts per cm^2, a calorimeter is exposed to the same radiation and the heat absorbed by the calorimeter is determined. The Ångström scale is defined with the aid of the Ångström compensated strip pyrheliometer. One of two similar metallic strips is exposed to solar radiation and the other is heated by an electric current; the value of the current is adjusted until both the strips are at the same temperature. From known values of the resistance of the strip and the absorptance of its surface it is possible to establish a standard scale of radiant flux in watts cm^{-2} in terms of the current in amperes.

In 1932, the Smithsonian Institution introduced an improved form of calorimeter, and reexamined the accuracy of the scale which had been in use since 1913. The result of this study was that the Smithsonian announced that the measurements made on the 1913 scale had been 2.5% too high. This finding was confirmed by later measurements made in 1934, 1947 and 1952. However, the Smithsonian continued to standardize instruments in terms of the 1913 scale so as to preserve continuity.

The Ångström scale was originally established in 1905. It is based on two main types of instruments. For one type of instruments the original calibrations were made at Uppsala, Sweden, and now they are being made at Stockholm, Sweden; the source of energy is the sun and the conversion from current in amperes to energy in watts cm^{-2} is made from the

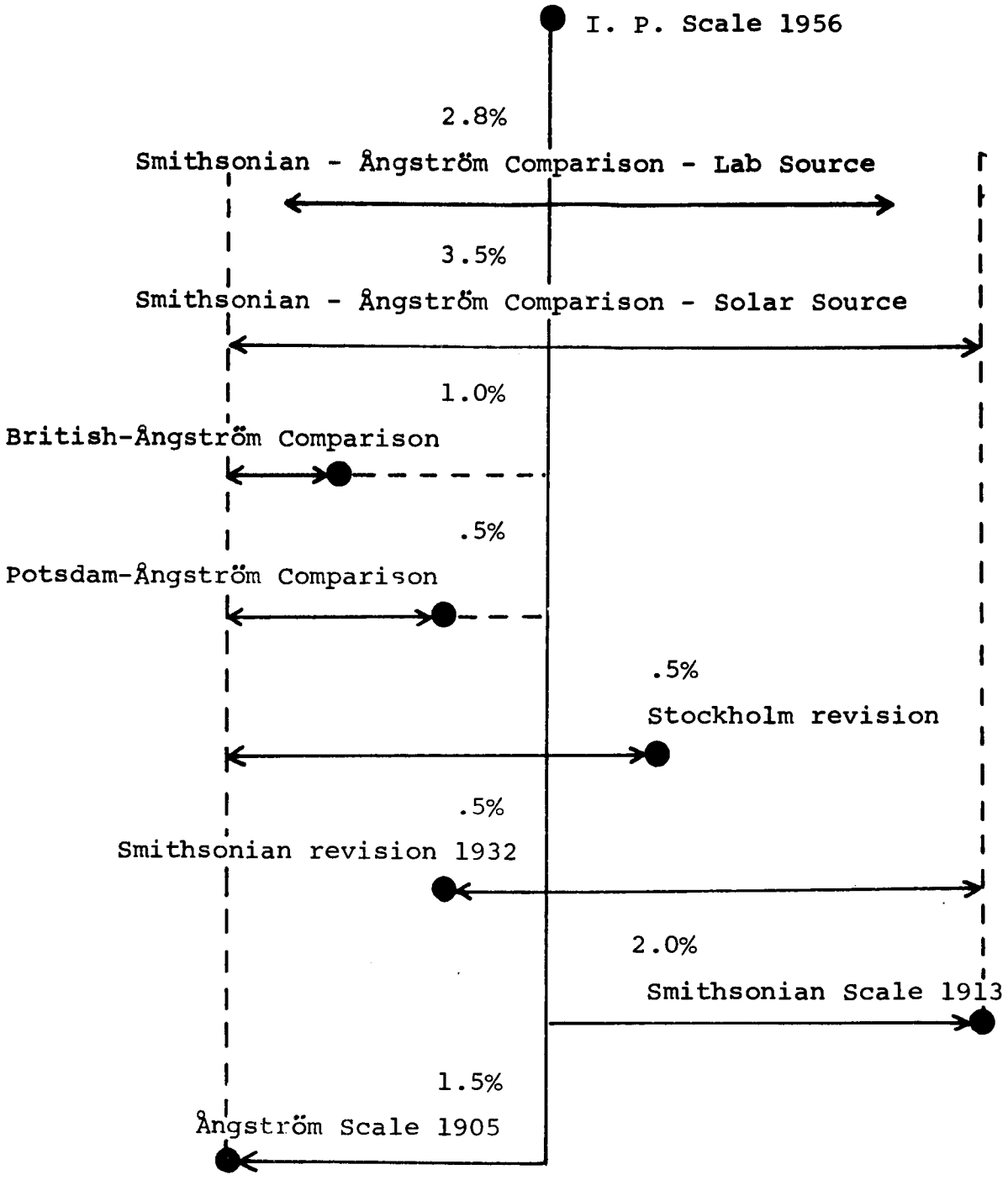
I. P. Scale 1956
2.8%
Smithsonian - Ångström Comparison - Lab Source
3.5%
Smithsonian - Ångström Comparison - Solar Source
1.0%
British-Ångström Comparison
.5%
Potsdam-Ångström Comparison
.5%
Stockholm revision
.5%
Smithsonian revision 1932
2.0%
Smithsonian Scale 1913
1.5%
Ångström Scale 1905

Each black dot represents a scale of radiation, and its relative distance to the right or to the left of the vertical line shows by what percentage the readings on that scale are higher or lower than the readings on the International Pyrheliometric (I. P.) scale 1956. By definition of the I. P. scale 1956, the Ångström 1905 scale is low by 1.5%, and the Smithsonian 1913 scale is high by 2.0%. The Smithsonian revision of 1932 makes the Smithsonian 1932 scale 0.5% lower than the I. P. scale 1956. The Stockholm revision makes the corrected Ångström scale 0.5% higher than the I. P. scale 1956. Both the British and German scales are lower than the I. P. scale 1956.

These relatively large differences between the different scales should be borne in mind when comparing the values of the solar constant given by different authors.

A question of special interest is: on what scale is based the Johnson value, 2.00 cal cm^{-2} min^{-1} of the solar constant? What Johnson attempted was a revision of the Smithsonian data. According to the Smithsonian, the solar constant, on the scale of 1913, is 1.981 cal cm^{-2} min^{-1}. But readings on this scale are too high. Aldrich and Hoover[4] stated in a paper in 1952 by how much the value should be lowered; the amount is 2.37 per cent, which is slightly less than the 2.5 per cent of the 1932 revision. It is this correction that Johnson accepted as a starting point: 1.981 (1 - 0.0237) = 1.934. Thus the Johnson value is based on a scale 0.37 per cent lower than the International Pyrheliometric Scale 1956.

III. REVIEW OF MAJOR CONTRIBUTIONS

1. Smithsonian Institution

The most extensive investigations on the solar constant and the spectral distribution of solar radiant flux are those made by the Smithsonian Institution of Washington, D. C. The work was started at the beginning of the century, and was continued for over fifty years.

The main steps of the Smithsonian procedure are shown in figure 1, which is adapted from Johnson[1] and Tousey[14]. There are two independent measuring instruments, one a pyrheliometer which measures the total energy without any spectral resolution, and the other, a spectrobolometer which measures on a relative scale the solar spectral radiant flux. The pyrheliometer reading is used for converting the relative values of the spectrobolometer to an absolute scale. But the two instruments do not have an identical wavelength range. The spectrobolometer is limited to the wavelength range 0.346 to 2.4 microns, whereas the pyrheliometer registers the energy of the entire spectrum as transmitted by the atmosphere. Hence one has to add to the integrated area under the curve given by the spectrobolometer a correction factor. The correction factor is equal to the area under the two ends of the curve of spectral radiant flux. With this correction factor the spectrobolometer curve is extended to the whole range of the pyrheliometer, and the area under the curve is equated to the pyrheliometric reading.

Thus the relative scale of the spectrobolometer is converted to an absolute scale and values of spectral radiant flux in watts cm^{-2} are available for the range 0.346 to 2.4 μ.

These values, however, refer to the solar energy received at the surface of the earth. The table of values thus obtained for different wavelengths are next extrapolated to zero air mass by comparing the data for different zenith angles. For large zenith angles the assumption that the optical air mass, m, is equal to the secant of the zenith angle does not hold good, and the modifications given by Bemporad[15] for the curvature of the atmosphere and refraction are to be applied.

The extrapolation to zero air mass gives the curve for spectral radiant flux in the range 0.346 to 2.4 μ outside the earth's atmosphere. The area under the curve is determined by integration. To the integrated value is added the zero air mass corrections, namely, the areas under the curve of solar spectral radiant flux in the ultraviolet range below

0.346 μ and in the infrared beyond 2.4 μ . The final result of this procedure is the solar constant.

The Smithsonian procedure has remained practically the same over the years, but the value of the solar constant has often been revised, partly due to improvements in methods of measurements and data reduction, and partly due to revision of the pyrheliometric scale.

2. Parry Moon's Analysis

A contribution of major importance in our current knowledge of the solar radiant flux was made by Parry Moon in 1940. Moon's main purpose was to propose standard solar radiation curves for engineering use. He attempted to collate and compare available data on questions such as variation of solar illumination with seasons of the year, hours of the day, latitude of location, height above sea level, etc. In doing so, he made a systematic study of the absorption effect of the atmosphere and the spectral distribution of radiant flux outside the atmosphere.

Parry Moon made a detailed analysis of the absorption effects of the atmosphere. The results are presented in a series of tables and graphs which it is not necessary to reproduce here. The main results are summarized in figure 2, reproduced from P. R. Gast, which gives four curves related to solar spectral radiant flux. The lowest curve which has a large number of sharp dips is the spectral radiant flux as observed by a ground - based instrument when viewing solar radiation at zenith angle zero, that is, when the path of sunlight is normal to the earth's surface.

The smoother curve shown above the experimentally observed curve is what the spectral distribution would be in the absence of the major molecular absorption effects of O_2, O_3, H_2O and CO_2.

The third curve is the solar spectral radiant flux for

air mass zero. This curve, however, is based not on Moon's computation, but on the later and more accurate revision of Smithsonian data given by Johnson. A fourth curve, the blackbody radiation curve for 6000°K, is shown for purposes of comparison.

Another major contribution by Moon was a comparison of the Smithsonian results with those of other independent observers. This is shown in figure 3. Smithsonian's best results are believed to be the weighted average of the measurements of 1920 - 22, which is shown in the figure by circles, and the circles are joined together by a short dash curve. Three other sets of Smithsonian data shown in the figure are from earlier periods: 1903 - 1910, 1903 - 1910 omitting quartz results, and 1916 - 1918. These results are compared with those from three other independent sources, Wilsing's measurements made at Potsdam[16], Pettit's measurements[17] and those of Fabry and Buisson[18]. The data of figure 5 are in arbitrary units, on a log-log scale, and hence the shape of the curves appears different from those of figure 2. The log scale for spectral radiant flux permits one to shift any set of points up or down to secure maximum agreement with all the other sets. The blackbody distribution shown in figure 3 by long dash curve is for 6000°K; this temperature was chosen because the maximum of the 6000°K blackbody distribution occurs at about the same wavelength as for the Smithsonian 1920 - 22 results. The standard curve which Moon proposed as the best fit after due weighting for all published results is shown by the heavy continuous curve.

Moon's proposed curve follows the data of Fabry and Buisson in the wavelength range below 0.32 μ and the data of Pettit for the range 0.32 μ to 0.40 μ. He considered these more reliable for the respective ranges. The Smithsonian values were apparently too high because of scattered light in the spectrograph. In the range 0.40 to 0.60 μ the Smithsonian results are in general agreement with other results. Moon's curve departs again from the Smithsonian results in the longer wavelength range. In the range 0.60 to 0.75 μ the Smithsonian values are lower than all the other values which are in close agreement.

For the range 0.50 to 1.0 μ the depression of the solar curve below the 6000°K blackbody curve is so well established experimentally that Moon felt there is no justification in following the Planckian curve in this range. In the infrared, beyond 1.25 μ up to 2.5 μ , the 6000°K Planckian curve seemed sufficiently close to all available experimental data other than the Smithsonian 1920 - 22 data. In the range beyond 2.5 μ experimental data are scarce. Water vapor and carbon dioxide have strong absorption bands in this range, so that the extrapolation of ground - based measurements to zero air mass is subject to large errors. Hence Moon suggested the 6000°K Planckian curve for the range beyond 1.25 μ .

The total area under the solar spectral distribution curve proposed by Parry Moon is 0.1322 watts cm^{-2} or 1.896 cal cm^{-2} min^{-1}. The value is based on the 1913 Smithsonian scale and hence must be increased by 2 per cent to agree with the International Pyrheliometric scale 1956. In order to compare Moon's results with the more widely accepted Johnson's results, all values on Moon's scale should be multiplied by 1.026, which is the ratio of Johnson's and Moon's values of the integrated solar radiant flux in the wavelength range of Moon's table, that is, for λ greater than 0.29 μ.

3. National Bureau of Standards, Stair and Johnston

Ralph Stair and Russell G. Johnston made in 1955, and in earlier years, a series of extensive measurements of the spectral radiant flux of the sun. They attempted to eliminate some of the major sources of error of the Smithsonian data. The authors observe that in the Smithsonian work the solar beam was reflected into a spectrobolometer by a metal coated mirror whose reflectivity was subject to change with age. The light is incident on the mirror at different angles, which introduces another factor of uncertainity in the reflection coefficient of the mirror. The solar image is focussed on the slit of the spectrograph, and hence the spectrograph views only a very small portion of the solar disc at a given time. Large and rather uncertain correction

factors are involved in attempting to calculate the energy of whole solar disc from such measurements.

Another source of error in the Smithsonian data is that a pyrheliometer is used to integrate the energy of the whole spectrum and to obtain the result in absolute units. This involves several assumptions based on inadequate observational data concerning the absorption of energy by the atmosphere and the spectral limits of the pyrheliometer.

Stair and Johnston adopted an experimental arrangement which eliminated automatically several of these sources of error. The apparatus was set up at a location where the effects of the atmospheric absorption were considerably less than at sea level in a densely populated city. The location chosen was Sunspot, New Mexico, at an altitude of 9200 feet. The spectrum was scanned by a Leiss double quartz prism spectrograph. It was mounted on the polar axis and driven across the sky. Hence the corrections for oblique incidence of light on heliostat mirrors could be eliminated. A specially designed amplifier circuit ensured a high degree of linearity of response. Tungsten ribbon standard lamps calibrated at the National Bureau of Standards were used to reduce the readings to absolute intensity values.

Measurements were made on four days, June 3, 4, 6, and 7, 1955, in the spectral range 0.3 to 0.54 microns. On four other days, June 16, 17, 18 and 19, measurements were made in the range 0.32 to 2.6 microns. The effect of atmospheric attenuation was determined by the conventional method of assuming that the pathlength through the atmosphere is proportional to the secant of the zenith angle. A complete discussion of the methods of data reduction are given in various publications of Stair and his coworkers[19,20, 21, 6].

The solar constant is calculated from the area under the spectral radiant flux curve for zero air mass. The experimental curve is for the actual sun-earth distance at the time of the measurement. In order to get the values of spectral radiant flux for the average sun-earth distance, the

observed values were multiplied by 1.0244. No data for the spectral radiant flux are experimentally available for the ultraviolet range below 0.3 μ or for the infrared range above 2.6 μ. For the ultraviolet, the curve is arbitrarily assumed to drop down to zero at about 0.2 or 0.22 μ. A correction factor of 0.06 calories per sq. cm. per minute is assumed to be the probable solar energy of wavelength beyond 2.5 μ, based on a blackbody curve at the solar temperature. With the addition of these correction factors, the value of the solar constant is 2.05 calories per sq. cm. per minute.

According to the authors this value is probably correct to less than 5 per cent, and "is in general agreement with recent estimates, being a little higher than those usually reported by the Smithsonian Institution." Johnson's value is 2.00 cal cm^{-2} min^{-1} which is only 2.5 per cent less than Stair's value, and hence well within the percentage accuracy claimed by Stair. The infrared correction of 0.06 cal cm^{-2} min^{-1} assumed by Stair is 2.93 per cent of the total, and is slightly below Johnson's estimate for this range, which is 0.065 cal cm^{-2} min^{-1} or 3.27 per cent of the total.

In their discussion of the data, Stair and Johnston stress the complicated nature of the steps involved in gathering and evaluating the measurements. There are numerous sources of uncertainty and error. Hence the accuracy cannot claim to be better than plus or minus a few per cent. They also observe that the results they obtained at Sunspot were slightly different from those they had reported earlier from their measurements at Climax[20] and at Sacramento Peak[21]. This is probably to be attributed to improvements in the experimental technique or may also be due to solar changes within the interval. Another important source of uncertainty which the authors have stressed is the radiometric standard. The values currently adopted for the spectral emissivity of tungsten are subject to revision, and such revision, if later found necessary, will alter the values of the solar constant and the solar spectral radiant flux.

4. Naval Research Laboratory, Dunkelman and Scolnik

Another set of measurements which should be reviewed in

some detail were made by Dunkelman and Scolnik. These measurements were made in 1951, but were not reported in detail until eight years later in 1959[2]. The conventional method used by Stair, Moon and earlier workers was adopted to extrapolate from ground-based measurements to zero air mass. The observation station was situated on the top of a flat rock, at an elevation of 8025 feet, on Mount Lemmon, near Tucson, Arizona. But it was a real disappointment to the observers that the sky about Mt. Lemmon was overcast with clouds during most of the period, September 20 to October 17, 1951, which they spent on the mountain top. Useable data were obtained only on one day, October 4. On that day a total of 25 spectral scans were made at different times from early morning till late in the evening.

The spectrum was produced and the energy scanned by means of a Leiss quartz double monochromater, detected by a 1 P 21 photomultiplier tube, amplified and presented on a strip chart recorder. The wavelength covered was from 0.303 to 0.700 μ, the only range where the 1 P 21 detector is sufficiently sensitive. In this small range, wavelength-wise, only 8 per cent of the entire range of 0 to 5 μ of the solar spectrum is contained about 40 per cent of the total solar energy. The purpose of the observers was not to chart the entire spectrum or to evaluate the solar constant, but to provide a calibration standard whereby the relative measurements of the rocket data collected by the Naval Research Laboratory in the little known ultraviolet range could be reduced to absolute values of radiant energy.

The equipment was calibrated frequently by using the spectrum of the tungsten lamp. The tungsten lamp which operated at a temperature of 2800°K had previously been calibrated at the National Bureau of Standards with reference to a blackbody, in accordance with the Bureau's well established procedure. There is no reason to doubt the N. B. S. calibration technique, and it was decidedly the best available at that time. However, it should be noted that the N. B. S. does not claim an accuracy better than 5 per cent for its calibration table. The method which was used in 1951 involved a series of difficult calculations from the color temperature to the true temperature, and thence through blackbody radiation functions and spectral emissivity curves of tungsten to the spectral radiance of the

tungsten ribbon as viewed through a quartz window. This method has since been replaced, and the present calibration tables give the spectral radiance at selected wavelengths for a specified current.

The block diagram of the apparatus used by Dunkelman and Scolnik is reproduced in figure 4 from their original paper[2]. Light from the sun or from the standard source, L, is introduced into the Leiss double monochromator from the magnesium carbonate block C. The lamp current and the voltage are monitored continuously by means of the voltmeter V and ammeter A, and adjusted when necessary by a variac VA. The mirror M_L is interposed in the path of the beam from the siderostat when a calibration run is to be made. The signals from the photomultiplier PM are amplified by a D. C. amplifier and recorded on a stripchart recorder. A bucking box B serves to subtract the dark current.

A major contribution of Dunkelman and Scolnik was the detailed comparative study they made of the data obtained by different observers. The results of this study are presented in figures 5 and 6, also reproduced here from their original paper.

In figure 5 are given the better known measurements of the entire solar disc made prior to 1949. The Smithsonian data[22,23] are usually shown in relative units only, though they are basically absolute. Pettit[24] normalized his spectral solar radiance data to agree with those of the Smithsonian at 0.45 μ. In figure 5 both the Smithsonian and Pettit's curves have been readjusted downwards to make them conform to the new absolute energy values for the solar spectrum given in the Ninth Revised Edition of the Smithsonian Physical Tables[25]. The short curve for the range 0.3 to 0.33 μ is based on Stair's absolute measurements of 1947[26]. The data of Hess[27], Reiner[28], and Gotz and Schonmann[29] were published only on a relative scale. Dunkelman and Scolnik normalized these curves against Pettit's at 0.4725 μ in order to make a meaningful comparison. The large differences in the wavelength range below 0.4 μ are probably due to stray light in the spectrograph, uncertainties in the calibration of the tungsten standard, and errors in the extrapolation to zero air mass in a wavelength range of high absorption.

In figure 6 is shown a comparison of Dunkelman and

Scolnik's measurements with more recent data, those of Pettit and of Stair and Johnston. The curves are based on integrated energy values and do not show the fine details of figure 5. Stair and Johnston's curve agrees closely with that of Dunkelman and Scolnik in the wavelength range below 0.5 μ, whereas Pettit's values are lower by about 25 per cent. In the range above 0.5 μ, the results of Stair and Johnston are high, whereas those of Dunkelman and Scolnik and of Pettit are in fairly close agreement. Solar spectral radiant flux at 0.6 is 1.81 $\mu w\ cm^{-2}\ A^{-1}$ according to Dunkelman and Scolnik and 1.963 $\mu w\ cm^{-2}\ A^{-1}$ according to Stair and Johnston. Francis Johnson had concluded that the original scale of Dunkelman and Scolnik had to be raised by 9 per cent in order to conform to the Smithsonian data and the NRL rocket data. The value 1.81 is on this raised scale. The value on the original scale is 1.66 $\mu w\ cm^{-2}\ A^{-1}$ which is different from Stair's value by 18.2 per cent. This large difference occurs in a wavelength range which might be considered the most favorable for accurate solar measurement, a range where the solar energy is high, atmospheric absorption is low, detectors are highly sensitive and the tungsten standard is sufficiently strong. Concerning this difference, however, Dunkelman and Scolnik[2] make the following observation: "The results of Stair between 5000 and 7000 A are high, and are not in agreement with any previous work including his own earlier measurements. Furthermore they lead to a value of extra-terrestrial illuminance that is higher than recent measurement of Karandikar[30], and most previous solar illuminance measurements."

5. Revision of Smithsonian data by Francis S. Johnson

Francis S. Johnson and his co-workersat the Naval Research Laboratory undertook a major revision of the solar constant and of the solar spectral radiant flux. This work was stimulated by the new measurements in the range 0.22 to 0.34 μ made by rocket-borne spectrographs[31,32] and by the Mount Lemmon data of Dunkelman and Scolnik. Johnson's discussion of this revision was reported in 1954 in the Journal of Meteorology[1]. In 1957 an abridged report was published by R. Tousey in Nuovo cimento[14]. Johnson's revision started from the measurements which had been made for over half a century by the Smithsonian Institution. A

number of corrections are involved in deriving the solar constant from the Smithsonian data, and Johnson attempted to reevaluate these corrections with the aid of the more recent NRL data.

The starting point for Johnson's revision was the Smithsonian value 1.934 cal cm^{-2} min^{-1}, which is on the so-called "true" scale. Subtracting from this the Smithsonian zero air mass correction of 0.061 in the UV below 0.346 μ and 0.038 in the IR above 2.4 μ, Johnson obtained 1.835 cal cm^{-2} min^{-1} as the radiant flux for zero air mass in the range 0.346 to 2.4 μ. To this value Johnson added three correction factors, 0.006 an increase due to the revised UV spectrobolometer correction based on Mt. Lemmon data, 0.085 the revised UV zero air mass correction based on NRL rocket data and Mt. Lemmon data, and 0.076 the revised IR zero air mass correction based on the assumption that in the IR from 2.4 to at least 14 μ, the solar spectral radiant flux for zero air mass is that of a 6000°K blackbody. This assumption had been made earlier by P. Moon, and was apparently justified by the work by A. Adel[33,34] and R. Peyturaux[35]. These three corrections when added to 1.835 cal cm^{-2} min^{-1} yield the final value of the solar constant 2.002 cal cm^{-2} min^{-1}. Tousey[14] observes: "We prefer to call it 2.00 since we feel that the probable error may be of the order of ± 2 per cent." Thus we have the value most frequently cited in literature, 2.00 cal cm^{-2} min^{-1}, and referred to as the NRL value or the Johnson value.

Johnson's revision of the Smithsonian data also yielded a new table for the solar spectral radiant flux. The starting point is a curve of the spectral radiant flux on a relative scale, the same as for the solar constant. This curve is based on three sources which Johnson considered the most reliable, the NRL rocket data for wavelengths shorter than 0.318 μ, the Mount Lemmon data for the range 0.318 to 0.60 μ and Parry Moon's results for the wavelength range beyond 0.60 μ. The normalization procedure for converting the relative scale to an absolute scale is based on the reevaluation of the spectrobolograms corrections and the zero air mass corrections. Johnson[1] has discussed in detail the steps involved in the procedure.

Johnson's data on solar spectral radiant flux is given in table I. It is reproduced from a more recent publication edited by Johnson, Satellite Environment Handbook[36]. The same data are also presented in figure 7, which shows some of the finer details which are usually omitted in reproductions of the Johnson curve. Figure 7 is a reduced photograph of a drawing made on large scale graph paper of all the data points of table 7.

IV. CONCLUSION

In view of the discussions in the previous sections, it would seem highly desirable that a new attempt be made to obtain more accurate and complete experimental data on the solar constant and the spectral distribution of the solar radiant flux. Johnson's work was mainly one of revision, and the experimental data for the revision had been obtained many years earlier by the Smithsonian Institution. The observations of Dunkelman and Scolnik were made on one single day, and were limited to the visible portion of the spectrum. The data of Stair and Johnston were averaged over eight days, but the authors themselves emphasize the large uncertainties inherent in the method.

The task of accumulating new experimental data with a degree of accuracy considerably superior to that of currently available data, will necessarily be a huge one. The justification for attempting such a task lies mainly in the importance of the solar constant in many areas of physics and engineering. The thermal balance of the earth depends on the energy from the sun. The attenuation characteristics of the atmosphere remain uncertain because the energy received above the atmosphere is uncertain. The solar radiant flux is an important parameter in most problems of astrophysics and solar physics. It is indeed a disturbing situation that so important a physical constant has an uncertainty of a few parts in a hundred, when standard tables of the physical constant, such as the velocity of light, electron charge, Planck's constant, etc., quote the values with an accuracy of one part in a million or a billion.

The uncertainty in the solar constant and the solar spectral radiant flux has serious consequences for solar

simulation and the thermal balance of spacecraft. This aspect of the question has a special interest for those engaged in building and testing satellites, since one of the more accurate methods of improving upon current data is to make measurements from above the atmosphere by satellite-borne instruments. The information which the satellites need for ensuring their operational stability can best be obtained by the satellites themselves. We have discussed earlier to what extent errors in the solar constant and the solar spectral radiant flux would effect the equilibrium temperature of spacecraft. A vast amount of effort is now being made in building and maintaining solar simulators for pre-launch testing of satellites and space probes. The operational assumption in such testing is that if the satellite fails to maintain the required thermal balance under the simulated conditions it will also fail to do so under actual conditions. High energy radiant sources, as for example, the carbon arc or the mercury-xenon arc, illuminate the test floor with energy which matches, as far as practicable, the energy of the sun both in spectral distribution and in total energy. It is obviously impossible to simulate accurately something unknown or uncertain. However, it should be pointed out that at the present time the degree of error in our knowledge of the solar energy is not the only obstacle or the major obstacle for adequate solar simulation. The margin of tolerance permitted or realistically attainable with high energy solar simulator sources is larger than the assumed margin of error in the published values of the solar constant and the spectral distribution of solar radiant flux. However, as efforts are being made to improve the energy output and the spectral characteristics of solar simulators, a parallel effort should be made to ascertain more accurately what one is trying to simulate. The large uncertainties in the ultraviolet region, referred to by P. R. Gast, may also have unpredictable effects on the rapid deterioration of certain surface materials.

R. Tousey[14] concluded his discussion of the NRL revision of the solar constant with this remark: "I feel that new work on the solar constant is in order, but it will not be easy to improve on the accuracy attained by the Smithsonian. Attempts to make measurements directly from rockets have been made, but not yet with completely satisfactory results. The values obtained were of the order of 2.0 however. Measurements

from the ground could now be made with increased accuracy due to the present day availability of many new radiation measuring techniques. To do this will require a long series of painstaking measurements, preferably, from two independent stations located at widely separated points on the earth."

Tousey's observations were made in 1957 at the threshold of the satellite age. The intervening years have witnessed a rapid progress in satellite technology. Satellites of the near future give promise of larger and bolder experiments.

The severe limitations which existed in earlier years on the size and mass of the experimental package and on the available supply of power are now being removed. The obvious advantage of a satellite experiment to measure the solar spectral radiant flux is that the spectrograph is outside the earth's atmosphere and that the difficult and highly doubtful corrections for atmospheric absorption are unnecessary. Measurements can be made over a prolonged period of time, and many repeated values can be taken so as to average out all random experimental errors.

However, every precaution should be taken to forestall systematic errors which might wholly vitiate the results. The measurements of the Smithsonian, N.B.S. and N.R.L. were made by experienced observers who always had ready access to the apparatus and could make readjustments whenever necessary. A completely automated experimental package presents problems of a different order of magnitude. But the solutions to these problems are within reach for present day satellite technology.

A quartz double prism monochromator might well be the main unit in the experimental package. More than one energy sensing device will be needed to cover completely all ranges of wavelength. Some form of 'on-board' calibration, as for example, with a secondary standard of spectral radiance, will be necessary. Adequate shielding should be provided for stray radiation from the earth or from the body of the satellite itself; or these will have to be corrected for. The satellite should have the attitude control for pointing constantly to the sun, and the optical system should be such as to view the whole solar disc.

A total energy sensor might well be needed as an auxiliary piece of apparatus. R. Hanel[37] and his co-workers have suggested a compact unit of this type, and the original design is now being improved upon. Readings of the total energy sensor would provide an additional means of calibration, in the same manner as the Smithsonian pyrheliometer was used to convert the relative scale of the spectrobolometer to an absolute scale.

Due attention will have to be paid also to small percentages of energy in the ultraviolet and the infrared wavelength ranges where the quartz prism is an effective absorber. The N.R.L. rocket-borne spectrographs and the albedo measuring devices of the Tiros satellites provide many helpful suggestions for mapping accurately these relatively inaccessible regions of the spectrum.

The prism spectrograph with the auxiliary units for calibration provides one method of approach and perhaps the best. A slightly different method is to employ a series of narrow-band-pass filters. Many different types of filters are commercially available. The relative ruggedness and simplicity of an experimental package with a series of filters and a thermopile might more than compensate for the lack of detailed spectral resolution. But considerable research still needs to be done on the stability of the transmission characteristics of the filters and on the method for obtaining a curve for the spectral radiant flux from the energy transmitted by the filters.

Richard Tousey[14] justly pointed out the desirability of more ground-based measurements, since new radiation measuring techniques are now available. He also said that measurements should preferably be made from widely separated points on the earth. More ground-based measurements are undoubtedly of great value. One objection to ground-based measurements is that they would tell us more about the characteristics of the atmosphere than about the solar radiant flux. Abundant data about the upper atmosphere and about the earth albedo are now available from satellite experiments. These data might well serve for a more reliable extrapolation to zero air mass than was previously possible. The problem of extrapolation can be considerably

reduced if the measurements are made not from a mountain top but from a high flying aircraft such as the X-15, A-11 or U-2, or from a balloon. These provide an alternate approach to the satellite experiment.

A major problem in all absolute measurement of energy is the standard of spectral radiance and total radiant flux. Data of any degree of accuracy which are cited in literature, whether of Smithsonian, N.R.L. or N.B.S., refer ultimately to the spectral radiance standards of the N.B.S., or to the Smithsonian pyrheliometer. There is no complete agreement between different countries and different national laboratories concerning the standard of energy. If a determined and massive effort is made to reevaluate the solar constant and the solar spectral radiant flux, an essential part of that effort will be to define an internationally acceptable standard of energy.

V. ACKNOWLEDGMENTS

This study was prompted partly by a conference on Solar Simulation Research and Technology, held on February 27-28, 1963, at the Headquarters of the National Aeronautics and Space Administration, Washington, D. C. Several of the panelists raised questions regarding the reliability and degree of accuracy of our current knowledge of the solar constant and of the solar spectral radiant flux which the space environment simulators are trying to match. The author wishes to thank the members of the panel and in particular Conrad P. Mook of the Office of Advanced Research and Technology, NASA, the moderator of the Conference, for several helpful suggestions. The author is particularly indebted to Dwight C. Kennard, Technical Assistant for Advanced Research and Technology, Test and Evaluation Division, Goddard Space Flight Center, NASA. His keen interest in this study, the constant encouragement and many helpful discussions, and the items of information which he gathered from different sources about the feasibility of further measurements were a major factor towards the completion of this work. Thanks are due to two other members of the T&E Division, GSFC, Elias Klein, Director of the Summer Workshop, and Henry Maurer, Jr., Head, Thermodynamics Branch. Brief discussions which the author had with Richard Tousey, Ralph Stair and Lawrence Dunkelman proved highly beneficial; all three have made rich contributions to this field; their help is gratefully acknowledged.

REFERENCES

1. F. S. Johnson, "The Solar Constant", J. Meteor. 11, 431(1954).

2. L. Dunkelman and R. Scolnik, "Solar Spectral Irradiance and Vertical Atmospheric Attenuation in the Visible and Ultraviolet", J. Opt. Soc. Am. 49, 356(1959).

3. P. Moon, "Proposed Standard Solar Radiation Curves for Engineering Use", J. Franklin Institute, 230, 583(1940).

4. L. B. Aldrich and W. H. Hoover, "The Solar Constant", Science, 116, 3(1952).

5. C. W. Allen, Astrophysical Quantities, University of London, London (1955).

6. R. Stair and R. G. Johnston, "Preliminary Spectroradiometric Measurements of the Solar Constant", J. Research Natl. Bur. Standards, 57, 205(1956).

7. P. R. Gast, in Handbook of Geophysics, Chapter 16-3, "Solar Radiation" Pp. 16-14 to 16-30,(McMillan Co., New York, 1960).

8. R. J. Stair , R. G. Johnston, and T. C. Bagg, "Spectral Distribution of Energy from the Sun", J. Research Natl. Bur. Standards 53, 113(1954).

9. "Nomenclature for Radiometry and Photometry", J. Opt. Soc. Am., 43, 809(1953).

10. G. G. Gubareff, J. E. Janssen, and R. H. Torborg, Thermal Radiation Properties Survey, (Honeywell Research Center, Minneapolis-Honeywell Regulator Company, Minneapolis, Minn. 1960) p. 254.

11. R. G. Stair, R. G. Johnston and E. W. Halbach, "Standard of Spectral Radiance for the Region 0.25 to 2.6 Microns", J. Research Natl. Bur. Standards, 64A, 4, 291(1960).

12. IGY Instruction Manual, Part VI, Radiation Instruments and Measurements, (Pergamon Press, London 1957) P. 378. A. J. Drummond, "The International Scale of Radiation", W. M. O. Bull, 5, 19(1956). A. J. Drummond, "A Contribution to Absolute Pyrheliometry", Quarterly J. R. Met. Soc. 82, 481 (1956).

13. F. Lindholm, "On the Ångström Absolute Pyrheliometric Scale", Tellus, 10, 249(1958).

14. R. Tousey, "The Solar Constant", Nuovo cimento 6, X, 413(1957).

15. Smithsonian Physical Tables, Ninth Revised Edition (1954), Table No. 811.

16. J. Wilsing, "Uber die Helligkeitsverteilung im Sonnenspecktrum nach bolometrichen Messungen", Astrop. Obs. Potsdam, Publikationen, 32, No. 72, 91(1917).

17. E. Pettit, "Measurements of Ultraviolet Solar Radiation", Astrosphys. J. 75, 185(1932).

18. C. Fabry and H. Buisson, "A Study of the Ultraviolet End of the Solar Spectrum", Astrophys. J. 54, 297(1921).

19. R. Stair, "Ultraviolet Spectral Distribution of Radiant Energy from the Sun", J. Research Natl. Bur. Standards, 46, 353(1951).

20. R. Stair, "Ultraviolet Radiant Energy from the Sun Observed at 11,190 Feet", J. Research Natl. Bur. Standards, 49, 227(1952).

21. R. Stair, R. G. Johnston, and T. C. Bagg, "Spectral Distribution of Energy from the Sun", J. Research Natl. Bur. Standards 53, 113(1954).

22. C. G. Abbot, F. E. Fowle, and L. B. Aldrich, "The Distribution of Energy in the Spectra of the Sun and the Stars", Smithsonian Misc. Coll. 74, No. 7, 15(1923).

23. C. G. Abbot, Gerlands Beitr. Geophys. 16, 4, 343(1927).

24. E. Pettit, "Spectral Energy-Curve of the Sun in the Ultraviolet", Astrophys. J. 91, 159(1940).

25. W. E. Forsythe, Ed. "Absolute Energy Values for Solar Spectrum", Smithsonian Physical Tables, Ninth Revised Edition (1954) Table No. 812.

26. R. J. Stair, Research Natl, Bur. Standards, 40, 9(1948).

27. P. Hess, "Untersuchungen uber die spectrale energieverteilung im sonnenspektrum von 350 mμ bis 500 mμ, "Inaugural-Dissertation", Universität Frankfurt a.M. (1938).

28. H. Reiner, Gerlands Betr. Geophys. 55, 2, 234(1939).

29. F. W. P. Gotz and E. Schonmann, Helv. Phys. Acta. 21, 151(1948).

30. R. V. Karandikar, J. Opt. Soc. Am. 45, 483(1955).

31. Johnson, Purcell, Tousey and Wilson, Rocket Exploration of the Upper Atmosphere (Pergamon Press, London, 1954) Pp. 279-288.

32. Wilson, Tousey, Purcell, Johnson and Moore, Astrophys. J. 119, 590(1954).

33. A.Adel, "Atmospheric Absorption of Infrared Solar Radiation at the Lowell Observatory", Astrophys. J. 89, 1(1939).

34. A. Adel, "An Estimate of Transparency of the Atmospheric Window 16 to 24", J. Opt. Soc. Am. 37, 769(1947).

35. R. Peyturaux, "Contribution a l'étude du fond continu du spectre solaire dans la proche infra-rouge", Ann. Astrosphys. 15, 302(1952).

36. F. S. Johnson, (Editor) Satellite Environment Handbook (Stanford University Press, Stanford, Cal. 1961) P.79.

37. R. A. Hanel, "An Instrument to Measure the Solar Constant from a Satellite", National Aeronautics and Space Administration, Washington, D. C. TN D-674, April 1961.

CAPTIONS FOR FIGURES

1. Flow Chart of Smithsonian Procedure
2. Curves Related to Solar Energy
3. Parry Moon's Curve
4. Block Diagram of Apparatus
5. Data Prior to 1949
6. Data of NRL, Pettit and Stair
7. The Johnson Curve

CAPTION FOR TABLES

I. Johnson's Data on Solar Spectral Radiant Flux

CONTENTS

FIGURE I

FLOW CHART OF SMITHSONIAN PROCEDURE

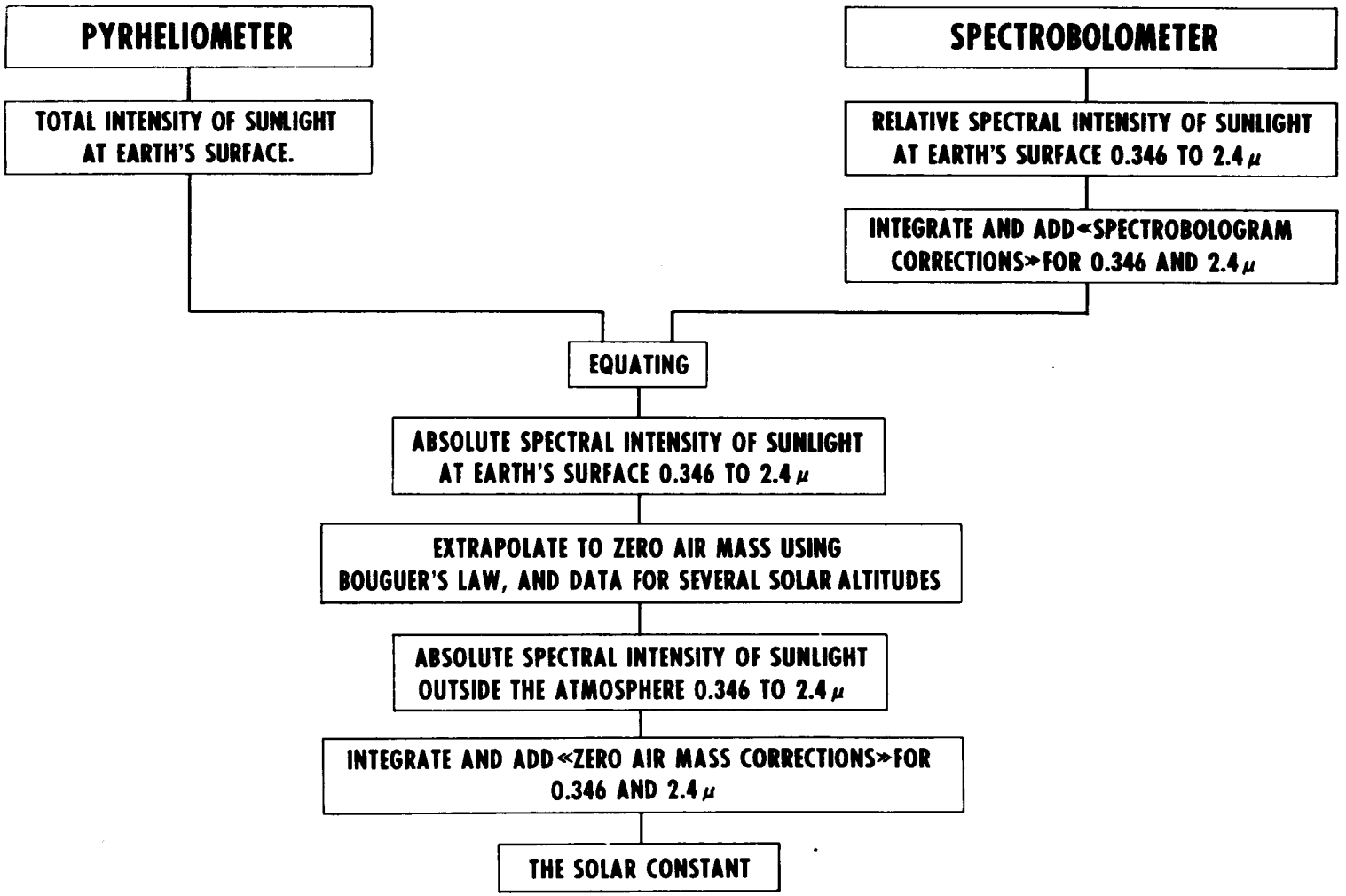

FIGURE 2

CURVES RELATED TO SOLAR ENERGY

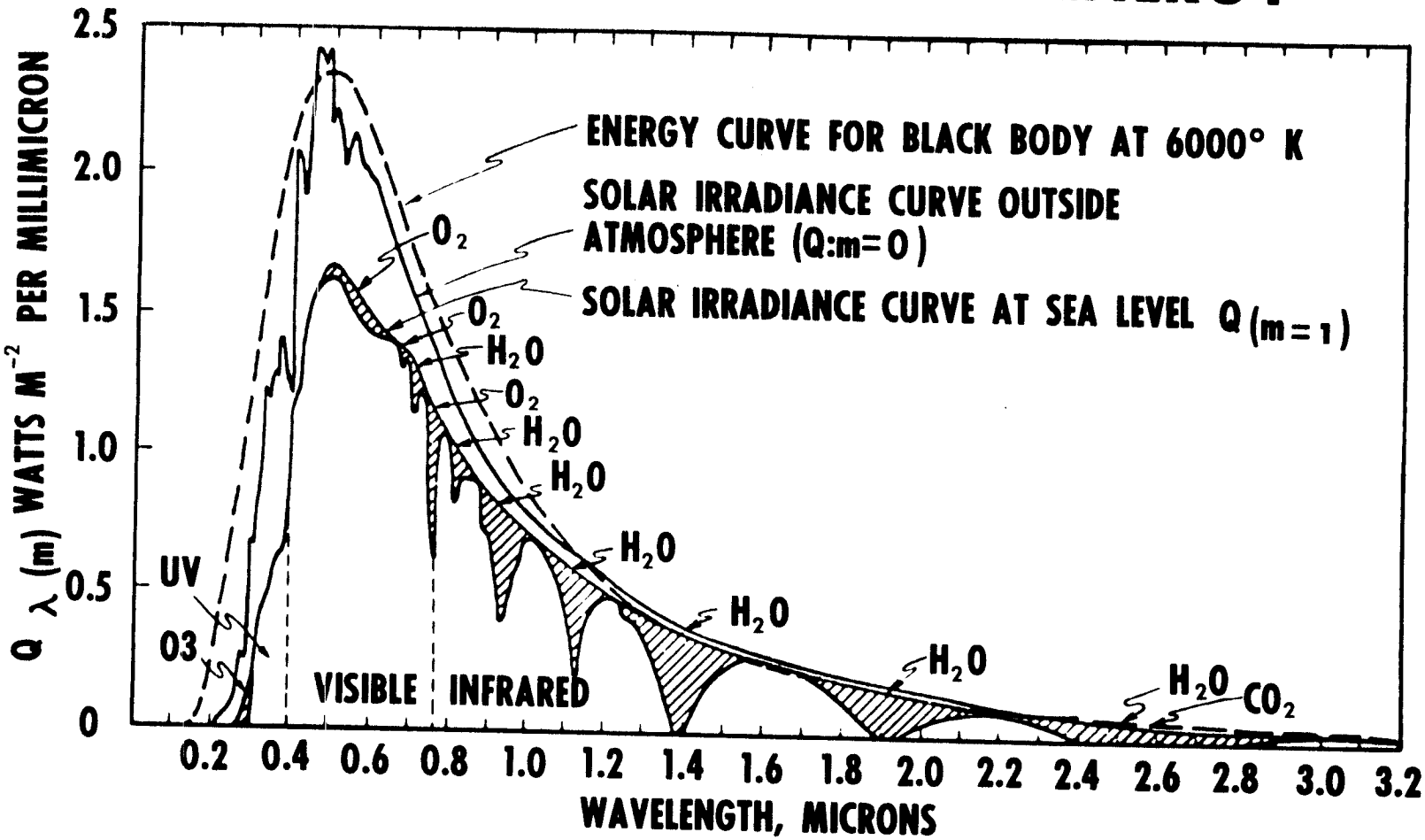

FIGURE 3
PARRY MOON'S CURVE

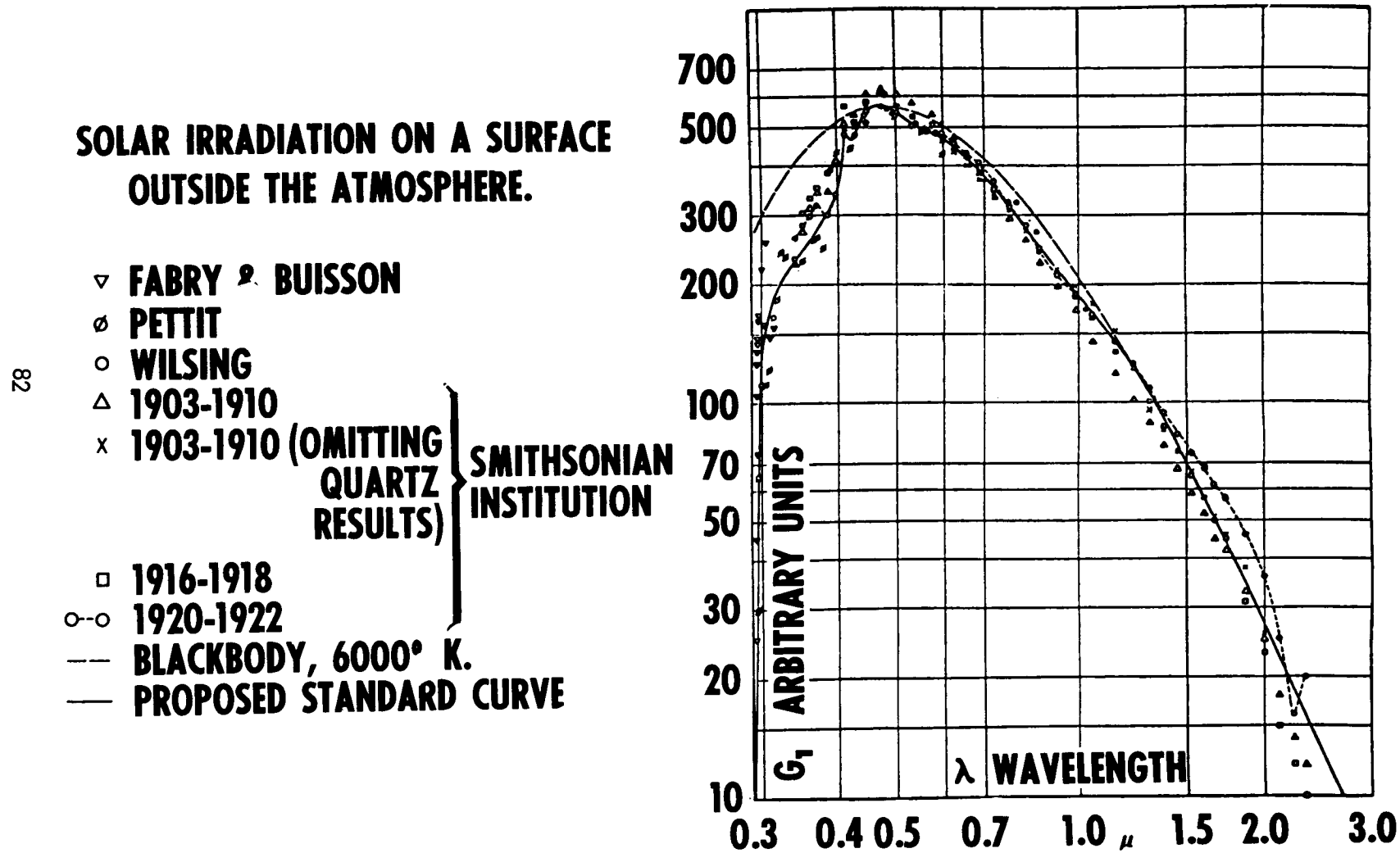

FIGURE 4

BLOCK DIAGRAM OF APPARATUS

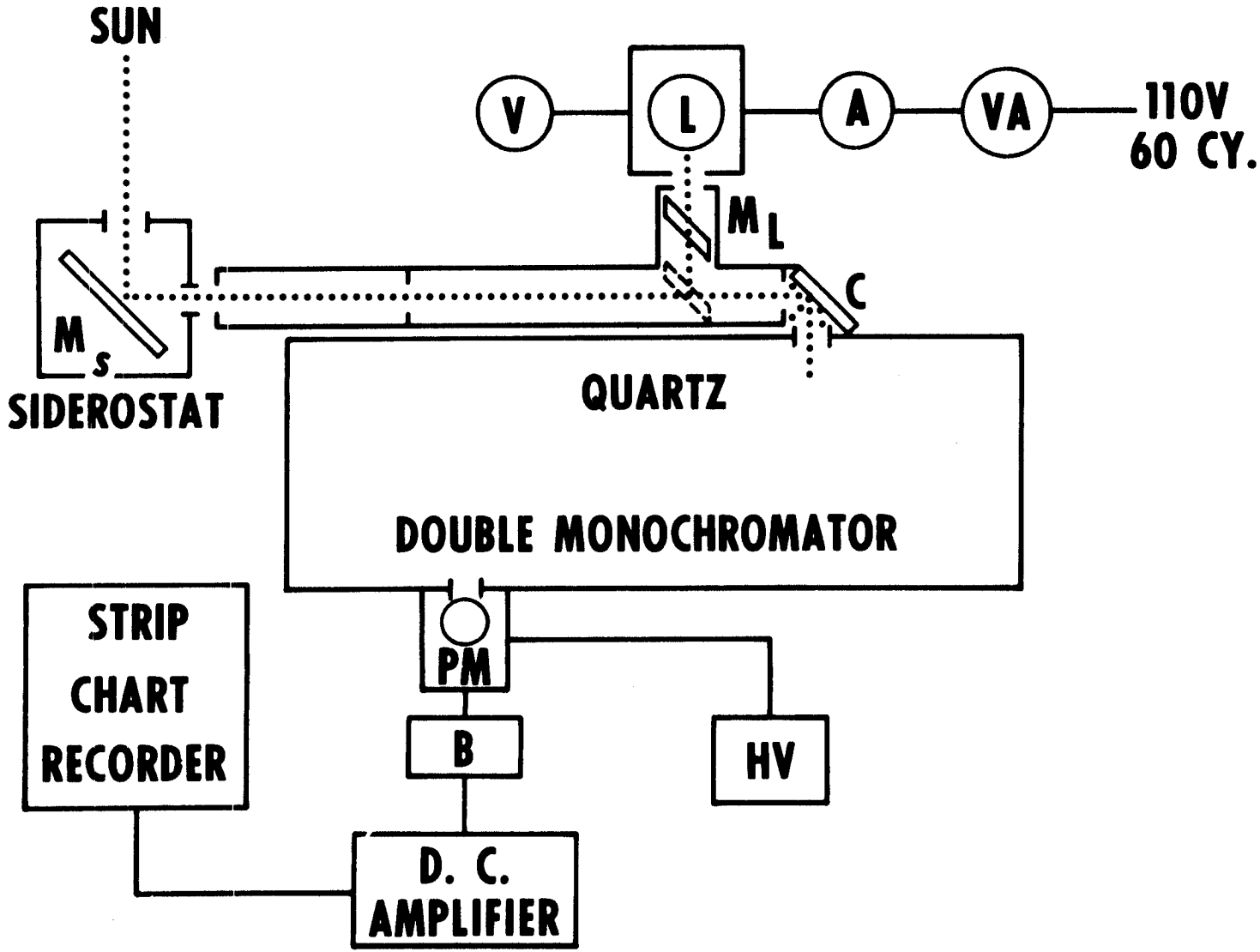

FIGURE 5

DATA PRIOR TO 1949

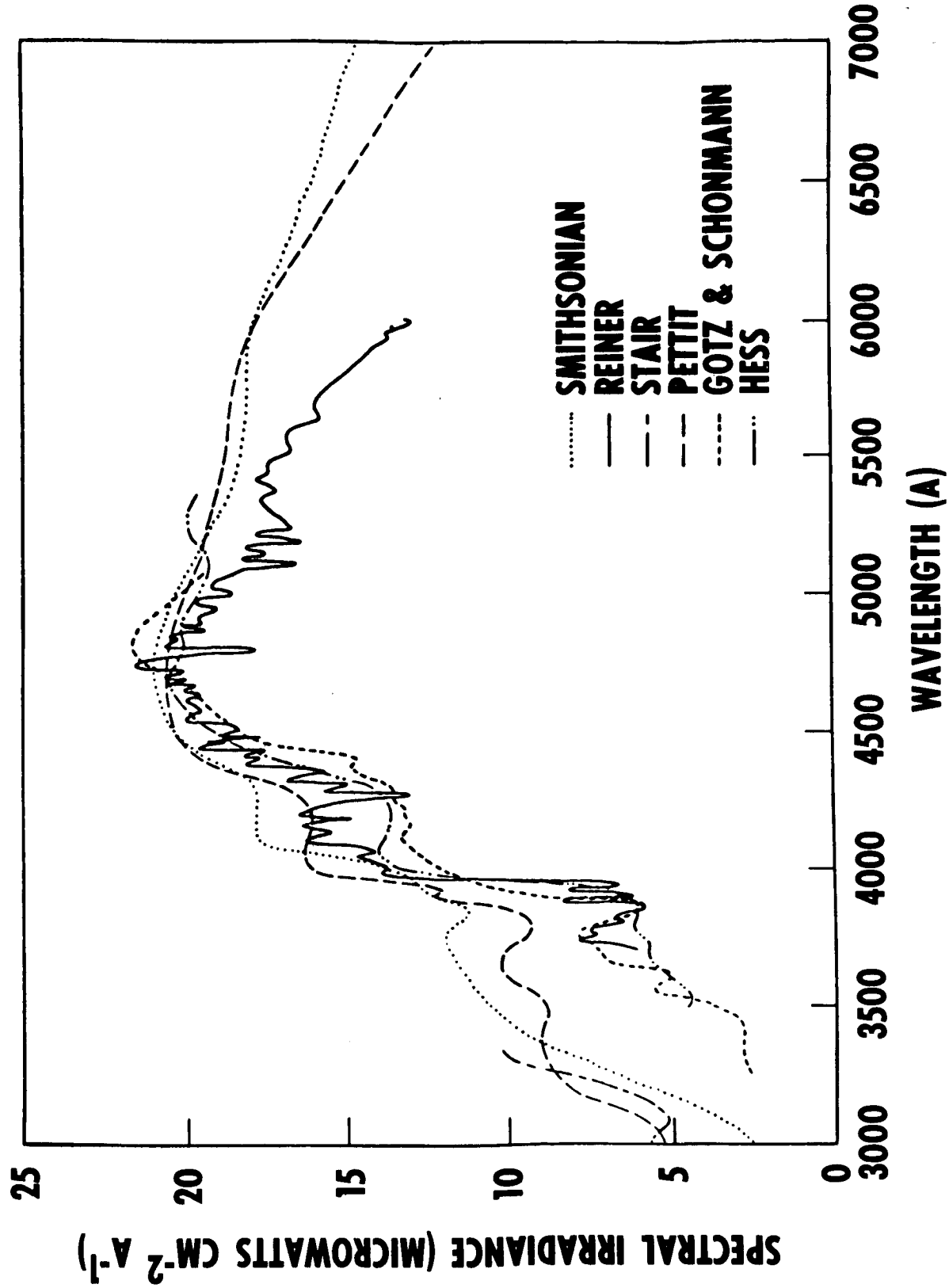

FIGURE 6

DATA OF NRL PETTIT AND STAIR

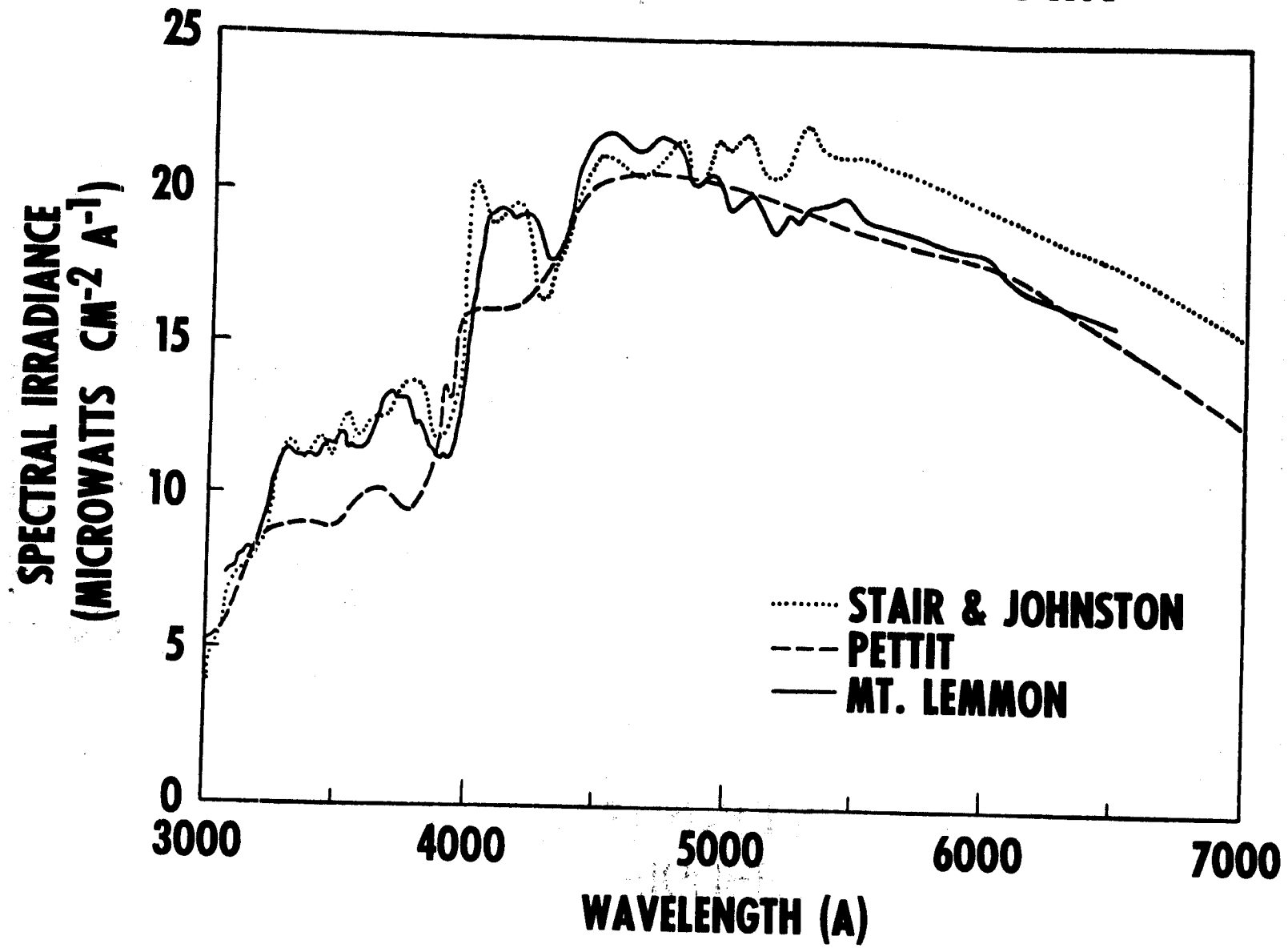

FIGURE 7

THE JOHNSON CURVE

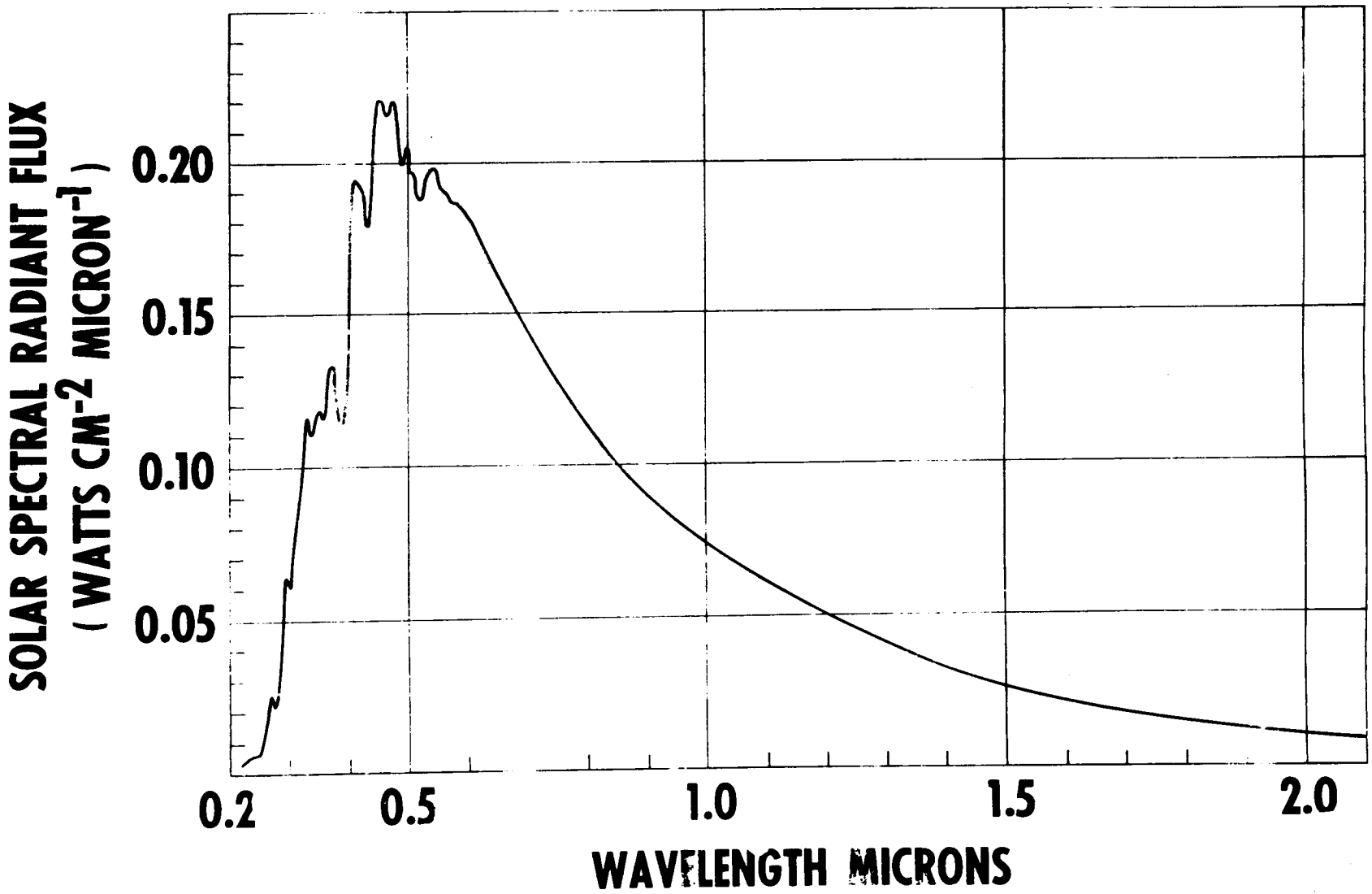

Table I. Johnson's data on solar spectral radiant flux (denoted by P_λ) for air mass zero
λ in microns; P_λ in watts cm^{-2} μ^{-1}. Third column is the cumulative percentage of energy.

λ (μ)	P_λ (w/cm²μ)	cum. (%)	λ (μ)	P_λ (w/cm²μ)	cum. (%)	λ (μ)	P_λ (w/cm²μ)	cum. (%)	λ (μ)	P_λ (w/cm²μ)	cum. (%)
0.22	0.0030	0.02	0.395	0.120	3.54	0.57	0.187	33.2	1.9	0.01274	93.02
0.225	0.0042	0.03	0.40	0.154	9.03	0.575	0.187	33.9	2.0	0.01079	93.87
0.23	0.0052	0.05	0.405	0.183	9.65	0.58	0.187	34.5	2.1	0.00917	94.58
0.235	0.0054	0.07	0.41	0.194	10.3	0.585	0.185	35.2	2.2	0.00785	95.20
0.24	0.0058	0.09	0.415	0.192	11.0	0.59	0.184	35.9	2.3	0.00676	95.71
0.245	0.0064	0.11	0.42	0.192	11.7	0.595	0.183	36.5	2.4	0.00585	96.18
0.25	0.0064	0.13	0.425	0.189	12.4	0.60	0.181	37.2	2.5	0.00509	96.57
0.255	0.010	0.16	0.43	0.178	13.0	0.61	0.177	38.4	2.6	0.00445	96.90
0.26	0.013	0.20	0.435	0.182	13.7	0.62	0.174	39.7	2.7	0.00390	97.21
0.265	0.020	0.27	0.44	0.203	14.4	0.63	0.170	40.9	2.8	0.00343	97.47
0.27	0.025	0.34	0.445	0.215	15.1	0.64	0.166	42.1	2.9	0.00303	97.72
0.275	0.022	0.43	0.45	0.220	15.9	0.65	0.162	43.3	3.0	0.00268	97.90
0.28	0.024	0.51	0.455	0.219	16.7	0.66	0.159	44.5	3.1	0.00230	98.08
0.285	0.034	0.62	0.46	0.216	17.5	0.67	0.155	45.6	3.2	0.00214	98.24
0.29	0.052	0.77	0.465	0.215	18.2	0.68	0.151	46.7	3.3	0.00191	98.39
0.295	0.063	0.98	0.47	0.217	19.0	0.69	0.148	47.8	3.4	0.00171	98.52
0.30	0.061	1.23	0.475	0.220	19.8	0.70	0.144	48.8	3.5	0.00153	98.63
0.305	0.067	1.43	0.48	0.216	20.6	0.71	0.141	49.8	3.6	0.00139	98.74
0.31	0.076	1.69	0.485	0.203	21.3	0.72	0.137	50.8	3.7	0.00125	98.83
0.315	0.082	1.97	0.49	0.199	22.0	0.73	0.134	51.8	3.8	0.00114	98.91
0.32	0.085	2.26	0.495	0.204	22.8	0.74	0.130	52.7	3.9	0.00103	98.99
0.325	0.102	2.60	0.50	0.198	23.5	0.75	0.127	53.7	4.0	0.00095	99.05
0.33	0.115	3.02	0.505	0.197	24.2	0.80	0.1127	57.9	4.1	0.00087	99.13
0.335	0.111	3.40	0.51	0.196	24.9	0.85	0.1003	61.7	4.2	0.00080	99.18
0.34	0.111	3.80	0.515	0.189	25.6	0.90	0.0895	65.1	4.3	0.00073	99.23
0.345	0.117	4.21	0.52	0.187	26.3	0.95	0.0803	68.1	4.4	0.00067	99.29
0.35	0.118	4.63	0.525	0.192	26.9	1.0	0.0725	70.9	4.5	0.00061	99.33
0.355	0.116	5.04	0.53	0.195	27.6	1.1	0.0606	75.7	4.6	0.00056	99.38
0.36	0.116	5.47	0.535	0.197	28.3	1.2	0.0501	79.6	4.7	0.00051	99.41
0.365	0.129	5.89	0.54	0.198	29.0	1.3	0.0406	82.9	4.8	0.00048	99.45
0.37	0.133	6.36	0.545	0.198	29.8	1.4	0.0328	85.5	4.9	0.00044	99.48
0.375	0.132	6.84	0.55	0.195	30.5	1.5	0.0267	87.6	5.0	0.00042	99.51
0.38	0.123	7.29	0.555	0.192	31.2	1.6	0.0220	89.4	6.0	0.00021	99.74
0.385	0.115	7.72	0.56	0.190	31.8	1.7	0.0182	90.83	7.0	0.00012	99.86
0.39	0.112	8.13	0.565	0.189	32.5	1.8	0.0152	92.03			

SOLAR SIMULATION TESTING OF AN EARTH SATELLITE AT GODDARD SPACE FLIGHT CENTER*

by
R. E. Bernier, R. H. Hoffman
A. R. Timmins, and E. I. Powers
Goddard Space Flight Center

INTRODUCTION

The use of solar simulation to evaluate the thermal performance of a spacecraft is still relatively new and controversial. Reference 1 reports successful use of carbon arcs in testing the Telstar spacecraft. Additional information on the use of the carbon arc as a solar source should be useful in evaluating its effectiveness as a thermal design technique. At Goddard Space Flight Center carbon arcs have been used for achieving the solar simulation testing of spacecraft sized for the Delta and Scout boosters. This report presents data and experience from such testing, using the results from the flight backup Ariel II (UK-2/S-52) international satellite† as an example.

OBJECTIVES OF THE TEST

The primary purpose of exposing a spacecraft to a simulated solar atmosphere is to verify the thermal design of the spacecraft in full operation.

An additional objective is to check the operation of experiments in the vacuum chamber with simulated solar energy. Some experiments are directly stimulated by the sun, as in the case of ozone measurement experiments on the UK-2/S-52. Others, such as the micrometeoroid detector, use sunlight as a secondary medium by measuring the amount of sunlight passing through the punctures in a foil. Spacecraft subsystems also use sunlight as an event marker, switching operational modes as a sunrise or sunset condition is encountered.

A benefit derived from a solar test of a spacecraft is the exposure of spacecraft coatings and exposed surfaces to the thermal radiation environment encountered in orbit. In this way, possible physical incompatibilities may be discovered.

---

*Presented by Mr. Bernier at the Institute of Environmental Sciences 1964 Technical Meeting and Equipment Exposition, Philadelphia, April 13-15. Published in *1964 Proceedings*, pp. 209-216.

†Ariel II was launched successfully March 27, 1964 (designation: 1964-15A). The initial orbital temperature data compared favorably with prelaunch predictions.

For these reasons, as well as the basic desire of environmental testing groups to demonstrate spacecraft performance under the simulated environment, a solar test of the UK-2/S-52 international satellite was conducted.

THERMAL DESIGN AND PREDICTIONS

As previously stated, the primary purpose of conducting a solar test is to verify the thermal design of the spacecraft. Therefore, a brief discussion of the radiation inputs and the thermal model is presented so that a better appreciation of the test results may be possible.

For the UK-2/S-52, internal power dissipation is relatively small, compared with the total radiation input, and does not have a significant effect on the satellite mean temperature. In general, the magnitude of this effect depends on the emittance ϵ and the surface area (e.g., with a surface of low absolute ϵ, internal power may raise the temperature significantly because the skin has a limited capacity for reradiation).

Direct solar heating, earth-reflected solar heating (albedo), and earth-emitted radiation (earthshine) represent the significant inputs to the satellite. It is apparent that an adequate thermal design is predicated on a reasonably accurate knowledge of these thermal radiation inputs. The major source of energy–direct solar radiation–is, fortunately, the most accurate obtained. Since the sun's rays impinging on the satellite are virtually parallel, the problem is simply one of determining the instantaneous orientation of each external face with respect to the solar vector.

Determination of the Thermal Model

Of prime importance in the thermal analysis of a spacecraft is the determination of the thermal model. The model, an approximate mathematical representation of the satellite, is composed of a number of isothermal nodes or areas. The selection of these nodes is governed partly by convenience in working around interfaces, by accuracy requirements, and by a desire to minimize engineering and computer time.

First inspection of the UK-2/S-52 (Figure 1) showed that the broadband ozone detector mounted on top of the spacecraft was essentially independent of the spacecraft itself. Therefore, separate thermal models were developed for the main spacecraft and the detector and were thermally coupled by radiation and conduction interchange. The spacecraft was divided into 20 nodes, and the broadband ozone detector into 19 nodes.

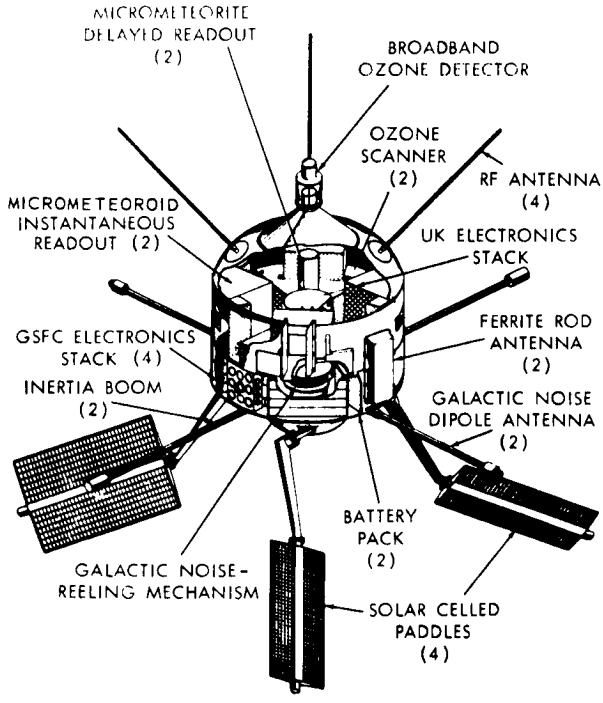

Figure 1–Flight backup Ariel II.

2

The thermal model of the ozone detector is shown in Figure 2. The most critical elements of this experiment are the monitor cell and the thorium-coated glass-enclosed tube at the top, each of which must be maintained below 60 °C.

The thermal model of the spacecraft is shown in Figure 3. Since the satellite is spinning about its longitudinal axis, skin temperatures tend to be uniform about the axis. This, together with the symmetrical design of the spacecraft, greatly simplifies the thermal considerations. As Figure 1 illustrates, there are a few components exposed to space: the ferrite rod antennas mounted in two fiber glass containers, the foil of the four micrometeoroid experiments, and the four apertures of the ozone scanners. There are also several openings in the bottom dome around the boom and paddle arm mounts which expose certain internal elements to space.

Since elements exposed to space generally undergo significant fluctuations in temperature, three of the ten external nodes were assigned to the ferrite rods, micrometeoroid foil, and the ozone scanner apertures. Of the ten internal nodes, five are structural elements and five relate to the experiments. The experiments on the upper shelf were considered as one node, since each is similarly influenced by the temperatures of of the upper dome and midskin while the power dissipated is negligible. The equipment on the lower shelf also was considered as one node.

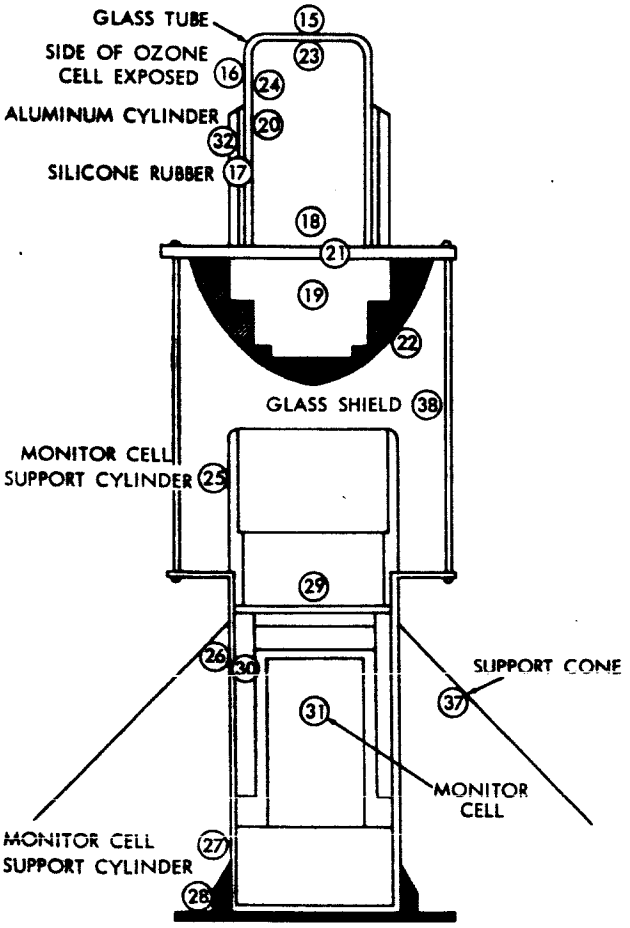

Figure 2–Broadband ozone detector node locations.

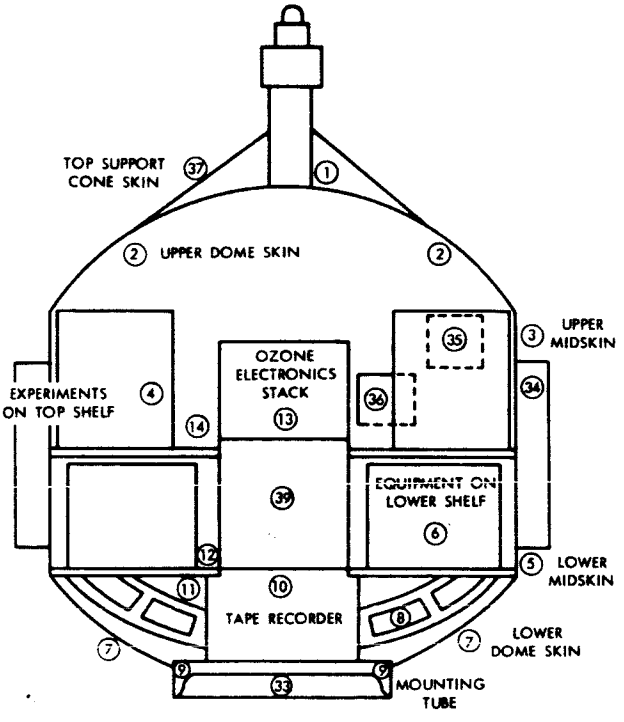

Figure 3–Thermal model for flight backup Ariel II, main body node locations.

The batteries, however, were investigated in further detail because of local hotspots while being charged. The three remaining internal nodes represent the ozone electronics stack, the galactic noise-reeling mechanism, and the tape recorder.

Conduction and Radiation Interchange

Every node is thermally coupled to one or more nodes by conduction and/or radiation interchange. External nodes also radiate to space. To determine the radiative coupling, the shape-factor area product and the effective emittance between nodes were determined. The shape-factor calculations were simplified by reducing the internal nodes to simple geometric forms (flat plates, cylinders, spheres, etc.) and by employing sources such as Reference 2. Almost the entire interior of the spacecraft was painted black to minimize thermal gradients. The effective emittance values were, therefore, approximately equal to 1.

The conduction interchange presented a problem in some cases since there was no way of accurately determining the conductance across joints. In these cases the extremes were considered, assuming both perfect contact and virtual isolation of the two nodes to determine how large a gradient might exist. Ten percent of perfect contact area was usually used for a nominal value.

Solar Input

As mentioned earlier, the major source of heat input to an orbiting satellite is direct solar radiation. The solar radiation absorbed by an external surface is $SA_p\alpha$, where S is the solar constant, A_p is the projected area to sunlight, and α is the solar absorptance of the surface.

Determining the projected areas of each surface element or node for different positions around the spin axis and for various aspect angles was accomplished by taking pictures of a one-fifth-scale model of the spacecraft. The satellite was designed to operate within solar aspect angles (angle between the solar vector and spin axis) of 45 to 135 degrees. However, for a complete analytical study the projected areas were determined for all aspect angles at 15-degree increments.

Albedo and Earthshine

A computer program (Reference 3) was employed to determine the values of albedo and earthshine incident upon the rotating surfaces throughout the orbit. Average orbital values were used for the two orbits considered. Albedo and earthshine account for approximately 15 to 30 percent of the total external heat input, albedo being greater in the minimum sunlight orbit.

Modifications in the Thermal Analysis

In altering the thermal analysis for use in the solar environment test chamber, the energy inputs of albedo and earthshine were equated to zero since no attempt was made in the test to simulate them. The effect of paddle shading at high aspect angles also was removed from the computer analysis since the test was conducted without the solar paddles fixed to the spacecraft.

Calibration tests were performed on samples of the spacecraft coatings to determine their absorptance properties when illuminated by the solar simulator in the test chamber. These properties were then inserted into the thermal model in place of the values used for orbital predictions. It is noted here that the difference between the orbital absorptance properties and the carbon-arc chamber values for the UK-2/S-52 coatings was negligible. However, the practice of using test-condition absorptance properties to predict test temperatures can be extremely important when a source with a poor spectral match is used on a coating whose absorptance response is not flat in the source wavelength region.

The thermal model was used to predict spacecraft temperatures from carbon-arc radiation intensity values which were introduced as input fluxes to the external nodes of the spacecraft. Agreement between predicted and actual test temperatures would then corroborate the thermal design of the spacecraft. Differences in predicted versus test temperatures would indicate areas requiring more study, either in the design or in the test technique.

DESCRIPTION OF THE SOLAR SIMULATION TEST

The test was performed in a 7-foot-diameter, 8-foot-long, cylindrical thermal-vacuum chamber. Located at one end of the chamber is a 1-foot-diameter quartz port through which the carbon-arc beam was introduced (Figure 4).

The spacecraft was mounted on a rotator-gimbal mount which provided two-axis motion: spin about the centerline of the spacecraft at 3 rpm, and inclination relative to the incident simulated solar radiation. Because of the physical limitations of the facility size, the inertia booms, galactic noise experiment dipole booms, and solar paddles were not included in the test configuration. Also, shortened telemetry antennas were substituted for the full-length antennas during this test (Figure 5). Two modes of information were available from the spacecraft: normal telemetry

MANUFACTURER
Goddard Space Flight Center (Prime)

TEMPERATURE (HEAT SINK)
-173°C (100°K)

SOLAR SIMULATION
1400 watts/m^2 over a 91 cm (3 ft) diam. circle by carbon arc

ULTIMATE VACUUM
5×10^{-8} mm Hg

TIMES TO PRESSURES
1×10^{-6} mm Hg — 3 hours
5×10^{-8} mm Hg — 15 hours

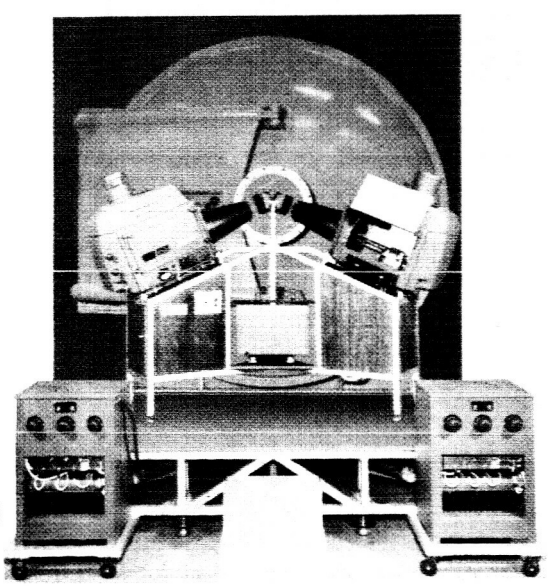

Figure 4—The environment simulator

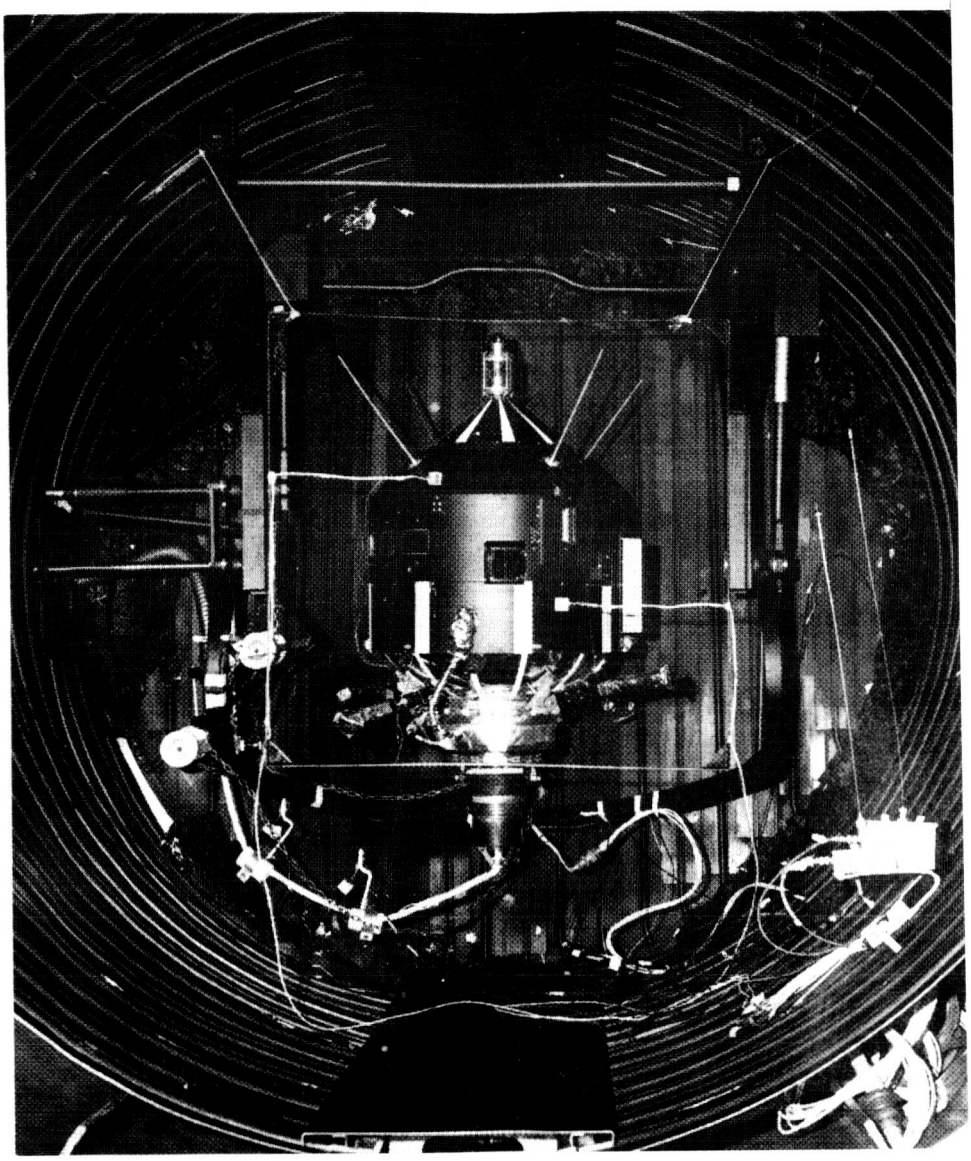

Figure 5–Flight backup Ariel II mounted on rotator-gimbal in the thermal-vacuum chamber.

transmission and command receiver, and a test hardline-slipring combination for power and supplementary data. The former system provided information in the same format as its orbital operation, while the latter provided the capability of recharging the on-board batteries and transmitting data from temperature sensors mounted for test purposes. These sensor outputs were scanned during the test to minimize the number of sliprings.

The pressure environment was in the range of 1×10^{-7} mm Hg, while the chamber walls were at approximately liquid-nitrogen temperature, -190°C. The simulated solar radiation was set at an equivalent 1 solar constant, as described in the next section of this report. The spacecraft was fully operational from an experiment and subsystem basis while rotating on its spin axis.

The spacecraft was separated from the rotator-gimbal mount by a nylon insulator. Heat was supplied to the mount to such a degree that a small temperature gradient existed at all times. This minimized the energy flow between the spacecraft and mount. Since the temperatures were monitored throughout the test, approximate values of heat gain or loss were calculated. These values were introduced into the thermal model, to be reflected in the spacecraft energy balance and test temperature predictions.

Three spacecraft-incident solar radiation aspects were tested. They consisted of the 90-degree aspect or broadside solar exposure, the 45-degree aspect or maximum top-to-bottom temperature gradient expected in flight, and the 135-degree aspect or maximum bottom-to-top temperature gradient expected.

The variation of sun exposure in orbit is from 63 to 100 percent. The 63-percent exposure consisted of a series of cycles of 55-minute sunlight–32-minute shade periods. The 90-degree aspect position was tested at both of the above exposures to determine the effect on mean spacecraft temperature. The remaining aspects of 45 and 135 degrees were tested at the 100 percent sunlight condition only, because the primary objective was to study the internal temperature gradients resulting from these aspects.

PROBLEMS ASSOCIATED WITH SOLAR SIMULATION

Some of the difficulties encountered in attempting to simulate solar radiation are related below. The efforts to compensate for these problems are discussed in detail.

The choice of radiation source in large part is dictated by the desire to match as closely as possible the spectrum of the sun at orbital altitude. In addition, the ease of handling the source during the test must be considered.

Spectrum

Any significant departure in the spectral distribution of the simulator source from the sun's spectrum, as defined in the Johnson Curve, may cause a change in the absorbed energy of the exposed surface.

The carbon arc was chosen as the solar source because of its close spectral match with the Johnson Curve. Open-arc sources, however, present several operational problems, as discussed in the following paragraphs.

Uniformity and Degradation of the Carbon-Arc Solar Simulator

The carbon-arc system consisted of two modified reflector arc lamps. The system contained no optics except the quartz port in the vacuum chamber. Two arc lamps were used for two reasons: (1) the carbon-rod feed mechanism created a shadow on the reflector and a discontinuity in

the intensity of the beam from a single lamp; (2) the necessity for replacing the consumable rod in each lamp every hour warranted the use of multiple lamps to minimize the interruption of radiation energy input to the spacecraft.

The use of a reflector system is beneficial from a power and efficiency standpoint but creates uniformity and degradation problems. The exposure of the reflector to the open arc permits the deposit of vaporized carbon on the reflector surface, resulting in loss of reflectance efficiency and an ever-changing intensity distribution in the projected beam. To compensate for this condition during the test, intensity mappings of the projected beam were made at selected intervals in the test cycle. A rolled-ribbon thermocouple radiometer mounted on an X-Y plotting board was used for this mapping procedure. This provided an in-test calibration of the radiation beam and also a reference point for total intensity adjustment to compensate for reflector degradation.

Determination of Carbon-Arc Intensity

The first step in determining the arc intensity or solar flux on the spacecraft is to determine the effective α/ϵ of the total spacecraft when illuminated by the natural sun. This is combined with the carbon-arc intensity I_c and the natural sun intensity I_s as follows:

$$I_s \, (\alpha/\epsilon)_s = I_c \, (\alpha/\epsilon)_c \quad . \tag{1}$$

The effective α/ϵ is determined by the following equations:

$$\alpha_{eff} = \bar{A}_1 \, \alpha_1 + \bar{A}_2 \, \alpha_2 + \cdots \bar{A}_n \, \alpha_n \quad , \tag{2}$$

$$\epsilon_{eff} = \bar{A}_1 \, \epsilon_1 + \bar{A}_2 \, \epsilon_2 + \cdots \bar{A}_n \, \epsilon_n \quad , \tag{3}$$

$$(\alpha/\epsilon)_{eff} = \frac{\alpha_{eff}}{\epsilon_{eff}} \quad , \tag{4}$$

where

$\bar{A}$ = ratio of coating area to total exposed area (as given in Table 2),

α = absorptance,

ϵ = emittance.

Table 1

Spacecraft Coating Thermal Properties

Coating	Solar			Chamber		
	α	ϵ	α/ϵ	α	ϵ	α/ϵ
Black	0.96	0.86	1.12	0.96	0.86	1.12
White	0.27	0.86	0.31	0.26	0.86	0.30
Evap. aluminum	0.12	0.04	3.0	0.11	0.04	2.77

By referring to Tables 1 and 2, which give the coating thermal properties and their areas, respectively, the following effective α/ϵ ratios are derived:

$$(\alpha/\epsilon)_{eff,\ solar} = 1.04 \quad , \tag{5}$$

$$(\alpha/\epsilon)_{eff,\ chamber} = 1.03 \quad . \tag{6}$$

Table 2

Spacecraft Coating Area Evaluation

Spacecraft Surface	Area (sq ft)	Percent of Total Area	White (%)	White (% of total area)	Black (%)	Black (% of total area)	Evap. Al (%)	Evap. Al (% of total area)	Al Foil (%)	Al Foil (% of total area)
Top dome	2.82	23.7	0	0	100	23.7	0	0	0	0
B. B. support dome	1.16	9.8	25	2.5	75	7.5	0	0	0	0
Upper mid-skin	2.50	21.0	0	0	100	21.0	0	0	0	0
Lower mid-skin	2.58	21.7	20	4.3	80	17.4	0	0	0	0
Bottom dome	2.53	21.3	10	2.1	0	0	90	19.2	0	0
Mounting ring	0.30	2.5	0	0	0	0	0	0	100	2.5
Total area:	11.89			8.9		69.6		19.2		2.5

Combining Equations 1, 5, and 6, gives, assuming I_s = 1 solar constant,

$$I_c = 1.01 \text{ solar constant} \quad (7)$$

Intensity Calibration and Monitoring of the Carbon-Arc Solar Simulator

The lack of an absolute solar standard detector made it necessary to use a secondary method of intensity calibration. The method chosen was the integrating black-ball technique in which a thin-shell aluminum ball, the approximate size of the spacecraft, is placed in the test chamber in the exact location the spacecraft will occupy during the test. The integrating ball has a small thin-shell ball suspended in its center. The inner ball temperature is measured by a thermocouple. Both balls are coated with a black paint of known absorptance and emittance. A calculation is made to determine the stabilization temperature of the ball for a flux of 1.01 solar constant. The chamber is then evacuated, and the shrouds are flooded with liquid nitrogen to simulate the same environment that the spacecraft will encounter. The arc output is adjusted so that the ball system stabilizes to the predetermined temperature. Once this focus adjustment is made, the arc beam is mapped for uniformity and intensity with the radiation detector on the X-Y plotting board located external to the chamber. The readings of the detector are then bench-marked to the intensity incident on the black ball and are used throughout the test of the spacecraft as a relative monitoring point.

The use of the black-ball technique for calibrating the arcs serves a dual purpose: (1) arc calibration as described above, and (2) inclusion of inherent chamber energy (reflected or radiative) in the calibration of total energy absorbed by the black ball. The black coating of the ball is spectrally flat in its absorption characteristics, and therefore arrives at the desired stabilization temperature by summing the energies from the carbon arcs and the inherent chamber sources.

This technique is applicable if the spacecraft to be tested also is essentially spectrally flat in its absorption characteristics, as in the case of the UK-2/S-52.

Beam Collimation

The radiation beam projected by the solar simulator is divergent with a 7½-degree half-angle. This permits the system to project a 36-inch-diameter beam at the centerline plane of the spacecraft. This divergence rate is not considered severe enough to cause unnatural shadowing; however, a measured energy change per unit area of approximately 1 percent per inch of depth variation is produced in the test volume. Therefore, incident intensity compensation was made to the thermal model of the spacecraft to take into account this change of intensity with depth.

Determination of Local Solar Intensity Input to the Spacecraft

The thermal model segments the spacecraft into thermal nodes. Figure 6 shows the nodes used for this test, along with the definition of aspect angles used in the test series.

The intensity-uniformity of the projected beam was mapped with an X-Y plotting board, as previously described. Figure 7 shows a typical uniformity distribution plot taken with a radiometer; the numbers are millivolt output readings which, when used in conjunction with a

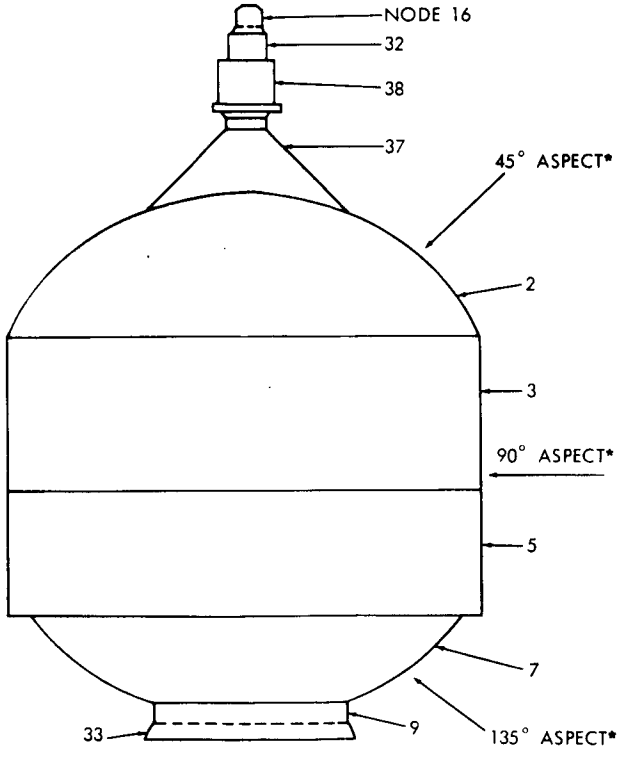

*Angle represents spacecraft-sun aspect, and arrow represents sunlight.

Figure 6—Computer thermal nodes and spacecraft aspect angles.

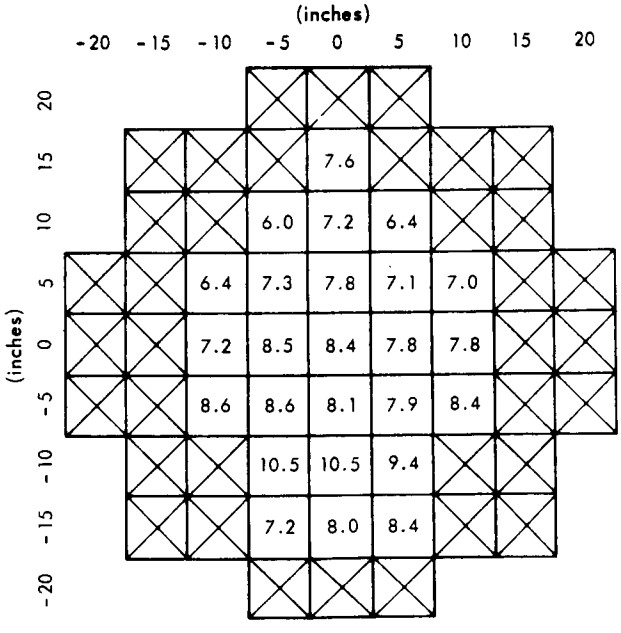

Figure 7—Carbon-arc uniformity distribution survey.

calibration curve, yield relative intensity readings. The uniformity plots were used to determine the local intensity at the individual thermal nodes given in Figure 6. Three planes of intensity perpendicular to the incident beam were plotted: at the spacecraft centerline, 6 inches nearer the beam source, and 12 inches nearer the beam source. This was done to determine the change of intensity with distance from the source, since the beam is diverging at the rate of 7½-degree half-angle. This calibration indicated a change of 6 percent intensity for each position, or a range of 12 percent over the full 12 inches of the beam depth covered. The above information was then used in refining the local intensity values to be used in the thermal analysis.

It should be noted again that, in a reflector-focus arc system, the reflector degrades in performance as it becomes coated with carbon deposit from the open arc. This degradation decreases the total intensity for a given focal length and randomly changes the uniformity pattern as some areas of the reflector receive carbon deposit. Because of this condition, in-test monitoring is necessary to change the arc focal length, compensating for the reflector degradation. Since no adequate real-time in-chamber monitoring device was available, the detector and an X-Y plotting board were used whenever the test schedule called for a simulated shade period in an orbit cycle. These external in-test uniformity plots were then used to indicate the status of the solar flux just prior to the shade period. In addition, they were used to determine what refocusing was necessary to restore the total intensity to the desired 1.01 solar constant. Therefore, a test prediction is made from intensity plots obtained during the test. Table 3 presents the intensity values used for test predictions.

Table 3

Test Chamber Total-Intensity Inputs to the Predict Program*

Spacecraft Node (See Figure 6)	90° Aspect, 100% Sun I_T	90° Aspect, 63-37% Sun I_T	45° Aspect, 100% Sun I_T	135° Aspect, 100% Sun I_T
2	550	597	529	0
3	470	505	492	529
5	468	500	454	484
7	581	496	0	495
9	522	478	0	518
9*	-27	-18	-17	+1.0
16	330	365	728	490
32	330	365	715	504
37	583	729	592	0
38	390	400	689	525

*Notes: 1. Units, Btu/hr-sq ft
2. Total intensity I_T represents available energy to the nodes
3. Node 9* input is conductive energy across the spacecraft rotator interface

SOLAR SIMULATION TEST RESULTS

Figures 8 through 10 present typical thermal profiles that have been included to show the comparison between predicted and test temperatures. From the total data available, the following observations are made:

1. The effect of aspect angle on the mean temperature of the spacecraft, as represented by the battery, was 23 °C.

2. The effect of sunlight-shade exposure time on the mean temperature of the spacecraft was 33 °C. Figure 11, presenting a sample of data from this test, is valuable as an indicator of the interactions of spacecraft structure and components.

3. The temperature excursion of the broadband ozone detector due to sun aspect angle was about 85 °C (69 °C to -17 °C) from test data,

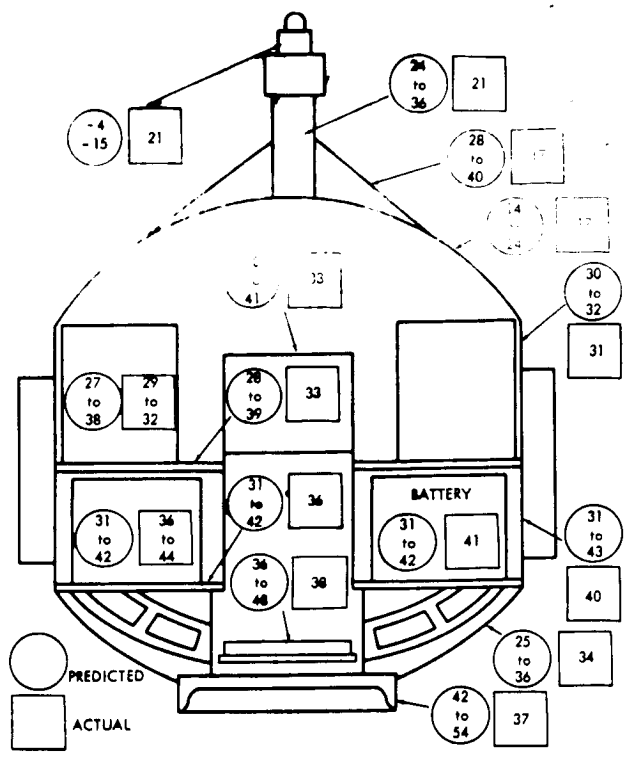

Figure 8—Temperature predictions versus actual test in °C, with 100% sun cycle and 90° aspect angle.

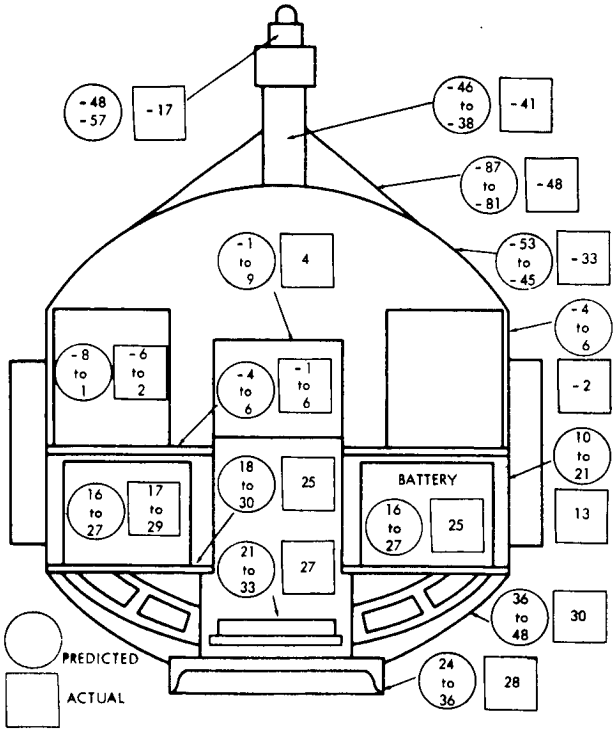

Figure 9—Temperature predictions versus actual test in °C, with 100% sun cycle and 135° aspect angle.

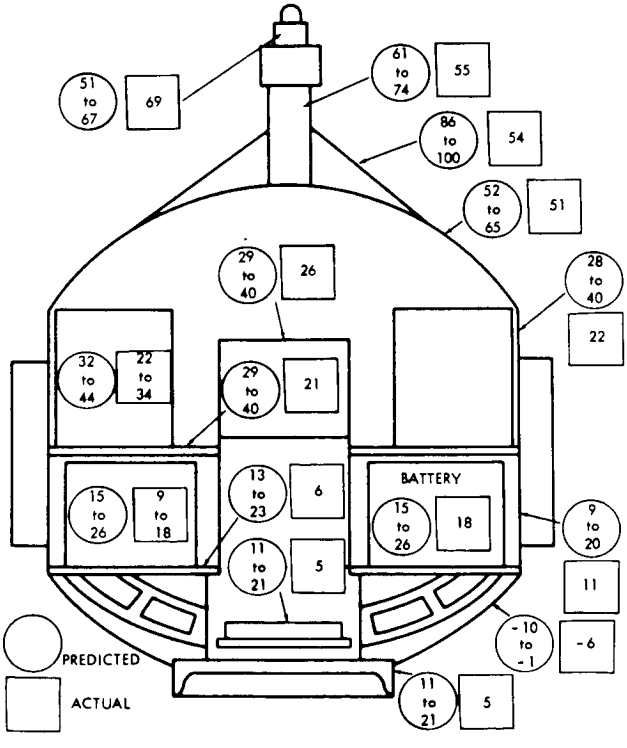

Figure 10*—Temperature predictions versus actual test in °C, with 100% sun cycle and 45° aspect angle.

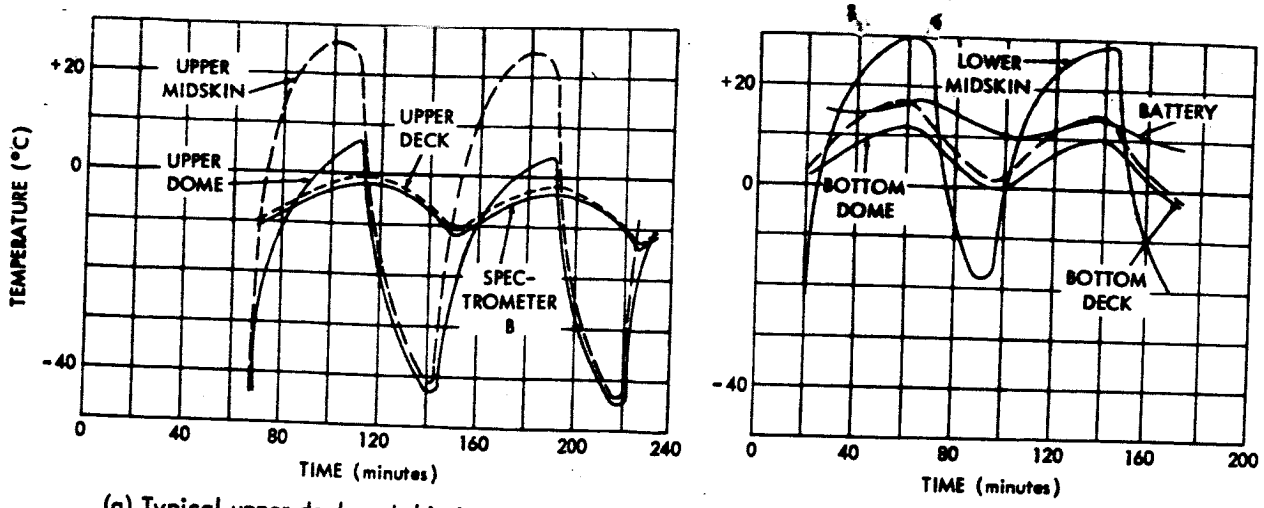

(a) Typical upper deck and skin interaction during cycles

(b) Typical lower deck and skin interaction during cycles

Figure 11—Typical cyclic data.

whereas the predicted excursion was approximately 110°C (59°C to -52° C). The test results indicate that the external portion of the detector does not reach the extreme temperatures that are predicted but more closely follows the temperature of its enclosed base, the support cone, and the top dome.

In addition, it should be noted that two of the experiments required solar energy for activation; thus complete performance was obtained under simulated space conditions.

Also, the occurrence of a coating failure directed attention to a review of the adhesion characteristics under stress and the preparation of surfaces to be painted.

The spacecraft was fully operational throughout the test, and no problems were experienced with components or ground station. One minor exception was an occasional noise interference between the carbon arcs and the spacecraft programmer which controls operating modes of the spacecraft.

CONCLUSIONS

Based on the test results obtained, the following conclusions were reached:

1. The solar simulation test verified the assumptions made for the thermal model, excluding the broadband experiment.

2. The spacecraft should operate satisfactorily under space conditions.

3. The satisfactory performance of the two experiments that were stimulated by simulated solar energy indicates that successful operation should be obtained in space.

4. The carbon arc is a useful solar simulation source although a simulator utilizing optics, rather than reflector focus, would provide better uniformity.

*In Figure 10, test ended prematurely because of data failure, resulting in some low internal temperatures.

5. The nonuniformity of the arc beam intensity can be adequately compensated by the rotating spacecraft and the nodal energy input to the computer program.

(Manuscript received June 12, 1964.)

REFERENCES

1. Hrycak, P., Unger, B. A., and Wittenberg, A. M., "Thermal Testing of the Telstar Satellite," *Proceedings of the Institute of Environmental Sciences, 1963,* p. 377.

2. Hamilton, D. C., and Morgan, W. R., "Radiant-Interchange Configuration Factors," NACA TN-2836, December 1952.

3. Powers, E. I., "Thermal Radiation to a Flat Surface Rotating About an Arbitrary Axis in an Elliptical Earth Orbit: Application to Spin Stabilized Satellites," NASA TN D-2147, January 1964.

DEVELOPMENT AND PERFORMANCE OF THE JPL GLASS-LINED METAL REFLECTORS FOR THE SOLAR SYSTEM IN THE 25-FOOT SPACE SIMULATOR

* * * *

H. N. Riise
Section 374
3/25/64

Jet Propulsion Laboratory

N. Riise
3/25/64

DEVELOPMENT AND PERFORMANCE OF THE JPL GLASS-LINED METAL REFLECTORS FOR THE SOLAR SIMULATOR IN THE 25-FOOT SPACE SIMULATOR

I. INTRODUCTION

The optical system initially delivered to JPL for solar simulation in the 25-foot space chamber (see Figure 1) included stainless steel mirrors in three positions as follows:

Mirrors	Size	No. Req.	See Fig. No.
1. Turning mirror (pseudo-parabola)	33 in dia.	19	2
2. Fly's eye (pseudo-hyperbola)	8.4 in. hex.	19	3
3. Virtual source	3/4 in. hex.	1200	4

These mirrors were unsatisfactory when compared with glass, mainly from a maintenance point of view. The fact that these mirrors required refiguring when they were recoated was both costly and time consuming.

The preference would also be with glass when comparing maximum reflectivity or rate of reflective surface degradation. This assumes, of course, that glass mirrors could be used.

II. REASONS FOR INITIAL SELECTION OF STAINLESS STEEL REFLECTORS

The energy flux designed to impinge the virtual source and fly's eye mirrors is about 11,000 w/ft^2. If the reflectivity is 75% (many were lower than this), the exposed surface will absorb 2750 w/ft^2 or about 9000 BTU/hr.

If a heat sink is provided through one inch of reflector material, and this is the only means by which heat is dissipated, the temperature difference between the exposed and cooled surfaces will be:

[redacted]	6 deg. F.
Silicon	7 "
Brass	12 "
Stainless Steel	76 "
Silica Glass	800 "

It was a calculation similar to this which led Bausch & Lomb to the decision to make these mirrors of metal. Almost any metal would be satisfactory from a surface temperature point of view, but glass is such an inferior thermal conductor that it would probably fail from thermal shock. If this did not happen, the reflective coating would degrade rapidly from the high operating temperatures.

III. PROBLEMS WITH THE STAINLESS STEEL REFLECTORS

Stainless steel mirrors were subsequently fabricated by Bausch & Lomb and installed in the system.

Reflectivity of the virtual source mirrors degraded below a useful value before the lights in the chamber were initially turned on. When the evaporated aluminum coating was stripped from the mirrors, the surface appeared corroded. They were, therefore, polished before being recoated with evaporated aluminum. Later, when it was determined that the figure was not correct, it was generally believed that the polishing operation had destroyed the initial contour to which the mirrors had been polished.

IV. NEW MIRROR MATERIALS CONSIDERED

Before JPL actually took possession of the space chamber, a new set of virtual source mirrors was ordered (see Figures 5 & 6). These mirrors were of different size, different contours, and different materials than the original B & L installation.

The materials to be used in the new mirror fabrication were specified as follows:

1. Stainless steel
2. Brass
3. Brass - nickel plate and refigure before aluminizing.
4. Silicon
5. Glass-lined aluminum - see Figure 6

V. RESULTS OF MIRROR MATERIALS EXPERIMENTS

The glass-bonded-to-aluminum mirror was superior in every respect to the other materials tried except the silicon. Temperature rise in the glass from bond line to the reflective surface is estimated to be 50 deg. F.

The silicon mirrors, from the standpoint of initial reflectivity, durability of coating and ease of maintenance (cleaning and recoating) was as good as, or slightly better than the glass. However, this slim edge in

performance was more than offset by high cost. The very high thermal conductivity (nearly that of aluminum) of silicon may bring it back into consideration if flux densities should increase to the point where surface temperatures of the glass would again become a problem.

All of the other metal substrates appear to react with the aluminum reflective coating in such a way that the polish of the substrate is degraded. It is probable that moisture, ozone, or some other contaminant in the atmosphere enters into or catalyzes this reaction.

It might be mentioned that these glass-lined mirrors survived a bond strength test of reduction to liquid nitrogen temperatures and return to ambient.

VI. GLASS-LINED METAL FLY'S EYE (Pseudo-Hyperbolic) MIRRORS (Figure 3 & 7)

After successfully glass bonding the virtual source mirrors, it was decided to take similar action on the fly's eye mirrors. A spare set was ordered which was identical with those which were in place except that the exposed surface was glass and the base metal was copper. When these were installed in the system, a thin layer of glass was bonded to the original stainless steel mirrors. This provides a complete set of spares.

The performance of both these sets of mirrors is satisfactory. No difference can be seen in their operation even though it is obvious that the copper-base mirrors operate at a lower surface temperature than the stainless-base mirrors.

VII. GLASS-LINED METAL HEADLAMP REFLECTORS

The original headlamp collectors furnished by Bausch & Lomb were 16-in. latus rectum reflectors with a 4-in. first (see Figure 3) focus. In our need for more power into the solar system, a 5-KW lamp was installed in place of the 2.5-KW lamp originally furnished. The reflectors could not withstand the additional thermal shock.

Since the glass-lined metal reflector seemed to be resistant to thermal shock, it was decided to move the lamp cluster to the position of the turning mirror (see Figure 8) if a satisfactory reflector could be fabricated for this position. This would decrease the size of the collector to 7 1/2 in. dia. and increase its performance requirements proportionally, but it was believed from our experience with the virutal source and fly's eye reflectors that such a mirror was practical (see Figures 9 and 10).

This modification would increase energy into the solar system in the following ways:

1. It would eliminate the energy absorbing reflection of the turning mirror.

2. It would collect the more readily available part of the energy polar of an Xenon lamp.

3. It would permit the use of more powerful lamps in the system.

VIII. PERFORMANCE OF THE 7 1/2 IN. GLASS-LINED HEADLAMP REFLECTOR.

If its acceptance angle is not changed, the energy which impinges a fly's eye mirror from a cluster of seven headlamps is proportional to the energy in the solar beam. This fact makes the headlamp and reflector combination readily adaptable to bench testing.

Calorimeter measurements were made on an area representing a fly's eye mirror to determine the energy increase into the system that can be expected using the new reflectors.

Comparison of data taken with various lamp and reflector combinations is as follows:

N. Riise
3/25/64

Mfg.	Type Lamp	Power Rating	Power into Lamp	Energy into Calorimeter Watts	Comments
Hanovia	HgXe	2½ KW	2½ KW	1180	Original Bausch & Lomb configuration, 16-in. dia. reflector cluster of 7 lamps (Figure 1)
Hanovia	HgXe	2½ KW	2½ KW	1960	New configuration with 7½ in. dia. glass-lined reflectors. Cluster of 7 lamps (Figure 8)
Osram	Xe	2.5 KW	3 KW	3040	New configuration with 7½ in. dia. glass-lined reflectors. Cluster of 7 lamps (Figure 8)
Osram	Xe	6.5 KW	6.5 KW	6800	New configuration with 7½ in. dia. glass-lined reflectors. Cluster of 7 lamps (Figure 8)
Osram	Xe	6.5 KW	8.0 KW	7160	New configuration with 7½ in. dia. glass-lined reflectors. Cluster of 7 lamps (Figure 8)
Ushio	Xe	5.0 KW	5.0 KW	4360	New configuration with 7½ in. dia. glass-lined reflectors. Cluster of 7 lamps (Figure 8)
Ushio	Xe	5.0 KW	6.2 KW	5340	New configuration with 7½ in. dia. glass-lined reflectors (Figure 8)

IX. CONCLUSION

Glass-metal reflectors can intercept high energy solar radiation without damage to the reflective coating, the glass, the bond, or to the substrate metal itself.

The combination should not be used in mirrors requiring a highly accurate figure since the glass and metal have different coefficients of expansion and the combination will change figure with temperature. An attempt is made to minimize this deformation by:

1. Making the mass of the metal large compared to that of the glass.

2. Keeping the temperature as constant as possible by making the substrate metal highly conductive and water cooling this metal to minimize temperature rise.

It is probable that silicon substituted for the glass could survive much higher radiation flux since the temperature gradient through the silicon would only be about 1% of that through the glass.

The type of epoxy bonding material is probably not very important providing the bond thickness is kept below .005 in. Hysol 3X was initially specified for the virtual source mirrors after trying many different types.

Hysol 3X was too viscous to accomplish the thin bond line required for the larger fly's eye and headlamp mirrors so General Mills Genepoxy 175 with Furane #9633 hardener was tried and it has proved satisfactory.

It is important that the bond between the glass and the metal be cured at a temperature above which it will be operated. This will always keep the glass in compression...a force which it appears to survive very well.

The glass should be kept thin to minimize warpage and minimize the shear stress which develops at the bond line. The epoxy itself is stronger than the glass in shear so that if the glass thickness is increased, shear failure will occur in the glass near the bond line.

* * * *

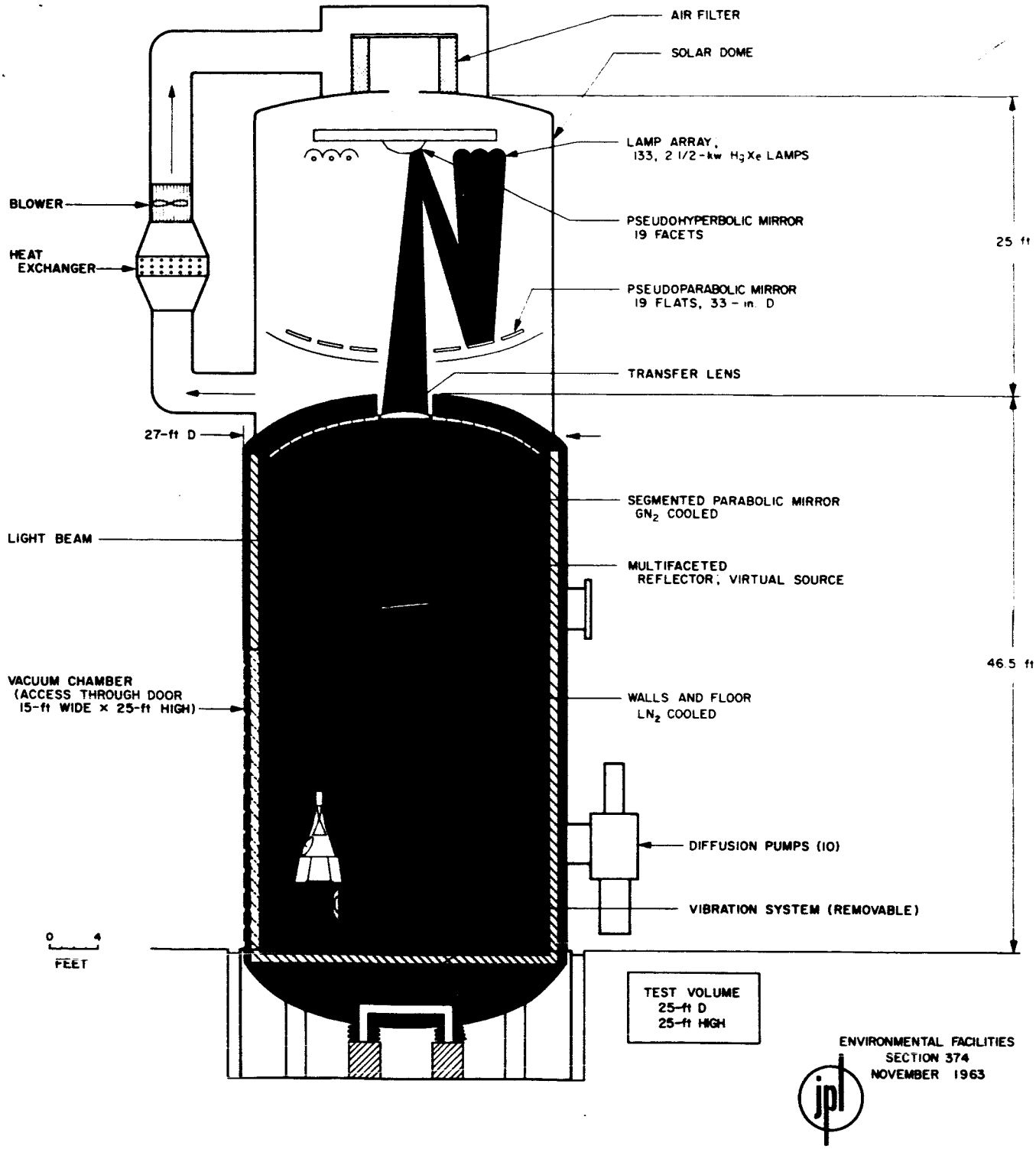

JPL 25-ft SPACE SIMULATOR

Figure 1.

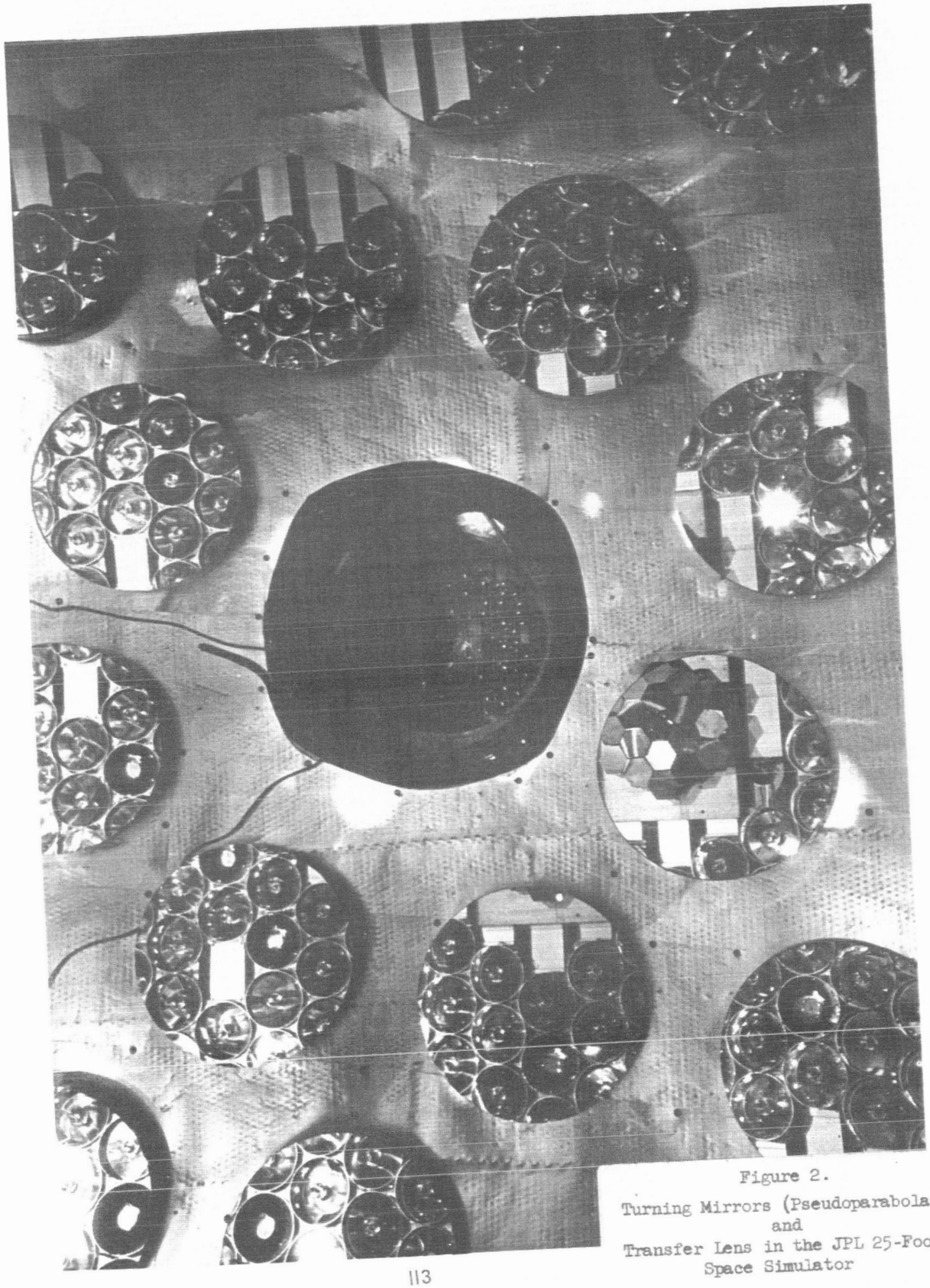

Figure 2.
Turning Mirrors (Pseudoparabola)
and
Transfer Lens in the JPL 25-Foot
Space Simulator

PRECEDING PAGE BLANK NOT FILMED.

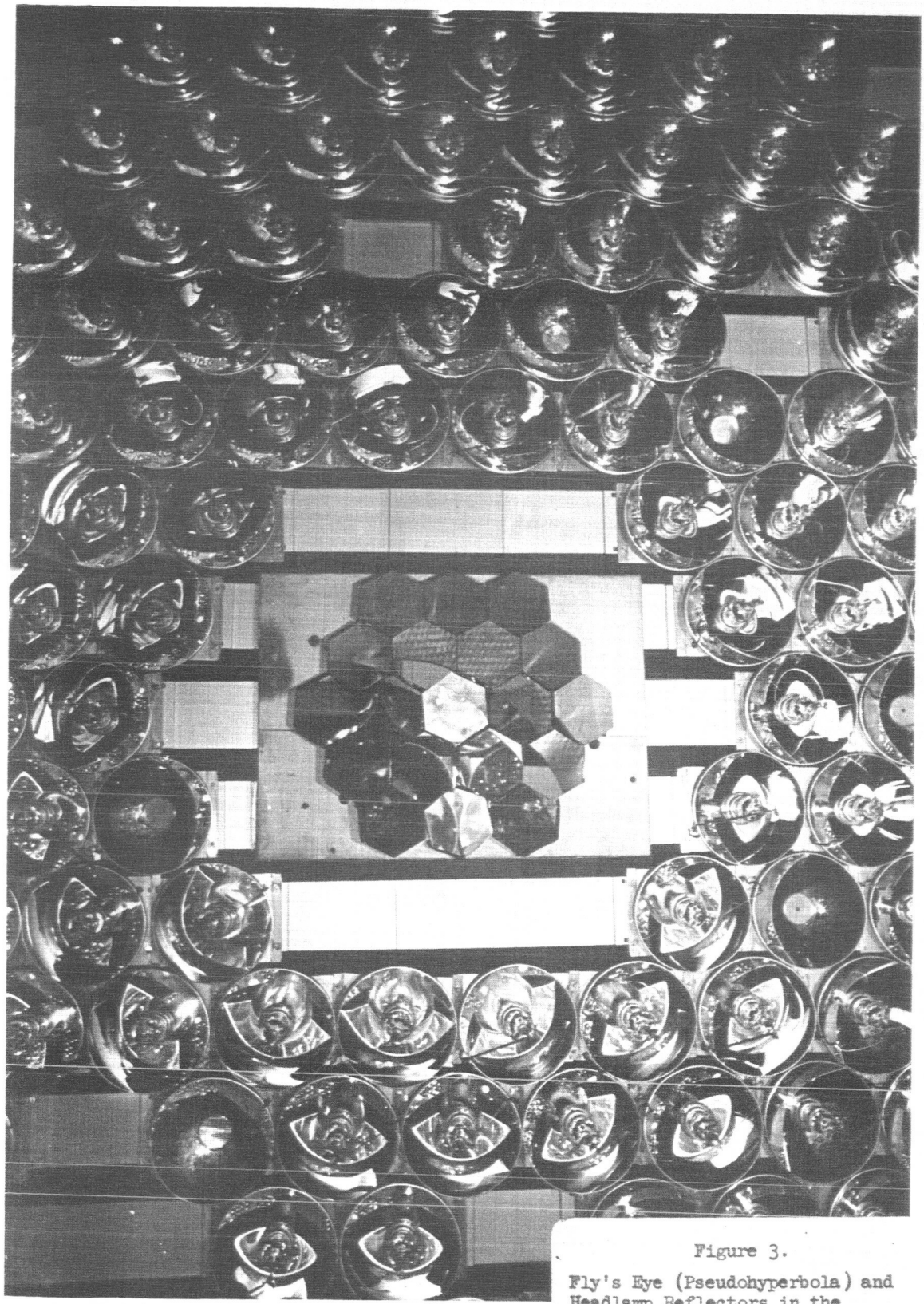

Figure 3.

Fly's Eye (Pseudohyperbola) and Headlamp Reflectors in the JPL 25-Foot Space Simulator

Figure 4.

Contractor Furnished Virtual Source Mirrors for the JPL 25-Foot Space Simulator

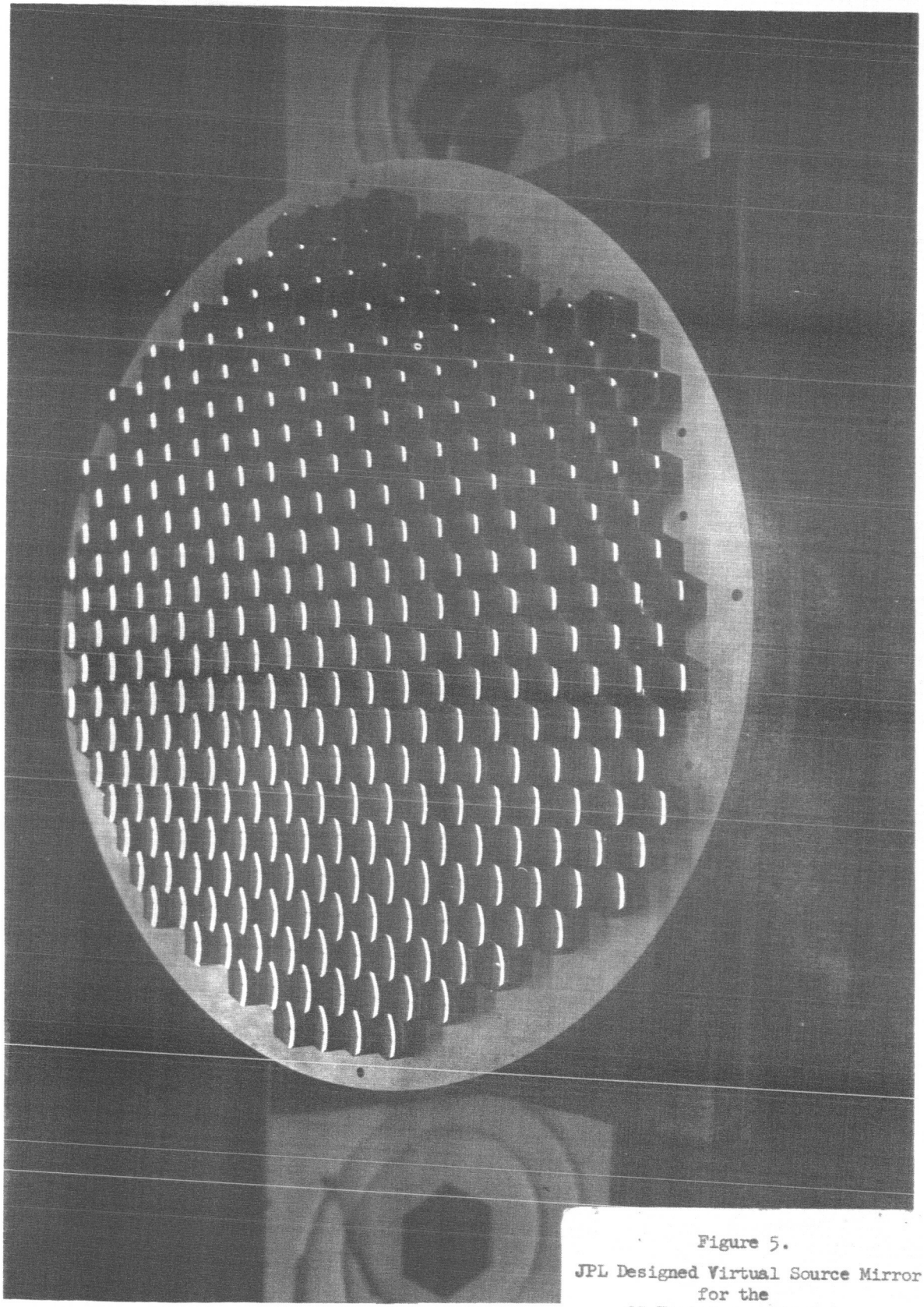

Figure 5.
JPL Designed Virtual Source Mirror
for the
25-Foot Space Simulator

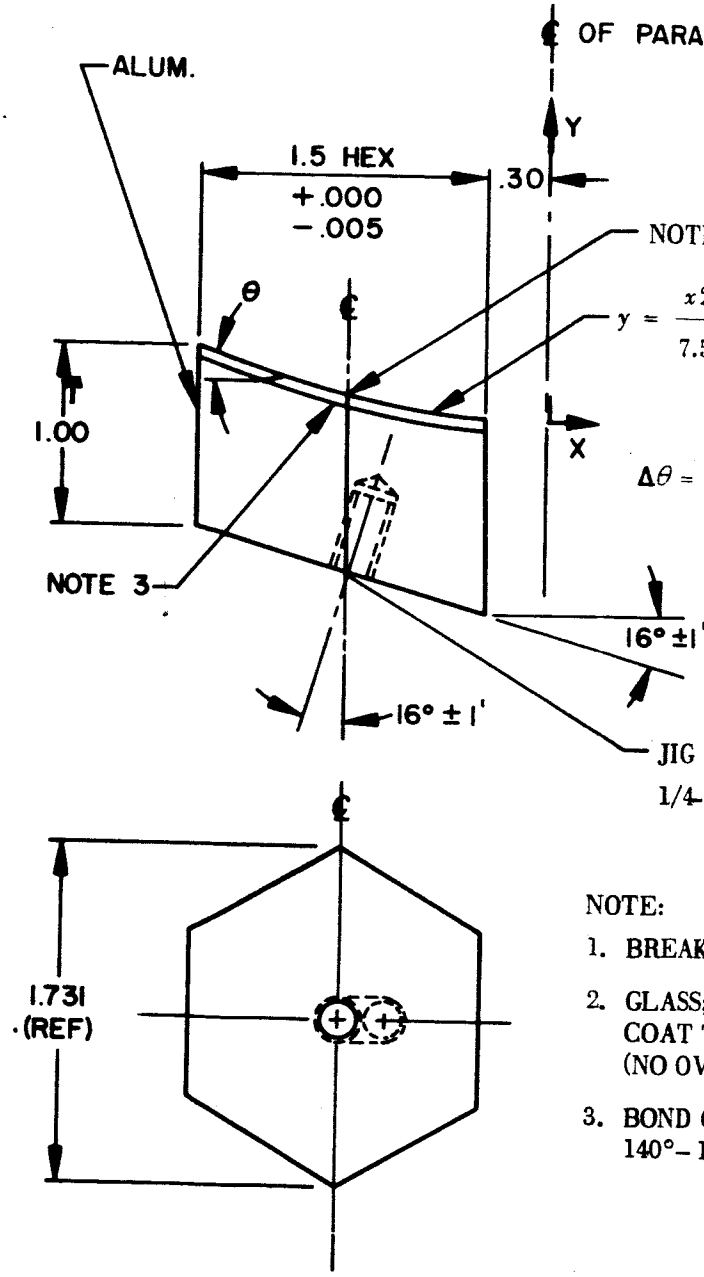

NOTE:

1. BREAK ALL SHARP EDGES EXCEPT OPTICAL SURFACES.
2. GLASS; MAX. THICKNESS, 06; POLISH SURFACE & ALUM. COAT TO 90% MIN. REFLECTIVITY TO SOLAR SPECTRUM; (NO OVERCOAT)
3. BOND GLASS TO METAL WITH EPOXY; SET EPOXY AT 140°– 150°F. MAXIMUM BOND THICKNESS – 0.005

Figure 6. Virtual Source Mirror - 7-ft Solar Beam

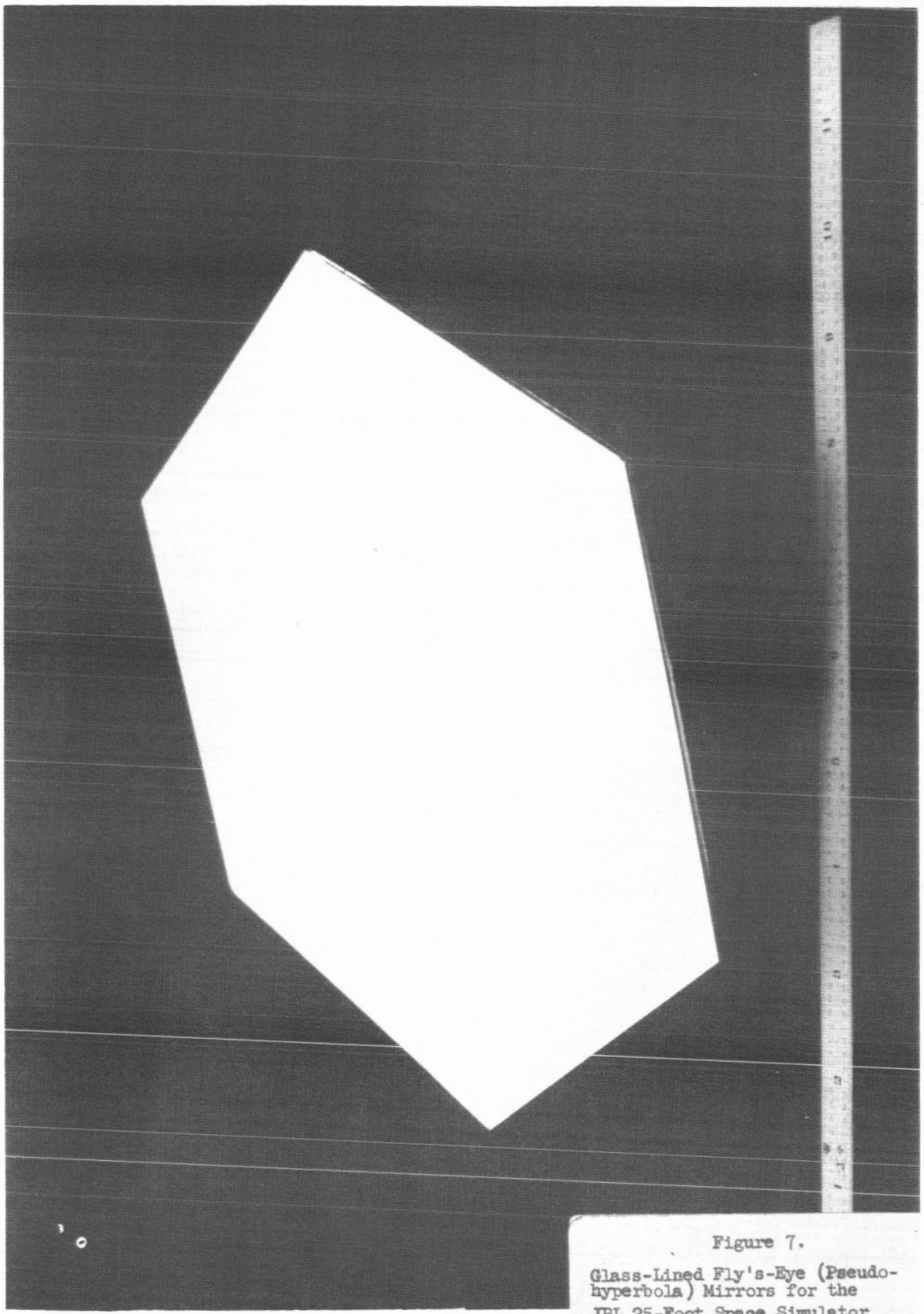

Figure 7.

Glass-Lined Fly's-Eye (Pseudo-hyperbola) Mirrors for the JPL 25-Foot Space Simulator

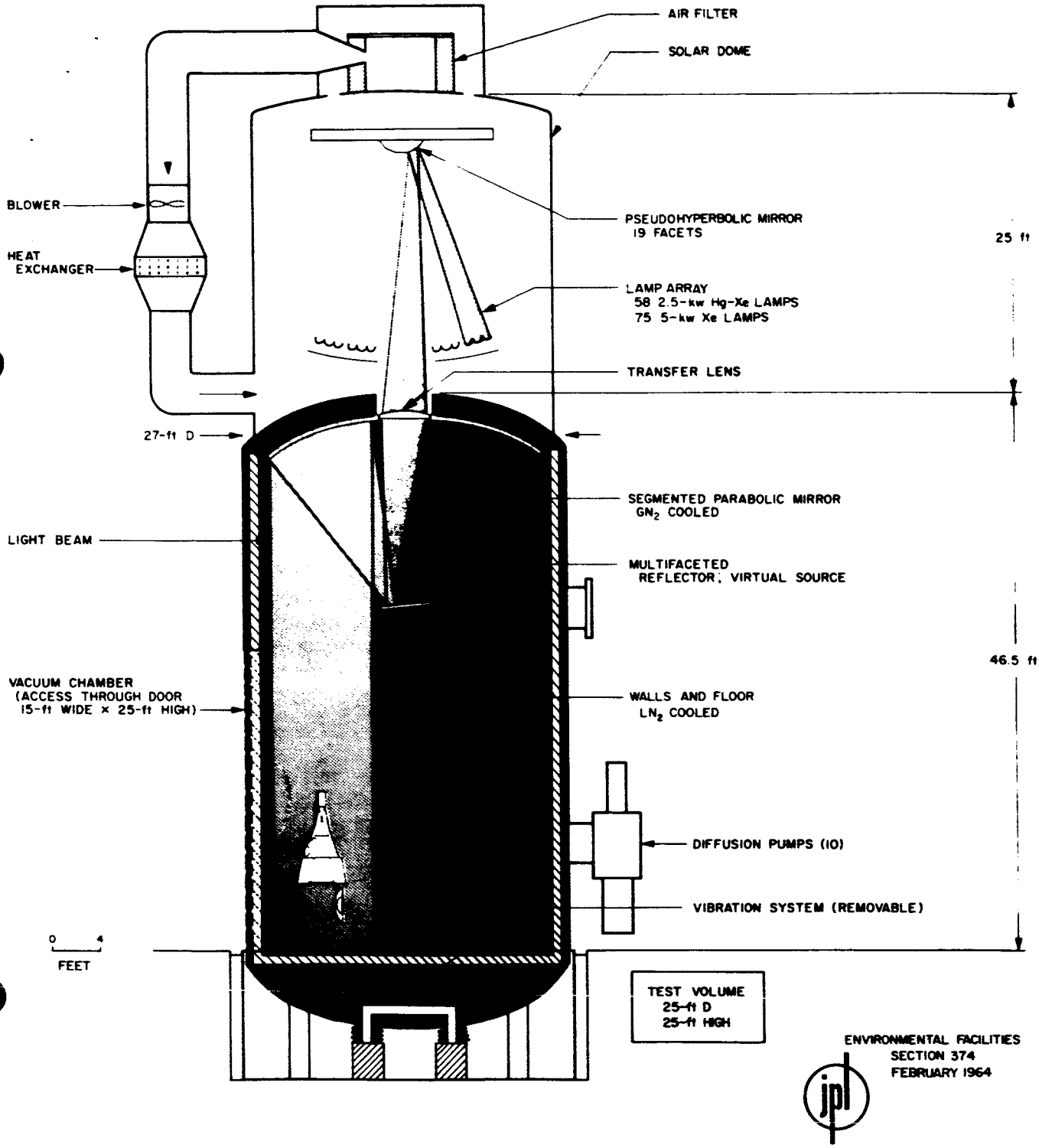

JPL 25-ft SPACE SIMULATOR

Figure 8.

Modified Solar System Proposed for the 25-Foot Space Simulator

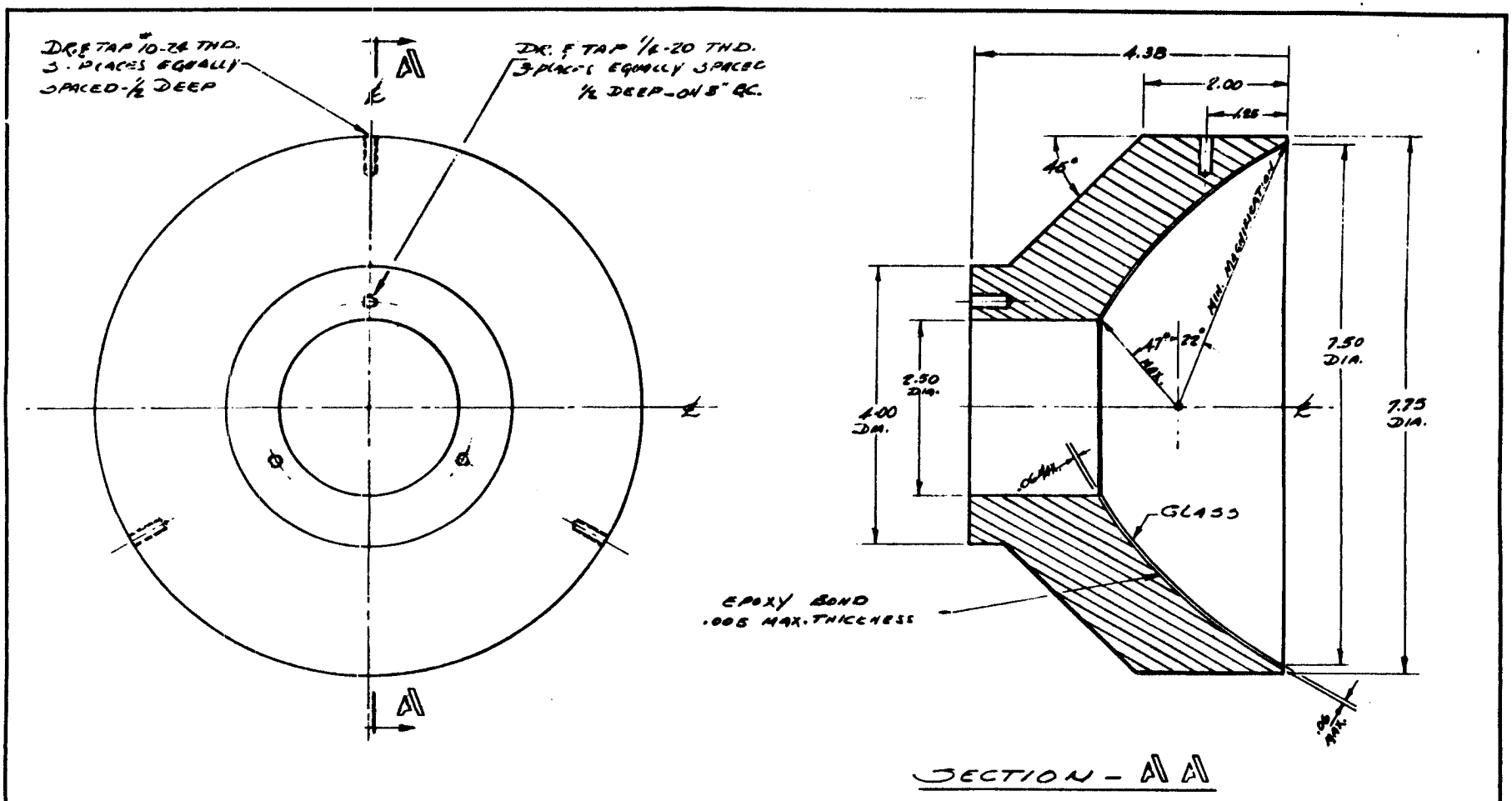

Figure 9.

Detail of 7½-in. Headlamp Reflector

MATERIAL - 6061-T6 ALUM.
FIGURE ELLIPSE - F_1 = 1.3"; F_2-F_1 = 130"
O.D. = 7.5 DIA.; TOLERANCE = ± 2 MIN.

NOTES: MAGNIFICATION = MAX=107, MIN.= 40

PART NO.	NAME	STOCK SIZE	MATERIAL
JET PROPULSION LABORATORY		CALIFORNIA INSTITUTE OF TECHNOLOGY	
7½" DIA. COLLECTOR SOLAR LAMPS 25' SIMULATOR			
UNCLASS	FULL	4-9373667	

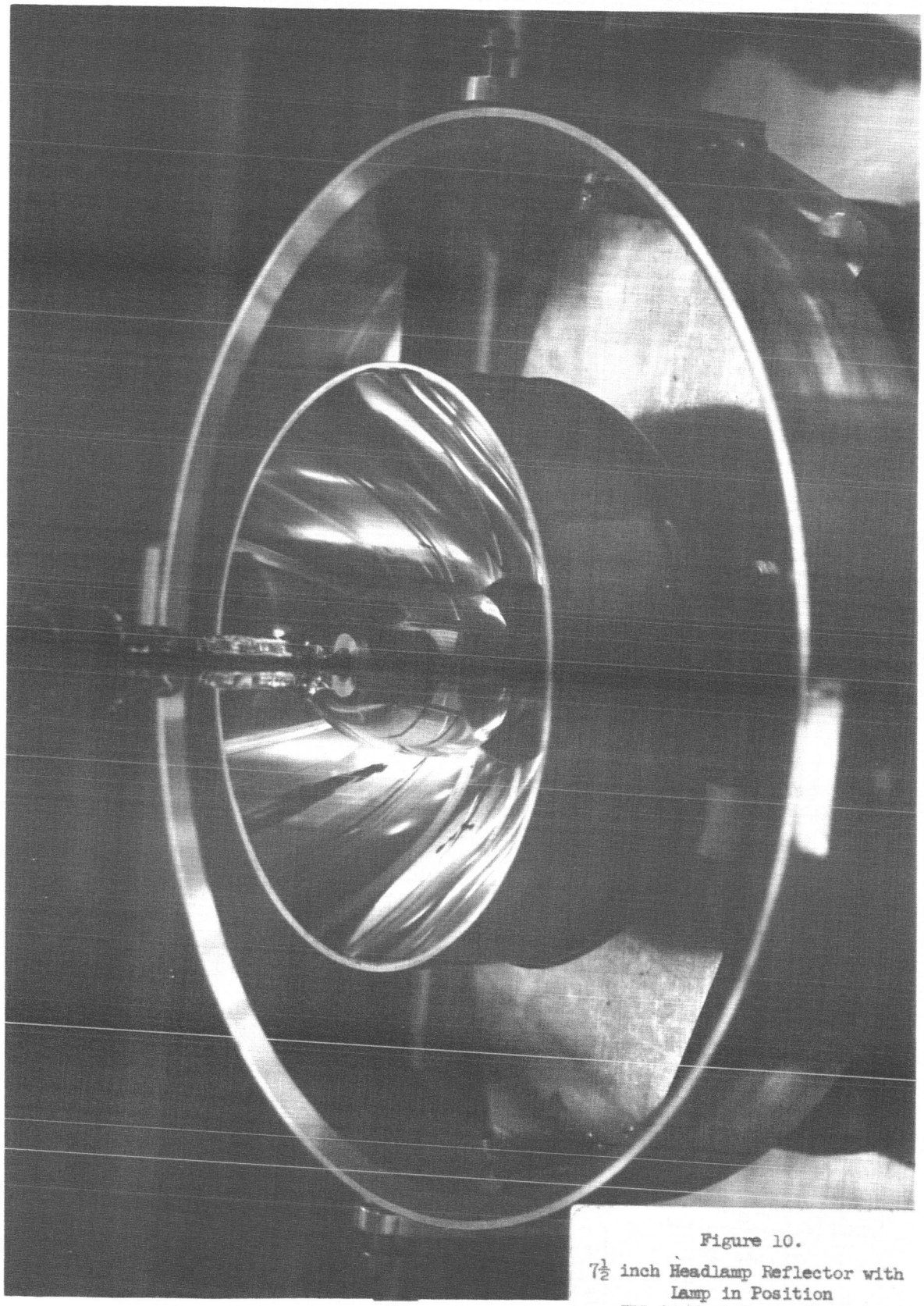

Figure 10.

7½ inch Headlamp Reflector with Lamp in Position JPL 25-Foot Space Simulator

THERMAL TESTING OF THE RANGER BLOCK III SPACECRAFT IN THE JPL 25 FT. SPACE SIMULATOR

Michael E. Kahn

Jet Propulsion Laboratory

In January, 1964, a test program was begun on the thermal design of the Ranger Block III spacecraft. The tests were performed in the newly operational JPL 25' Space Simulator over a period of 6 months. The objectives of these tests were two-fold:

A. To evaluate the 25' Space Simulator as a facility for proving the thermal design of spacecrafts, and

B. To verify the thermal design of the Ranger Block III spacecraft.

These two objectives are complimentary in the test series performed and are difficult to separate into distinct categories. An important part of the first objective was to learn what type of test preparation, instrumentation, and analysis was required for the meaningful evaluation of test data from the 25' Space Simulator tests. Although some experience had been gained in testing of components and incomplete spacecrafts in smaller solar simulation chambers during the early part of the Ranger program, we knew little about testing of a complete spacecraft in the 25' Space Simulator when this test program began.

Test analysis requires that the energy absorbed by various spacecraft components be known. This requires a knowledge of the area of solar absorption or sunlit area, the solar energy flux density

on the area, and the effective absorptance of that area. Most of the problems encountered were associated with the determination of the last two quantities since the sunlit area may be obtained directly by inspection of spacecraft surfaces. This paper will present a discussion of our experiences during the Ranger Block III thermal test series on the Thermal Test Model (TCM). The TCM was thermally equivalent to the flight type Ranger spacecraft except for the lack of an antenna dish and solar panels. Flight type structural hardware was used with surface finishes equivalent to those of the flight spacecraft. Aluminum blocks simulated the spacecraft electronics thermal masses with resistance heaters simulating the electronic power dissipation. The discussion will be presented in a semi-chronological order and will be divided into the following areas:

1. Determination of solar simulation flux density on spacecraft surfaces.
2. Problems related to decollimation of the solar simulation source.
3. Determination of effective absorptance in the solar simulation spectrum.

Determination of Solar Simulation Flux Density

Due to the uncertainties in the flux densities on the spacecraft surfaces resulting from reflections and non-uniformity of the solar simulation source, a detailed mapping of flux densities on the spacecraft was performed before each solar simulation test. The mapping was done under ambient conditions and consisted of readings with a calibrated solar cell at several hundred points on the spacecraft

surfaces for each flux density which was to be used during the vacuum cold-wall portion of the test. Solar cells were used for mapping because of their small size, fast response time, and principally for lack of a better device.

The first test was performed in January of 1963. The test object consisted of a thermal model of the RCA subsystem mounted on a plate which simulated the JPL bus as shown in Figure 1. Before the RCA subsystem was suspended in the chamber, flux density readings were made on the test fixture shown schematically in Figure 2. The discs of the test fixture had diameters equivalent to the fin diameters on the RCA subsystem and were spaced vertically at the proper positions. A solar cell calibrated against an air thermopile was used to measure the flux densities along the edges of each disc. After the RCA subsystem was suspended in the chamber, measurements of flux densities on the fin surfaces were made. When compared with the densities determined from the test fixture, it was found that a large amount of energy was being reflected from the skin of the subsystem to the top of each fin. The calibrated solar cell was used to monitor the flux density at the top of the RCA subsystem thermal model during the mapping and also during the vacuum cold-wall test with solar simulation.

The second test was performed in April of 1963. The test object was the complete TCM, consisting of the RCA subsystem mounted on the JPL bus as shown in Figure 3. For this test an Eppley thermopile was used to monitor the flux density during the mapping and the vacuum cold-wall test with solar simulation. This thermopile was mounted on a boom above the top of the spacecraft. Eight solar cells were mounted

in various locations on the spacecraft for the purpose of checking the mapping data during the vacuum test and also to detect any variations or warping of the solar simulation energy field during the test. During the mapping, calibrated solar cells were used to determine the flux density at each cell location on the spacecraft. It was found that a vacuum calibration was needed in order to check the absolute flux density at each cell location during the vacuum cold-wall test. However, it was possible to check the relative flux densities among the various cells using the air calibration. No warping of the solar simulation energy field was detected. At the completion of the test we still wanted a method of checking the mapping data obtained under ambient conditions with the flux densities encountered during the vacuum tests.

The third test on the TCM was performed in June of 1963. Before the spacecraft was installed in the chamber, ten solar cells were calibrated under vacuum cold-wall conditions against an Eppley thermopile. The test configuration is shown in Figure 4. The cells were mounted on a plate which could be rotated so that each cell could be positioned over the detector of the thermopile. Alternate readings of cell output and thermopile output were recorded for each cell while the temperature of the cells was controlled by a heater mounted on the rotating plate. A difference of approximately 10% in the calibration number was found between the air calibration and the vacuum calibration. The cells were then mounted on the spacecraft as was done in the second test and a thermopile was mounted on top of the spacecraft for flux density monitoring. During the test it was possible to check and verify mapping data obtained under ambient conditions with the flux densities at the cell locations under vacuum conditions.

In mapping, the cell was held horizontally above sunlit areas and held parallel to surfaces which were shaded or vertical. For a horizontal cell (vertical light beam), the mapping data is thought to be accurate to within 7 watts per square foot at one solar constant due to a 3% thermopile tolerance and an instrumentation accuracy of ±1 millivolt. This error could be considerably worse for the shaded or vertical areas due to the questionable reflectance characteristics of the solar cells at high angles of incidence.

Before the third TCM test, it was found that the calibration of the only available thermopile was seriously in doubt. This resulted in a 4-day delay while the thermopile was flown to Eppley Laboratories for recalibration. This experience emphasized the need for a planned calibration program for thermopiles, with back-up thermopiles available before each test, or on-site calibration capability.

Decollimation of the Solar Simulator Source

Before the test of the RCA subsystem thermal model, an attempt was made to evaulate the degree of decollimation of the solar simulator source. A large aperture camera was used to photograph the sun image at the top of the chamber. Measurements of shadow lines on the test fixture mentioned previously were also made. These two investigations indicated an effective decollimation half-angle of 4.7°. When the RCA subsystem was suspended in the chamber and the solar simulation lights turned on, it was found that approximately 40% of the polished aluminum skin was partially illuminated by the "sun" as can be seen in Figure 1. This furnished another check on decollimation half-angle which agreed with the value determined previously.

The results of this test were somewhat disappointing. The RCA subsystem ran approximately 40°C hotter than predicted from the mapping data. It was found that approximately 15.5% of the input energy could not be accounted for even if the absorptance of the skin was taken into account.

Before the first test of the complete TCM, the effective diameter of the RCA fins was increased by the addition of polished aluminum rings to the outside edges of the fins. These rings eliminated the impingement of solar simulation energy on the polished aluminum skin as shown in Figure 5. At the conclusion of this test, RCA was able to account for the input energy to its subsystem to within 2%, a considerable improvement over the results of the first test.

Profiting from RCA's experience on their first test, JPL installed shading strips at the top of its electronic chassis to shade the white painted fronts of these chassis. The fronts of these chassis may be seen in the illuminated condition in Figure 5 and in the shaded condition in Figure 6.

At this time there seems to be some uncertainty as to whether the extension rings should have been added to the RCA subsystem. Ranger 6 flight data indicated that the RCA subsystem ran some 20°C hotter than predicted. To date, no satisfactory correlation has been possible between the data of the first RCA subsystem test without the rings, subsequent TCM tests with the rings, and flight data. Ranger 6 flight data also showed that the JPL electronic chassis ran only a few degrees hotter in flight than had been predicted. This correlation problem is indicative of the difficulties involved in performing

meaningful solar simulation tests of this configuration and meaningfully interpreting data from these tests.

Determination of Effective Absorptance in Solar Simulation Spectrum

At the time these tests were performed, no monochrometer measurements of the 25' Solar Simulator spectrum had been made. This prevented calculation of the effective absorptance of the various spacecraft surfaces in the solar simulation spectrum. Therefore, these absorptances were measured experimentally with the device shown in Figure 7. Under vacuum cold-wall conditions, the six samples and black intensity standard were allowed to come to equilibrium temperature under solar simulation. The solar simulator was then turned off and internal heaters used to duplicate the temperatures obtained in the first part of the test. Calculations were then used to determine the effective absorptance of each sample. The values obtained from these measurements are given in Table 1.

Conclusions

The objective of verifying the Ranger Block III thermal design was largely satisfied in this series of tests. In addition, valuable experience was gained in pretest preparation, instrumentation, and test data analysis. Improvements remain to be made in areas such as mapping devices, better analysis techniques, and better measurements of solar simulation spectrum and absorptances in this spectrum. Hopefully, these improvements will be made within a reasonable period of time.

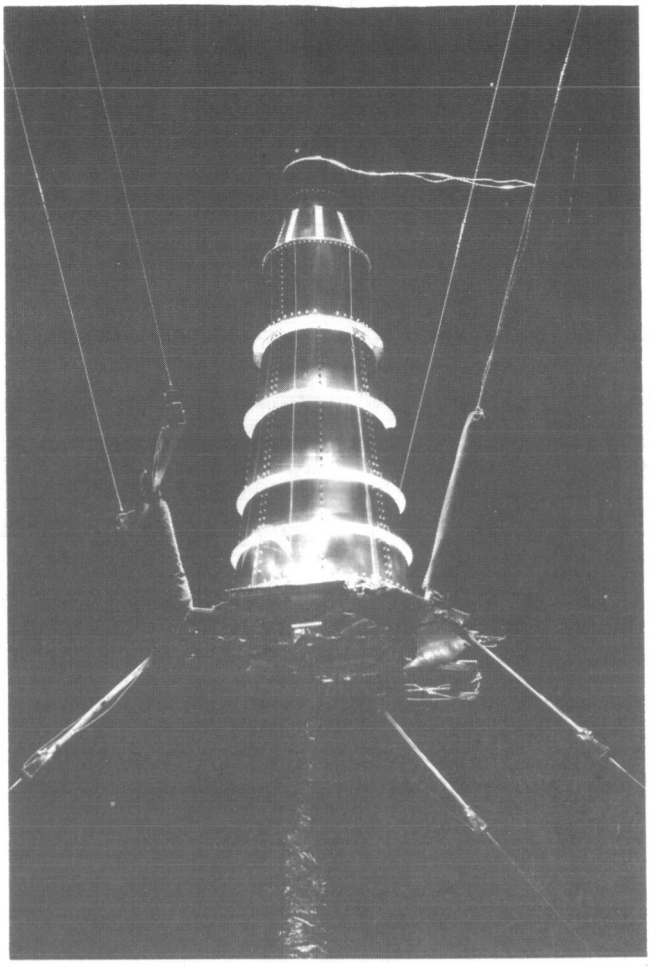

Figure 1. Thermal model of RCA subsystem suspended in JPL 25' Space Simulator for first test, January, 1963. Photograph taken with solar simulation lights on.

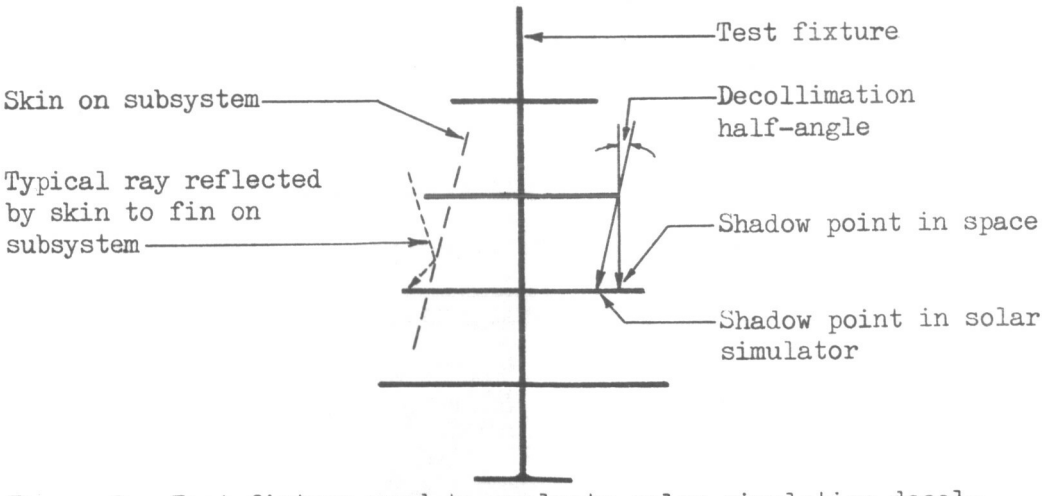

Figure 2. Test fixture used to evaluate solar simulation decollimation half-angle and amount of energy incident on RCA subsystem fins due to reflection from skin.

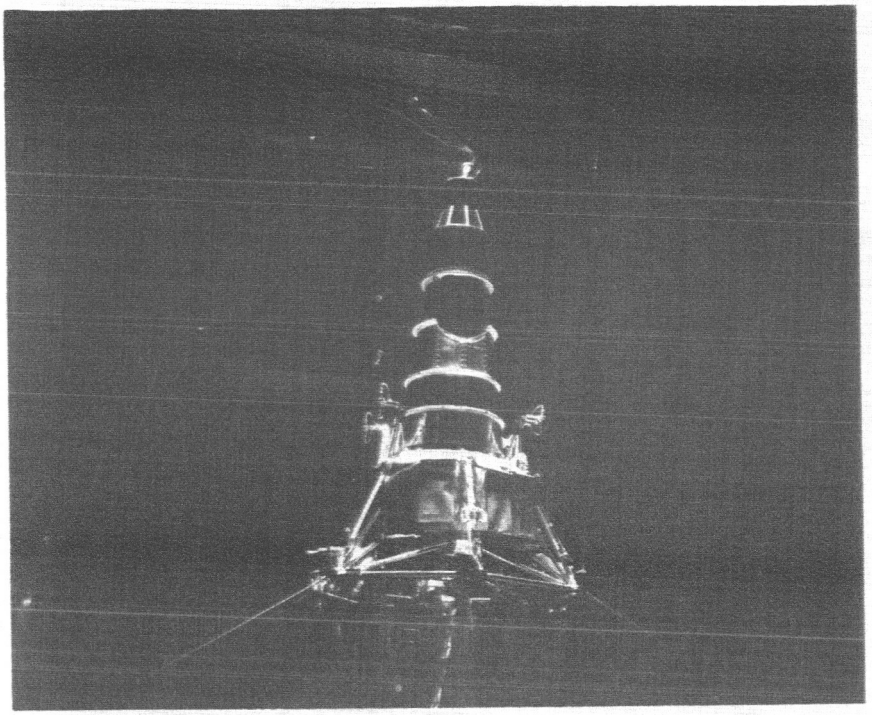

Figure 3. Ranger Block III TCM in JPL 25' Space Simulator.

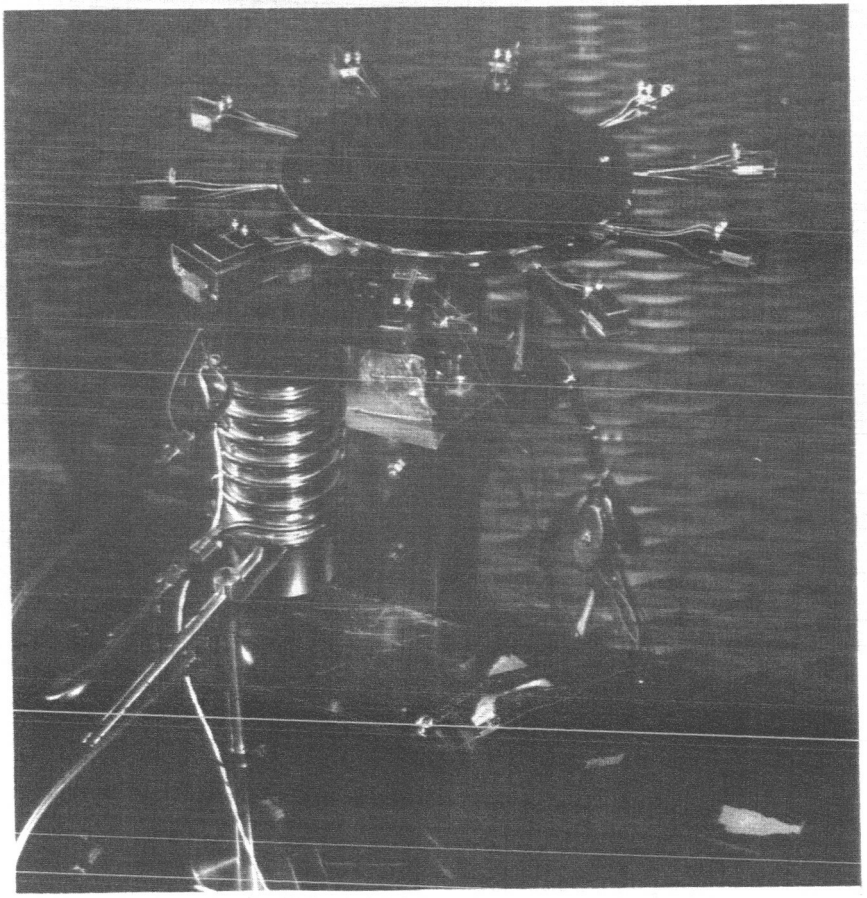

Figure 4. Apparatus used to calibrate solar cells against Eppley thermopile under vacuum conditions with solar simulation.

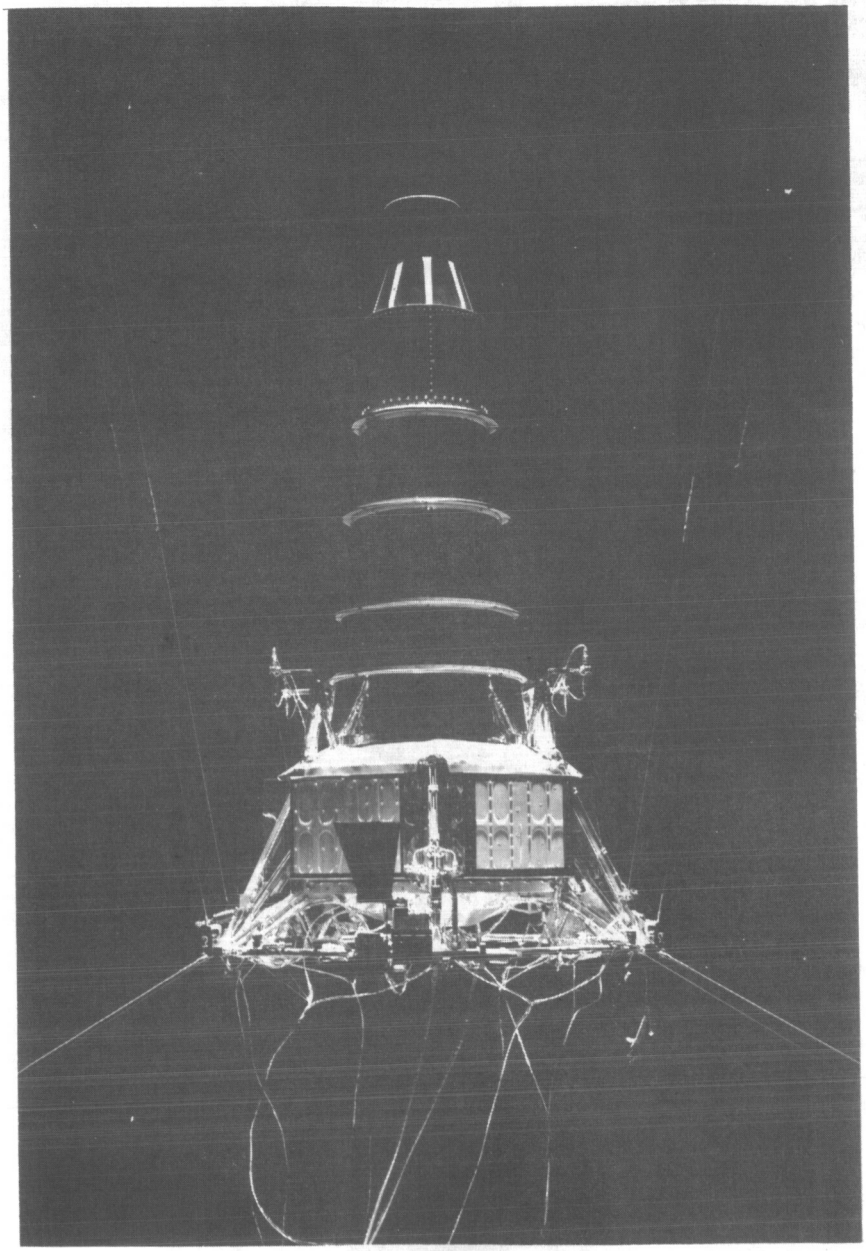

Figure 5. TCM after addition of fin extension rings on RCA subsystem but before addition of shading strips on top of JPL electronic chassis. Photograph taken with solar simulation lights turned on.

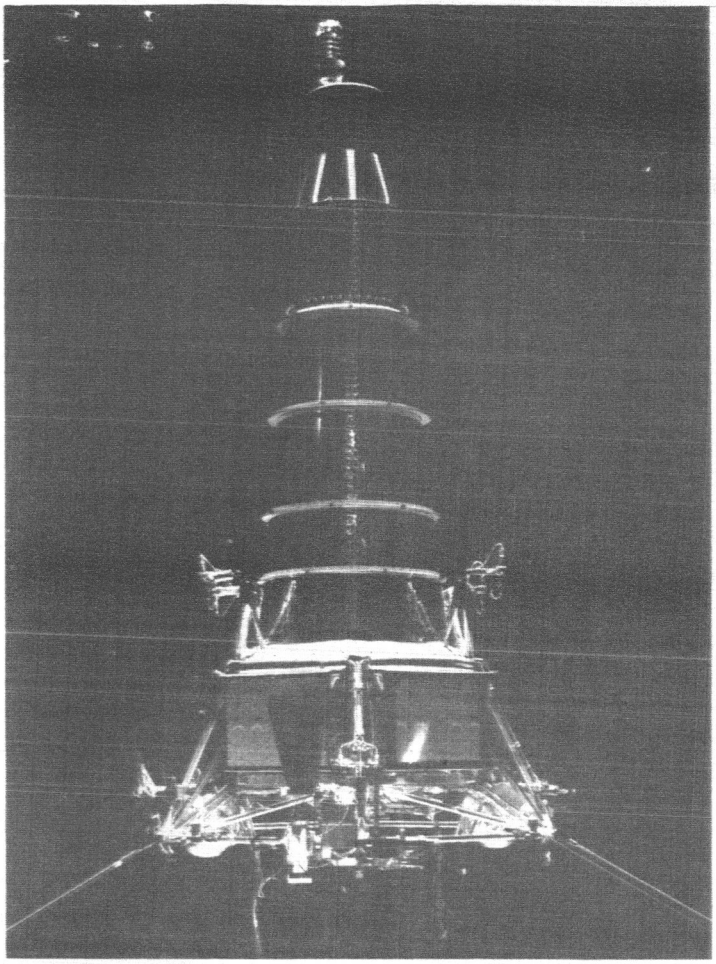

Figure 6. TCM after addition of fin extension rings on RCA subsystem and shading strips on top of JPL electronic chassis. Note thermopile mounted on top of spacecraft for intensity monitoring. Photograph taken with solar simulation lights on.

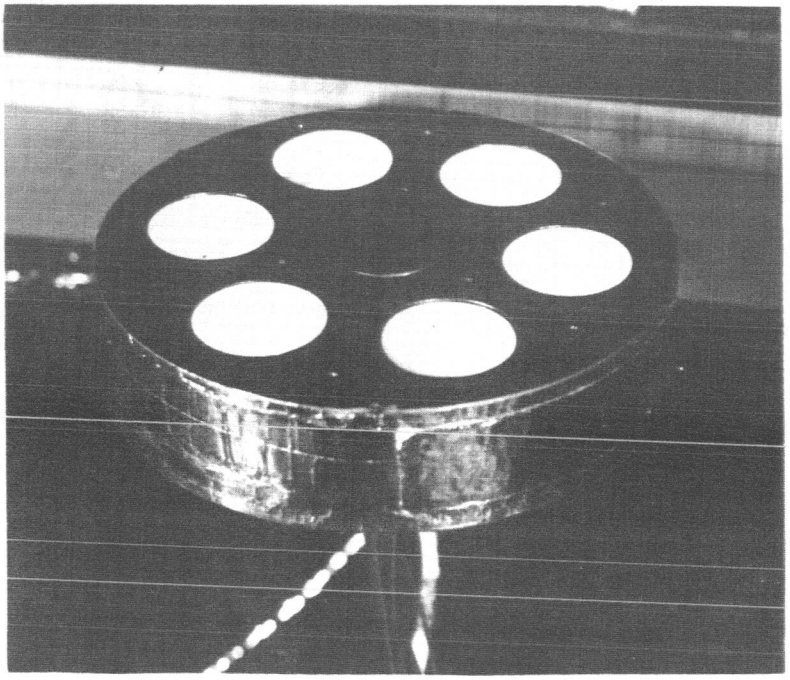

Figure 7. Device for measurement of absorptance in solar simulation spectrum. 1" diameter samples.

TABLE 1

Comparison of Measured Absorptance in 25' Space Simulator Hg-Xe Spectrum and Calculated Solar Absorptance for Several Surface Treatments

Surface	Hg-Xe	Solar	Error
Polished Aluminum	0.21	0.19	+11%
Polished Gold Plate	0.26	0.22	+20%
PV 100 White Paint	0.31	0.22	+41%
JW 40 White Paint	0.39	0.23	+70%
Cat-a-lac Black Paint	0.96	0.96	0%

NATIONAL AERONAUTICS AND SPACE ADMINISTRATION

MANNED SPACECRAFT CENTER

Clear Lake, Harris County, Texas

SOLAR SIMULATION IN THE MSC SPACE ENVIRONMENT SIMULATION LABORATORY

By

Joseph A. Muller

NASA Conference on Space Vehicle Thermal Radiation and Temperature Control

April 7-8, 1964

SOLAR SIMULATION

IN THE MSC

SPACE ENVIRONMENT SIMULATION LABORATORY

Abstract

The MSC Solar Simulator history and requirements for the Space Environment Simulation Laboratory (SESL) are briefly reviewed. A description is presented of the SESL, and a discussion is included of the solar simulator development and present status.

A Radiant Intensity Measuring System for the SESL is briefly described.

Introduction

Solar simulation activities at the MSC were initiated when a decision was made to construct the Space Environment Simulation Laboratory (SESL) for testing the Apollo spacecraft. The SESL includes two large space environment chambers designated Chambers "A" and "B"; Chamber "A" includes a top and side "sun" and Chamber "B" a top "sun" only. In addition to the solar simulators, a Radiant Intensity Measuring System (RIMS) is being provided for monitoring and calibrating the "suns" in both chambers. Plans for the "RIMS" have progressed from the conceptional design stage to fabrication of a pilot model system to be proof tested in a small environmental chamber that simulates the environment of chambers "A" and "B".

A contract for design, fabrication, and installation of complete solar simulator systems for Chambers "A" and "B" was awarded to the RCA Service Company in December 1962. The original design was based on an upgraded version of the Mark I prototype Solar Simulator Module then being planned for the AEDC at Tullahoma, Tennessee. The MSC system is modular in concept and resembles the original Mark I superficially. However, the MSC version will illuminate approximately four times the area of the Mark I. The development of the MSC module to its present status has required an extensive and continuing process of redesign and improvement of the original concept, particularly with respect to the carbon arc source and mirror fabrication. The radiant source, for example, has evolved to the point where it now represents a combination of a plasma arc and a conventional carbon arc.

SESL DESCRIPTION

The SESL chamber building shown in Figure 1 is a high-bay structure which houses the two large man-rated Space Environment Simulation Chambers, related services, and work areas. The larger of the two chambers provides simulated space and lunar surface environments and is primarily intended for combined tests involving men and operating Apollo spacecraft. The smaller space chamber will be utilized for life systems and astronaut training studies in addition to tests of single modules of the Apollo spacecraft.

Chamber "A" is a 65-foot diameter stainless steel vessel having an overall height of 120 feet. The chamber will handle a spacecraft of up to approximately 75 feet in height and 25 feet in diameter. There are four individually operated 25-ton hoists located above the top head of the vessel. The lifting hooks may be lowered through the removable sections in the top head.

Chamber "A" will support a spacecraft weight of 150,000 pounds in a vertical position on a rotating platform (lunar plane) 45 feet in diameter. The lunar plane rotation ($\pm 180^{\circ}$) can be controlled, manually or automatically, to a maximum rotational speed of 1-2/3 rpm. The lunar plane surface temperature can be controlled from 80°K to 400°K.

A side-hinged door for vehicle loading is located in the cylindrical section of the vessel with the bottom of the opening approximately four feet above the lunar plane level. The door provides a 40-foot diameter clear opening. The door is hydraulically opened, closed, and clamped from a remote control panel.

The chamber interior will be equipped with guarded walkways around the perimeter at the mid-manlock level and the upper manlock levels.

The chamber vacuum system consists of a combination of mechanical and diffusion pumps and a 20°K cryopump using gaseous helium. The chamber will pump down to 1×10^{-5} torr in nineteen hours with a gas leak load of 2/.6 torr-liters/sec.

The interior of the chamber is lined with black, nitrogen-cooled heat sink panels which will operate at approximately 80°K. To the maximum practical extent, all surfaces in the chamber viewed by the vehicle consist of heat sink panels. Cryopump surfaces, cooled by gaseous helium, are shielded from the test vehicle by heat sink panels.

Solar simulators of modular design are mounted external to the chamber walls on its side and top. The simulators irradiate the vehicle through penetrations in the wall with an intensity which can be controlled in the range from 00 to 137 watts/sq. ft. The solar simulators feature a

wavelength range from approximately 0.25 to 3.0 microns. The target area of the side sun is 13 feet wide by 33 feet high, expandable to 20 feet wide by 65 feet high. The target area of the top sun is 13 feet in diameter, expandable to 20 feet in diameter.

Chamber "B" is a 35-foot diameter stainless steel vessel having an overall height of 43 feet. The chamber will handle a maximum sized vehicle of 13 feet in diameter and 27 feet in length. Vehicle access is provided by a removable top head. A rolling bridge crane with a capacity of 50 tons will be utilized to remove the chamber head or insert spacecraft into the test chamber.

Chamber "B" will support a spacecraft weight of 75,000 pounds on a fixed simulated lunar plane 20 feet in diameter. The lunar plane surface temperature can be controlled from $80^{\circ}K$ to $400^{\circ}K$.

There will be one double manlock at the lunar plane level with the same provisions established for Chamber "A" manlocks.

The chamber vacuum system will consist of a combination of mechanical and diffusion pumps. The chamber will pump down to 1×10^{-4} torr in $3\frac{1}{2}$ hours with a gas load of 25.6 torr-liters/sec.

The heat sink description for Chamber "A" is applicable to Chamber "B". The Chamber "B" solar simulators are the same type as for Chamber "A". The target area for the top sun is 5.6 feet in diameter, expandable to 20 feet in diameter.

SOLAR SIMULATOR REQUIREMENTS

The following requirements were established after an investigation into the state-of-the-art:

FLUX DENSITY - 60 to 137 watts/sq. ft.

UNIFORMITY - $\pm$5 percent with 1.0 $ft.^2$ detector

$\pm$10 percent with 0.1 $ft.^2$ detector

SPECTRUM - Carbon arc

DECOLLIMATION - Less than $\pm$2 degrees

The final decollimation angle is expected to be considerably less than ±2 degrees. Present indications are that it will be near ±1 degree.

SOLAR SIMULATOR MODULES

General Description

The present Solar Simulator System consists of 80 modules, 73 in Chamber "A" and 7 in Chamber "B". The overall module length is 175 inches and the weight is estimated to be about 1,200 pounds. The modules will be supported by a structure which is completely separate from the chamber wall. Connections at the chamber wall for vacuum purposes are by flexible stainless steel bellows.

Optical System

The optical system shown in Figure 2 consists of two parts; a collector and a collimator assembly. The primary collector mirror and lens accept radiant energy over a 110-degree angle. Part of the radiant beam is reflected to the secondary collector mirror and is brought to a focus at the focal point of the collimator which is a modified cassegrain assembly. This assembly directs the radiant beam into the vacuum chamber. All of the mirrors are metal with aluminum coatings. Another part of the radiant beam is transmitted by refractors into the chamber. All refractor optics are quartz except the field lens and vacuum seal windows which are sapphire. The field lens and vacuum window are located essentially at the collimator focal point.

The refractor elements are utilized to prevent shadow formation by the cassegrain secondary mirror. Quartz flash plates are provided at a short distance in front of the radiant source to prevent degradation of optical components resulting from arc startup or sputtering during operations.

Module Operations

The mechanical arrangement is shown in Figure 3. The carbon arc burner assembly, along with the automatic feed system, intensity control aperture, and all other electronic and mechanical components, exclusive of the collimator assembly, are located outside the vacuum chambers.

The positive electrodes in the arc burner consist of 16mm diameter carbon rods. The negative electrode is a nonconsumable tungsten rod which is bathed in an inert gas to prevent oxidation.

The carbon electrode magazine in each solar simulator module is cylindrical and has tubular compartments that hold a 24-hour supply of carbons. Carbons are fed into an automatic joining device, through water-cooled copper jaws, and positioned at the focal point of the primary collector. Servo systems provide electrode position and module intensity control. The intensity control system consists of a variable aperture operated by a small servo motor and a photovoltaic detector. The aperture and servo motor are located approximately at the field lens and the intensity detector is located on one of the collimator support vanes in the vacuum chamber. All module components mounted outside the vacuum chamber are removable as a unit from the rear of the module for maintenance and calibration. In addition, all parts are interchangeable. The utilities are coupled at the rear of each module with quick disconnect junctions. Utility connections include the inert gas, water, and air inlets and outlets, and power. The power required is approximately 32 kw (400 amps at 80 volts). The air supply is circulated past the arc, mixes with the inert gas (either argon or nitrogen), and both gases are drawn out the rear of the module. The arc burner portion of each module is maintained at a temperature of 100°F or less by a water-cooled panel enclosure.

SOLAR SIMULATOR MODULE DEVELOPMENT

Status

A prototype solar simulator arc burner assembly, along with an automatic feed mechanism, has been fabricated and is undergoing development and operational tests to determine reliability factors and to eliminate design deficiencies. In addition to this burner, a total of three prototypes are being fabricated and will be utilized in simultaneous tests involving the various phases of a reliability program. The reliability program is divided into three categories:

1. Arc burner testing, which is currently underway. This will be concluded after a 1000-hour life test which was initiated recently. The 1000-hour test consists of four 250-hour tests. The module will be vertical for half the tests and horizontal for the other half.

2. Testing of a burner with optics under ambient conditions.

3. Environmental testing of a complete prototype module in environmental Chamber "E" at MSC, NASA. Chamber "E", which has a test volume of approximately $3\frac{1}{2}$ feet diameter by 6 feet in length, will be utilized to simulate the environments of Chambers "A" and "B".

A three-module cluster test will be performed subsequent to the 1000-hour life test and the environmental test. The optical elements for the three prototypes have been completed and are currently being installed on the burner assemblies. Development of the solar simulator prototype module to its present status has evolved some new concepts in optical design, radiant source operation, and optical alignment.

Radiant Source

The initial MSC design used a positive and negative carbon. During the course of module development, a new radiant source has been devised which has resulted in elimination of the negative carbon electrode. This carbon-tungsten source offers a number of significant advantages including:

1. Enhancement of reliability and reduction in maintenance through elimination of the complex negative carbon handler, feed mechanism, negative jaw, and positioning devices.

2. Reduction in positive electrode consumption by about 12 percent.

3. Elimination of light blockage by the negative carbon rod handler and jaw.

4. Reduction of carbon residue contamination by about 5 to 7 percent.

5. No module shutdown every 24 hours, which was required for negative carbon replacement.

The possible effects on spectral distribution caused by use of tungsten and an inert gas was investigated immediately following source development. Results of this study are shown in Figure 4. The spectral distribution of radiant energy of the carbon-tungsten arc using either argon-air or nitrogen and air is essentially the same as that of the carbon-carbon arc burning in air. The curve was obtained with an Eppley normal incidence pyroheliometer together with a series of interference filters. An NBS standard lamp was used during instrument calibration. The use of nitrogen does not produce as good a spectral match as argon; however, further economies could be realized by its use, if test requirements permit.

CARBON ELECTRODE DEVELOPMENT

The 16mm rod used in the MSC solar simulator module is referred to as a "hard pin" carbon. The core and shell are separately extruded and baked,

and then the core is inserted into the shell with a looseness of at least 0.005". This permits some differential expansion and core gases can escape without breaking the shell. The core is primarily a mixture of rare earth oxides (the rare earths are in the ratio of the normally mined rare earth ones), carbon, tungsten boride, potassium nitrate, and low temperature binders.

Two methods of extrusion of the core and shell material are used. One is the continuous screw type feed extrusion which is used for high production. This method usually results in a more uniform product material than the second method which hydraulically extrudes a single charge of material of $\frac{1}{4}$ to $\frac{1}{2}$ cubic feet in volume. The latter is the method presently being used on the 16mm rods because of production requirements.

It has been determined that the MSC module requires the following dimensions for carbon electrodes:

DIAMETER - 0.630 inches $\pm$0.002 inches

LENGTH - 25 inches $\pm$0.0625 inches

STRAIGHTNESS OR MAX. DEVIATION FROM A STRAIGHT LINE - one mil/inch of length

Although extensive improvements have recently been made on 16mm carbons, problems still exist in maintaining the required dimensional tolerances. Excess bow or thread misalignment are causes for malfunctions of the rod burning and changing mechanisms. The problem is a mechanical one and should be overcome by improved quality control during rod manufacture.

A spectrographic analysis has been made of the residue which collects in the exhaust system. This analysis indicated that the sputter material is basically rare earth compounds plus small amounts of yttrium and iron. The carbon supplier believes that the core binder material is probably the primary cause of arc sputtering. An effort is being made to improve this situation.

The MSC, NASA is in the process of funding a program to optimize 16mm positive carbon physical and operational characteristics, particularly with respect to the operation of solar simulators for Chambers "A" and "B". The program includes study and improvements in:

1. Physical dimensions
2. Carbon threading techniques
3. Reduction of arc sputtering and residue contamination
4. Increased operating power range

5. Spectral match

6. Constancy of burning

7. Quality control for production carbons

MIRROR FABRICATION

A study has been made of the various fabrication materials and techniques to determine which mirror types can withstand the Thermal-Vacuum environment and retain the necessary optical figure. As a result of this effort, mirrors for the three prototype modules have been fabricated of stainless steel. The secondary collector mirrors will be fabricated from wrought stainless steel plate. This is being done to minimize the substrate porosity and is possible for these mirrors because of their small curvature. The primary collector and collimator mirrors are made from 400 Series stainless steel sand castings. All mirrors were turned on a lathe and were individually ground and polished. These mirrors are of excellent quality and have an accuracy of 3 to 4 minutes of arc; however, their fabrication costs are relatively high.

RCA has recently given Electro Optical Systems Incorporated a contract to develop the means for mounting, cutting, and performing all operations for the primary collimator mirror from a 60-inch master by electro-formed replication. Comparative measurements of master and replica will be made to evaluate the adequacy of this technique, which is professed to have advanced in sufficient degree to solve the mirror replication problem. Also, tests are now being performed on an F/0.3, 23-inch diameter mirror of 2.0 minute accuracy, mounted by an EOS RTV11 aluminum structure. RTV11 refers to an arrangement whereby an electro-formed mirror is attached to an aluminum backup structure by a silicone elastomer. The tests will determine the adequacy of this configuration for the collector system.

Mirror supports for the cassegrain collimator are presently made of Invar. The weight of each support vane is relatively high (67 pounds), therefore, these supports will probably be replaced with aluminum to reduce the weight of this assembly. Uniformity of intensity and intensity measurements on the prototype modules will be performed under ambient conditions at the contractor's plant, Camden, New Jersey.

Mirror Cooling Techniques

Provisions for mirror cooling were not incorporated in the initial design; however, a review and subsequent reevaluation of the heating problems involved has resulted in a scheme to utilize water cooling for the secondary collimator mirror and emittance enhancement coatings for the primary

collimator mirror. The secondary mirror will be spirally grooved on its rear face with a closure plate provided for containment and sealed by "O" ring seals. Coupling tubing is fed through headers in each module and is routed in the shadow of the support vanes to eliminate obscurations.

Tests on emittance enhancement coatings have recently been completed. A total of 23 coating specimens were subjected in sequence to the following endurance cycle:

1. Cold soak at $77^{\circ}K$.
2. Irradiance of 2300 w/ft^2 for 8 hours at a controlled temperature of $170^{\circ}F$ and an environmental vacuum of 10^{-6} torr.
3. Film adherence and abrasion testing by scotch tape stripping, and by rubbing across each coating 200 times with a 3/8" diameter pad of cheesecloth $\frac{1}{2}$" thick bearing with a force of one pound.
4. Air bake at a temperature of $460^{\circ}F$.

An examination of the coatings was made by optical measurements, microphotographs, and visible comparison of the change in thin film characteristics. From the studies thus far, it was concluded that highly oxidized SiO coatings over aluminum protected by a Cr barrier coat on substrates cleaned by a bakeout cycle are comparable to the quartz coated aluminum, and should be used where thermal controls are needed (for example, in the vacuum environment). The quartz coated aluminum should be used where thermal control is not required.

AUTOMATIC FEED MECHANISM

The development test program for the automatic feed mechanism has succeeded in eliminating the majority of problems associated with this subsystem. The carbon jaw consists of two water-cooled copper blocks that form each half of the jaw. Two hemispherical silver inserts are used for electrical contacts. Mechanical wear and erosion of these inserts has been reduced significantly by widening the gap between jaws and allowing electrical contact only in the area of maximum cooling. Development is continuing in this area.

Substantial improvement has also been made in minimizing carbon dust accumulation. To reduce dust accumulation in the positive jaw and throughout the mechanism, covers have been placed over the carbon electrode at the threader and at the positive drive. At the latter position,

the rod is scraped to remove loose dust before it enters the jaw. Results thus far appear good.

SOLAR SIMULATOR MODULE ALIGNMENT

The problems associated with alignment are compounded because of the quantity of units involved and a requirement that alignment (and realignment) must be accomplished in the shortest possible time. The optical relationships of elements in a single module can be critically adjusted in the laboratory, but the alignment of one module with respect to another can be done only in the chamber. A special fixture has been designed for alignment of modules during installation. This fixture has been designed to clamp onto the fill-in lens cell casting of the collimator assembly. The fixture consists of three telescoping arms, each containing a pentaprism, an infinity-corrected telescope together with an auto-collimator eyepiece. The three telescoping arms serve a two-fold purpose; they provide a triplecheck on each module to eliminate zonal irregularities and they also permit alignment of two modules adjacent to a reference module.

RADIANT INTENSITY MEASURING SYSTEM (RIMS)

The RIMS will pretest calibrate the solar simulators and monitor the target radiant energy during tests. Traversing bars with radiometers mounted thereon will survey the target areas in Chambers "A" and "B". The system concept for Chamber "A" top and side "suns" is shown in Figures 5 and 6. Several cathode-ray tubes will display average intensities as a ratio of one solar constant for selected test zones.

A test operator will have the capability of selecting an automatic or manual model of radiometer bar traverse. In the automatic position, the bar will traverse the entire irradiated area, sending signals to the cathode-ray data display tube. In theevent of an out-of-limit intensity signal during the automatic mode, the test operator has the option of selecting a manual mode of operation for a more critical survey. Radiometer characteristics are shown in Figure 7.

A pilot model similar to the RIMS is being designed by MSC for use in environment Chamber "E". Operation of the pilot model will serve to minimize design deficiencies in the RIMS for Chambers "A" and "B". This pilot model is scheduled for completion in May 1964.

CONCLUSIONS

The MSC Solar Simulators contain a relatively large number of mechanical and electronic components. The reliability factors of these components have not yet been determined. It is apparent that this will be one of the most critical areas of module development; therefore, extensive efforts are being made to increase reliability through a comprehensive program of testing. The reduction in positive electrode burning rate, through use of the inert gas and tungsten rod, has been one step in the overall program to increase reliability. The reduced burning rate will result in less maintenance required for the automatic feed mechanism.

Improvements in carbon electrodes would also result in greater operational reliability. It is believed that the use of the continuous extrusion method to obtain large production orders will achieve much greater uniformity between carbons. This technique, combined with the MSC program for improving other carbon characteristics, should result in more efficient and reliable solar simulator operation.

Successful completion of the solar simulators on schedule will depend, to a great extent, on problems that may be encountered during optical system testing. These tests are scheduled to begin in April 1964. Solar simulator installation and checkout for Chamber "B" is schedule for completion in September 1964. Completion of solar simulation for Chamber "A" is scheduled for January 1, 1965.

NASA
S-63-4970

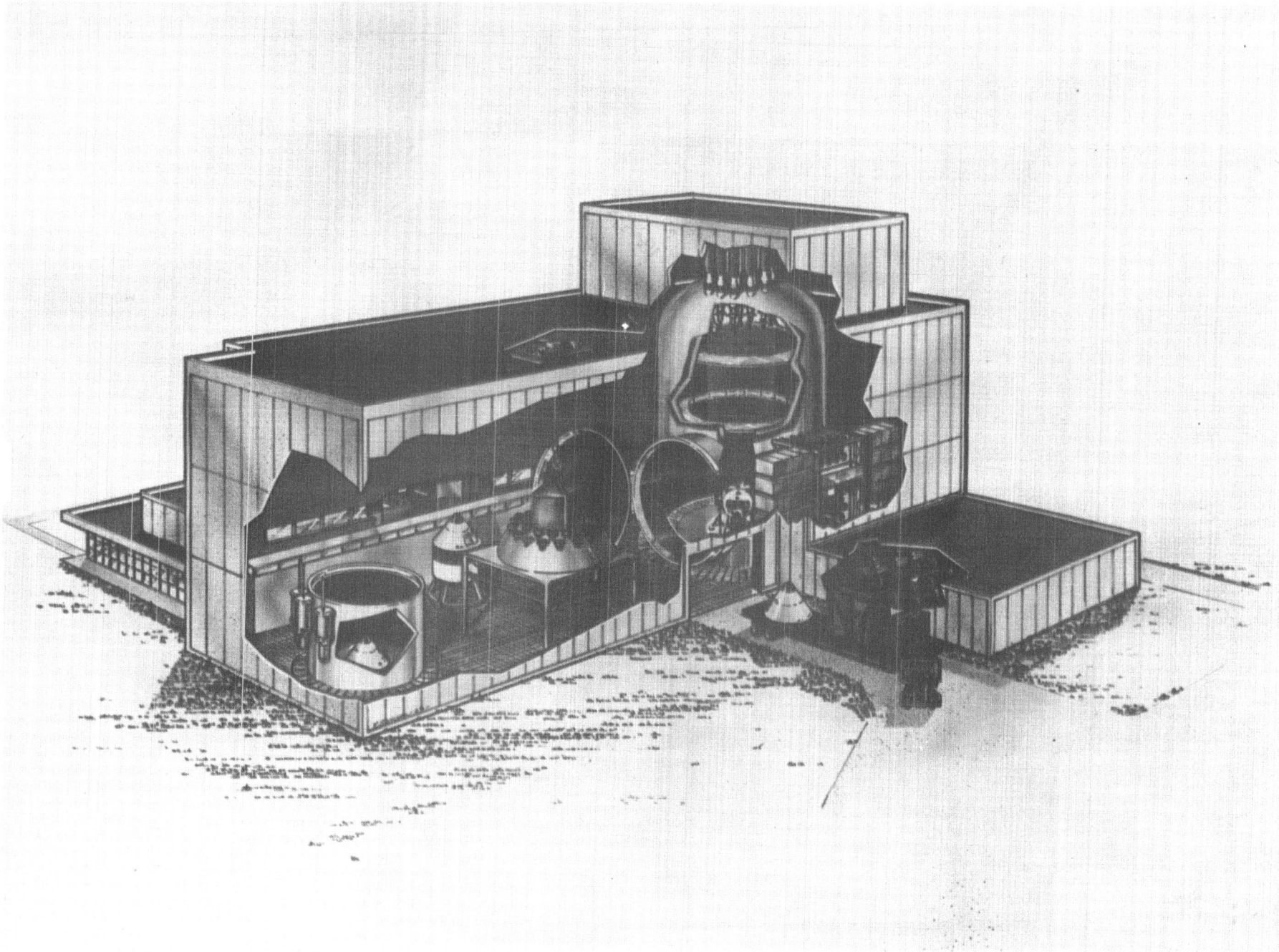

Figure 1

SOLAR SIMULATOR MODULE

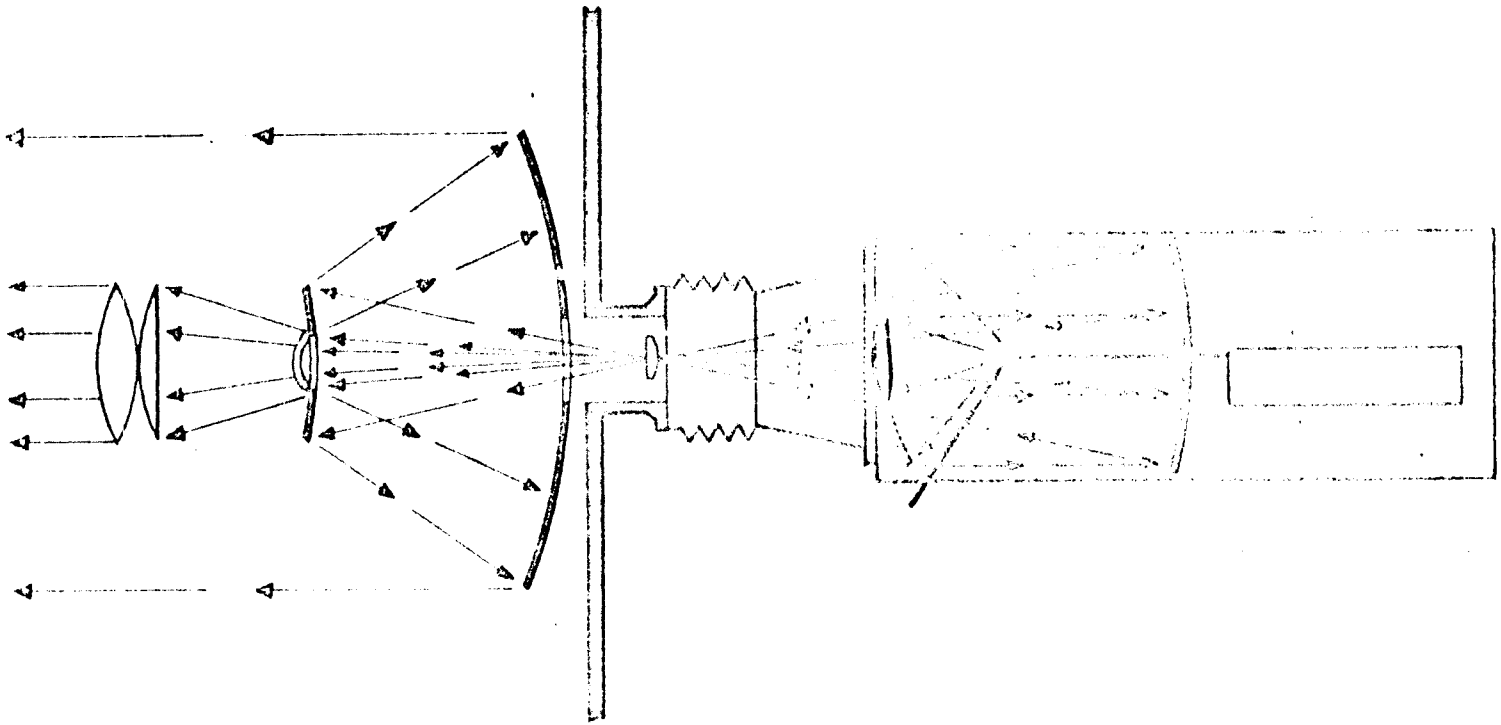

Figure 2

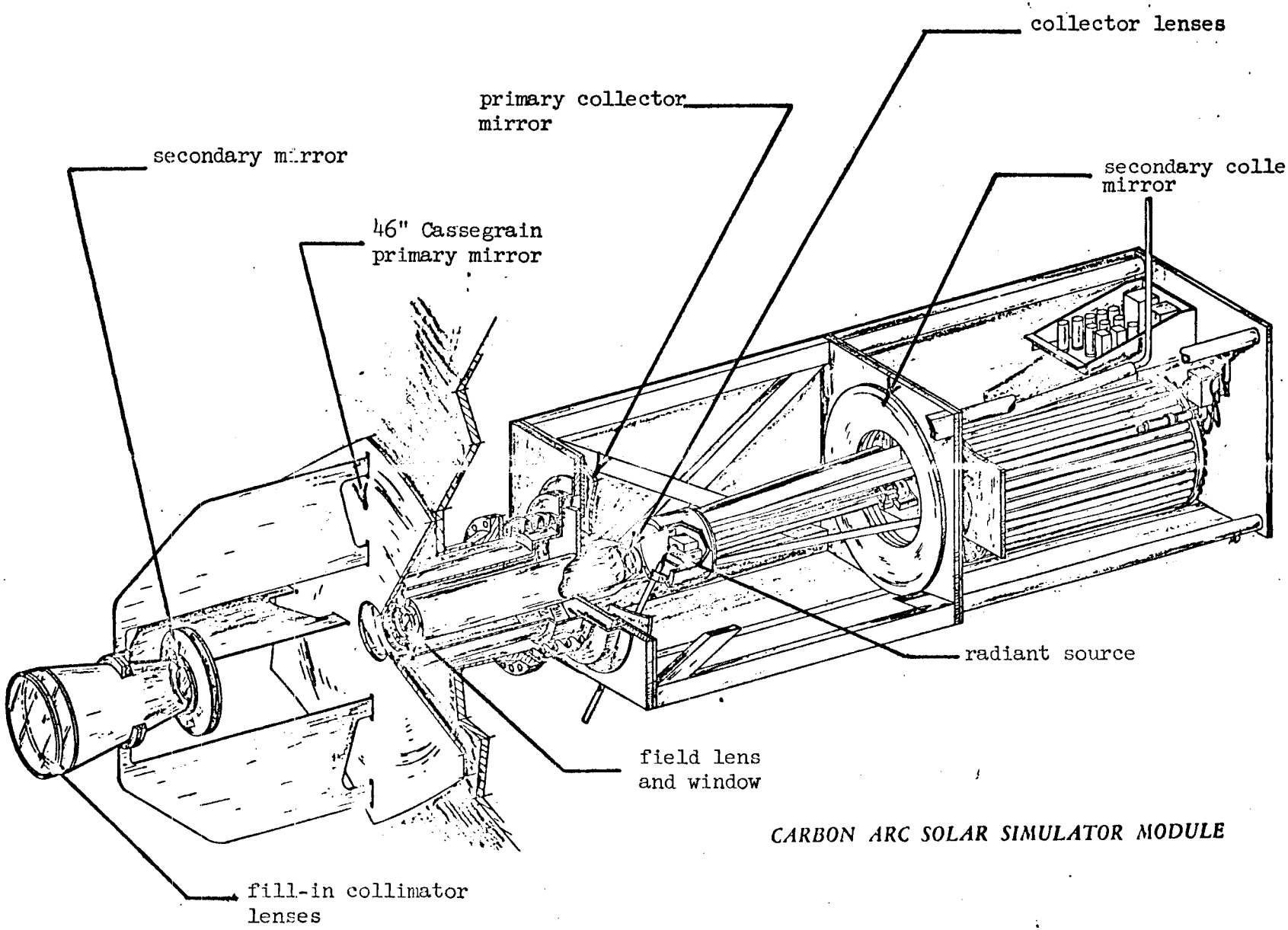

Figure 3

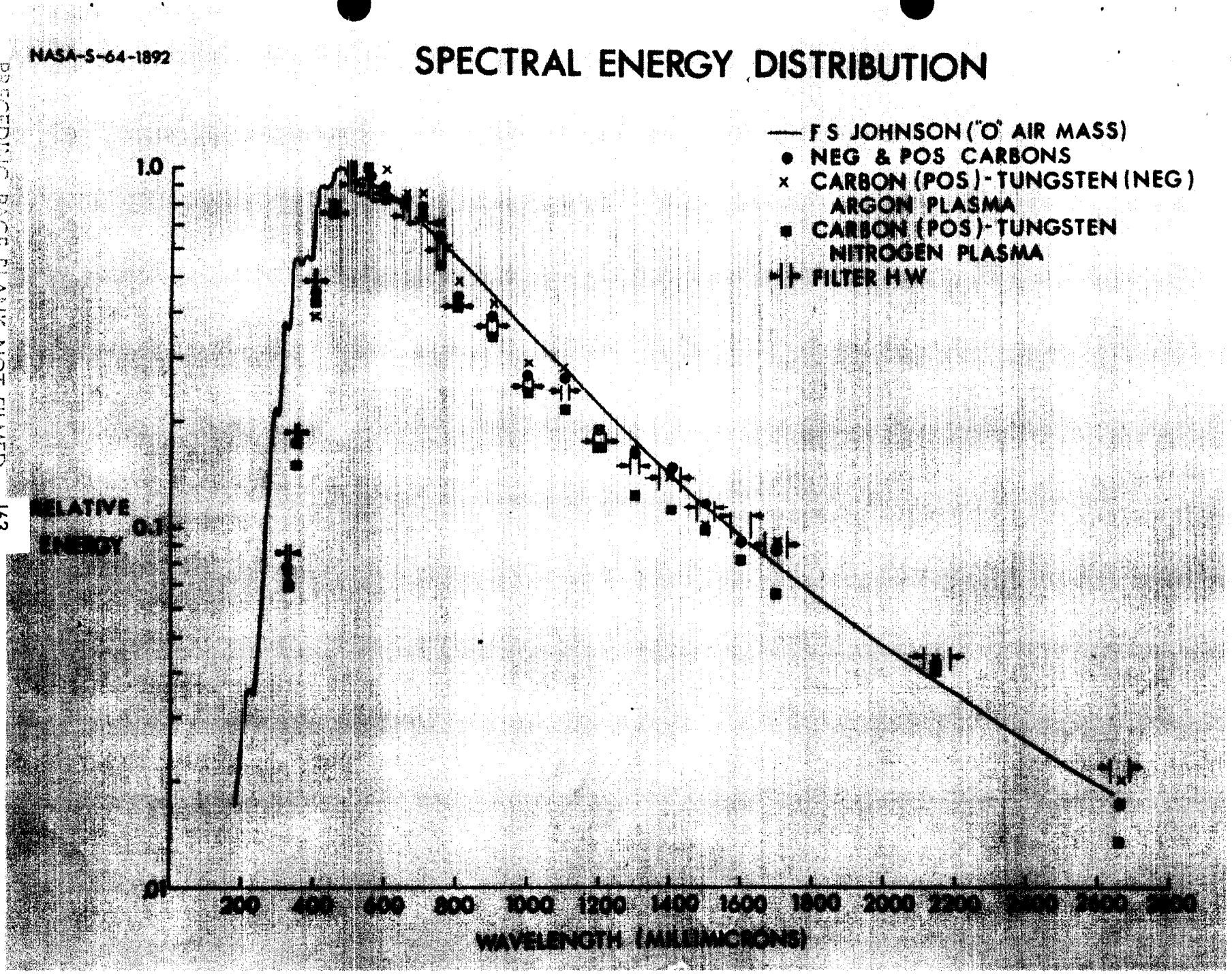

Figure 4

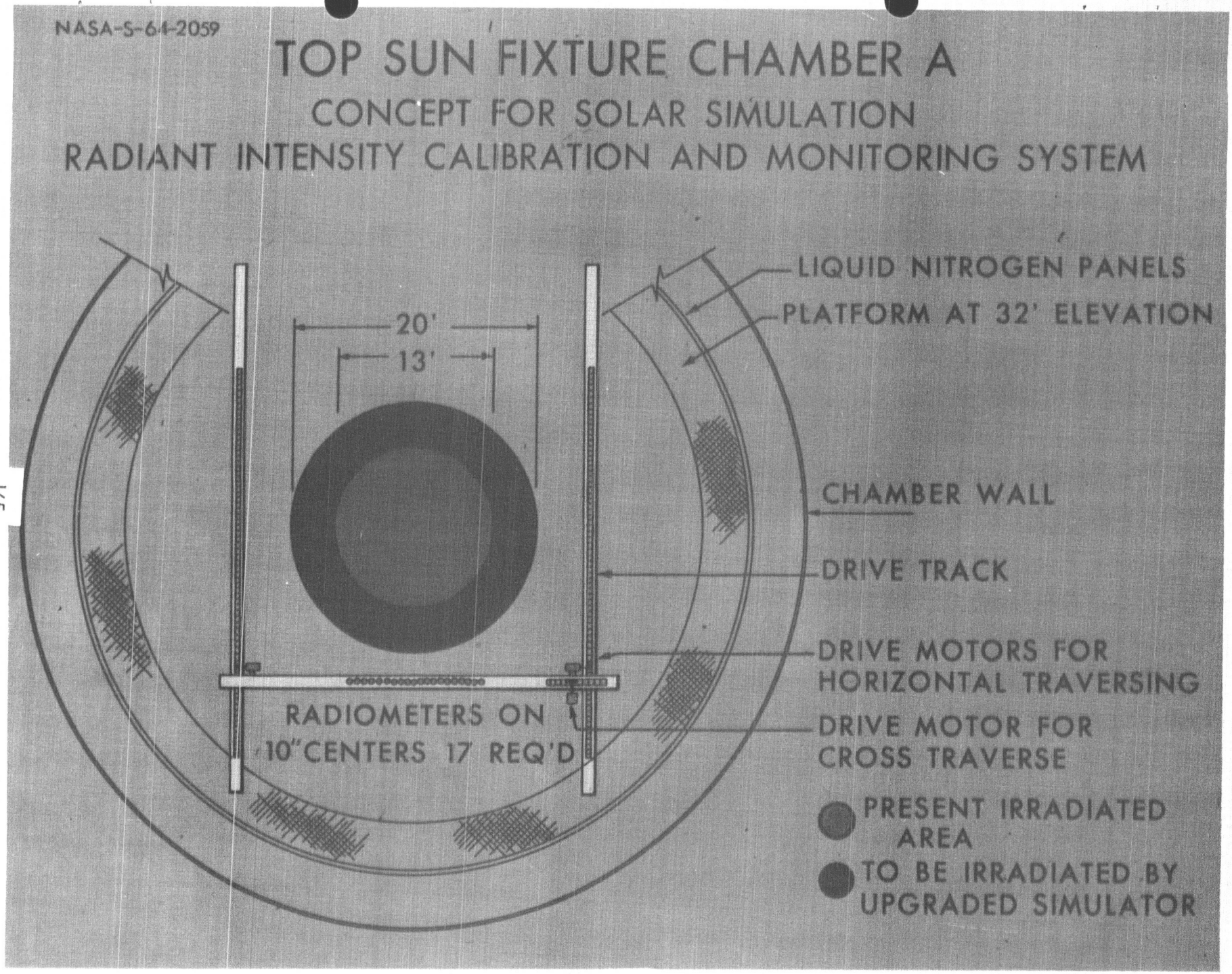

Figure 5

NASA-S-64-2058

SIDE SUN FIXTURE CHAMBER A

CONCEPT FOR SOLAR SIMULATION RADIANT INTENSITY CALIBRATION AND MONITORING SYSTEM

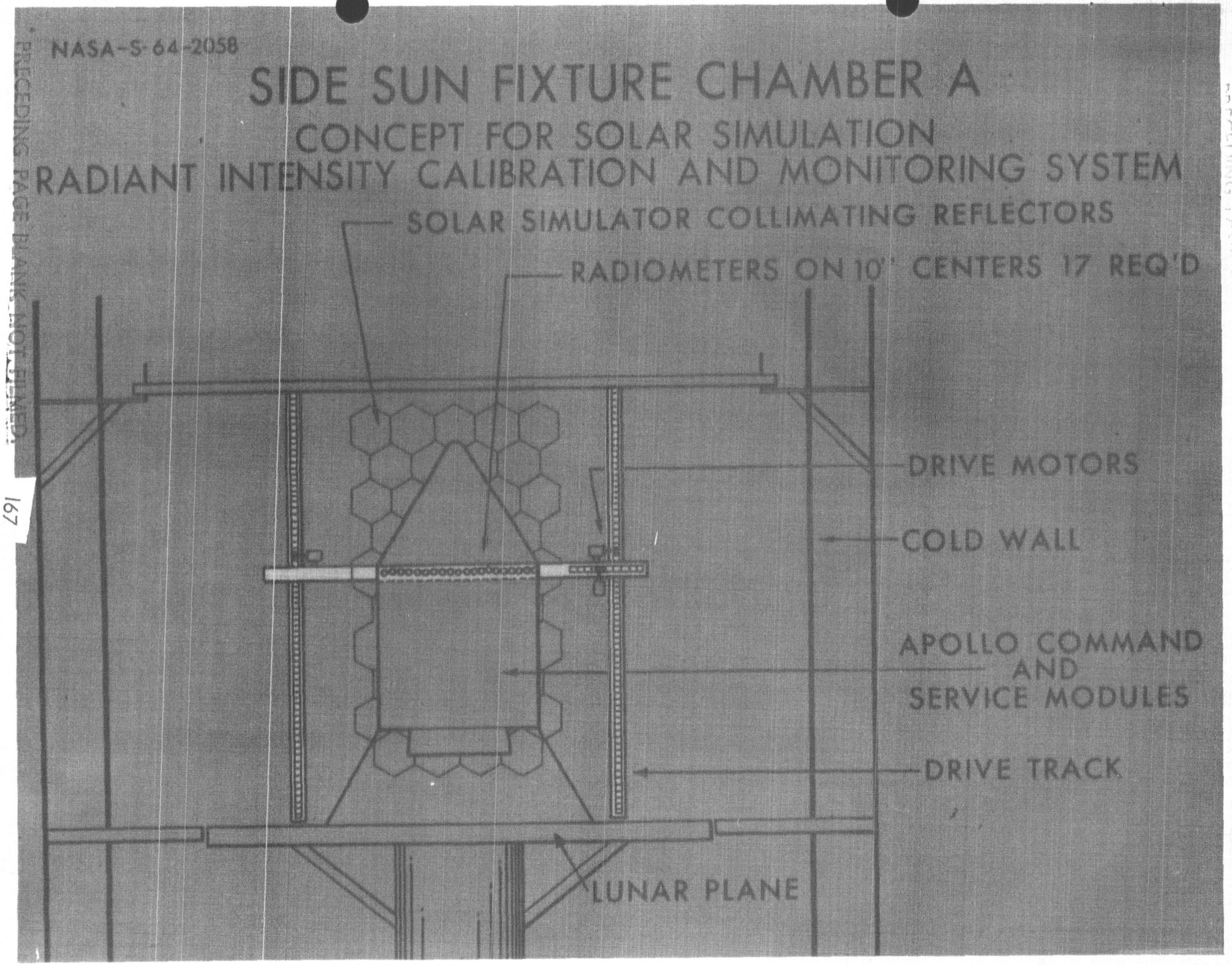

RADIOMETER CHARACTERISTICS

FLUX RANGE	0-3.0 "SUNS"
SENSITIVITY (ATMOS PRES.)	20.0 MV/SUN (MAX)
SENSITIVITY (10^{-5} TORR)	22.0 MV/SUN (MAX)
TIME CONSTANT	0.6 SECONDS
SIZE	2×2×1 INCHES
APERATURE	1.125 INCHES DIA
WINDOW	FUSED QUARTZ
NONLINEARITY	0.3% FULL RANGE

DEVELOPMENT OF THE JET PROPULSION LABORATORY SOLAR SIMULATOR TYPE A

By

Ralph E. Bartera
Roger M. Barnett

California Institute of Technology
Jet Propulsion Laboratory
Pasadena, California

Presented At The
Second Annual
NASA Conference on Solar Simulation

CONTENTS

I. INTRODUCTION

The Jet Propulsion Laboratory has been involved in solar simulation since 1960 in fulfillment of its obligations to the National Aeronautics and Space Administration. When it became apparent in 1962 that the solar system installed in the 25-Foot Space Simulator would not meet its initial performance specifications, which were inadequate at best, a program was initiated to devise techniques for improving upon that system. This activity led into a system development program which culminated in the production of what is now known as the JPL Solar Simulator Design Type A, six-foot diameter (JPL-SS-A6). A brief history of this development together with the outstanding actual performance of the JPL-SS-A6 are presented here.

II. HISTORICAL DEVELOPMENT OF THE JPL-SS-A SYSTEM

In order to appreciate the origin of the JPL-SS-A System, it will be necessary to examine briefly JPL's first large solar simulator. JPL's 25-Foot Space Chamber, as it was made operational in late 1962, utilized in its solar system a multifaceted, reflective optical element ("virtual source") at the focal point of a paraboloidal collimator in the configuration shown in Figure 1. The large number of small facets (each contributing light to the entire test volume) eliminates the non-uniformity inherent in the incident light; the shape of each facet (paraboloidal with the same aperature as the collimator) compensates for the non-uniformity which would otherwise be introduced by the large collimator aperature. A highly uniform beam of light is therfore obtained in the test volume. The large, non-useful skirt area (which contains about one-half the total energy) is primarily due to the presence of extended images of the field lens near the "virtual source", Figure 2. If a lens is placed at each image in such a way that we superimpose in the test volume images of each facet rather than unfocused light beams, the skirt in the test volume would thereby be greatly reduced. Since such a lens would interfere with the incident light, let us replace the reflective facets with refractive ones illuminated from the other side. Such an arrangement is shown in Figure 3. Since we have given up the reflective facets, we must restrict the collimator aperture, but this is a small price to pay for the greatly increased efficiency.

As the possibilities of this lens unit unfolded, patent applications were considered. We then discovered three rather interesting facts:

1) A patent was issued to Mr. Rantsch, et.al., in 1939 covering the application of this principle to motion picture projectors.
2) Ziess-Ikon has been selling for some time a projector which uses this principle.
3) A local company had developed independently of and almost concurrently with us a small solar simulator based on this same principle.

We were then in that unenviable position of having "invented" a device which was new at least 24 years ago. Be that as it may, this "re-invention" has become a significant advance in the short history of solar simulation.

III. THE JPL-SS-A6 SYSTEM

The design goal of the JPL-SS-A6 was as follows:

1. Intensity: 275 watts per square foot
2. Collimation (Worst angle): ± 2 degrees
3. Uniformity: ± 5% on any plane.
   ± 10% anywhere
4. Spectrum: Best obtainable with Xenon and Mercury Xenon compact arc lamps.

In order to fully exploit the possibilities of the lens unit, the simple system shown in Figure 4 was chosen. It consists of four subsystems:

1) Power Supplies:
   These are the standard 12.6 KW arc welding units shown in Figure 5.
2) Light Sources:
   These are 5 KW compact arc lamps (both Xenon and Xenon-Mercury types) mounted in latus rectum ellipsoidal reflectors with focal lengths of 4-in. and 420-in. Figure 6 shows one assembly and Figure 7 shows a twelve lamp array.
3) Lens Unit:
   Two views of the lens unit are shown in Figures 8 and 9. It has a 20-inch diameter and consists of two planes of nineteen lenses each. All lenses are four-inch hexagons fabricated from fused silica.
4) Collimator:
   This is a spherical surface with a 10-foot chord and a 40-foot radius of curvature (20-foot focal length). Figure 10 shows one which is composed of nineteen 2-foot segments. The center segment shows the lens unit as seen from the center of the test volume.

IV. SYSTEM ANALYSIS

When 5 KW lamps are placed in ellipsoidal reflectors and focused on the entrance to the lens unit, thirty five feet away, the energy distributions of Figure 11 are obtained there. The distribution from twelve Xenon lamps is shown in Figure 12. The distribution in Figure 12 was obtained with more precisely figured reflectors than were used for the distribution in Figure 11. The ordinates on both these curves are at four-inch intervals and represent individual lens channels. Note that the intervals labeled A and E in Figure 12 have an intensity gradient across them of about eight to one. An early experiment showed that this lens size provided sufficient integration of the light, i.e., if the five channels labeled A, B, C, D and E are superimposed (along with the other fourteen channels), the resulting distribution is highly uniform.

Refer to Figure 13 to see how the relative lens positioning is used to control this superposition. For clarity, we have drawn this figure out of scale and shown light passing through two lens channels only. It is evident that the location of the intersection at A and hence the plane of superposition is dependent on the angle α, which is determined by the relative locations of the lenses. The lamp array is centered on the intersection at B so that we may center images of it in each of the transfer lenses, Figure 14, and thus obtain efficient energy transmission, i.e., as the diameter of the lamp array is increased, images of it fill all transfer lenses at the same time.

In order to minimize the skirt losses, a real image of each condensing lens is formed in the test volume as illustrated in Figure 15. This is accomplished by forming a virtual image with each transfer lens and relaying a real image of that onto the superposition plane by means of the collimator. When this is done, it happens that the lens planes are separated by a distance equal to the average of the two lens focal lengths and thus form an acromatic unit. There are, therefore, no color gradations in the light beam. It should be borne in mind that since the quality of these images is not especially critical, the precision of the optical surfaces is not critical, e.g., the collimator can have slope deviations of several minutes of arc with no serious effects.

IV. SYSTEM ANALYSIS (Cont'd)

The collimator required has a 10-foot chord and a 20-foot focal length. Since it is easier to fabricate a spherical surface than a paraboloidal one (especially off-axis), we examined the aberations which might be introduced by a sphere. Figure 16 shows the computed effect of the spherical aberation. The sphere, of course, when illuminated by a point source at its focal point, does not produce a parallel beam of light, but one which is slightly convergent as indicated by the dashed line. This convergence (which amounts to a few minutes) will theoretically increase the outboard intensity in the manner that the curves in the same figure show. The cross-hatched area indicates the extent of the test volume. Notice the improvement over the curve, which is not a function of H/F, indicated for the paraboloid. This shows quite clearly that the spherical surface produces higher inherent uniformity and, therefore, a desirable fabrication technique. These curves were determined on a digital computer in two ways:

1) With a single point source at the focal point.
2) With nineteen point sources arrayed symmetrically around the focal point, i.e., one at the center of each lens. Identical results were obtained.

The simplified schematic shown in Figure 17 indicates the angular limitations imposed by the restricted collimator aperture. Since the ratio of i/h can only slightly exceed unity, the entrance or acceptance angle cannot be larger than the exit angle (collimator aperture). Any light incident on the lens unit from outside this angle does not reach the test volume.

V. FULL SCALE EVALUATION EXPERIMENT

A 10-Foot Space Chamber incorporating the JPL-SS-A6 was proposed by JPL as a second generation facility. A schematic diagram of this facility configuration is shown in Figure 18. It is expressly designed around the optical system. Because of the difficulties which all the large solar simulation systems were experiencing at that time, JPL decided that the JPL-SS-A6 should be demonstrated in full scale before the facility was constructed. Figure 19 shows the arrangement used for this multi-lamp, full-scale experiment. The experimental configuration differs from the proposed facility configuration in four ways:

1) The orientation is horizontal rather than vertical. This does not affect the test results.
2) No vacuum penetration window was used. This makes the experimental intensity measurements about ten per cent too high.
3) A folding mirror was used because the lamps must operate in a nominally vertical anode up direction. This makes the experimental intensity measurements about twenty per cent too low.
4) The ellipsoidal reflectors collect light from the anode (upper) half of the lamp rather than the cathode (lower) half. This makes the experimental intensity measurements about twenty-five per cent low.

These differences combine to make the intensity measured in the experiment about thirty-five per cent lower than what can be expected in the facility configuration.

The lamps, reflectors and lenses used were identical to those proposed for the new facility; the other optical element, the collimator, was not. While we plan to use a one piece component in the facility, the segmented one chosen in Figure 10 was used in the experiment. Because of the variations between segments, when they are alligned so that the normal to the center of each segment passed through a common "center of curvature", and are illuminated from a small source at the focal point, the pattern shown in Figure 20 is obtained in the test volume. With illumination from the entire lens unit, these variations produce a ripple in the test volume intensity surveys of which Figure 21 is typical.

V. FULL-SCALE EVALUATION EXPERIMENT (Cont'd)

The survey presented in Figure 22 was obtained by adjusting the collimator segments for the best allignment in one plane and direction. Unfortunately this optimum adjustment could not be obtained simultaneously throughout the test volume. The uniformity, however, represents that obtainable with a continuous surface reflector.

VI. SYSTEM PERFORMANCE

A. Intensity

The intensity of illumination in the test volume, as measured with an Epply thermopile, averaged over 120 watts per square foot when the lamp array contained ten Xenon and two Xenon-Mercury lamps. Increasing this by 35% as described above, we obtain a value of 162 watts/ft.^{2}. The new 10-foot space chamber facility will be constructed with 19 lamps installed (256 watts/ft.^{2}) and provision to add an additional 35 (54 total lamps).

Figure 23 is a view of the lens unit passing light from twelve lamps. Figure 24 is a view through the lens unit looking toward the lamp array. Firgure 25 shows the image of the lamp array in one lens channel. An examination of these figures, especially the last, shows that the optics can accept up to 61 lamps. There are, however, practical reasons which limit the number to 54 in the 10-foot space chamber. This implies a possible intensity performance in that facility of 825 watts/ft^2. This energy will probably be used to improve other parametors.

B. Uniformity

The uniformity of illumination in the test volume was a difficult measurement because of the inferior collimator used in the experiment. The actual measurements showed a variation of $\pm$ 10%. After eliminating the collimator effects, as described above, we obtain a maximum variation of $\pm$ 5% throughout the entire 10-foot high test volume.

C. Collimation

The degree of collimation of the JPL-SS-A system is a function of the lens unit diameter and collimator focal length. The JPL-SS-A6 experimental configuration was measured to have collimation angle (worst ray deviation from the test volume axis) of just over two degrees. The availability of the excess energy mentioned above allows for improvement of the collimation, e.g., if all but the center seven lenses of the lens unit are masked, a collimation angle of 1.5 degrees is obtained while retaining 60% of the light energy (from 36% of the original area). This is due to the fact that the "sun" is not uniformly bright, cf. Figure 12.

VI. SYSTEM PERFORMANCE (Cont'd)

D. Spectrum

The spectral distribution of energy in the test volume is identical to that of the lamps as modified by the optics. Since each lamp illuminates the entire test volume, a mixture of various types can be used to tailor the spectrum. Also, there is currently on the market a filter which modifies light from a Xenon compact arc lamp to a good solar spectrum. Which of these or other techniques should be used depends on the types of tests to be conducted. For our purposes, we have tentatively chosen a mixture of Xenon and Xenon-Mercury lamps. The lack of a good standard in the ultra-violet makes absolute energy measurements in that region very uncertain. We have made spectral measurements with a Beckman DK-2 spectrophotometer and obtained the date presented in Figure 26 and Figure 27

VII. CONCLUSIONS

The very high efficiency of the JPL-SS-A system allows us to expend the excess energy to improve any performance parameter; e.g. collimation. The system is quite flexible in yet another way. Since the lens unit effectively separates the lamp array from the test volume, we can make use of improved lamp or refelctor types as they become available.

We are currently studying spplications of this system to beam sizes in the 20-foot range. Since a direct scale-up becomes unwieldy, we are investigating techniques which might be used to increase the collimator aperture without degrading uniformity.

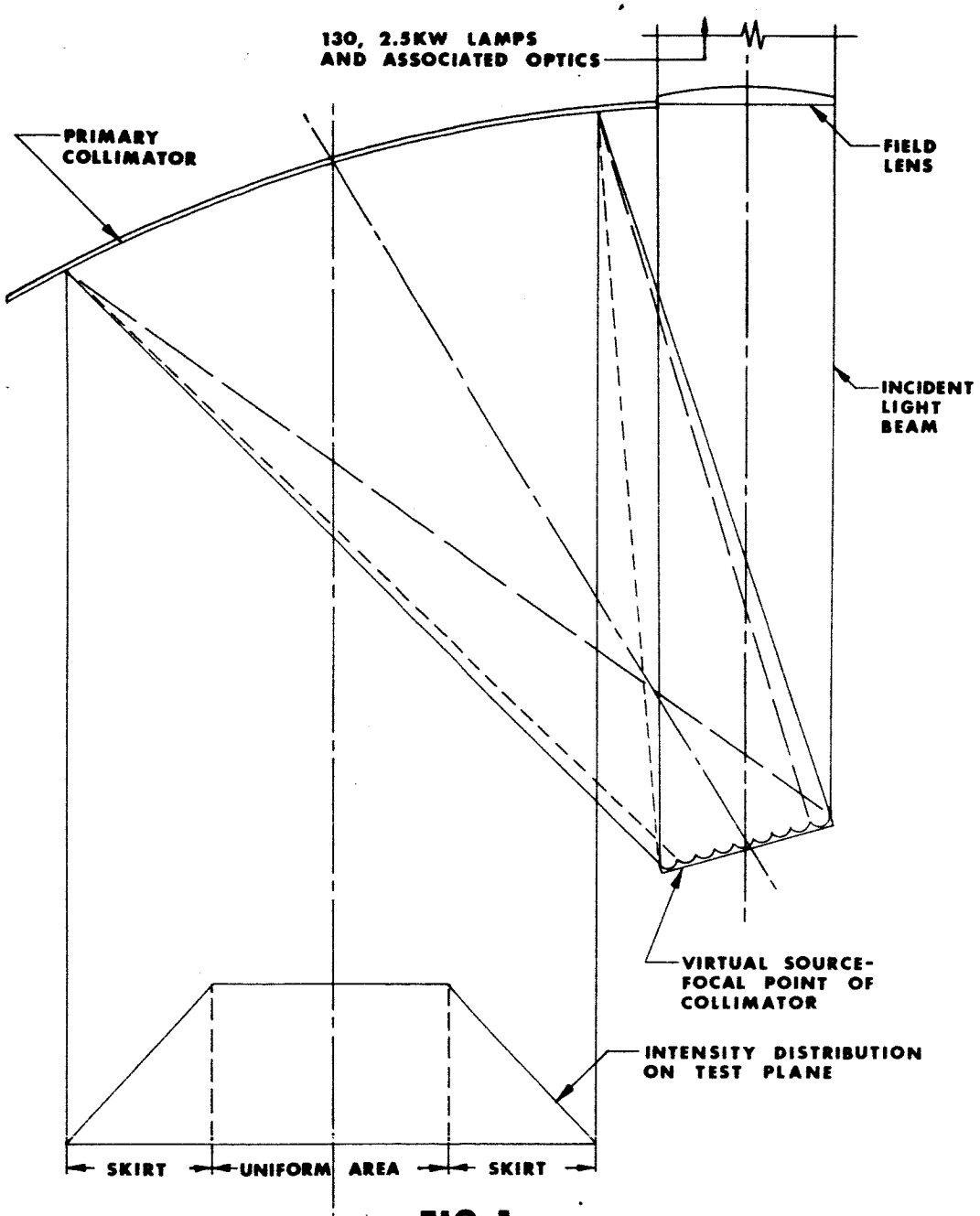

FIG. 1

PARTIAL REPRESENTATION OF THE SOLAR SIMULATION SYSTEM INSTALLED IN THE JPL 25 FT. SPACE CHAMBER

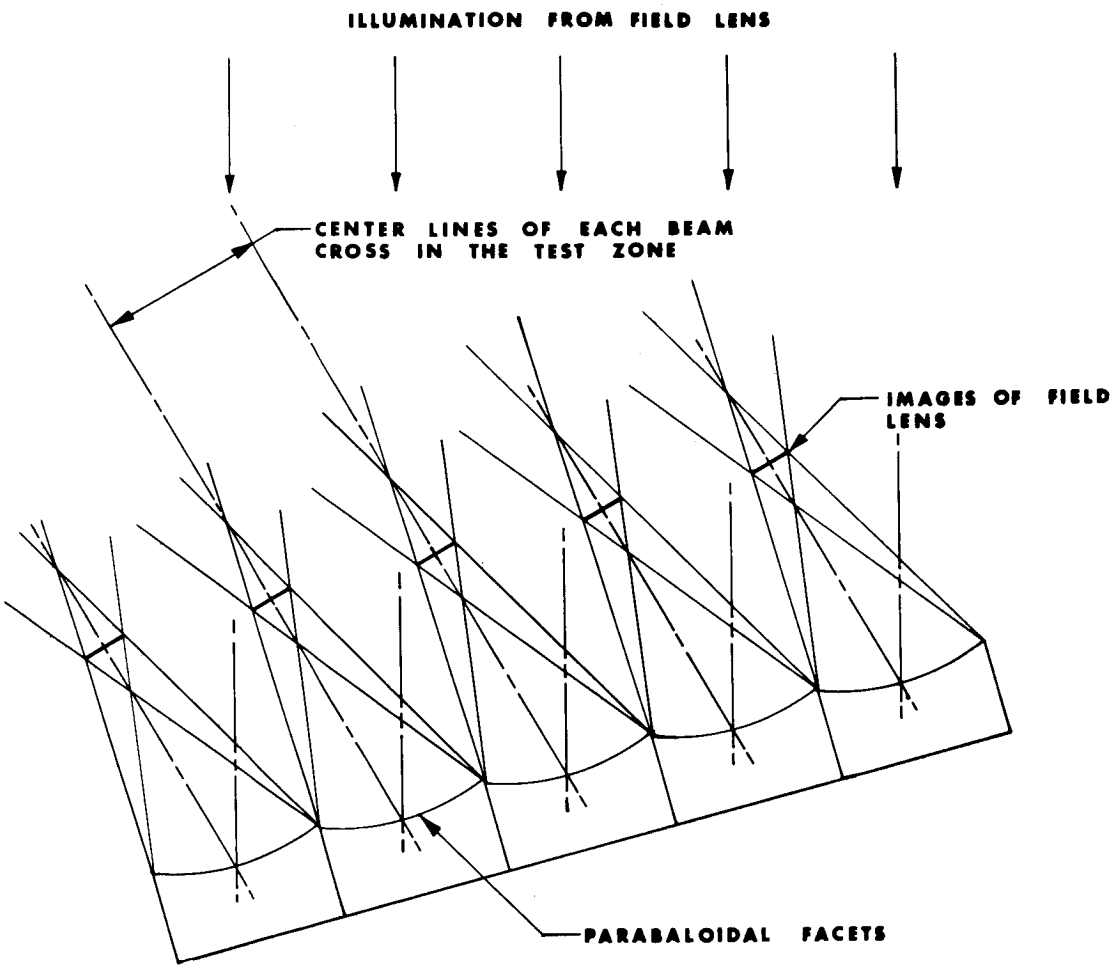

FIG. 2

IMAGE FORMATION NEAR THE VIRTUAL SOURCE IN THE 25 FT. CHAMBER

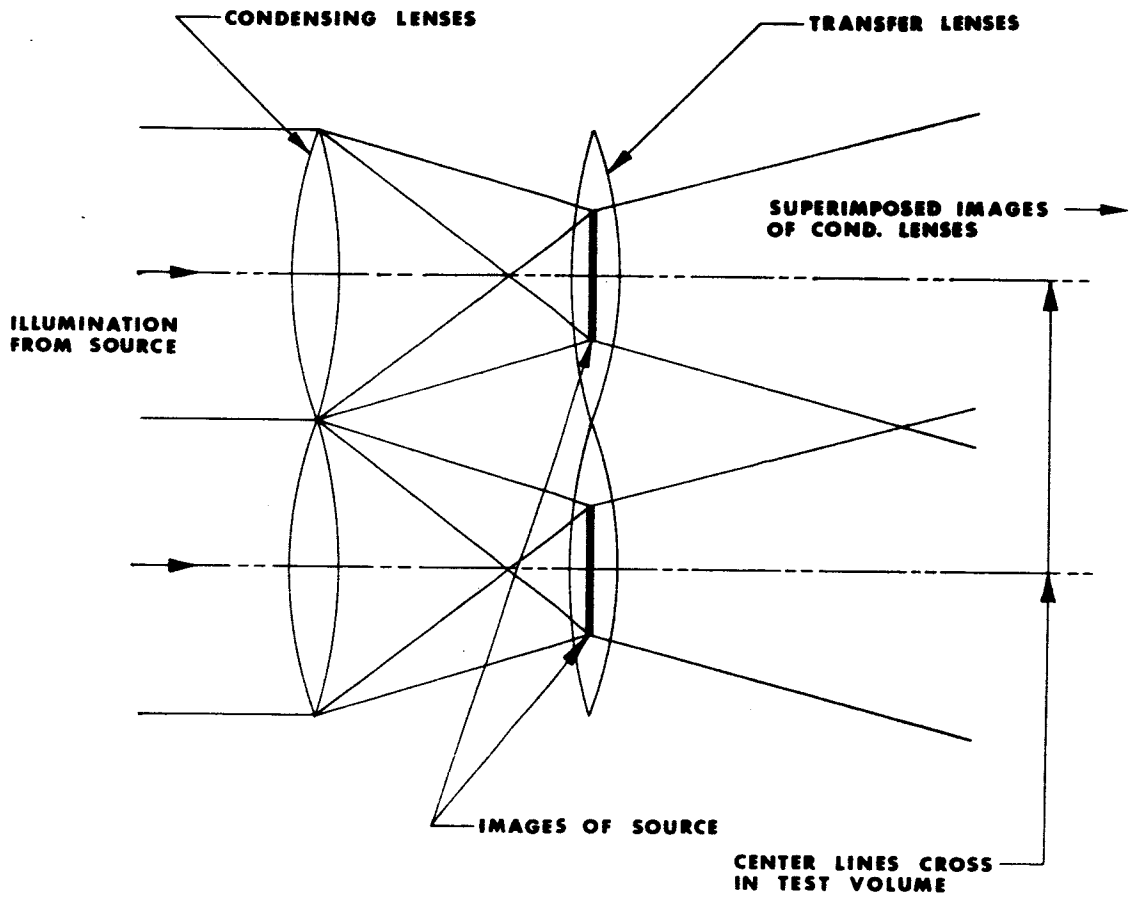

FIG. 3

INITIAL CONCEPTION OF THE JPL-SS-A LENS UNIT

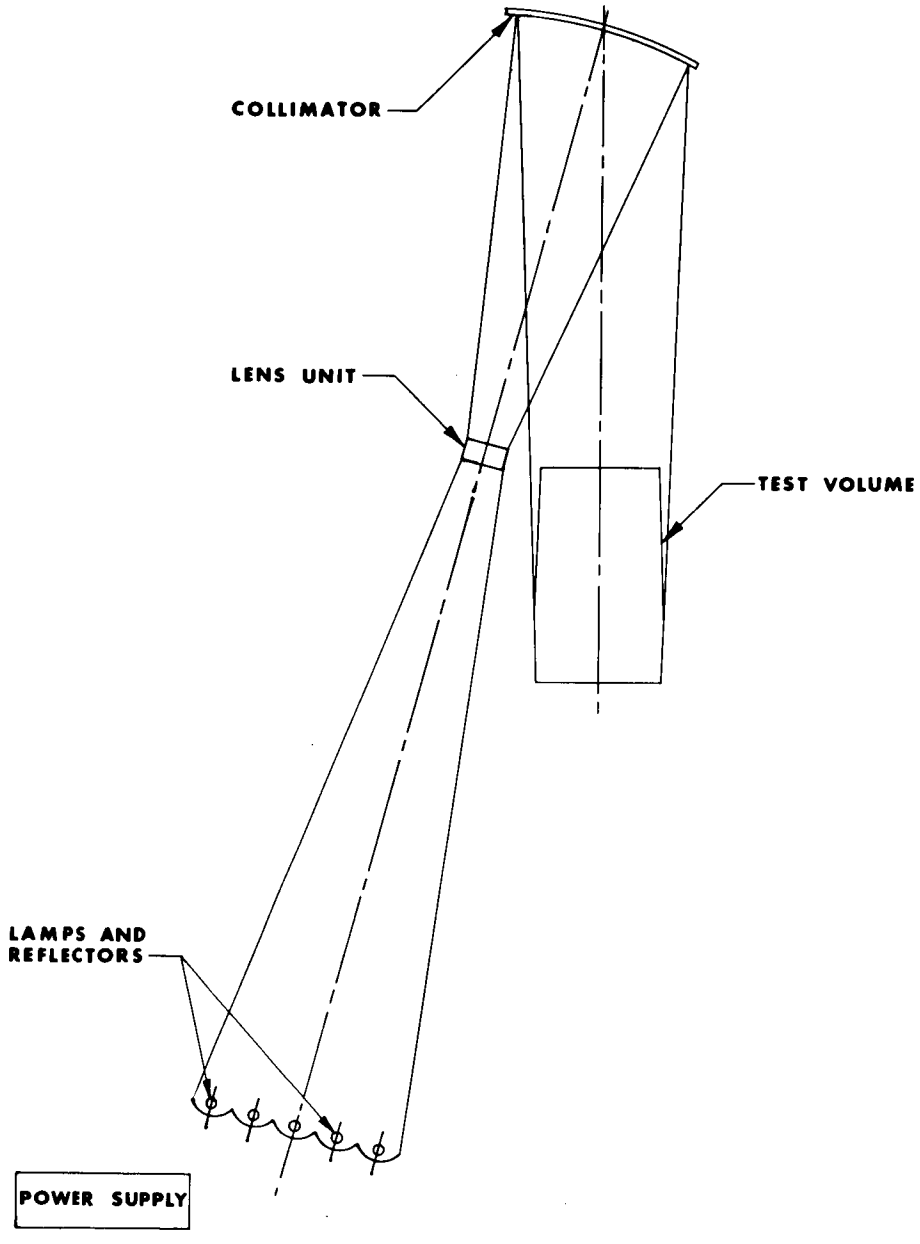

FIG. 4

JPL-SS-A LAYOUT

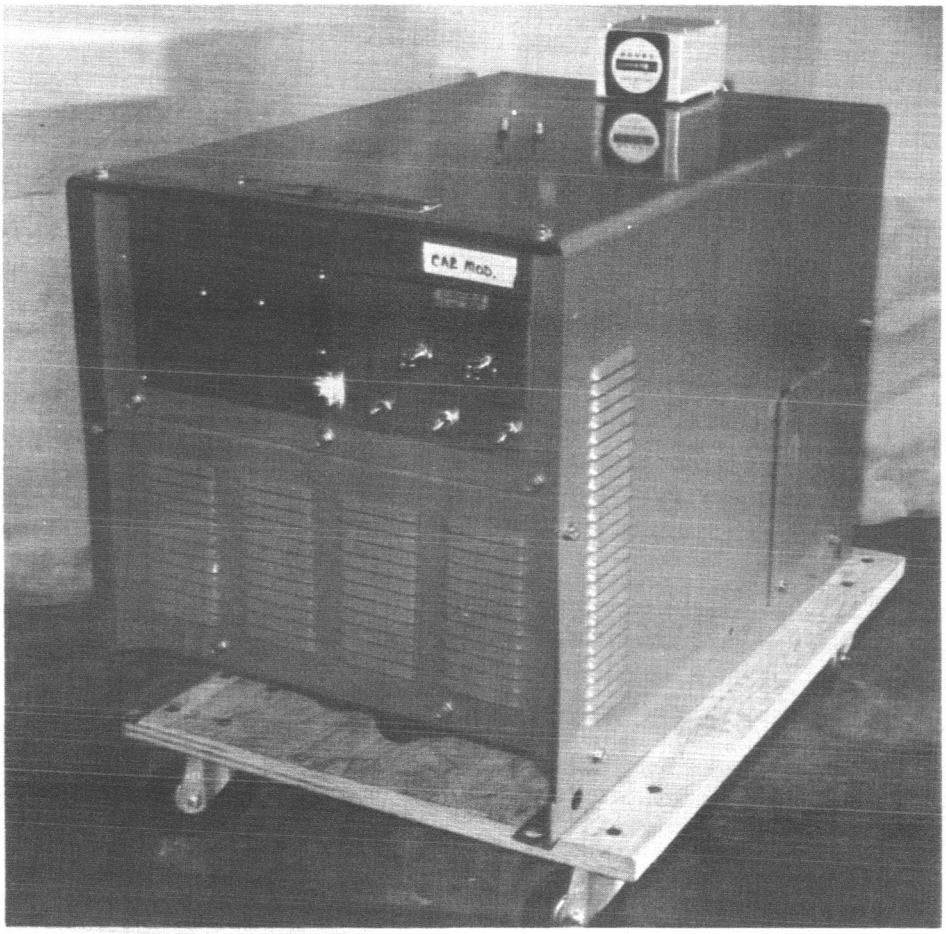

FIG. 5

POWER SUPPLY

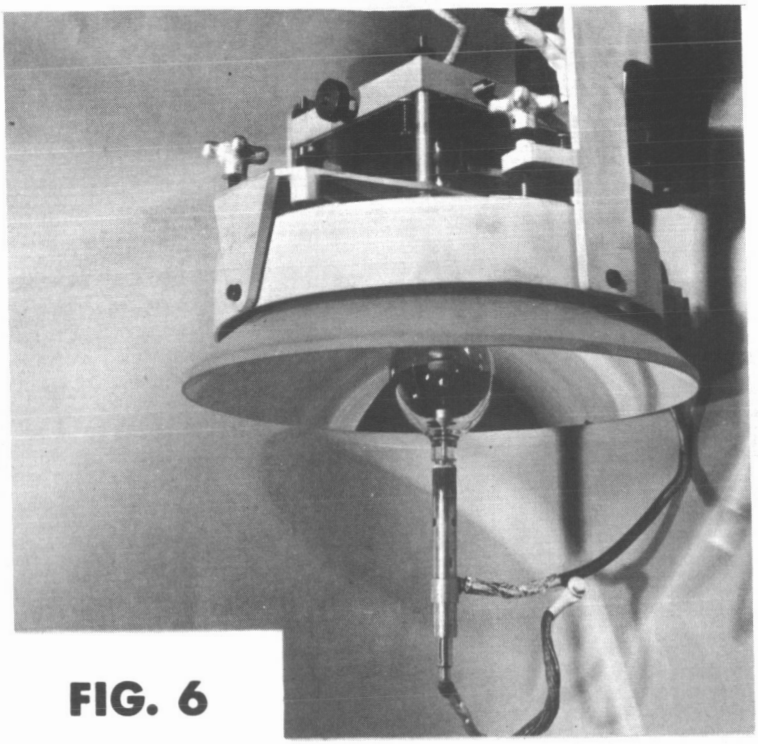

FIG. 6

LAMP-REFLECTOR ASSEMBLY

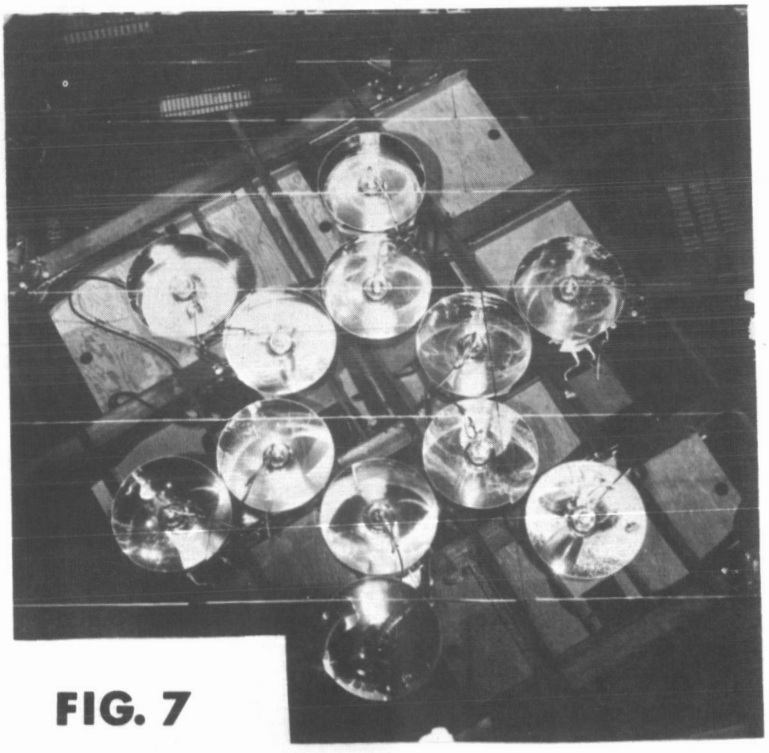

FIG. 7

LIGHT SOURCE ARRAY

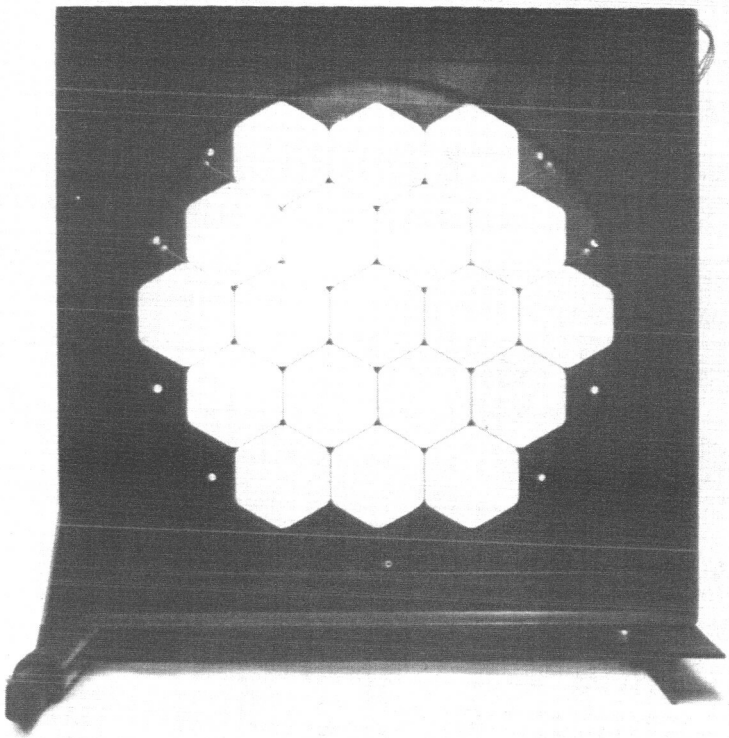

FIG. 8
LENS UNIT

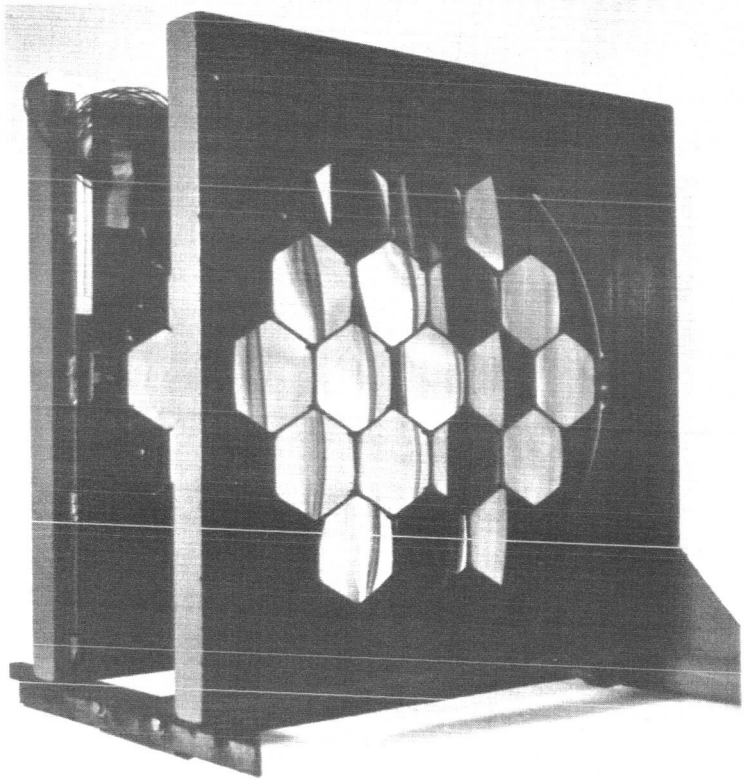

FIG. 9
LENS UNIT

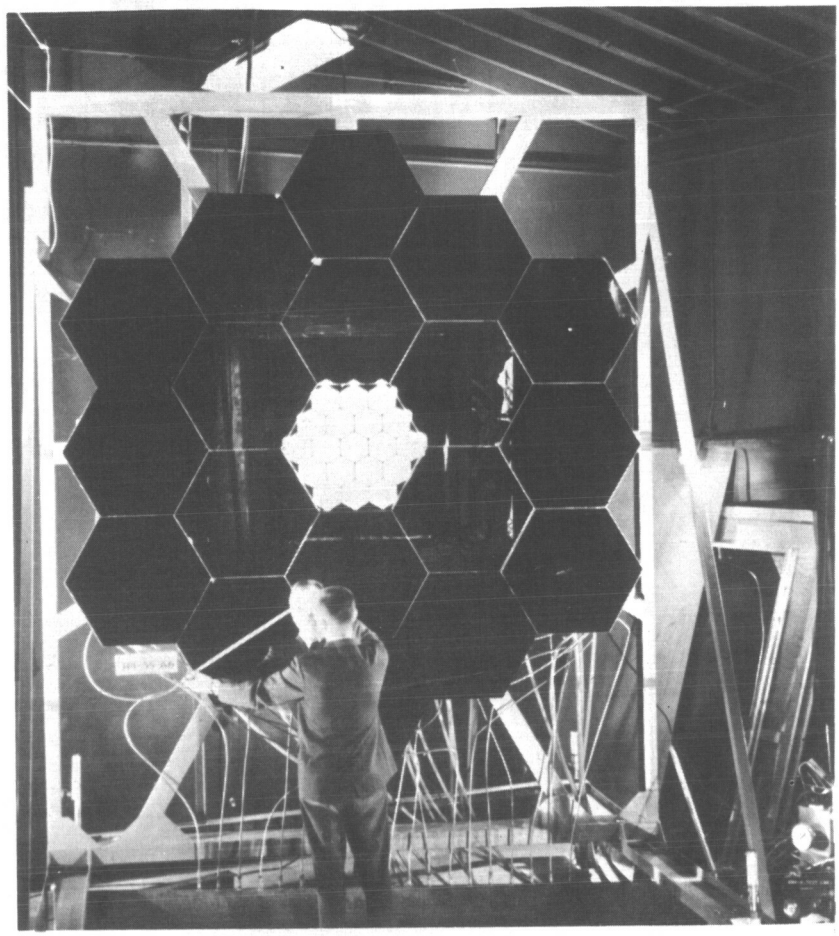

FIG. 10

COLLIMATOR USED IN THE JPL-SS-A6 EXPERMENT

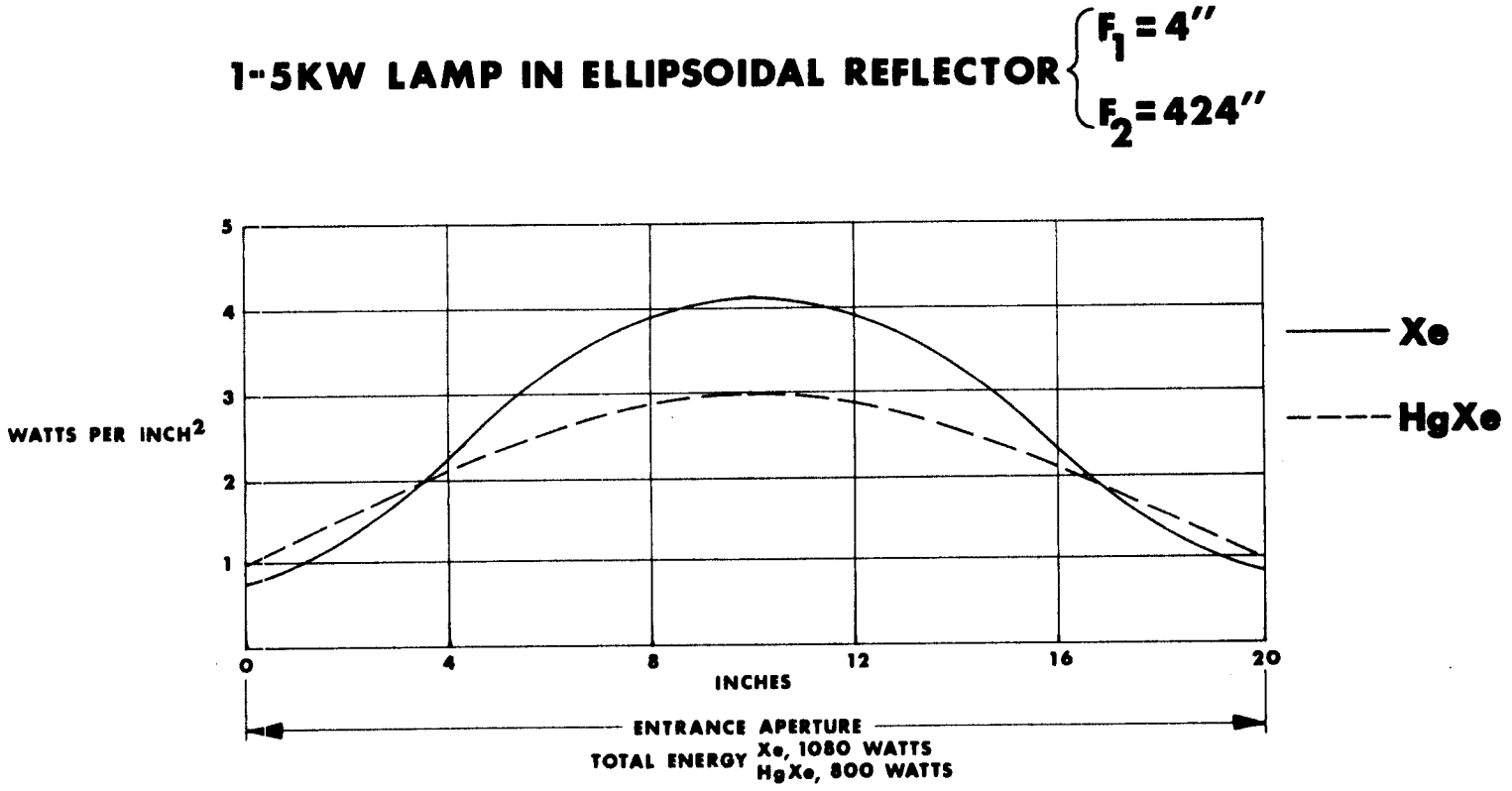

FIG. 11

ENERGY DISTRIBUTION ON THE ENTRANCE TO THE LENS

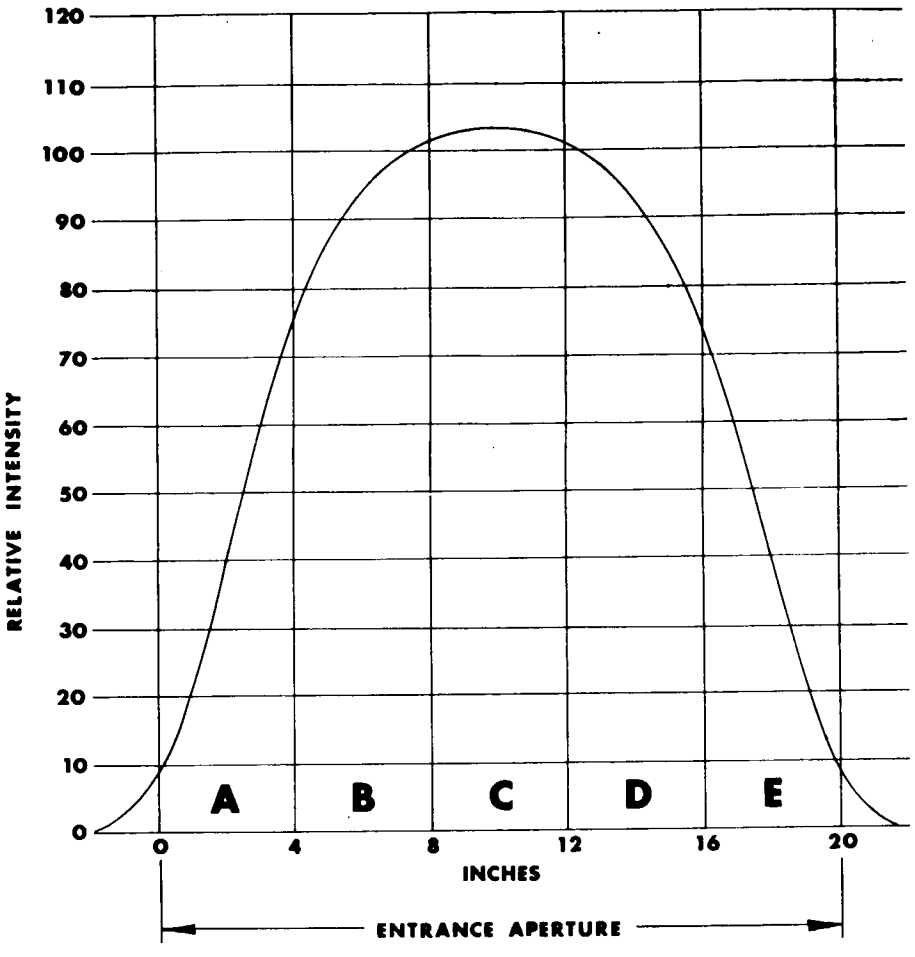

FIG. 12

ENERGY DISTRIBUTION ON THE ENTRANCE TO THE LENS UNIT FROM TWELVE 5KW LAMPS

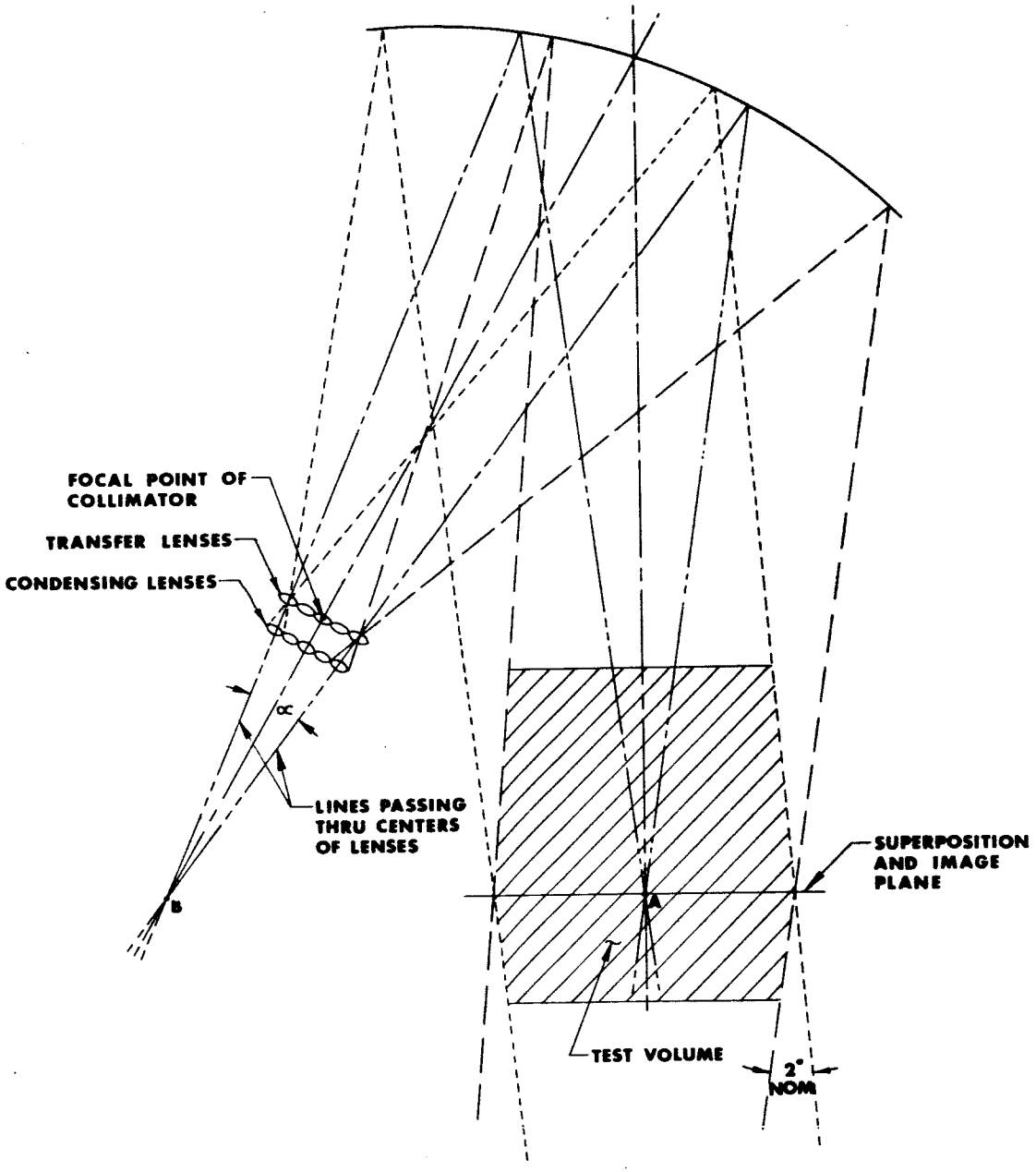

FIG. 13

ILLUSTRATION OF SUPERPOSITION

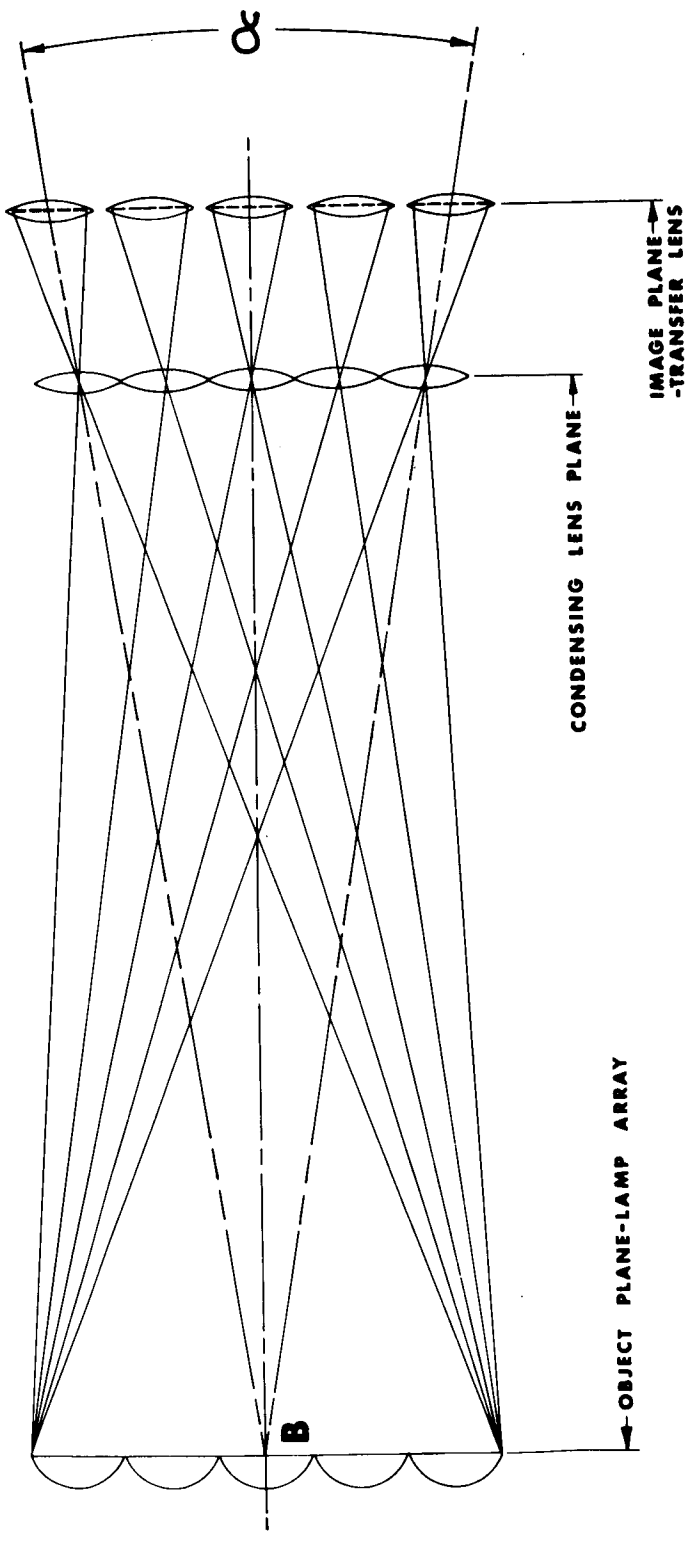

FIG. 14

IMAGE LOCATION-LAMP ARRAY

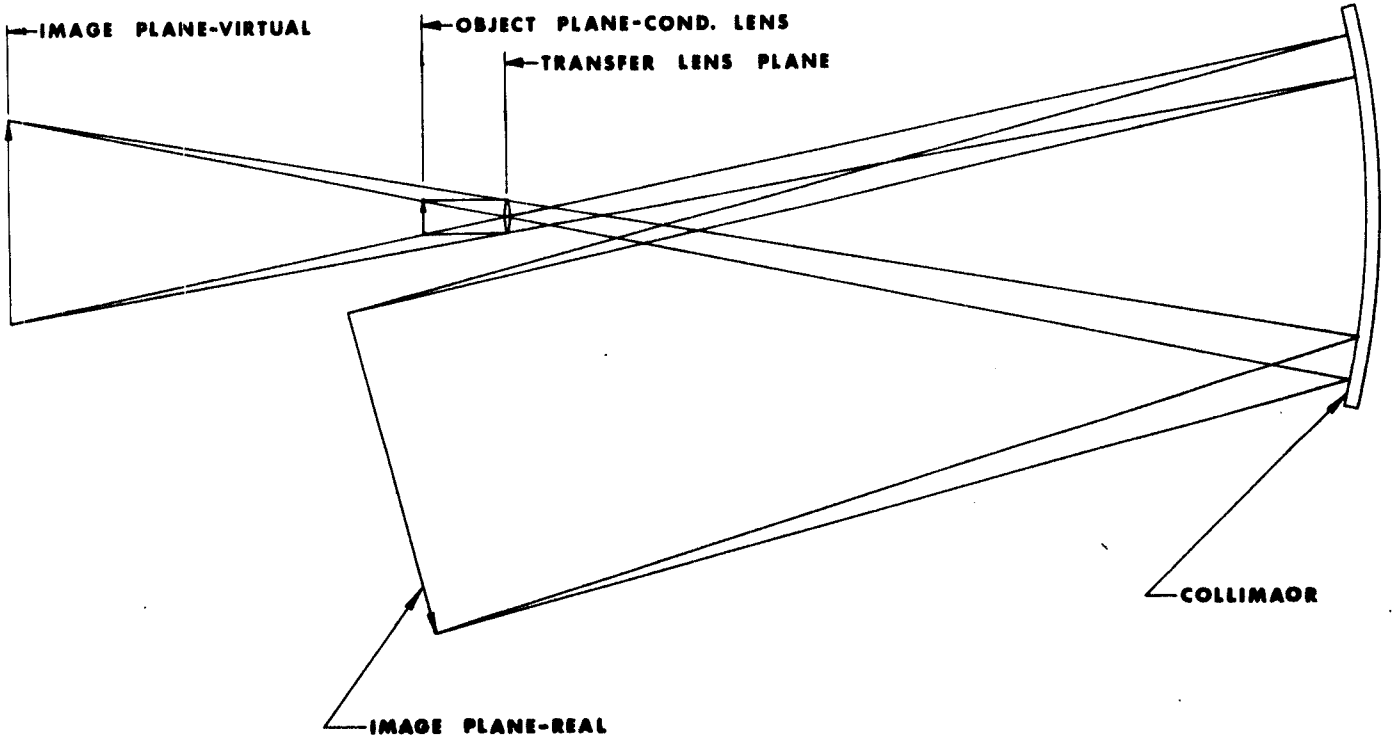

FIG. 15

IMAGE LOCATION-TEST VOLUME

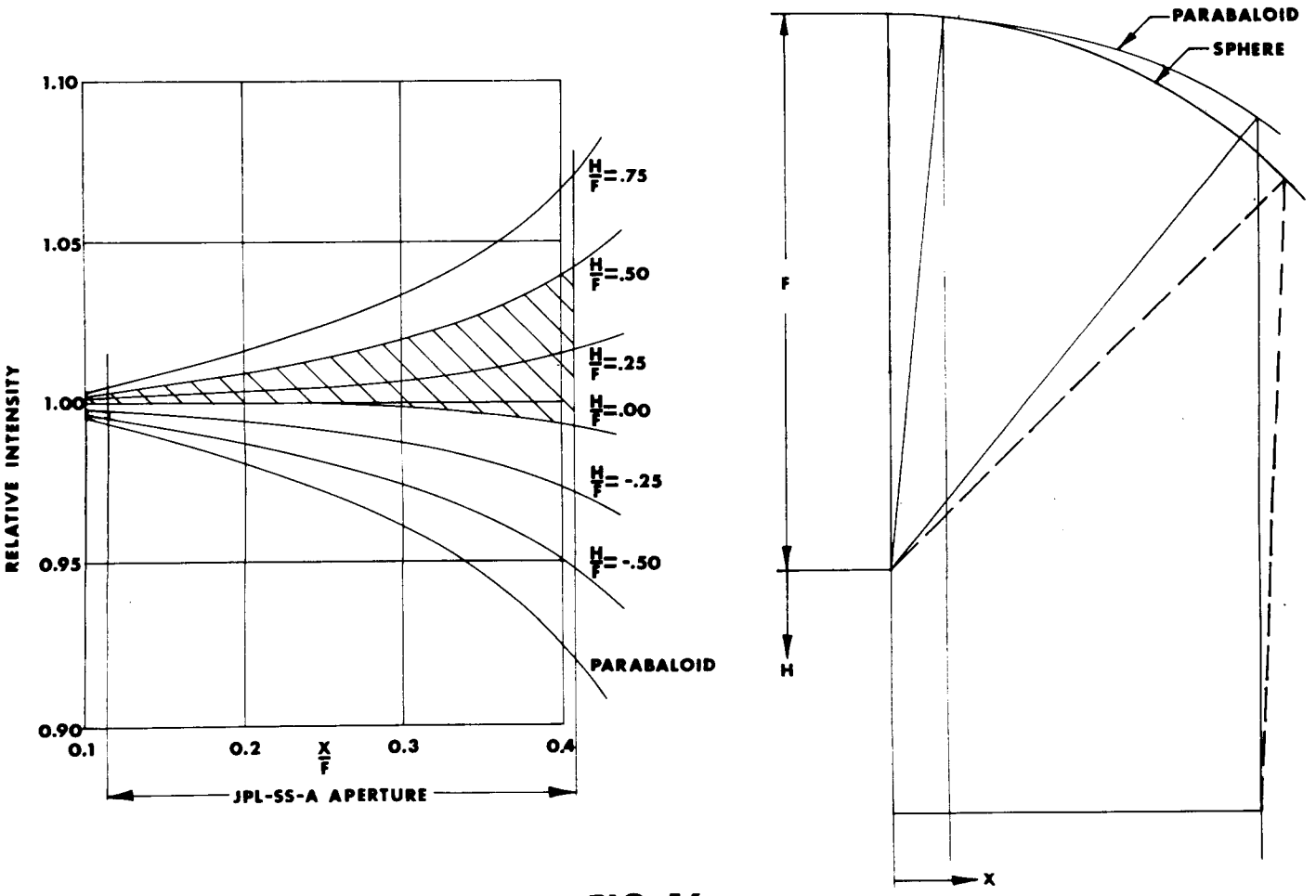

FIG. 16

SPHERICAL ABERATIONS OF THE COLLIMATOR

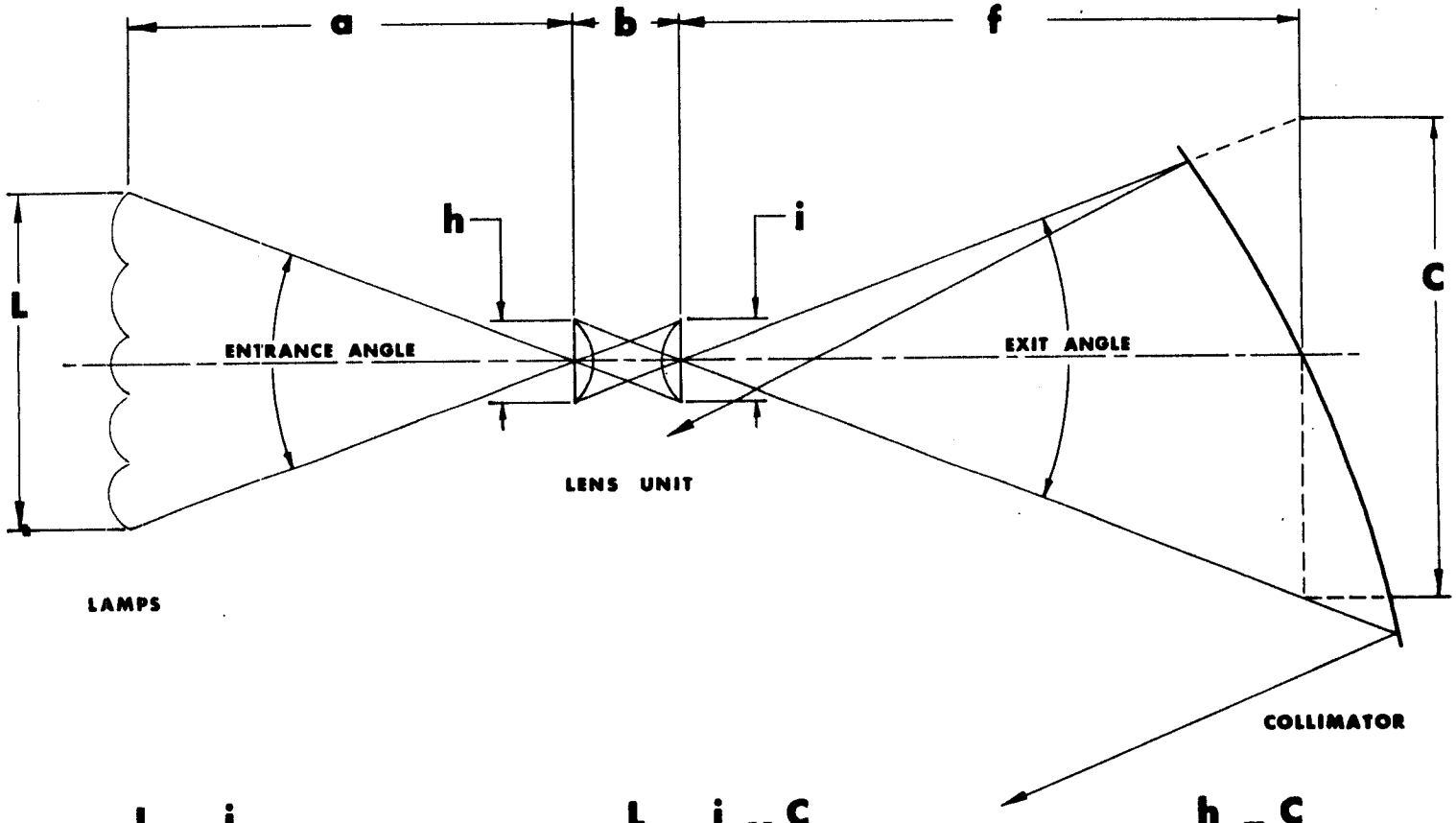

$$\frac{L}{a}=\frac{i}{b} \qquad \frac{L}{a}=\frac{i}{h}\times\frac{C}{f} \qquad \frac{h}{b}=\frac{C}{f}$$

FIG. 17

JPL-SS-A GEOMETRICAL LIMITATIONS

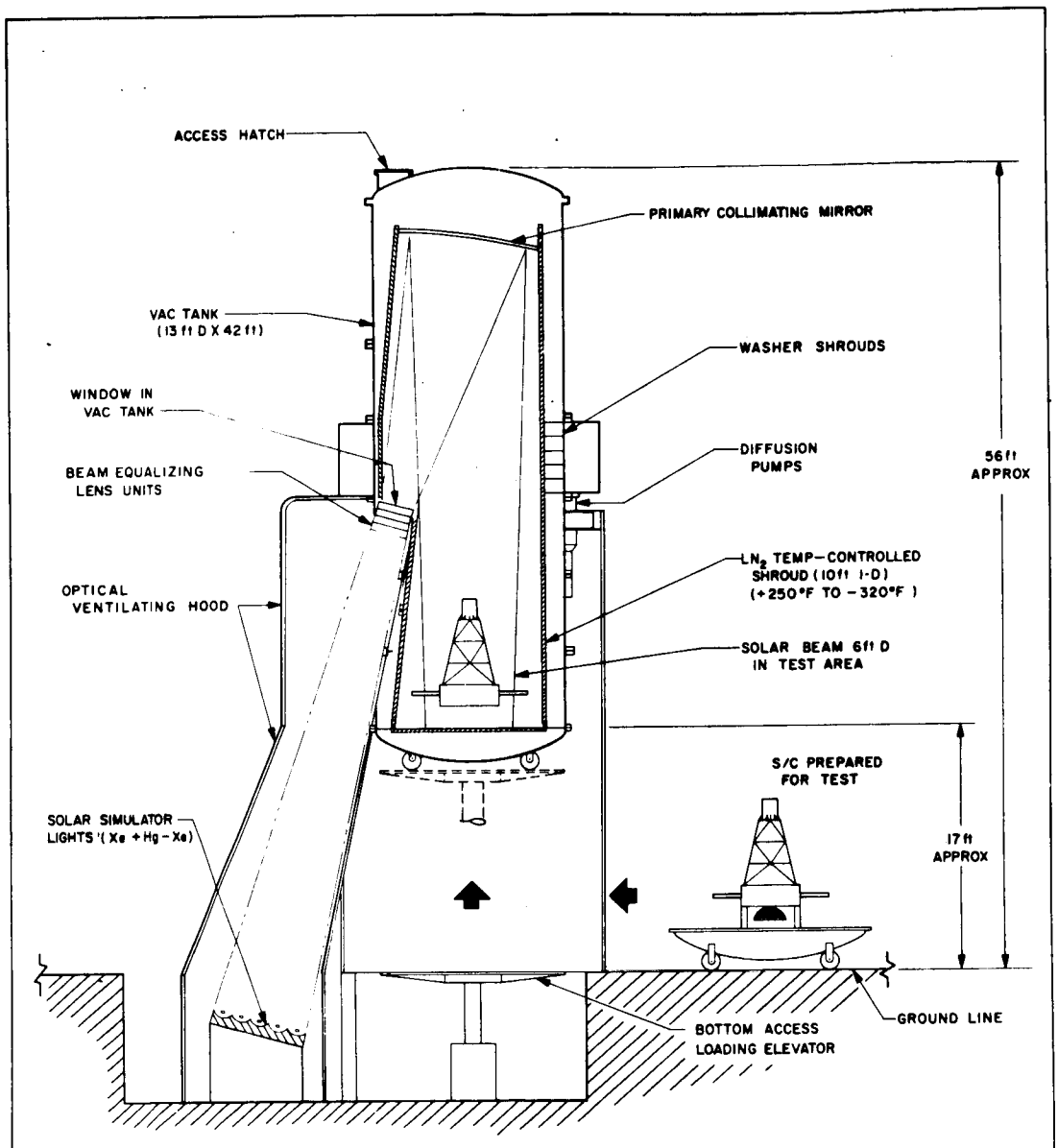

FIG. 18

REV 9/5/63

jpl TECH FACIL ENGR - 375 JUNE '63

PROPOSED
JPL-10 FT SPACE SIMULATOR
CROSS SECTION

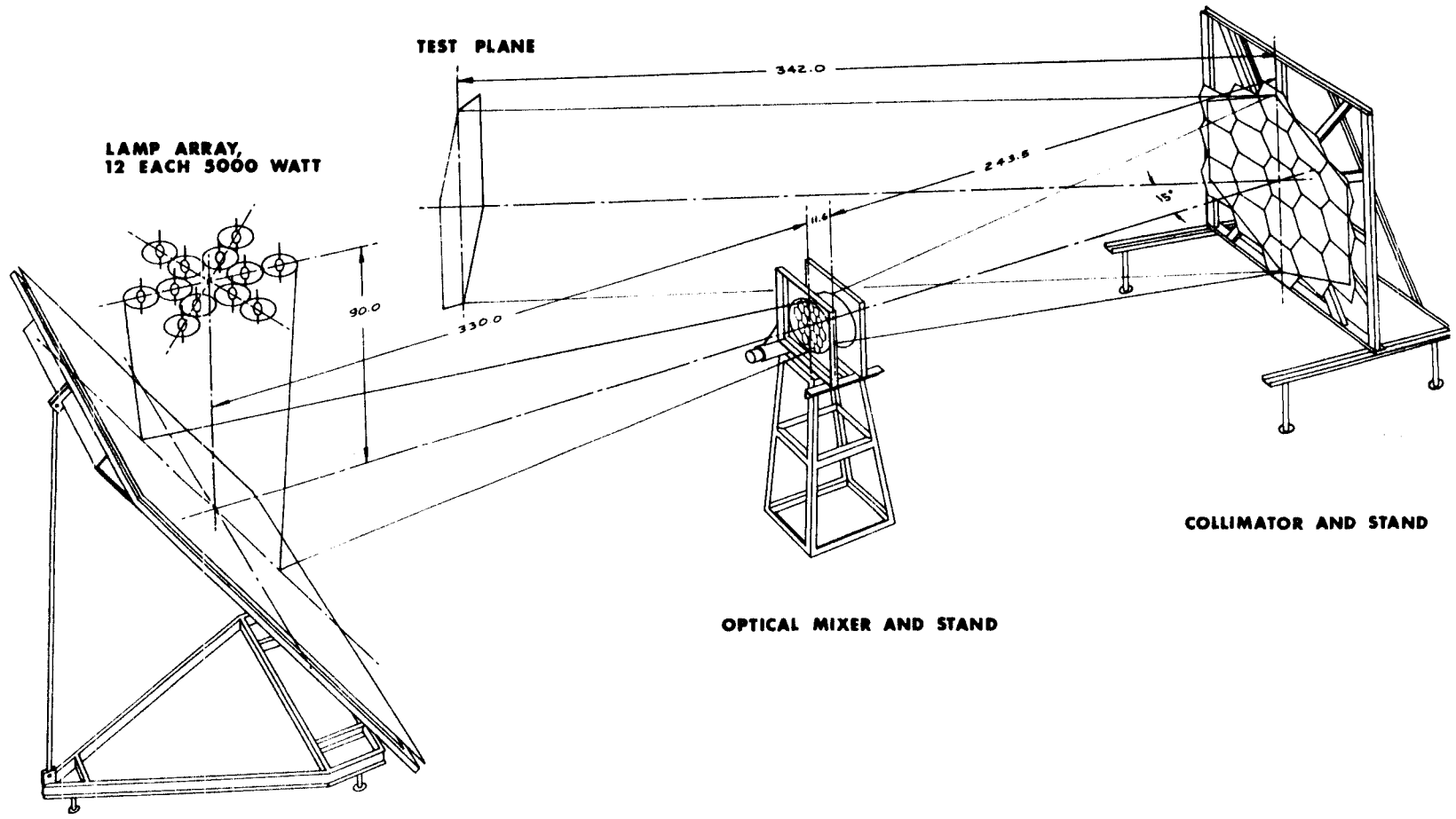

FIG. 19

FULL SCALE JPL-SS-A6 EXPERIMENT

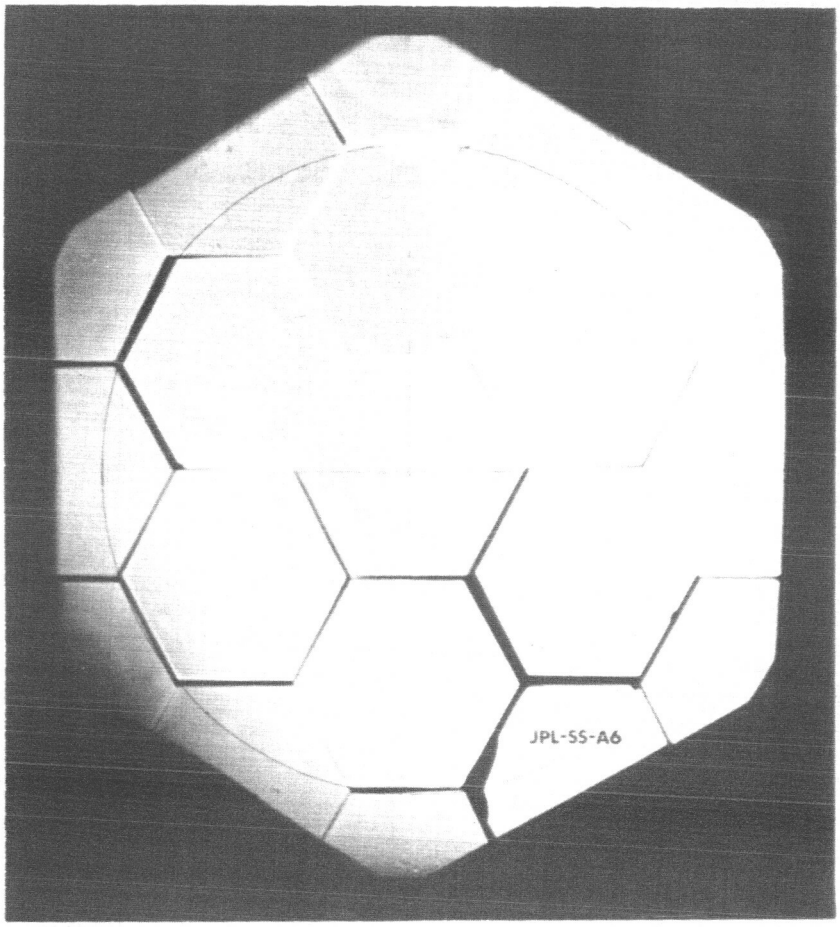

FIG. 20

TEST VOLUME
POINT SOURCE AT LENS UNIT

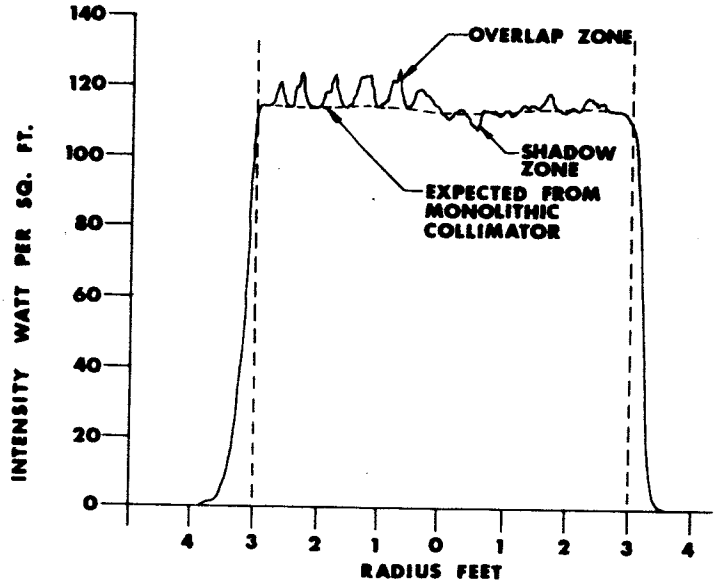

FIG. 21

TYPICAL UNIFORMITY DATA

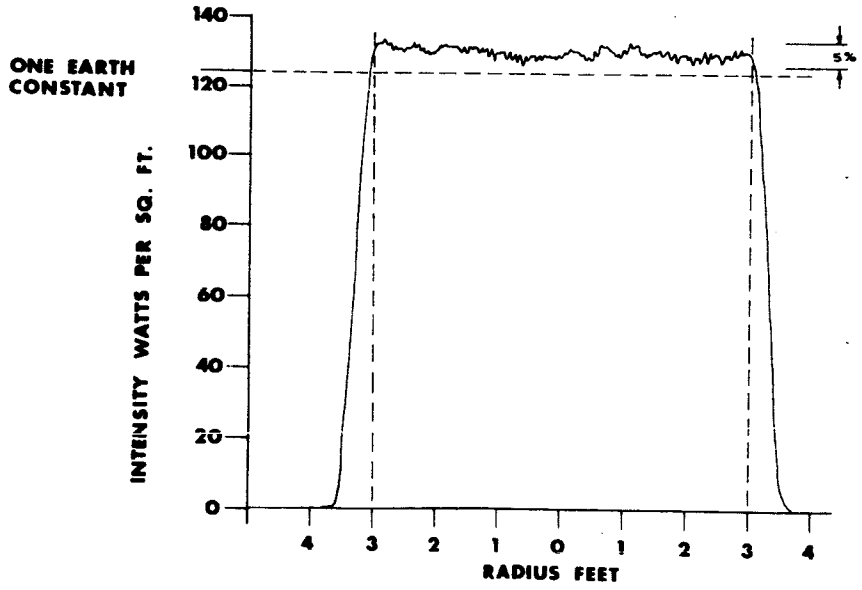

FIG. 22

INTENSITY SURVEY WITH OPTIMUM COLLIMATOR ADJUSTMENT

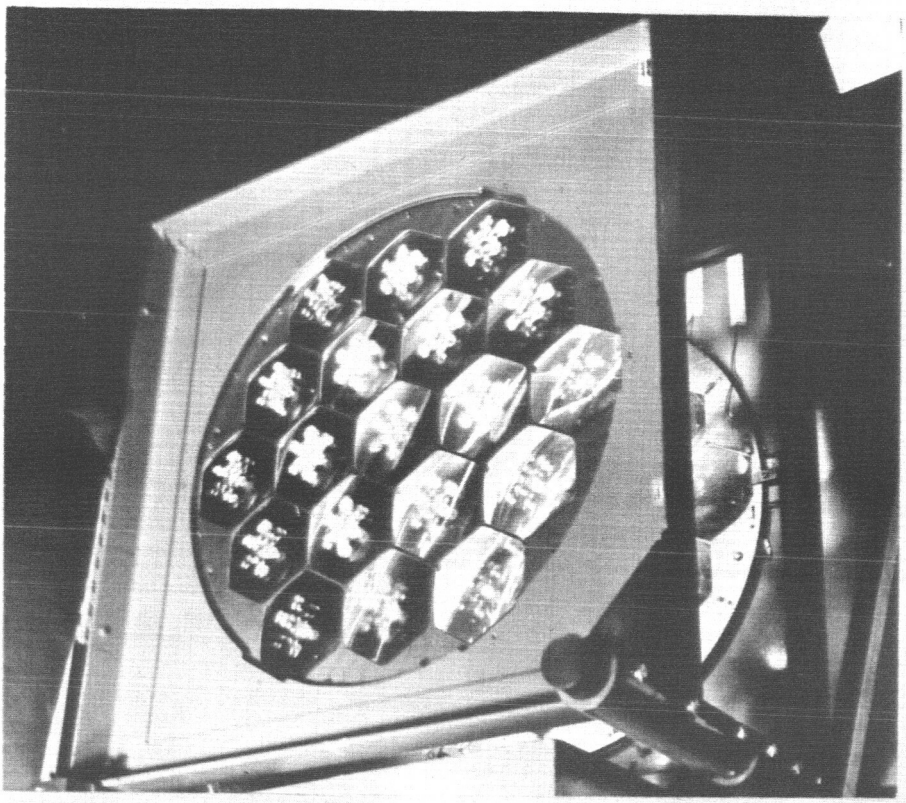

FIG. 23
LENS UNIT PASSING LIGHT

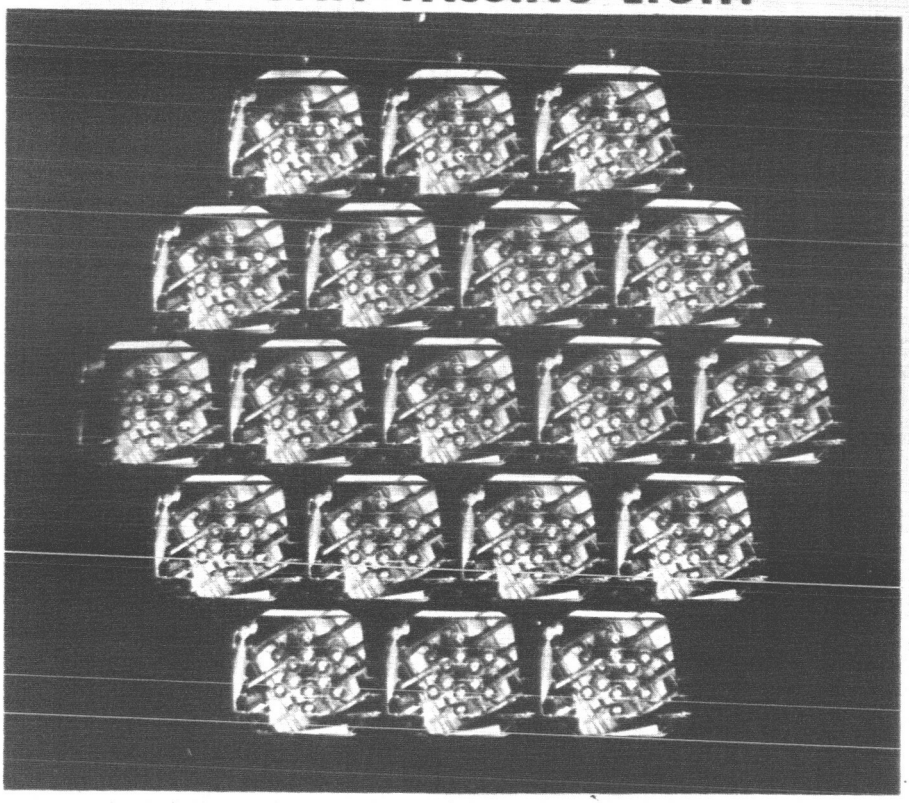

FIG. 24
LENS UNIT LOOKING TOWARD LAMP ARRAY

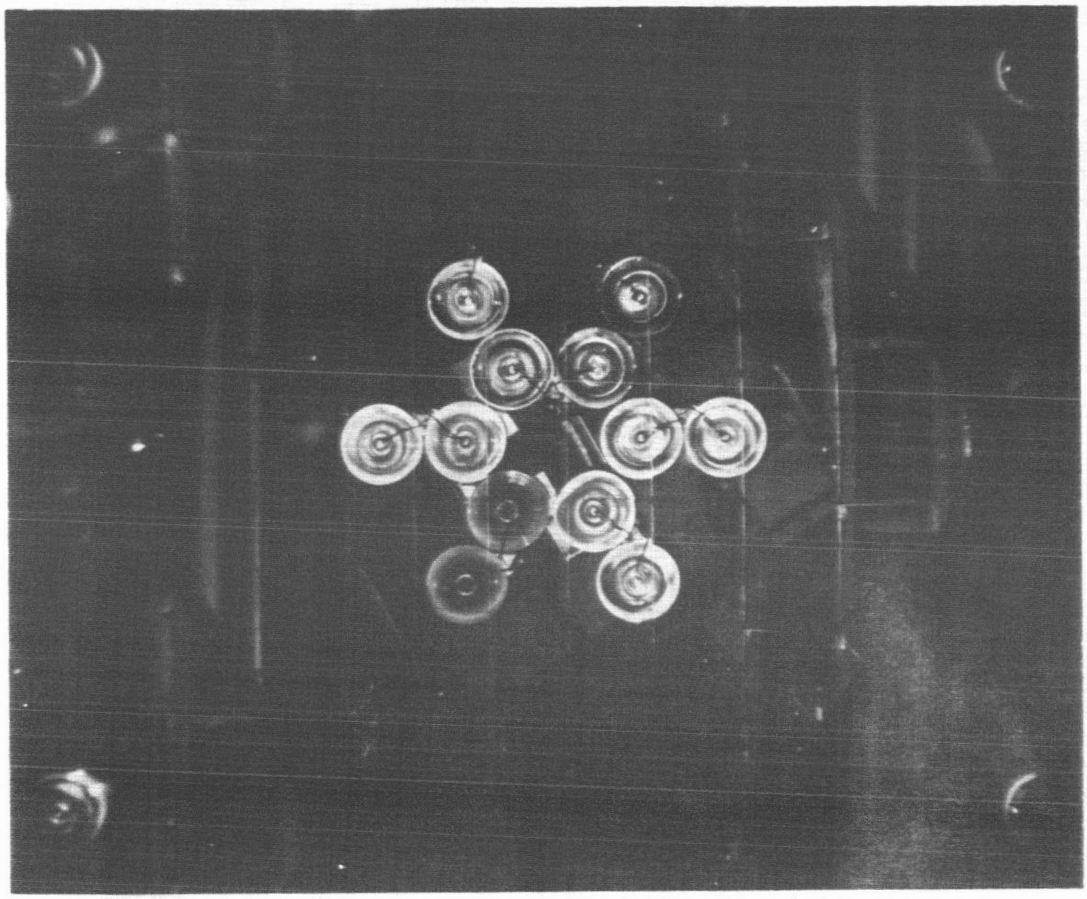

FIG. 25

IMAGE OF LAMP ARRAY IN ONE LENS CHANNEL

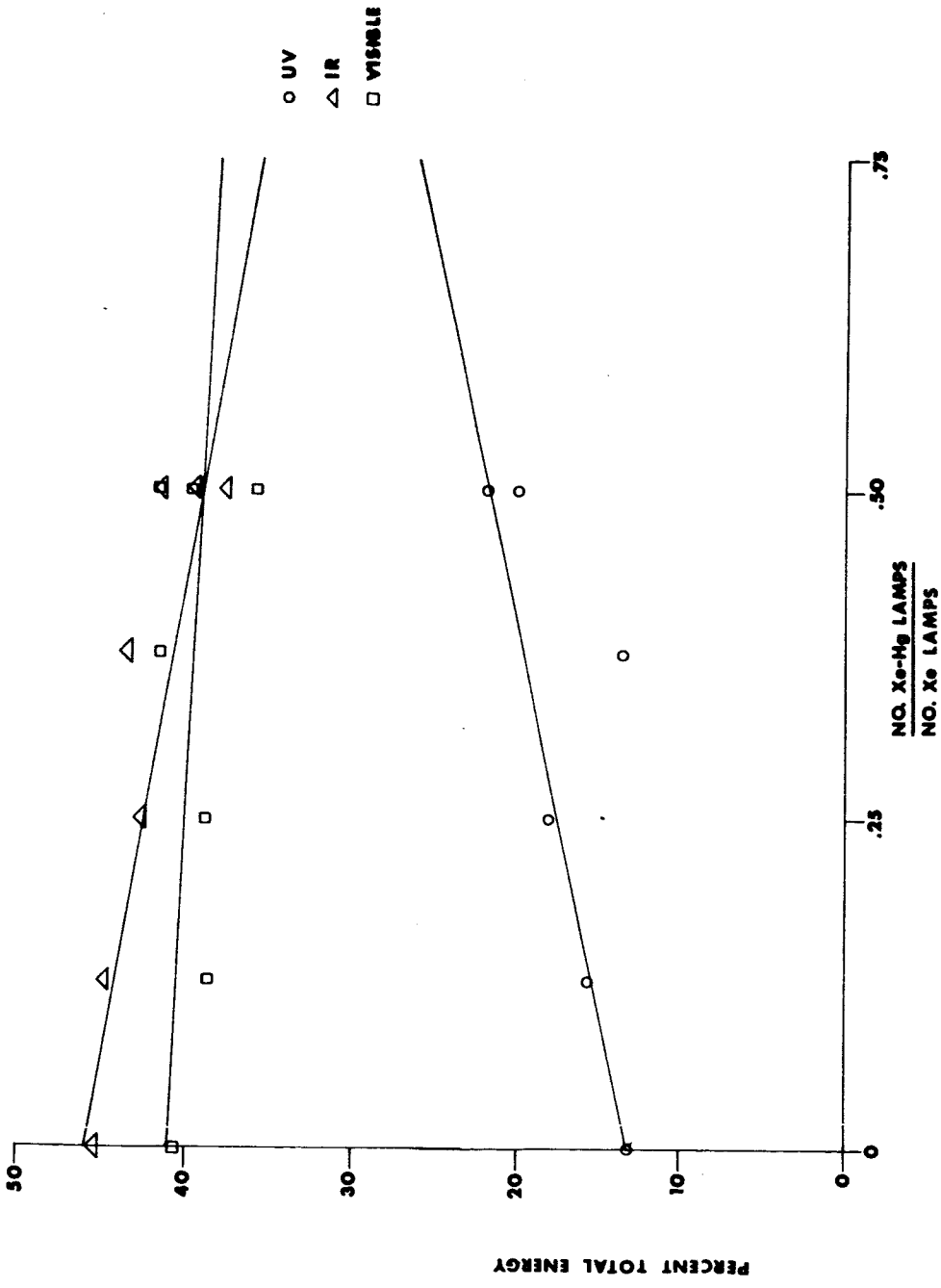

FIG. 26

EFFECT OF LAMP MIX ON SPECTRUM

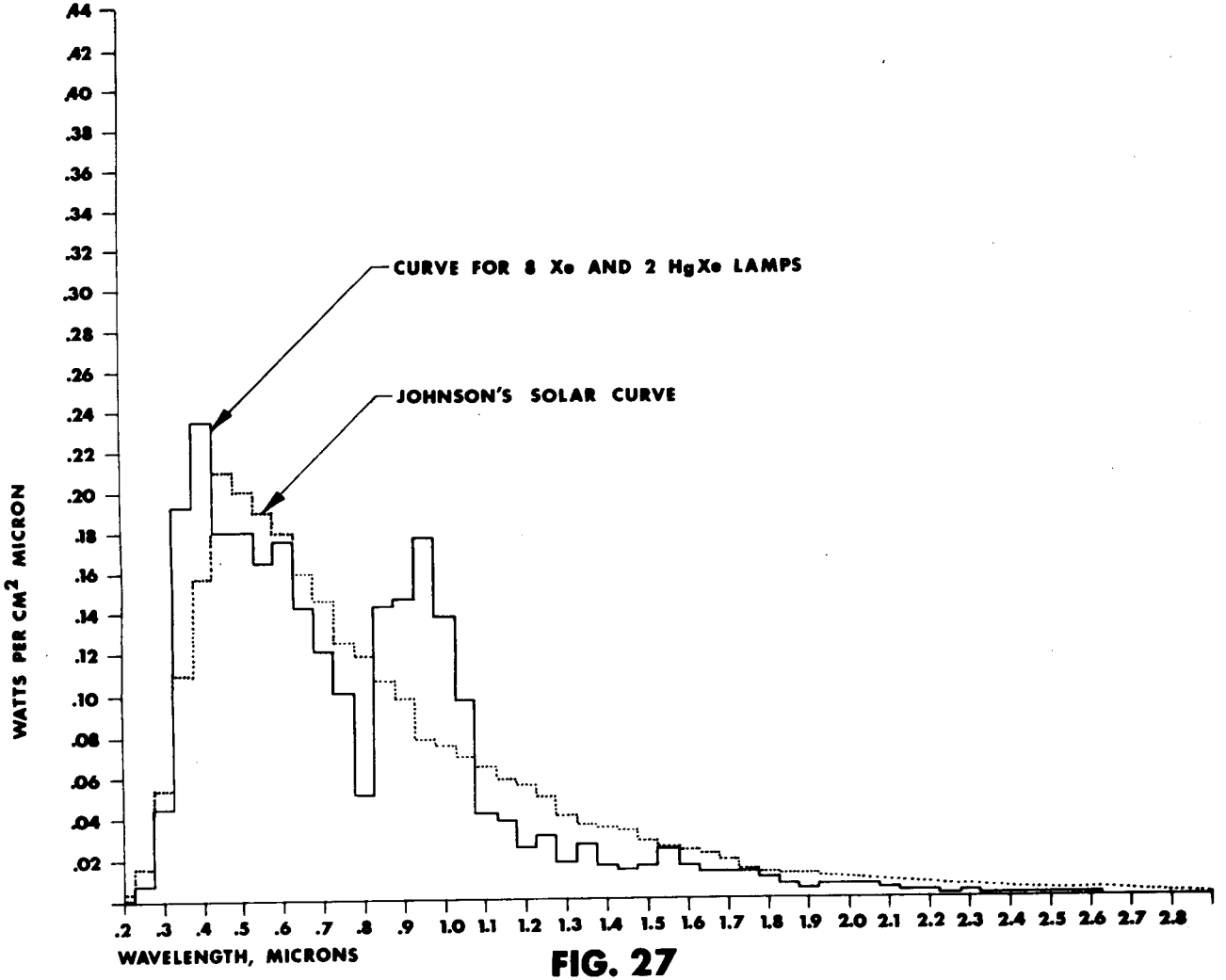

FIG. 27

JPL-SS-A6 SOUTH LESS 4 AND 9

National Aeronautics and Space Administration
Ames Research Center
Moffett Field, Calif.

PERFORMANCE CHARACTERISTICS OF THE AMES 10-SOLAR CONSTANT RADIATION SIMULATOR

By Donald L. Anderson

For presentation at Meeting to Discuss
Solar Simulation Research and Technology
NASA Headquarters
April 7-8, 1964

PERFORMANCE CHARACTERISTICS OF THE AMES 10-SOLAR CONSTANT SOLAR RADIATION SIMULATOR

By Donald L. Anderson

ABSTRACT

A brief review is made of the operating characteristics and present status of the Ames 10-Solar-Constant Solar Radiation Simulator. Performance test results of the recently completed system are compared to the design specifications. A spectral match is made between the simulator spectrum and the earth's zero air mass solar spectrum.

Instruments for measuring intensity, for uniformity mapping, determining collimation, and measuring the spectral distribution are described. The procedures used during the performance tests are discussed with particular emphasis on measurement technique.

PERFORMANCE CHARACTERISTICS OF THE AMES 10-SOLAR-CONSTANT SOLAR RADIATION SIMULATOR

By Donald L. Anderson

The topic of solar simulation has been discussed quite frequently in the past few years. Many simulators have been constructed; some are quite complex while others are very simple. The parameters by which the worth of a simulator is determined are dependent upon its ultimate use. Intensity, collimation, spectral match, uniformity-all play varying roles, depending upon the application. I know of one experiment that required a simulator of no greater degree of sophistication than the heating element of an electric stove. It was a real bargain at $4.00. Other experiments require a much higher degree of sophistication and consequently have a much higher price tag. The simulator I will describe today is in the latter category.

The specified requirements and proposed configuration of this simulator were presented in detail at the conference held here last year. Since simulators come in various sizes and shapes, I will briefly review the system specifications, the physical hardware, and then the demonstrated performance of the simulator.

Table I shows the specified system capability. The intensity was to be continuously variable from 65 to 1300 watts per square foot. The collimation was to be less than $\pm$ 5 degrees at the maximum output. The uniformity requirement of $\pm$ 5 percent is for the collimated portion of the beam. The collimated beam size was to be a minimum of 4.6 inches in diameter at the target plane. The regulation requirement was less than $\pm$ 2 percent variation in the intensity level. The individual lamps were to be regulated sufficiently to allow unattended operation over a week-end, approximately 100 hours.

Table II lists the desired spectral energy distribution as measured with a spectroradiometer having a maximum bandwidth resolution of 500 Angstroms. The specified energy match-percentages are the allowable deviations from the U. S. Naval Research Laboratory solar energy distribution curve for a zero-air mass sun (as published by Johnson in the Journal of Meteorology, December 1954, Vol. II, No. 6). The variation in these percentages is indicative of the relative difficulty in obtaining energy and the accuracy of absolute calibration of energy in these wavelength bands.

Figure 1 shows a cutaway assembly drawing of the 10-sun solar radiation simulator. A 13 unit, 2500 watt xenon lamp assembly is housed inside an eight-sided water-cooled chamber. Dry nitrogen gas is circulated inside this chamber as a cooling medium, rather than air, to preclude the generation of ozone. Transfer and collimation optics then direct the radiation from the array of arc lamps into the test chamber. The collimation lens assembly forms the vacuum seal between the solar simulator and the test chamber. This chamber is a four-foot internal diameter horizontal cylinder, five-feet long. The primary folding mirror is made of pyrex and is water cooled. The secondary folding mirror is a Kanigen coated aluminum plate, over-coated with an evaporated aluminum film. The other optical parts are made of high quality optical quartz. The system is designed so that each source irradiates the entire target area. Individual lamp failure therefore does not affect beam uniformity. This is very important for long-duration tests where a constant environment must be maintained. The beam intensity is controlled by varying the number of lamps and the power to each lamp.

Verification of the performance of a system is no small task. Special instruments and techniques must be utilized to accurately evaluate a system. The contract for this simulator included as a

requirement the delivery of instrumentation for measuring intensity, for uniformity mapping, determining collimation, and measuring the spectral distribution.

On January 15, 1964, performance tests of the completed simulator were conducted at the manufacturer's plant near Los Angeles. The following is a summary of these tests.

The instruments used for the intensity performance testing are shown in figure 2. The intensity level in the output beam was measured simultaneously with a calibrated Eppley Thermopile located in the target volume, with a thermopile located on a periscope ahead of the field lens, and with beam monitor solar cells. The high intensity thermopile is capable of reading intensity levels up to 14 solar constants. The calibration constant used in this test was supplied with the instrument by the Eppley Company. The beam monitor solar cells are four high-intensity photovoltaic sensors located on the periphery of the collimation lens. The output of the four cells are paralleled to provide an integrated measure of intensity during the operation of the simulator. The specification for the simulator required that the intensity of the collimated beam shall be variable from 65 to 1300 watts/ft^2. To provide this large beam intensity range, multiple patterns of lamps are utilized in conjunction with throttling of the radiation sources. Special achromatic filters were used for the low intensity tests.

Figure 3 shows the instrument used to measure the beam uniformity. The sensing element is a 1 x 1 cm solar cell and is mounted on an X-Y Scanner. Neutral density filters were used to reduce the intensity of the beam on the sensor to less than 2 solar constants. This is necessary to assure reasonably uniform sensor temperature and thereby linearity of readings. Horizontal and vertical scans were made at the 18 inch, 30 inch and 42 inch planes in the target volume. All beam intensities were recorded by a L and N Strip Chart Recorder. Figure 4 is typical of the data taken. The specifications required

that uniformity across the collimated beam be within ± 5 percent, and that this uniformity be exhibited over a diameter of 4.6 inches at the 42 inch target plane, when operating at 10 solar constants. The figure shows the measured uniformity which is well within this specification.

The problems involved in making spectroradiometric measurements are far too numerous to be treated in this paper. No new or unusual techniques were used in the calibration of this simulator, therefore, all of the usual problems were encountered. The equipment consisted of a double-prism monochromator employing photomultiplier detectors and a thermocouple bolometer.

Several independent tests were run and the results compared. By this means, it was possible to evaluate the test equipment and procedures. Measurements were made at various beam intensities and various positions within the beam to verify spectral uniformity throughout the target volume. Calibration of all measuring instruments was performed using a National Bureau of Standards calibrated quartz iodine filament lamp. The output of the standard lamp and solar simulator was compared at each wavelength and slit width setting of the monochromator. A white chalk block was used to deflect either beam into the entrance slit. These data were plotted in graphical form, as is shown in figure 5. This graph shows the relative intensity versus wavelength for both the simulator and the solar spectrum. The simulator intensity for this test was 10 solar constants. Numerical and graphical techniques were used to determine the match between these two curves within the specified wavelength increments. Figure 6 shows the energy in these integrated wavelength bands. The characteristic emission from the xenon lamp between 0.9 and 1.1 microns has been very effectively filtered to match the solar spectrum. In general, the simulator is rich in infrared energy and deficient in ultraviolet energy. In Table II this spectral match is given in percentage devi-

ations from the zero air mass Johnson curve. The specified energy match percents in the design goal regions proved to be somewhat optimistic for the ultraviolet region. The calibration in this region can, however, be somewhat inaccurate due to the low energy level of the calibration standard. New standards are being developed by the National Bureau of Standards which should increase the calibration accuracy.

A pin-hole viewer was used to measure the collimation angle for various lamp arrays. The collimation angle was determined for the combinations of lamps from 4 to 13, as they were used to achieve various intensity levels from one-half to 10 solar constants. The collimation half angle was within the $\pm$ 5 degree specification for all lamp combinations and intensities.

The stability of the simulator can be monitored by the photovoltaic cells, the periscope mounted thermopile, and the auxiliary thermopile located in the test volume. The photovoltaic cells mounted on the periphery of the collimation lens allowed continuous monitoring of beam intensity during a run. For the acceptance tests, a continuous run of thirteen hours at an intensity level of ten solar constants was performed. From the output of all the instrumentation, the stability of the simulator was verified to be within the $\pm$ 2 percent specification.

At the completion of the acceptance tests, the simulator was shipped from Spectrolab in Sylmar, California to the Ames Research Center. The simulator, with all its power supplies and controls, has been integrated with the vacuum chamber. Spectrolab personnel are scheduled to install the optical components within two weeks. At that time, the simulator will be operational and ready for research in the many areas where long-duration, high-intensity, solar radiation is required.

TABLE I

SPECIFIED SOLAR SIMULATOR REQUIREMENTS

INTENSITY	65 to 1300 watts per sq. ft.
COLLIMATION	less than $\pm 5^{\circ}$
UNIFORMITY	less than $\pm$ 5 percent
BEAM SIZE	4.6-inches in diameter at target plane
REGULATION	less than $\pm$ 2 percent of intensity
OPERATING TIME	100 hours continuous unattended

TABLE II

SPECTRAL ENERGY DISTRIBUTION MATCH

WAVE LENGTH RANGE ANGSTROMS	PERCENTAGE OF TOTAL ENERGY	SPECIFIED ENERGY MATCH PERCENT	ACTUAL ENERGY MATCH PERCENT
2200 - 2500	0.1	± 25 DESIGN GOAL	-60
2500 - 3300	2.9	± 15 DESIGN GOAL	-46
3300 - 4000	6.0	± 10	+3
4000 - 5000	14.4	± 8	-7
5000 - 6000	13.8	± 8	-7
6000 - 7000	11.9	± 8	+4
7000 - 8000	9.6	± 8	+3
8000 - 9000	7.7	± 8	+9
9000 - 11000	10.8	± 10	+18
11000 - 15000	11.2	± 10	+3
15000 - 20000	5.8	± 15	+22
20000 - 27000	3.1	± 15 DESIGN GOAL	+8

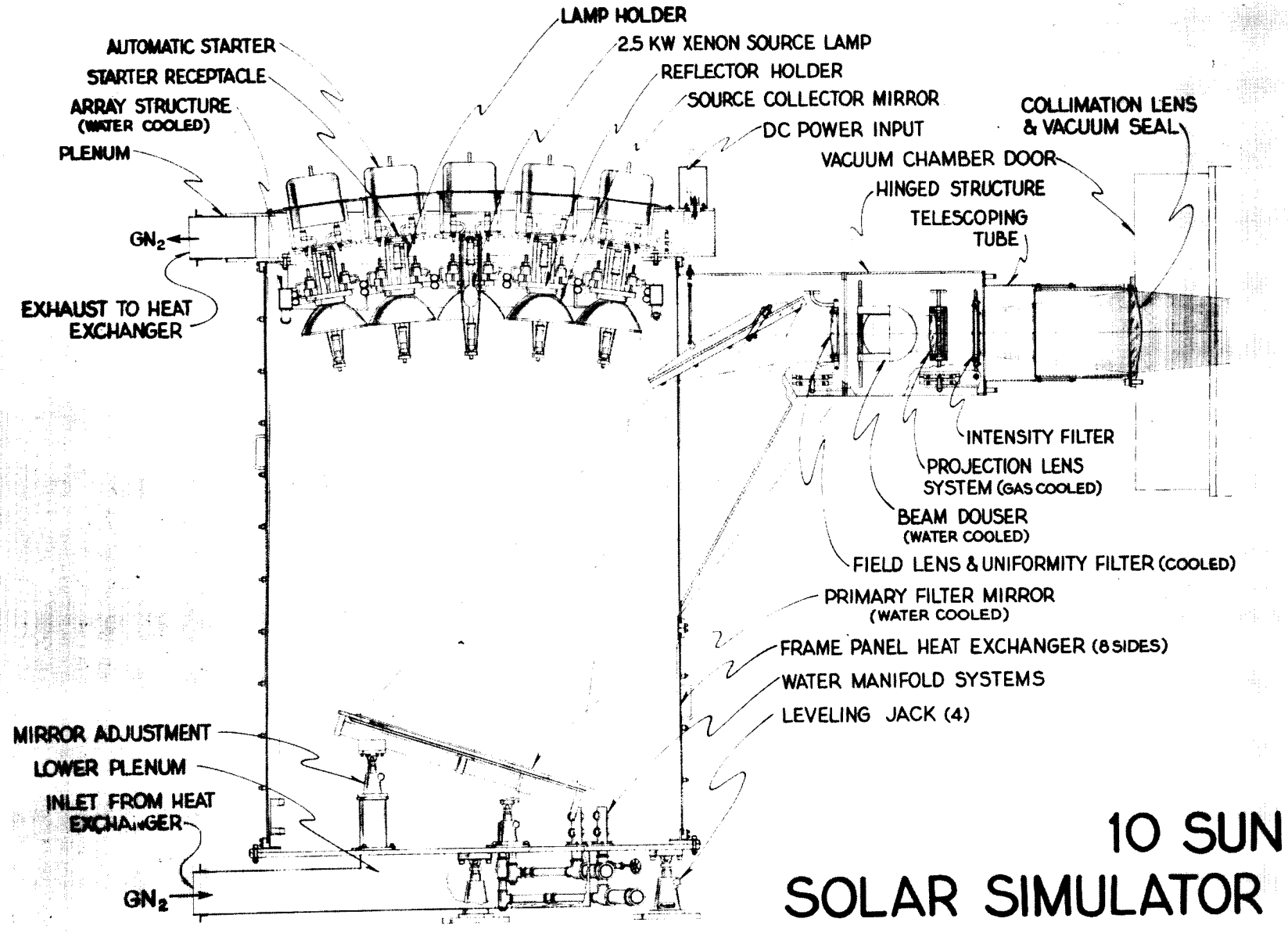

Figure 1. - 10 Sun Solar Simulator

NATIONAL AERONAUTICS AND SPACE ADMINISTRATION
AMES RESEARCH CENTER, MOFFETT FIELD, CALIFORNIA

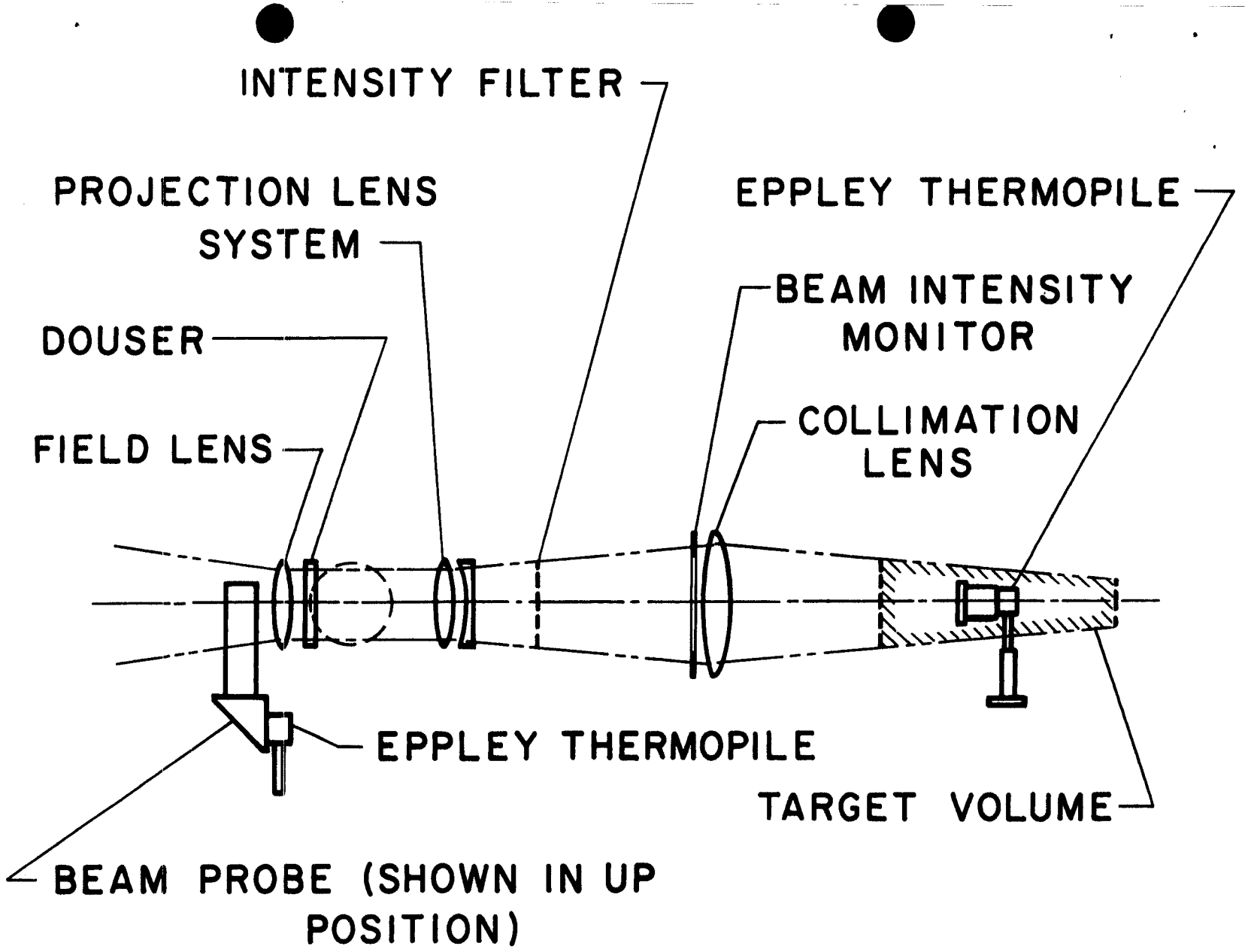

Figure 2. - Intensity Instrumentation

NATIONAL AERONAUTICS AND SPACE ADMINISTRATION
AMES RESEARCH CENTER, MOFFETT FIELD, CALIFORNIA

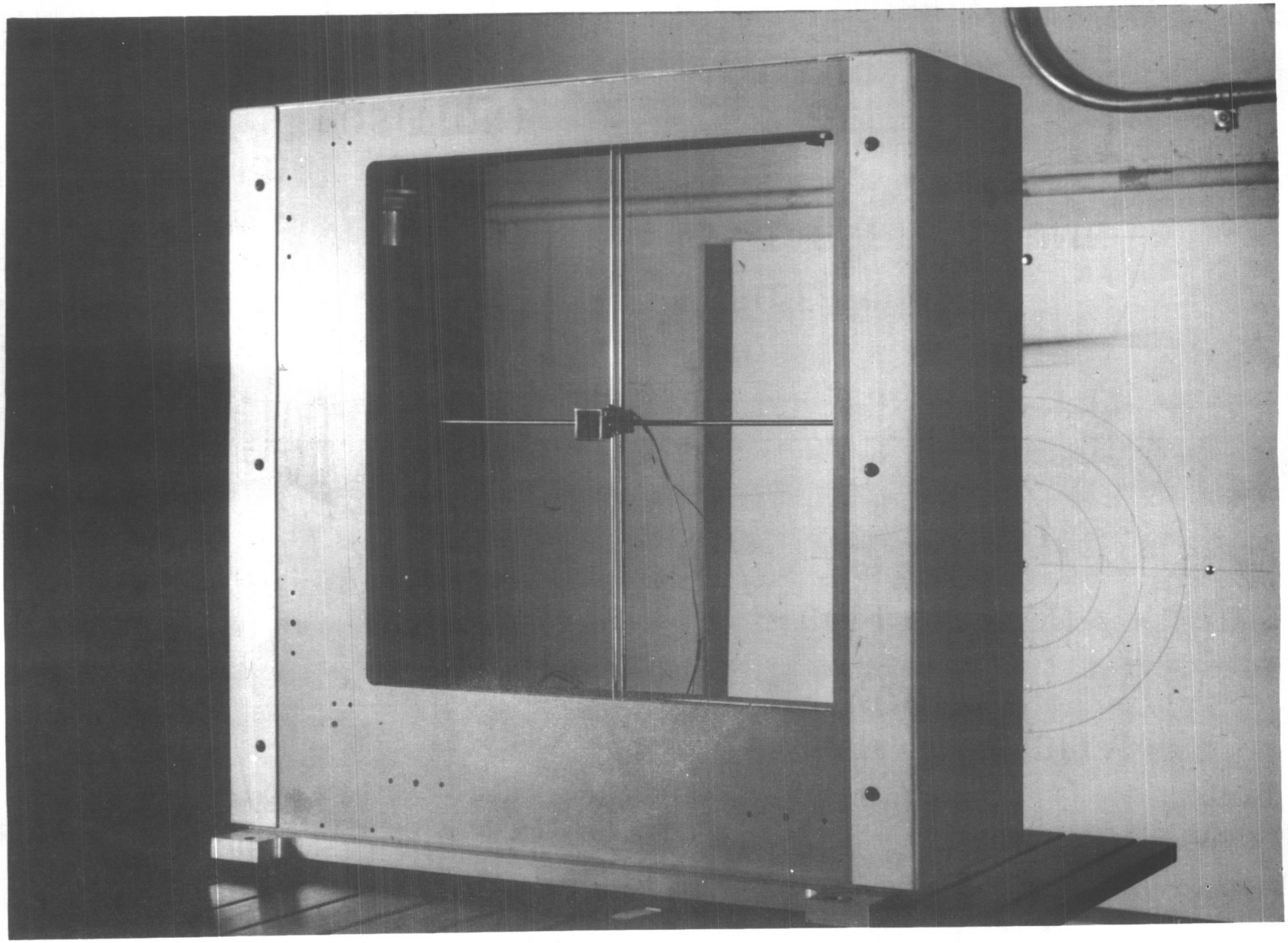

Figure 3. - Beam Uniformity Scanner

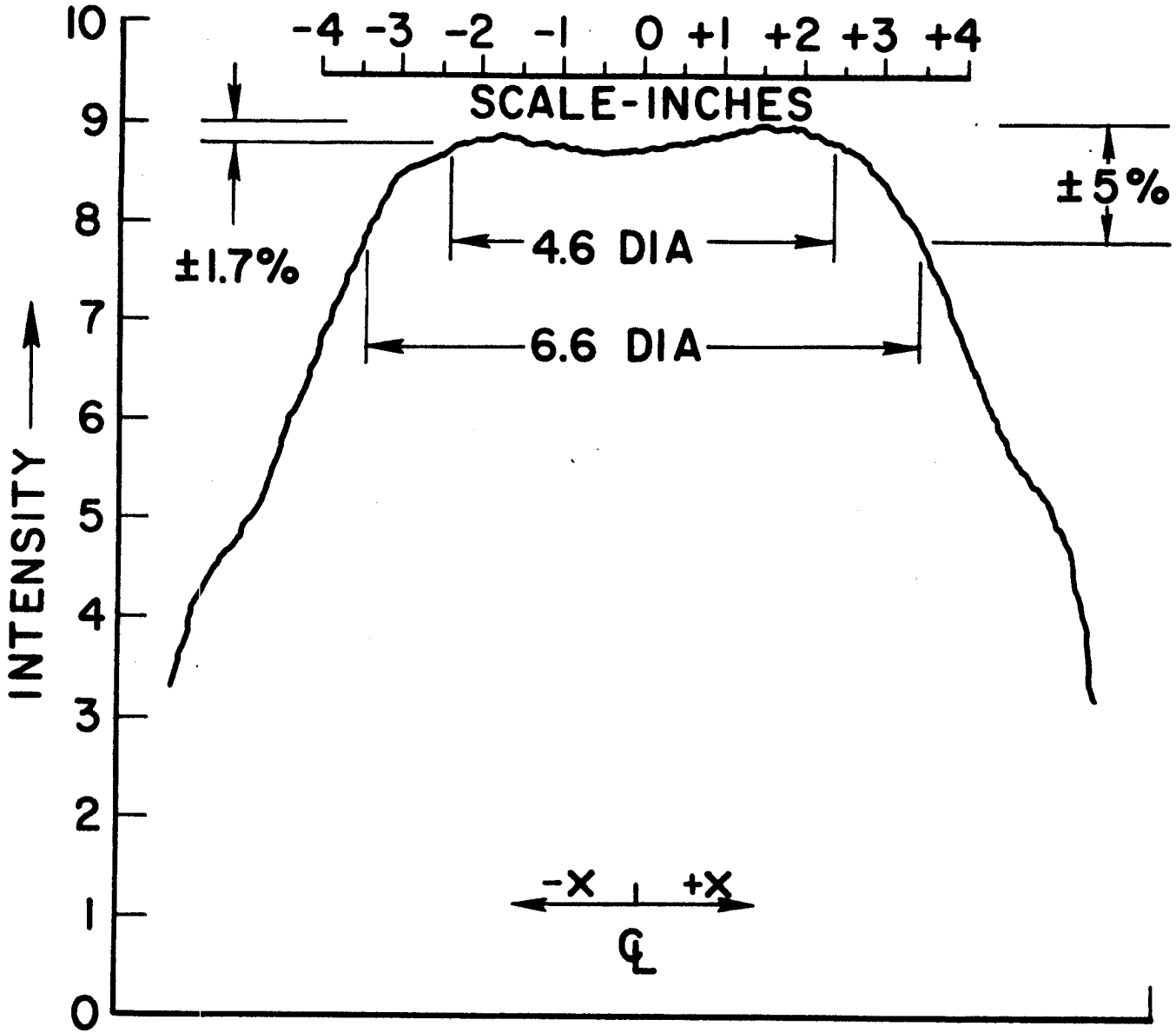

Figure 4. - Uniformity Scan Test Data

NATIONAL AERONAUTICS AND SPACE ADMINISTRATION
AMES RESEARCH CENTER, MOFFETT FIELD, CALIFORNIA

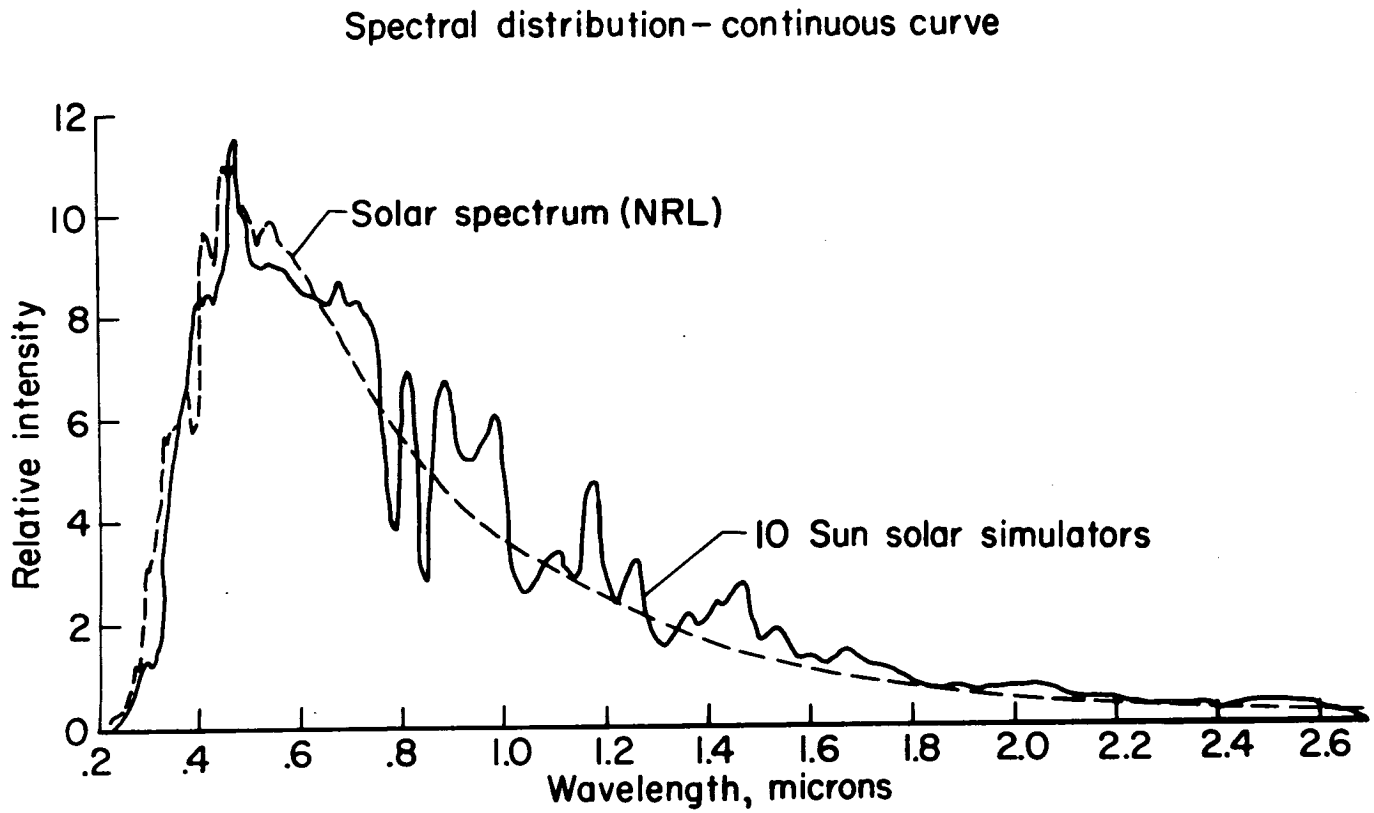

Figure 5. - Spectral Distribution-Continuous Curve

NATIONAL AERONAUTICS AND SPACE ADMINISTRATION
AMES RESEARCH CENTER, MOFFETT FIELD, CALIFORNIA

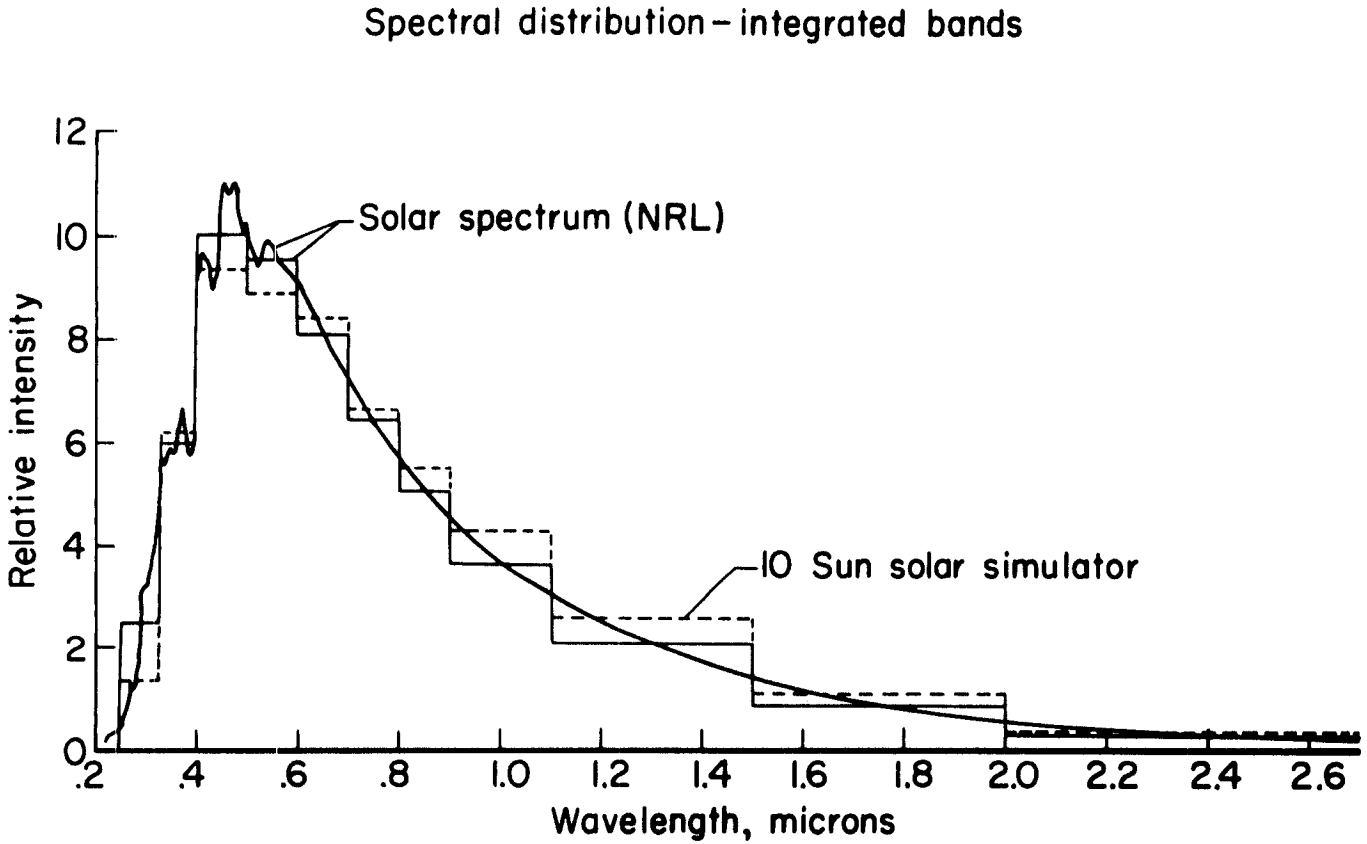

Figure 6. - Spectral Distribution-Integrated Bands

NATIONAL AERONAUTICS AND SPACE ADMINISTRATION
AMES RESEARCH CENTER, MOFFETT FIELD, CALIFORNIA

NATIONAL AERONAUTICS AND SPACE ADMINISTRATION

STATUS OF SOLAR SIMULATION AT LEWIS

by John L. Pollack

Lewis Research Center
Cleveland, Ohio

Prepared for

NASA Conference on Solar Simulation
Research and Technology
Washington, D. C., April 7-8, 1964

STATUS OF SOLAR SIMULATION AT LEWIS

by John L. Pollack

Lewis Research Center

This paper summarizes what has been done at Lewis during the last year, and presents our goals and plans for the future.

Our basic objectives have not changed. They are

(1) To develop an in-house capability to evaluate existing and proposed devices to produce solar simulation

(2) To upgrade and maintain our operational systems

(3) To furnish potential users with factual data on the state-of-the-art

(4) To support R & D on weak-link components of solar simulators in areas which are of specific interest to Lewis

In our paper last year, all our experience and work was in the use of solar simulators employing carbon arcs as sources. During this year much of our emphasis has shifted to evaluating the enclosed sources, not that we feel they are inherently superior, but because some of our requirements practically preclude considering carbon arcs.

The current level of effort at Lewis is six professionals in the Instrument and Computing Division. Two are working full time on the spectral irradiance measurements and the associated spectral radiation properties of materials.

In this area of spectral irradiance, last year Lewis contracted with Eppley Laboratories for independent measurements on our three carbon-arc solar simulators. Measurements on our 30-inch diameter beam were made under all conditions, including operational, - cold wall, and vacuum. Eppley's report to us was made available to the other NASA centers. We are pleased that the measurements by Eppley indicate the close approximation to the Johnson curve, but we are disturbed about the lack of agreement between these measurements and our own. In the following paper Mr. Goldman of our staff will present various methods for analysis of data obtained from filter radiometer measurements [redacted] paper will show our current disagreement between these results and the [redacted] obtained on disperseve instruments. His paper reinforces our opinion that the spectral irradiance remains the most serious unsolved measurement problem we have today.

Our philosophy in making the measurement with dispersing instruments is that it is absolutely required to destroy the geometry of the solar-simulator optical system before presenting the radiation to the instrument for measuring. We are working with integrating spheres, diffusing flats, and etched mirrors to

accomplish this and yet preserve enough energy from the standard sources to calibrate the instrument. To date we do not consider our efforts successful.

We are anxious to see what progress NBS is making on our contracts with them in this problem area. Also, we are waiting with interest the report by Eppley labs in which they made comparison measurements of GE's Valley Forge facility, using a Perkin Elmer "Spectracord" and their own filter radiometer. Incidentally, we mentioned last year our efforts to use a Macpherson arc as a high temperature standard of radiation (3810° K). We have shipped this lamp to Eppley. They will measure it on their dispersive device, and we will compare results.

To facilitate measurements on recently purchased incoming systems, we have set up an evaluation area. In the next few months we will measure constancy, uniformity, collimation angle and spectral irradiance, using a recently purchased filter radiometer from Eppley, on the following devices:

(1) Two Genarco ME6 - one with their conventional projection optics, the second modified by us to utilize mosaic lenses and a collimator

(2) The Strong Electric 75002, which utilizes a reflector-collector, mosaic lenses, and quartz projection lens

(3) A Minneapolis-Honeywell-Goddard module in a variety of modes of operation, which will be discussed later

The Measurement Facility has progressed to a point where we are in the process of instrumenting the area. The purpose of this area is to have available space, ventilation, power, and survey and measurement instrumentation to allow us to make the necessary measurements of simulator performance. The room is large; we have space for 50- to 60-foot vertical beam throws, and up to 100 feet horizontally. Up to 50 kilowatts of power will be available for various sources. A survey stand providing incremental linear and radial positioning over a 2-foot diameter field is available, and a larger 4-foot diameter stand is being built. These stands will allow precise, remote positioning of total or spectral radiometers in the beam of solar simulators with digital readout of position and angle of the scanning sensor as well as the scanning and fixed-sensor outputs. The purpose of the apparatus is to allow technicians to make simple, safe, accurate measurement of constancy and uniformity from a remote station.

It was mentioned earlier that we have had to turn our attentions to the consideration of compact-arc-modular type of solar simulation. Last year at this meeting we mentioned that Lewis had plans for a space environment facility at its Plum Brook Station (fig. 1). The space propulsion facility will have a cylindrical vacuum chamber 100 feet in diameter and 122 feet in height from the flat working floor to the top of the hemispherical dome. The vacuum chamber is surrounded by a 7-foot-thick concrete nuclear shield and containment vessel which is evacuated to 1/2 pound per square inch absolute. Inside the shield is an aluminum vacuum, cold wall structure. This large facility has been designed and a construction contract will be placed before June 1964. Estimated com-

pletion date is spring of 1967.

This large facility requires a solar simulator which can be used to irradiate a wide variety of test models of different sizes and shapes including the SNAP 8 space nuclear power generation system, chemical rocket upper stages, and other space vehicles and satellites. Initial model area to be irradiated is approximately 500 square feet.

Our studies and plans to provide a solar simulator for this facility by June 1967 has been influenced by the following factors:

(1) The unique construction of this large facility (the 7 ft.-thick walls) has made difficult the conventional approach of sources of radiation outside the chamber with optical penetrations in the chamber walls.

(2) The planned test programs for this facility also require that the solar simulator operate for long periods (100 hr minimum) without access to the system components.

(3) The large volume of the chamber provides a great degree of flexibility in model size and shape to be tested within it. It would be highly desirable to have similar freedom in positioning the solar simulator and in directing its radiation.

Consideration of these facts led us to the conclusion that for a large chamber employing this type of construction, a modular type solar simulator has to be designed that includes a radiation source that can operate entirely within the space environment. It is our opinion that the following advantages outweigh the attendant disadvantages:

(1) Complete flexibility to irradiate any shaped area from any direction

(2) Elimination of optical penetrations in the chamber walls

(3) Unitary construction of the module, rather than a design divided into parts inside and outside the chamber

The disadvantages of this design approach are

(1) Added heat load introduced into the chamber

(2) Necessity to pressurize the modules with attendant leak possibility

(3) Cooling and electrical power penetrations in the chamber wall

(4) Inaccessibility for source replacement during operation (this puts a premium on reliability, and indicates that we consider a system that employs redundancy)

(5) Eliminating of the consideration of carbon arc with its superior spectral distribution as a source of radiation

Implementing this basic decision (putting the radiation source inside) will be a major task during the next two years. The next decision required is the selection of the module design best suited for the Plum Brook system. If this decision were required today, our choice would be the Goddard-Minneapolis-Honeywell design because in our opinion it has the best over all guaranteed performance of any compact arc lamp module system available today.

Our basic premise is that a large system should be built around a proven module performance, and the only proof of module performance is evaluation of the actual operating hardware. Therefore, before actual expenditure of funds that are tentatively budgeted in fiscal year 1966 we will examine other promising approaches using as our minimum performance guidepost the performance of the Goddard module. Using this guideline will provide an opportunity for achievement of an optical performance superior to what is obtainable today by building onto the state-of-the-art.

Our method of implementing this plan is

(1) We have on order for delivery this month a flexible version of the Goddard Minneapolis-Honeywell module. This module will be furnished with interchangeable HgXe and Xe lamps of 2.5, 3.5 and 5.0 kilowatts. The Module will be capable (with various restrictions) of producing a vertical or horizontal beam. We will operate and measure the performance of the module to familiarize ourselves with its operating characteristics and to allow the intelligent prediction of the performance trade-offs possible for specific tests. First hand operation of the system will also allow better evaluation of the problems associated with enclosing the system in a pressure-tight container so that it can be operated within the space chamber.

(2) We intend to rent a second commercially available system (the Aerospace controls Lab compact arc lamp system employing mosaic lenses) to compare its performance to that of the Goddard system.

(3) We have a study contract in progress with Minneapolis-Honeywell (NAS3-5024) to design a pressure tight enclosure for an improved version of the Goddard module. This study is based on utilizing a 5-kilowatt xenon lamp. The module will operate vertically or horizontally; the study includes choosing materials compatible with nuclear radiation flux loads in which the solar simulator must operate. Module cooling, power requirements and control requirements as well as piping and wire sizes and methods of connecting to module enclosures are being determined. Required external cooling and electrical systems are being considered. The methods of installing, aligning, and supporting clusters of modules of variable size and shape are being worked out. The clusters will either be mounted off the test chamber floor in suitable racks or hung from the dome ceiling of the chamber.

The initial study will be completed in May, and detailed cost estimates will be furnished for the following:

(1) Completing the module detail design, and preparation of engineering plans and specifications

(2) Fabrication, test, and delivery of solar-simulator modules complete with power supplies and any other external system in groups of 50 and 200

(3) Installation in facility, alignment, and checkout of complete module system in groups of 50 and 200

Some data and preliminary conclusions are available now on this contract as a result of polar plot, microbrightness, and lamp aging tests on a variety of lamps in both vertical and horizontal operation. The results of early tests on mercury-xenon lamps in horizontal operation indicated the presence of a thermal tail flame which, even before it gave any evidence of envelope darkening, distorted the polar distribution of flux from the lamp and seriously reduced it locally upward (over the anode). Since the Honeywell design demands uniform polar distribution, use of this lamp in horizontal operation in the Goddard system would require cutting back the capture angle of the ellipse and reducing the overall module efficiency approximately 20 percent. The tests did show, however, that assuming the nonsymetrical polar distribution could be tolerated, the lamp could be operated for 200 hours with only the normal expected degradation in output even though the lamp blackened appreciably.

Since operation of the lamp in a both horizontal and vertical orientation is highly desirable for our application, the study was reoriented to consider xenon lamps. Figure 2 is a polar plot of a horizontally operated lamp. The dotted line (run no. 1) is the initial polar plot, the solid is the measurement after 503 hours continuous horizontal operation. This 5-kilowatt xenon lamp had no tail flame, and exhibited no bulb darkening. After 500 hours, however, vitrification of the quartz envelope in the vicinity of the cathode is indicated by a 15 percent local drop in intensity on the polar plot. The total and local degradation of radient output of the same lamp shown plotted vs time is shown on figure 3.

Based on the assumption that a 5-kilowatt xenon lamp would be used, a module was designed to cover 4 square feet (a hexagon 26-in. across the flats) with a maximum of 170 watts per square feet (1.31 SC).

Figure 4 is a drawing of the system as Minneapolis-Honeywell sees it today. In general except for scaling upward in size and an improvement in the condensing system to improve uniformity, it is similar to the Goddard system.

The enclosure is approximately 2 feet in diameter and 6 feet long and will weigh about 300 pounds. The entire module is constructed of aluminum with the exception of the nickel electroformed hyperbola. The parabola, which is of a finned design, is attached to the main structure. The critical seal is at the field lens. The coolant is tentatively a water alcohol mixture entering at 20° F through an inlet tube which is the support structure for the hyperbola, continues back following a parallel path into the container, through the coiled heat exchanger, and out. The container is filled with air or nitrogen at atmospheric pressure. A fan circulates the air around the outside of the ellipse through the heat exchanger, through the finned parabola, past the field lens, through three parallel paths between the condensers, and finally

around the lamp. The heat exchanger and water cooling removes 24,000 Btu per hour per unit, and each unit requires 2 tons of refrigeration. A coolant stabilized Hycal thermocouple detector on the hyperbola strut will monitor the module radiant output. The igniter is located in the area behind the lamp. Input power, fan power, and control wiring enter through the back.

It is planned to mount and support the modules in a horizontal array on the hexagonal bearing areas in the manner shown in figure 5. The modules will rest on one another to a height of 10 modules. The center of gravity is at this central support ring. A restraining harness will prevent shifting in the direction normal to loading. The utility supply tower has been designed for the horizontal array. It will consist of two vertical columns that provide the necessary supply and return lines to the modules.

Upon completion of this study contract (May 1964) it will be evaluated by the Lewis staff. We hope that actual operational data on the Goddard facility will also be available at that time.

If the decision is made to proceed, we will contract for final design, construction, and evaluation of a 1-3 module canned array. When the contractor's testing is complete, we will operate the array within a suitable environmental facility.

In spite of the fact that we consider the Goddard-Minneapolis-Honeywell module the best available today for our purposes, we are also providing limited contractual support to promising new schemes for producing solar simulation under the general conditions imposed by the Plum Brook space chamber.

We have entered into a contract with Linear Incorporated of Evanston, Illinois (NAS 3-2794) to design, construct, and evaluate the optical performance of an extremely simple modular design employing a minimum of components and utilizing the mosaic lens principle. Hoped-for results of the optical performance of the module would be (1) a gain of at least a factor of two in radiant energy transfer efficiency over the Goddard system, (2) a geometry which would allow dual or tertiary stacking of modules in both vertical or horizontal array, (3) a substantial decrease in the number and tolerance required on both the individual optical components and the alignment of components in the module.

We expect these gains to outweight possible losses in other areas of simulator performance, such as uniformity of irradiance. The linear concept is shown in figure 6. It consists of a grouping of on-axis modules for direct irradiation of the test zone. The flux source was chosen as a 2.5 kilowatt Westinghouse mercury-xenon lamp (SAHX-2500 F) so that a direct comparison of optical system results could be made with the Goddard module.

An ellipsoidal main reflector around the source, two lenticular or mosaic lenses, one of which might be a pressurized radiation window in the canned version, complete the module.

The reflector designed for slumping in rectangular quadrants has 3-point

adjustable mounts for each section. The elliptical form of the reflector is angularly displaced, and the image of the arc is actually an annular ring around the axis so that the flux will miss the end of the lamp and be more readily operated on by the lenticular plates. The collector intercepts practically all the source radiation. A secondary device is employed at the back of the reflector to complete the flux collection. Since no ray of flux is refracted by the lenses more than 12°, the chromatic aberration of this system is about one-eighth of the Goddard design.

A pair of lenticular plates accomplish the collimation and direction of flux to the test area covered by the module. The top lenticular plate is a combination of a prism and lenticular-lens array of hexagonal segments focusing and displacing an image of the arc so that images are formed in the center of the second lower array of pure-lens elements. The lower plate images the upper hexagonal segments onto the test zone. Each plate will be made up of many hexagonal elements, and the plates will be pressed from quartz or Vycor blanks.

Linear, Incorporated expects to be able to cover a 30-inch hexagonal area with one solar constant using one 2.5 kilowatt lamp. If they are successful and the reflector size remains as designed, it would be possible to intersperse a second or even a third array of modules as shown in figure 7. This interspersion would allow higher levels of irradiance or a redundant capability that would increase the reliability of the system. (In case one lamp failed the adjacent lamp could be burned on). Also, since this system is quite insensitive to polar symmetry of flux from the source, it would be possible to utilize Mercury-Xenon lamps operating horizontally in this system. The promise of increased efficiency is most attractive. For a system totally contained within a space chamber, it is a double advantage since the transmitted energy does not have to be removed as heat. If efficiency is doubled, cooling requirements are reduced to 40 percent.

One other area of interest to Lewis that is related to the general problem of obtaining a good reliable solar simulator for our Plum Brook space chamber will be discussed now. The 5-kilowatt lamp design of Minneapolis-Honeywell mentioned earlier requires approximately 130 modules to irradiate 500 square feet. In addition, there is general agreement that most of the problems associated with any solar-simulator design are directly traceable to the sources we must use. The present compact arc lamps are subject to the following limitations by design considerations:

(1) Limited power input (5 kw is maximum available)

(2) Vertical operation only - at least until more testing disapproves present practice

(3) Fragile and subject to explosive failure

(4) Require auxiliary cooling and ventilation

(5) Accelerating degradation during useful life

The plasma-jet radiant energy sources show promise of becoming second generation sources for solar simulation. They eliminate the limited power input and vertical operation requirement and are rugged and strong. By the nature of their operation the sources have a built-in cooling and venting system; they can be salvaged and rebuilt at the end of their useful life. Because the gas is recirculated through the lamp, they offer attractive possibilities of gas mixture and pressure variation to tailor spectral output. Through the co-operation of our Washington office, we are following the progress of various NASA and AEDC contracts that are directed toward evaluating and improving these sources, mainly the Plasmadyne source of Giannini Incorporated.

Another of these sources that appears particularly attractive to us because of our interest in the mosaic lens approach is the Westinghouse Radiant energy source.[1] This source is described by a report by Wolf & Hughes of that company and is shown in figure 8.

The source itself is a sealed-beam "headlight" design consisting of a rugged shell designed to withstand 600 pounds per square inch internal pressure. It incorporates water-cooled replaceable electrodes, and an integral elliptical mirror and lens. The gas enters, sweeps the lens and mirror to keep them cool and clean, and exits through the annular anode.

In our opinion this source is adaptable to our requirement of operating within the space environment. It is rugged and operates quietly and stably. The radiating area, from visual examination , appears to be much more of a compact-arc distribution than that of a line source. We have made rough measurements of radiant output from this source and reflector at the Westinghouse plant and concur with them that approximately 30 percent of the input power leaves the source as a directed beam.

Some advantages of the integral source reflector design of Westinghouse are

(1) Greater separation between arc and nearest optical surface that results in

   (a) Less deposition on the optical surface

   (b) Better cooling of the optical surface

   (c) Less obstruction to the projected beam

(2) Allows use of a dome-shaped window (lens) that results in

   (a) The window being able to support a much higher gas pressure

   (b) A longer distance from arc to window, therefore, reduced temperature rise in window

[1]Available from Westinghouse Electric Co., Industrial Systems, Public Works Province, Pittsburg 35, Pa. (P.O. Box 10560).

(c) Less intensity of radiation through the window, reducing the effect of window degradation by ultra-violet radiation

(3) A system that is more compact and, hence,

(a) Simplifies the introduction of magnetic stabilization

(b) Better suited for modular arrays, allows a greater number of units to be used for either higher irradiance, or for reliability.

In view of these possible advantages we are attempting to place a contract with Westinghouse to modify, improve, and life test one of their sources in order that we may examine it for our future requirements. Because of their proximity to Lewis, we will be able to take our own measuring equipment to the plant to measure its performance. The source now is conservatively rated at 10 hours at 10 kilowatts although it has been run up to 20 kilowatts. Westinghouse simply has not sufficient experience with it to predict its final performance. Target performance for our contract would be at least 100 hours at 25 kilowatts or more with the use of a recirculating gas specified by Lewis. We hope to complete negotiation of this contract in May 1964.

In conclusion, since we feel the basic purpose of these in-house meetings is the exchange of information, we will upon request make available to any other center the progress and final reports of any of our contracts as well as any significant progress in our in-house activities.

NASA
C-64141

LEWIS - PLUM BROOK SPACE PROPULSION FACILITY

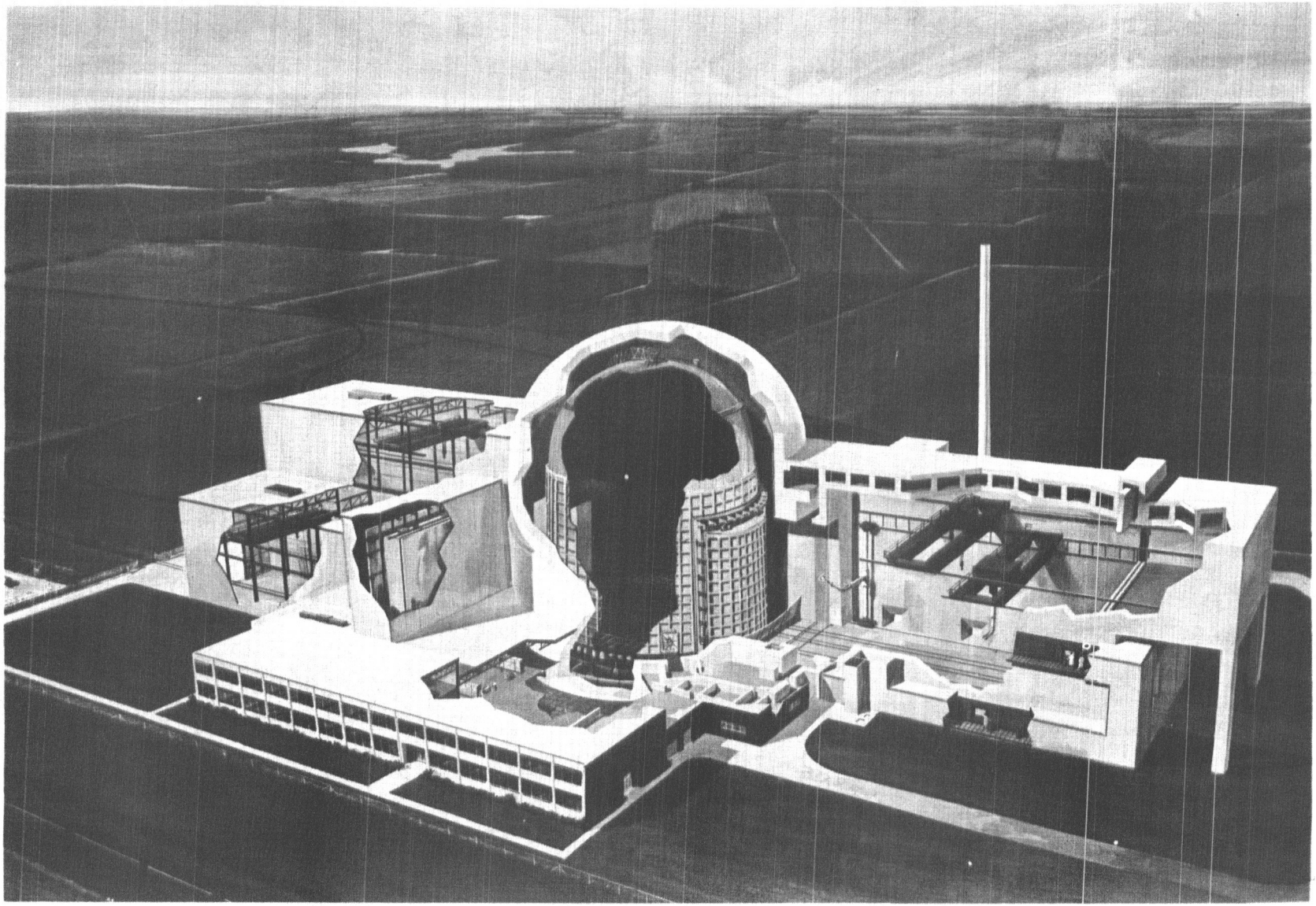

FIGURE 1

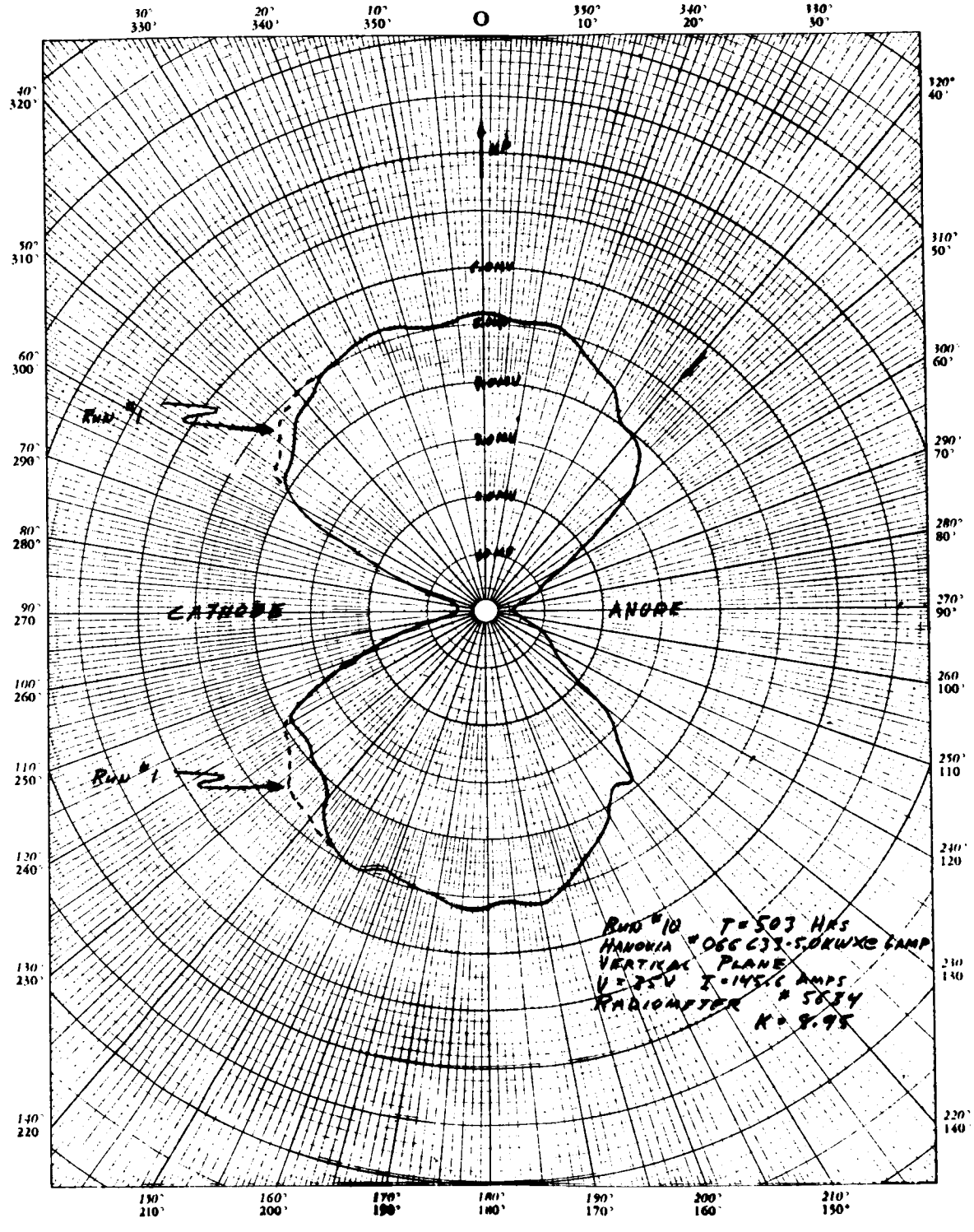
CATHODE
ANODE
Run #1
Run #1
Run #10 T=503 Hrs
Hanovia #066 C33-5.0KW/XE LAMP
VERTICAL PLANE
V=75V I=145.6 AMPS
RADIOMETER # 5634
K=8.95

Figure 2

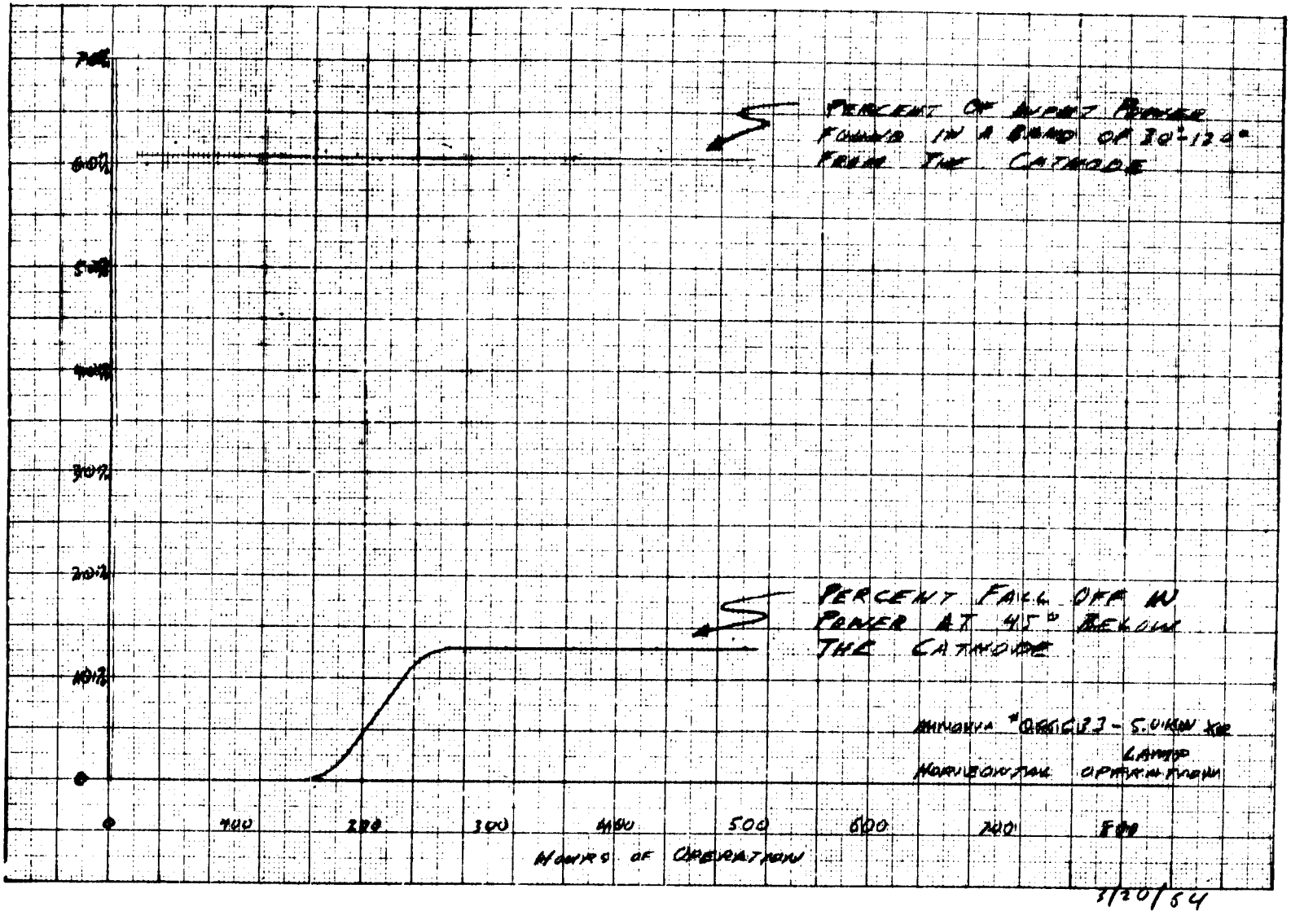
PERCENT OF INPUT POWER
FOUND IN A BEAM OF 30°-120°
FROM THE CATHODE
PERCENT FALLING OFF IN
POWER AT 45° BELOW
THE CATHODE
AMMONIA "OPTICAL" - SUITABLE FOR
LASER
MODULATION OPERATION
100
200
300
400
500
600
700
800
HOURS OF OPERATION
3/20/64

Figure 3

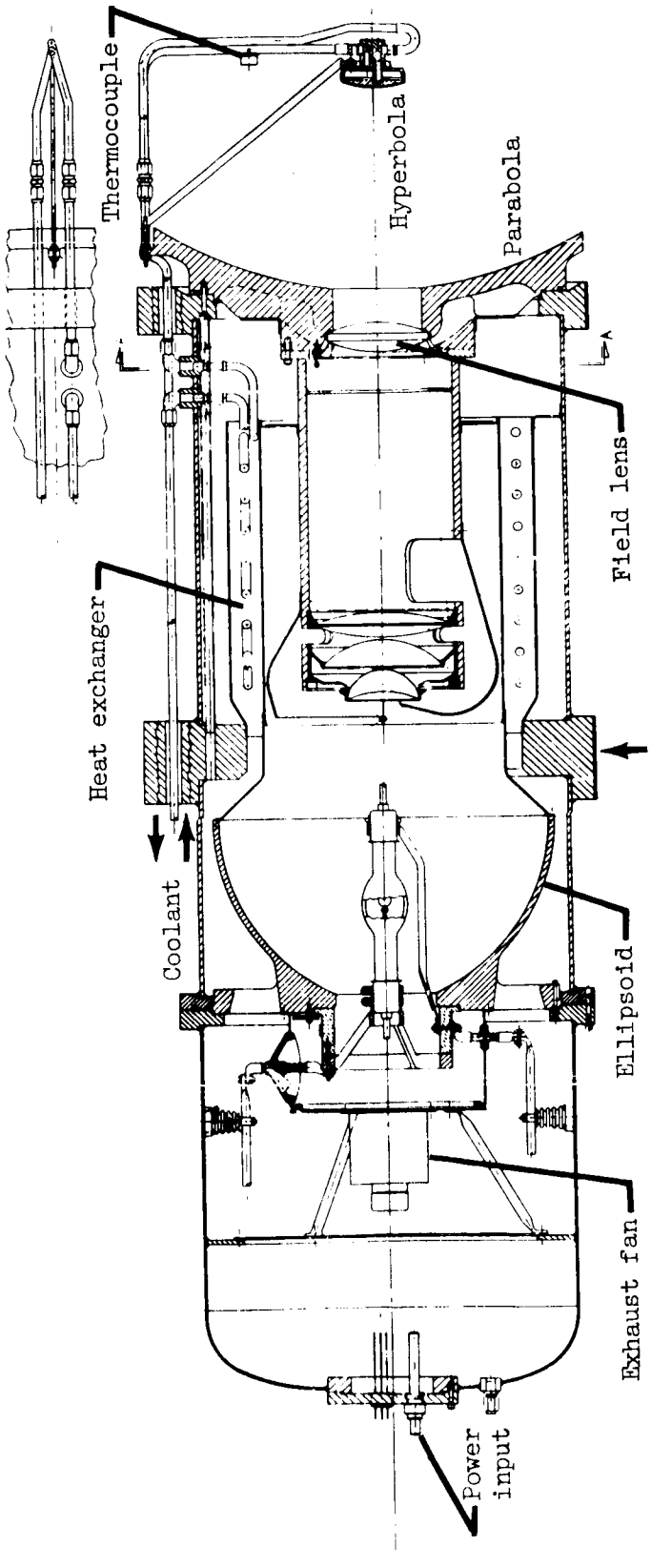
Thermocouple
Hyperbola
Parabola
Field lens
Heat exchanger
Coolant
Center of gravity
Ellipsoid
Exhaust fan
Power input

Figure 4

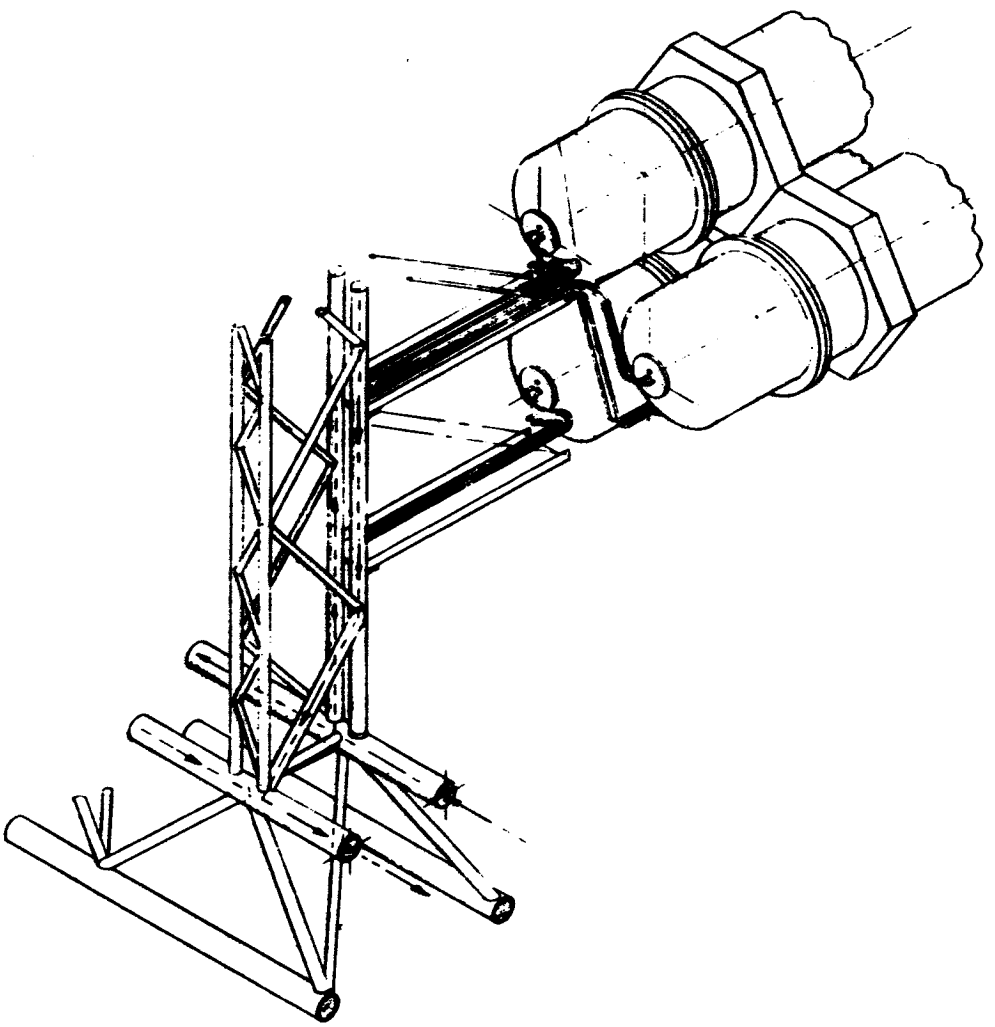

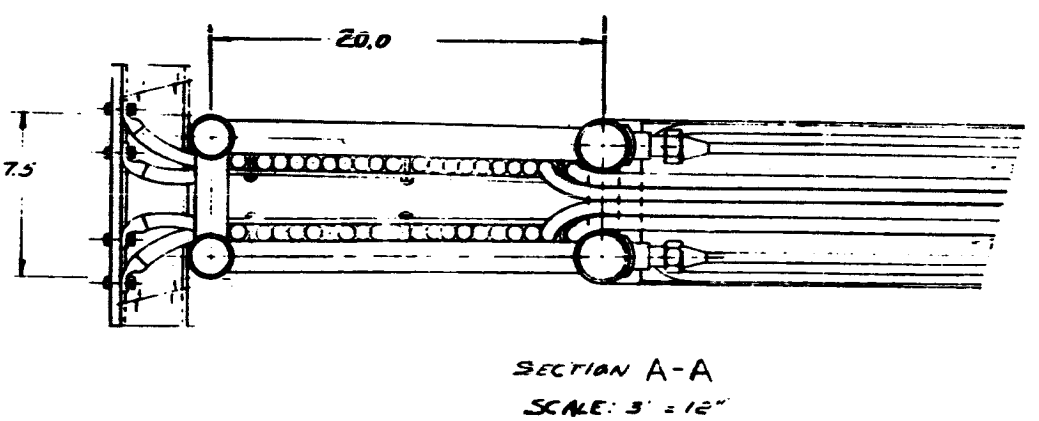

Figure 5

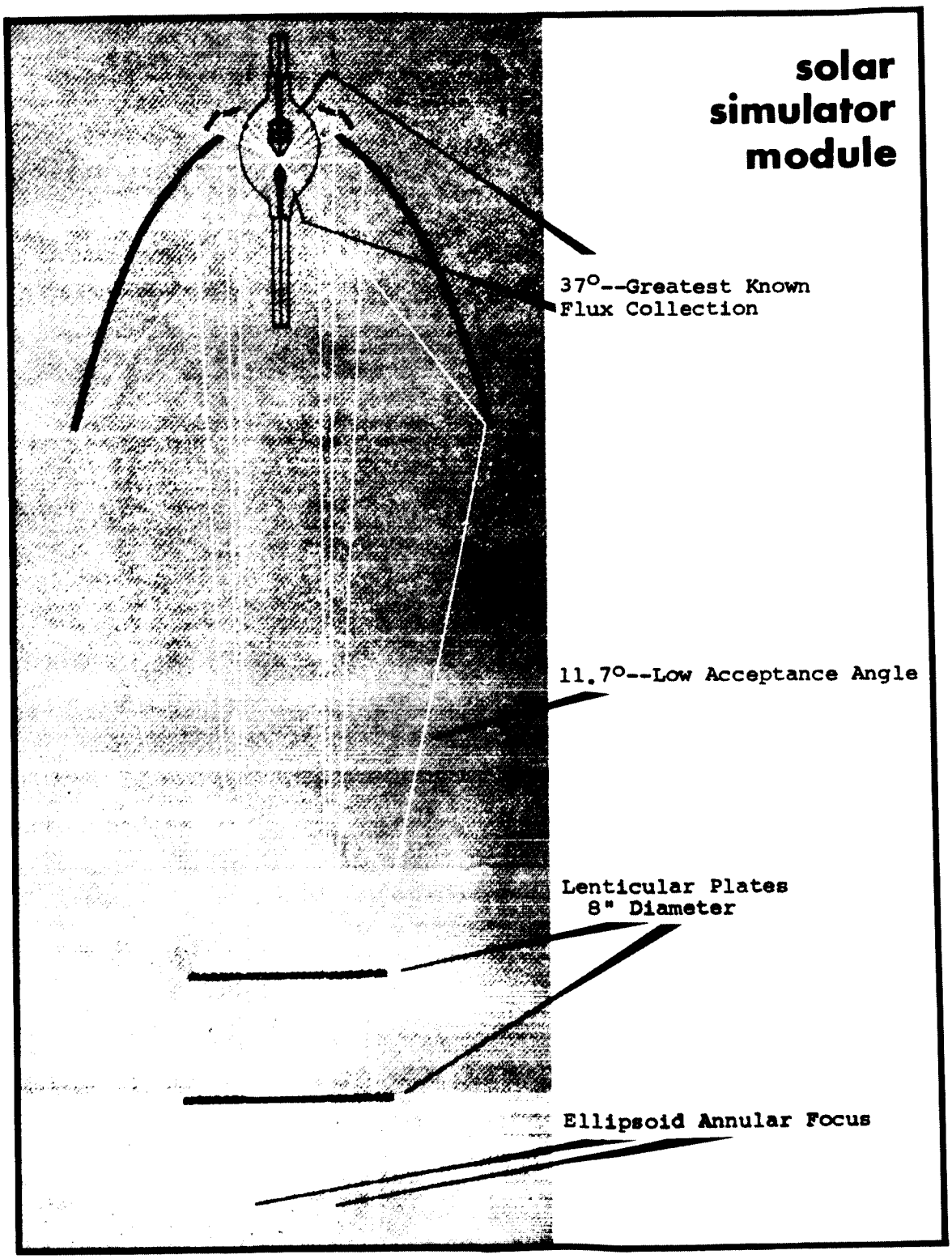
solar
simulator
module
37°--Greatest Known
Flux Collection
11.7°--Low Acceptance Angle
Lenticular Plates
8" Diameter
Ellipsoid Annular Focus

Figure 6

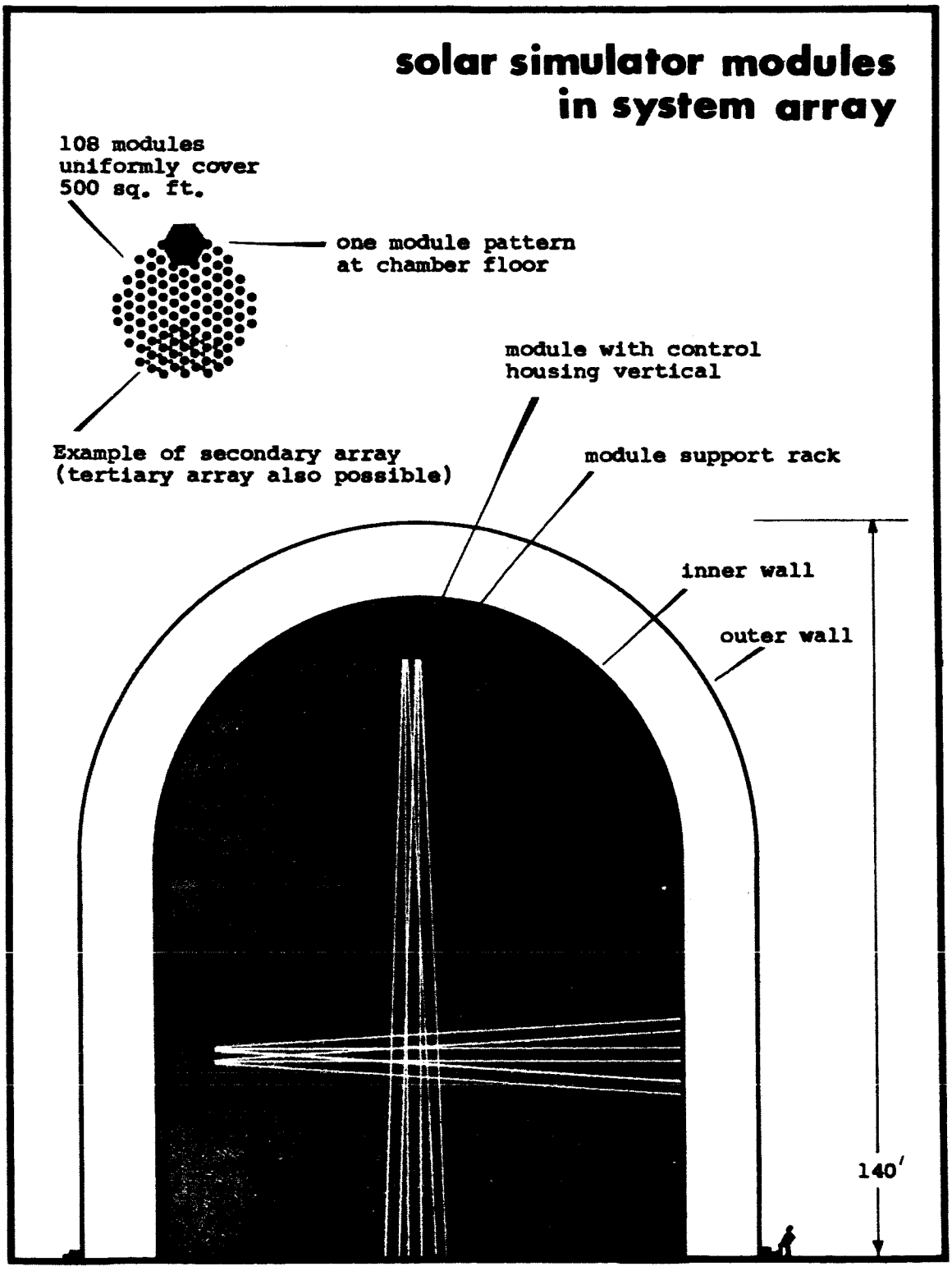
solar simulator modules
in system array
108 modules
uniformly cover
500 sq. ft.
one module pattern
at chamber floor
module with control
housing vertical
Example of secondary array
(tertiary array also possible)
module support rack
inner wall
outer wall
140'

Figure 7

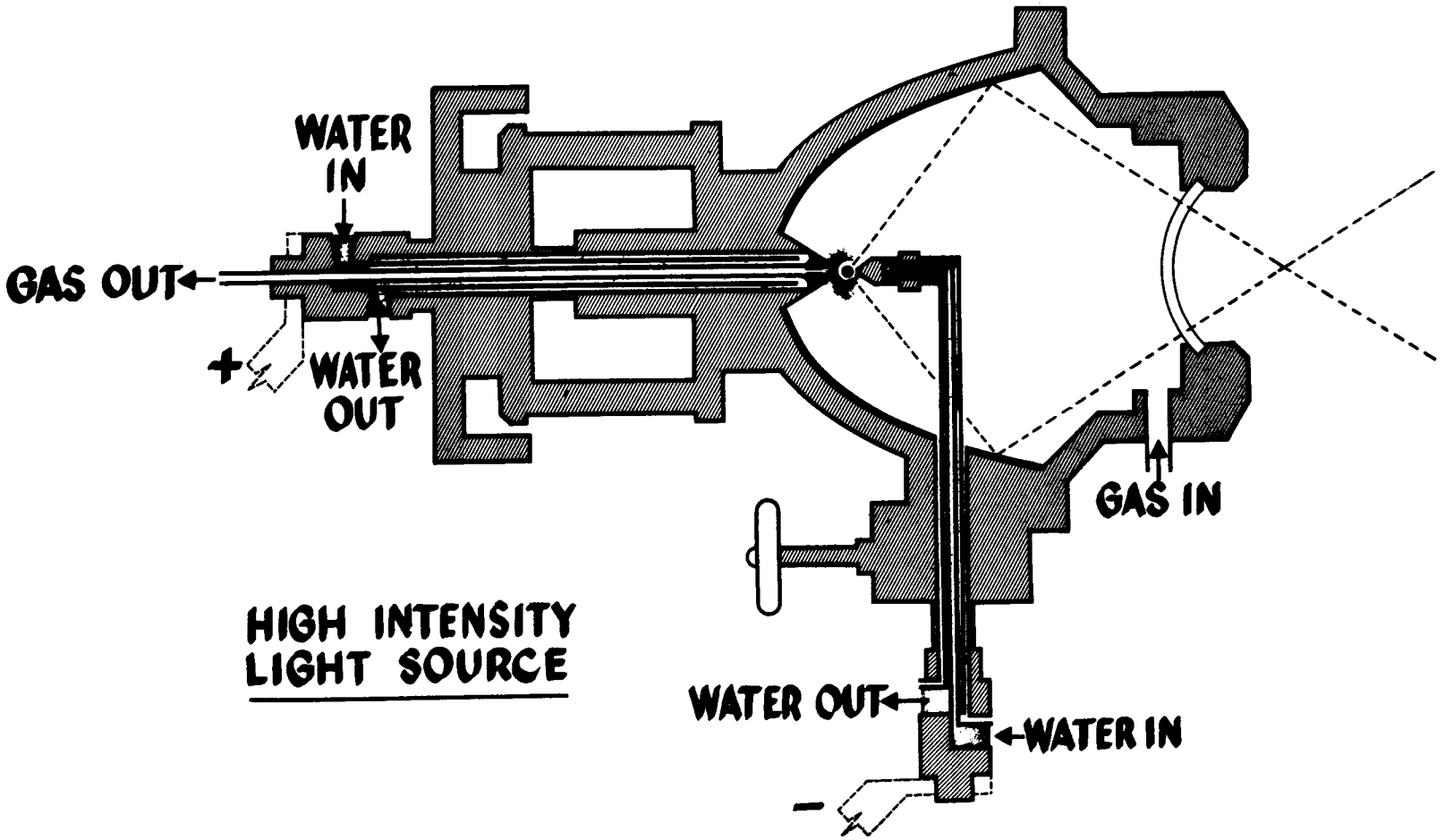
WATER IN
GAS OUT
+
WATER OUT
GAS IN
HIGH INTENSITY LIGHT SOURCE
WATER OUT
WATER IN
−

Figure 8

THERMAL TESTING OF UNMANNED LUNAR AND INTERPLANETARY SPACECRAFT

Elmer M. Christensen

Jet Propulsion Laboratory

Pasadena, California

Presented at NASA In-House Conference on Solar Simulation

NASA Headquarters

7-8 April 1964

THERMAL TESTING OF UNMANNED LUNAR AND INTERPLANETARY SPACECRAFT

Elmer M. Christensen

Jet Propulsion Laboratory

The achievement of temperature control of JPL sun-oriented spacecraft, i.e., Ranger and Mariner, has required a blend of analysis and testing. The first part of this report presents a brief description of these spacecraft. It enumerates the difficulties involved in temperature-controlling these spacecraft, describes the general thermal philosophy and methods of solution, discusses some testing experiences and test lessons, and comments on the flight results. The second part summarizes some of our expected future thermal test facility requirements and the interrelationship of spacecraft design and testing as they pertain to our future spacecraft. The temperature control requirements and constraints of most spacecraft are highly individualized. Thus, specific design and test implementation are required and cannot necessarily be generalized.

I. PAST EFFORT AND EXPERIENCES

A. SPACECRAFT WITH DIFFICULT-TO-ANALYZE HEAT TRANSFER CHARACTERISTICS

The comments in this report are relative to sun-oriented spacecraft such as Ranger, Mariner, and similar types that we expect to design in the future. In order to give a better understanding of the difficulties involved in analyzing the heat transfer of these spacecraft, refer to Figure 1. This is a model of the first and second Ranger spacecraft. It consists of a hexagonal-shaped basic structure with six electronic chassis, two wing-like solar panels, a parabolic-shaped antenna, a science experiment on a boom, an oil derrick-like superstructure containing many of the science experiments, and a hat-like omni antenna on the top. Sun sensors, coupled by a logic unit to gaseous nitrogen attitude control jets, point the spacecraft roll axis to the sun and maintain this orientation. In this sun-orientation cruise mode, the sun's rays are normal to the solar panels and illuminate the

superstructure or top side of the spacecraft. An earth sensor, coupled to the jets, points the parabolic antenna at the earth, thus providing roll stabilization.

The later Ranger spacecraft have, in addition, a midcourse and a terminal maneuver where the sun-oriented attitude is lost for a period of time. The Mariner II, a Venus probe, had a midcourse maneuver and a large change in solar intensity.

Figure 2 is a photograph of Ranger 1. Obviously, it was not taken in space during the sun-oriented cruise mode because of the strong side illumination and the wrong shadow pattern. However, we have learned that there is more illumination on the sides and bottom, than was originally thought, because of the multiple reflection of solar energy. Note the large number of varying-shaped external surfaces.

The classic simple formula for determining the equilibrium temperature of a body in space, i.e., the energy in equals energy out, subtly hides the difficulties of temperature-controlling these spacecraft. When a number of bodies or components are grouped together, as in Figures 1 and 2, the analytical formulation complexities rapidly increase. The external thermal radiation is difficult to predict because of the multitude of surfaces that see each other in varying attitudes and/or orientations. There are problems with the varied view factors, the variety of absorbing and reflecting diffuse and specular finishes, the curved and flat surfaces facing a variety of directions, and the full or partial shadowing dependent upon precise spacecraft orientation to the sun. The conduction of the exterior surface materials cannot be ignored because of the various thicknesses, the various material conductivities, and the various types of joints with the unknowns associated in various contact pressures.

Internal to the spacecraft, approximately 100 to 120 watts of electrical power are dissipated in the six electronic assemblies. This power, unfortunately, is not equally distributed nor constant with time. In order to prevent large thermal gradients within the electronic area, the units which are dissipating larger amounts of energy must be mounted with a good conduction path to an external radiating area.

Figure 3 shows a segment of a Ranger mainstructure and the electronic chassis assemblies. The chassis to the right is in the in-flight position. The chassis to the left is open for inspection or disassembly. Note the electronic modules in the open chassis. Figure 4 displays a typical electronic module.

B. METHODS UTILIZED IN SOLVING THE THERMAL PROBLEM

The task of the temperature control engineers is to control the spacecraft heat transfer characteristics such that the temperatures of the multitude of components will remain within tolerable limits throughout the flight. Early in this effort, we realized that we did not possess adequate knowledge nor the capability of analytically solving the temperature control problems involved in these necessarily complex spacecraft configurations, nor were facilities available that would permit solution by test alone. Thus, we have used various combinations of hand computations, machine computations, component tests, subsystem tests, and tests of complete spacecraft and then correlated these results as best we could. There is no set way in which we blend these together; instead, it depends upon the spacecraft, the money, the time, and the manpower available. Hopefully, by launch we shall have done the job with sufficient rigor and thoroughness to achieve an acceptable degree of confidence in the temperature control design.

Arbitrarily, the temperature control task can be divided into control of the internal and the external heat balance. The external heat balance can be defined as the local temperature distribution of the spacecraft exterior that results from the exchange of energy to and from space and the other exterior surfaces of the spacecraft. The internal heat balance is the spacecraft internal temperature distribution. For our spacecraft, most of the difficulties and effort are involved with the exterior heat balance where the unknowns are the largest.

In the case of the first Ranger, the general configuration, structure, etc. were essentially finalized before the magnitude of the thermal difficulties was recognized and accepted. As a result, the temperature control effort had to be within these gross configurational and material constraints. Thus, a major emphasis was placed upon minimizing the thermal uncertainties by local design techniques.

Examples of how design techniques were used follow. The uncertainties in the radiation to and from the six structural legs were reduced to acceptable values by finishing the legs with low-emittance surfaces. The chassis outboard surface has a high-emittance coating and the other chassis surfaces have low-emittance finishes. This procedure yields the most predictable electronic temperatures because the high-emittance surfaces have the best view of space and the least thermal radiation interaction with the remainder of the spacecraft. Generally, the heat transfer uncertainties associated with the complex conduction and radiation geometries interior to the hex have been avoided. This has been accomplished by attempting to make all chassis or bays maintain the same equilibrium temperature by external heat balance and by maximizing the internal emittance. Thus, the ΔT across the bus is not large, and the available conduction and radiation even out the temperatures.

A typical electronic module consists of two printed circuits with all the associated electronics which, in turn, are bonded to opposite sides of a metallic plate. An integral flange completely surrounds this plate. The external surface on the flange side opposite the connector is machined. Good heat transfer conduction to a radiator is provided when the machined surface is bolted to a machined inside surface of a chassis. The module is additionally supported by the two ears evident in Figure 4. Normally, the heat flow is from the electronic components, through the printed circuits to the center web, through the web to the flange, through the flange to the external chassis or radiator. Generally, high-power dissipation units are mounted toward the right side in order to shorten the thermal path to the radiator.

When the space effort was initiated, there was a great disparity of knowledge on material properties. Five years ago, there was a fair amount of information on the thermal absorptivity and emissivity of surfaces. However, it was of a general nature and did not specify the finish, the history of the material, nor the method of processing. Today we know that these factors are important in order to have truly repeatable surface properties as are required for spacecraft temperature control. The stability of some of these surfaces in space and/or the repeatability was not known. There was insufficient knowledge relative to how these surfaces could be protected from man-made and from natural environments prior to launch and after launch. These are continuing but decreasing limitations to spacecraft temperature control.

C. EARLY THERMAL TESTS

Late in 1960, a six-foot diameter by seven-foot-high vacuum facility became available. This facility had liquid nitrogen-cooled walls.

The six-foot tank, in addition to smaller vaccum cold wall facilities, provided the initial testing capability for Ranger temperature control. In early 1961, the six-foot facility capabilities were amplified by the addition of solar simulation--or perhaps we should call it "visible light" simulation.

Figure 5 illustrates the light sources as they were mounted above the vacuum tank. The light sources consisted of four movie projection-type carbon arc lamps--standard Strong projectors--mounted in a near-vertical position. I tend to call this visible light simulation, rather than solar simulation, because the optical axis of each projector was approximately 20° from the vertical axis of the chamber. The light beam from each projector spread out $\pm 20^{\circ}$ from its own optical axis. The four projectors were set so that the four beams of light were superimposed inside the chamber approximately two to three feet above the bottom of the chamber. The intent was to obtain a relatively uniform area of illumination at one test plane. The obvious disadvantages were the lack of collimated light and the variation of intensity and uniformity above and below the primary test plane. At the time of the initiation of this facility, the disadvantages were recognized as such; but these limitations were not recognized to be as significant as they turned out to be for the Ranger spacecraft.

Prior to the completion of the visible light simulator, tests were initiated on the Ranger hexagonal structure and electronic chassis in the six-foot vacuum cold wall facility. At that time, we had a thermal testing "baptism" for these "open" spacecraft and learned a number of things. For example, the conduction around the hexagon was less than it was thought it might be (Figure 6). The six main supports, or "legs,"

were finished with a low-emittance surface because of the uncertainties in the analytical predictions of the heat radiated from these complex shapes. The tests proved that heat losses from the legs, although unpredictable, were minimized and produced a minor effect on the electronic module temperatures. Initially, the spacecraft was supported by standoffs with heater guards to thermally isolate the spacecraft from the chamber. This was not satisfactory, so the spacecraft was hung by rope. As we proceeded, we learned to make our own electrical heaters which were strapped or taped onto the spacecraft in various appropriate places to simulate solar inputs. Later, infrared lamps supplemented these heaters by beaming energy into various inaccessible places.

When the visible light simulation became available, more tests were performed on the basic hex of Ranger 1 (Figure 6). It was hoped that more meaningful thermal tests could be performed than had been previously. Because of the highly decollimated light system and the small tank, the tests had to be limited to the spacecraft without its superstructure, antennas, etc.

The light from the four beams was superimposed on a plane even with the top of the six chassis. At this plane, light intensity dropped off just outboard of the chassis. The simulated solar energy input to legs and outboard components was reduced and generally indeterminate due to this light intensity dropoff, the complex configuration, and the additional decrease in light intensity as the distance from the light source increased. The tests resulted mainly in obtaining thermal balances of the chassis. Consequently, the value of the visible light was largely negated because electrical heater simulation for the chassis turned out to be of comparable or better value.

The visible light test results were not the most valid. However, they were informative and test techniques did evolve. These tests were started on the basis that the tops of chassis were illuminated with a light intensity of 0.8 solar constant. After four or five tests, by the use of solar cells and pyroheliometers the light intensity was judged to be between 0.5 and 0.6 solar constant. In Figure 6, note the cooled white shadow shield above the hex and the many uncovered cables leading into the spacecraft. Later, in order to reduce the indeterminate heat losses from these cables, they were wrapped with aluminized mylar, low-emittance surface out.

Thermal tests were performed on all the scientific experiments mounted on the superstructure of Ranger 1. These tests were performed singly or in groupings of the instruments. An example of how the light simulator was used effectively, and in a way that could be called solar simulation, was in the testing of the magnetometer as shown in Figure 7. The magnetometer is a rubidium vapor device consisting of a sphere connected to a lamp by a long plastic tube. The two parts required thermal coupling. However, the sphere was within the truncated cone with the lamp mounted below the cone, i.e., between the two IR lamps as shown in Figure 7. At the junction of the top of the inverted cone and the top cylinder is a screened annulus. During the sun-oriented phase of the flight, sunlight enters this annulus and impinges either directly upon the magnetometer sphere or is reflected to some part of the magnetometer. For the test, the axis of the magnetometer was canted in the chamber to correspond to the optical axis of one lamp. Thermally, this was very difficult to analyze but we believed that the one lamp test was worthwhile.

During this period, a number of facility problems occurred which are probably typical of those encountered with any new facility. For example, the ports or vycor windows, through which the solar energy enters the chamber, became darkened and muddy; the lenses in the optical systems became dirty and cracked at times; and the light intensity in the test volume varied as much as plus or minus 30% within a few minutes. In time, it was realized that this last difficulty resulted because the projectors were made for horizontal, not vertical operation. The feed system for the carbon rods did not move them uniformly. After rework, this intensity variation was reduced to approximately $\pm$ 6% at a given place in the test volume. Contamination within vacuum facilities continues to be a problem. One might say that 49% of the problems are caused by the test item and 49% are facility problems. For example, the test specimens had tape, insulation, heaters, mock-ups, etc. that outgassed and contaminated the facility. Today, our spacecraft have FEP teflon insulation, the heaters are ceramic and metallic, and the use of a number of materials is prohibited in order to reduce outgassing. The facilities have caused problems also, especially in the backstreaming of oil from the diffusion pumps. As a result, many unhappy days were passed in cleaning spacecraft and chambers. It could be said that the other 2% of the contamination was caused by such things as a dead mouse. (Actually, the remainder of a mouse was found after one test.)

Instrumentation is an important aspect of testing and, as the rest of our technology has progressed, it has also grown and improved. Originally, we started by using copper constantan thermocouples. Shortly after that, we switched to chromel constantan thermocouples.

The chromel constantan thermocouples have approximately a 50% increase in voltage per unit temperature difference. The thermocouple lead feed-through (air to vacuum) problem was a thorn. This has been cured as is illustrated in Figure 8.

Initially, thermal test instrumentation was planned and implemented on an individual test basis, because of limited time and manpower. The equipment was portable and largely nonstandardized. Today this situation has been improved by the development of instrumentation setups for a given facility. Thus, the problems associated with moving and changing lead-ins, measuring and recording equipment, etc., have been reduced or eliminated. A particular improvement is the concept of a preassembled spacecraft thermocouple harness as a unit. The harness can be placed on the spacecraft shortly prior to the test, thermocouples attached, and harness continuity checked. This reduces test preparation time, both for the facility and the test hardware. The 25-foot space simulator now uses a Pace reference as the standard thermocouple cold junction. The cold junction is inside the simulator, thereby eliminating all possible thermoelectric effects caused by temperature gradients in the leads where they come through the simulator wall. There also are less leads through the simulator wall per thermocouple. Experimentation is proceeding on the possible use of a floating cold junction reference and a thermocouple commutator which could be mounted within a spacecraft during a test.

Many of the test techniques and results were crude. Consequently, it is easy to view this history in a derogatory manner. However, without apologizing, I wish to say that these tests were performed under very limited money, manpower and schedule, and in a pioneering

situation and spirit. It is always interesting to ponder what might be the best course of action under similar circumstances.

D. EARLY FLIGHTS OF RANGER SPACECRAFT

Ranger 1 was launched into a close-earth orbit; the booster failed to inject the spacecraft away from the earth, and the spacecraft could not function in a normal manner. However, to my knowledge there were no spacecraft failures. The spacecraft would acquire the sun but then would lose lock as it went into the earth's shadow. Under these circumstances, a true sun-oriented, non-earth-influenced thermal balance was never obtained. On the basis of quick calculations after the flight, we decided that there was not sufficient information nor significant enough known differences from preflight estimates to warrant a change in the temperature control for the next flight.

Ranger 2 was launched but, again, only an earth orbit was obtained. This orbit trajectory was lower, shorter, and less informative than that of the first flight. Thus, a realistic temperature control flight test of the first model Ranger was not achieved.

Rangers 3, 4 and 5 were considerably modified from the first two. The new mission was to hard-land a seismometer capsule on the lunar surface. This mission required additional spacecraft capabilities such as a midcourse correction maneuver, a terminal maneuver above the lunar surface, a controlled deceleration of the capsule, etc. In Figure 9, the spherical capsule is mounted on top of the retro rocket, the lunar altitude radar is on the left side, the omni antenna is at the top left, and the aluminized mylar is crumpled around the nozzle of the retro motor. Except for the undeployed radar antenna, the spacecraft is in the terminal maneuver configuration. Prior to the final flight phase,

the mylar shield encloses the retro rocket in order to prevent excessive cooling. However, at ignition, the mylar must not interfere with the retro separation and spin-up. The solar panels, the high-gain antenna, and the basic hex structure remain essentially the same. However, there are additional electronics and changes to the previous electronics.

Ranger 3 in the flight premidcourse cruise configuration is shown in Figure 10. Note the highly reflective aluminized mylar shield around the retro rocket and the spherical gamma ray spectrometer adjacent to the radar antenna. Before flight, the gamma ray sphere in the photograph was replaced by a highly polished aluminum sphere with precisely-determined white paint spots, i.e., a thermal control mosaic.

A special innovation was devised for the testing of Ranger 3. This consisted of cutting the spacecraft hex into 1/6 and 1/3-pie-shaped segments. As a result, tests with solar simulation coverage of the complete test item could be performed in the STL facility. The light from two carbon arc projectors was blended into one diverging light beam with a one-solar-constant intensity at a 40-inch diameter. The maximum divergence from the optical axis was seven to eight degrees. These tests were considered to be worthwhile and significant under the existing temperature control state-of-the-art. An interesting aspect of these tests was the observation that the test team equilibrium temperatures were constant with one facility operator but varied as much as $10^{\circ}F$ with a second operator. This was caused either by carelessness or the incapability of the second operator to maintain a constant solar simulation intensity.

The flight of Ranger 3 was largely a success from an engineering viewpoint. The spacecraft achieved and maintained sun orientation, had

a midcourse maneuver, reacquired sun orientation, had good power and communication operation, and provided a temperature control flight calibration. The temperature distribution of the hex electronics was not as uniform as expected, and the temperatures averaged about 25°F warmer than the nominal midband prediction. However, this was considered quite good under the circumstances. A particular thermal problem was the gamma ray sphere. The flight temperatures exceeded the nominal predictions by more than 60°F in the close-in position (Figure 10) and by more than 40°F in the post-midcourse extended position. A telescoping tube extended the sphere approximately five feet in a direction normal to the spacecraft roll axis. The reason for the warm gamma ray sphere has never been fully determined, but it is suspected that the multiple reflection of solar energy was a major contributor.

Photographs of two tests performed after the flight of Ranger 3 are shown in Figures 11 and 12 and are examples of typical tests and techniques which have evolved as our capability and technology have grown. The following items are noteworthy in these photographs: (1) the flight-like structures, mechanical components and assemblies that were utilized specifically for temperature control tests; (2) the method of cutting the electronic chassis and structure in the middle of a bay, assuming that an adiabatic condition exists there and across the inside of the hex, and the construction of an adiabatic boundary with a multiple layer radiation shield; (3) the highly reflective thermal shield that enclosed the Ranger 3 retro rocket, modified by the addition of a flat black exterior cloth; and (4) the gamma ray sphere flight paint pattern. In this test, the sphere was utilized only for its thermal effects upon the thermal balance of other components.

On Ranger 4 we drew a blank. The spacecraft became inoperative at separation or shortly thereafter.

Ranger 5 had a power failure at sun acquisition. However, the spacecraft functioned until battery depletion. This was long enough to essentially reach thermal equilibrium and thus provide another flight calibration. The adjustment of the paint patterns from Flight 3 spacecraft to Flight 5 spacecraft worked well, with the exception of the gamma ray sphere which again was warm. To our knowledge, there were no problems caused by temperature. In all these flights, however, there were limited numbers of flight measurements and the temperatures of remote areas of the spacecraft were not obtained. Fortunately, the location of the power failure was narrowed to a specific module by the local temperature rise of one of the few temperature measurements.

E. MARINER II

The Mariner II spacecraft is shown in Figure 13. As you will note, it has the gross appearance of the early Rangers. There are many subtle-appearing differences, as there were between Rangers 1 and 2. However, the Mariner differences are quite major in actuality. From a thermal viewpoint, it was a new spacecraft requiring new concepts, new devices, new analysis, and new testing. The Mariner II had to function throughout the near-doubling of the solar intensity from Earth to Venus. Thus, the top of hex was blocked from sunlight by a multilayer radiation shield. The outboard surface of one electronic chassis had a set of bimetallic-operated louvers that varied the chassis radiation capability.

The JPL 25-foot space simulator was completed in time for some testing of the Mariner R. However, the solar simulator did not function to an acceptable and usable extent, and only vacuum cold wall tests with

heaters on the Mariner R were performed. This was the first opportunity to thermally test a complete spacecraft of the class referred to in this report.

The Mariner II became excessively warm during flight. After the flight when the JPL solar simulator became operational, the Mariner III was tested (Figure 14). Note the significant amount of reflected solar energy. The light beam covered a four-foot area with an intensity of up to 170 watts per square foot. The resulting test temperatures were between the flight and earlier test temperature but were closer to the flight results. The correlation to flight temperatures was limited by a lack of good knowledge of the facility and the interactions of facility and spacecraft. However, this latest test more accurately represented space than did the vacuum cold tests.

The Ranger Block III tests followed chronologically and are described in detail in the reference cited below.*

II. SOME FUTURE SPACECRAFT THERMAL TEST CONSIDERATIONS

A. FACILITY REQUIREMENTS

It is not difficult for temperature control engineers to specify the quality of solar simulation they desire, but it is difficult to specify an achievable quality of simulation that will provide technically and economically appropriate test capability in a timely manner. The "testing figure of merit" for any particular solar simulation system should be rated on the basis of the items to be tested; e.g., a facility

---

* Kahn, M. E., "Thermal Testing of the Ranger Block III Spacecraft in the JPL 25-Foot Space Simulator," presented at NASA In-House Conference on Solar Simulation, NASA Headquarters, April 7-8, 1964.

which can provide a good test for a sphere may be totally unacceptable for an "open" configuration spacecraft. Consequently, important parameters in rating a facility are: the spacecraft mission requirements, the thermal requirements imposed by the spacecraft system design, and the spacecraft configuration. Unfortunately, these factors are undefined until a spacecraft project is in design. Then it is many months to a few years too late to specify the facility test capability requirements for that project. Accordingly, it is necessary to make assumptions concerning these factors relative to future projects. This is where a Gallup Poll, a crystal ball and an "ouiji board" are required.

Estimates of acceptable solar simulation quality requirements are becoming more severe as time passes. Low-quality simulation is less and less appealing, as the ability to design spacecraft on the basis of past analysis, test, and flight results is further developed. At the same time, spacecraft system requirements on the thermal control system have become more severe, and estimates of the difficulty of obtaining satisfactory design answers are growing. Therefore, it is anticipated that future requirements for spacecraft temperature control test facilities will be more demanding. In addition, better quality solar simulation will permit better spacecraft temperature prediction capability and thereby lessen the restrictions that temperature control will place upon future missions. The writer's belief, that higher quality light is the highest priority space simulator facility requirement, is reaffirmed in the light of tests that have been performed to date. In referring to high-quality solar simulation, the two prime factors that call for continued emphasis in future JPL requirements are decollimation and spectrum. This is true at JPL because of the present facility approach where light intensity and uniformity are, by comparison, relatively good.

The concept of each lamp's illuminating all the test volume is a proven concept. In contrast, the concept of each lamp's illuminating small adjacent areas is highly undesirable for JPL type spacecraft thermal control testing. This is a result of the operational difficulties experienced in maintaining individual lamp operation. It appears that a facility which has a lamp for a discrete area has difficulty in providing constant known intensity, uniformity of intensity, and spectral distribution throughout the test volume during a complete test. These conditions would provide serious limitations for meaningful tests on spacecraft configurations similar to those of JPL. From a testing viewpoint, there are enough uncertainties without superimposing these problems.

B. INTERRELATIONSHIP OF SPACECRAFT DESIGN AND TEST

1. The prime objective in our spacecraft thermal testing is to narrow the range of temperatures predicted for the cruise portion of the flight beyond that possible by analysis. For Ranger and Mariner-type spacecraft, the fundamental temperature control information required prior to flight is the predicted spacecraft equilibrium temperatures during the sun-stabilized orientation. For planetary flights, this includes the quasi-equilibrium temperatures at the earth and the planet.

2. A cruise orientation thermal balance test of flightlike spacecraft in the best available space simulator has always been mandatory for our spacecraft. For the thermal balance test, all extraneous equipment which can influence the heat balance must be removed from the facility. This is in contrast to the spacecraft mission test in which the electronic functioning of the spacecraft is checked and which requires additional mazes of cabling, monitoring units, etc.

3. The decision as to whether the spacecraft thermal balance test shall be with or without solar simulation is dependent upon the available solar simulation and the configuration of the test item. Generally, solar simulation is required for the more "open" configuration spacecraft. The quality of the solar simulation required is equal to some exponential power of the spacecraft openness and the nongreyness. The definition of an "open" configuration is a spacecraft with numerous external components and/or segments which require individual thermal balances. In contrast, a "closed" configuration would have a continuous external surface, i.e., a sphere, cylinder, parallelopiped, etc. A thermally grey surface is one with the same absorptivity for all wavelengths.

4. Localized cooling or heating transients, except for the immediate post-launch phase, will commence from the cruise temperatures during flight. Some of these transients can be approximated by tests.

5. Thermal testing of individual components and/or segments of a spacecraft are desirable or, in some instances, necessary in order t determine a conductance, etc., that cannot be adequately analyzed. This permits design adjustments during the evolution of a particular spacecraft design.

6. Thermal testing of a Temperature Control Model (TCM) is an accepted fact of life at JPL. It provides a capability for iterative testing and analysis, especially of the spacecraft external heat balance. The advantage of the TCM is its continual availability to the temperature control engineers, for thermal tests and modifications, months before flight hardware can be tested. The TCM consists of a full-size flightlike structure and all external members that significantly influence the spacecraft external thermal balance. Internal

components and their power dissipations are usually simulated by heaters and sometimes by equivalent masses although thermally critical components can be used. Thus, generally, the internal thermal gradients are not determined by TCM testing.

7. Thermal balance tests of a Proof Test Model (PTM) verify the spacecraft external and internal heat balances. The PTM is a complete spacecraft, identical to a flight spacecraft, but it is assembled for comprehensive test purposes only and is not intended for flight.
8. Thermal balance tests of a flight spacecraft may be required. This is primarily a function of the magnitude of the particular spacecraft temperature control task, the adequacy of the prior testing, and the project schedule and monies status.
9. Prediction of test results prior to initiation of a thermal test are required. These predictions are based upon the best available information about the test facility, the test item, and the interactions between them.
10. Post-test comparison and analysis of the predictions versus the results is very important in acquiring a better understanding of spacecraft heat transfer, the ability to thermally test spacecraft, and of a facility's capabilities and limitations.
11. Spacecraft design should be directed toward the reduction of and/or the elimination of the difficult-to-analyze areas or conditions.
12. Spacecraft design should be directed toward the reduction of and/or the elimination of the difficult-to-test areas or conditions.
13. Generally, it is possible to raise or lower the equilibrium temperature that a component or grouping of components will attain in space by changes prior to launch. Often, surface finish changes

can appreciably raise or lower the temperatures. The difficulty is in predicting, after analyses and testing, whether the mean temperature must be lowered or raised and how much.

14. Accurate electrical power dissipation profiles are necessary for the PTM and each flight spacecraft.

15. Thermal adjustments for subsequent flights should be predicated upon previous flight results in order to permit long-range correlation of spacecraft heat transfer characteristics.

16. For some spacecraft areas or components, a thermal uncertainty or unaccountability reserve should be added for flight temperature predictions. This is advisable for cases in which the temperature control engineer cannot rationally explain variations between preflight predictions and flight temperatures.

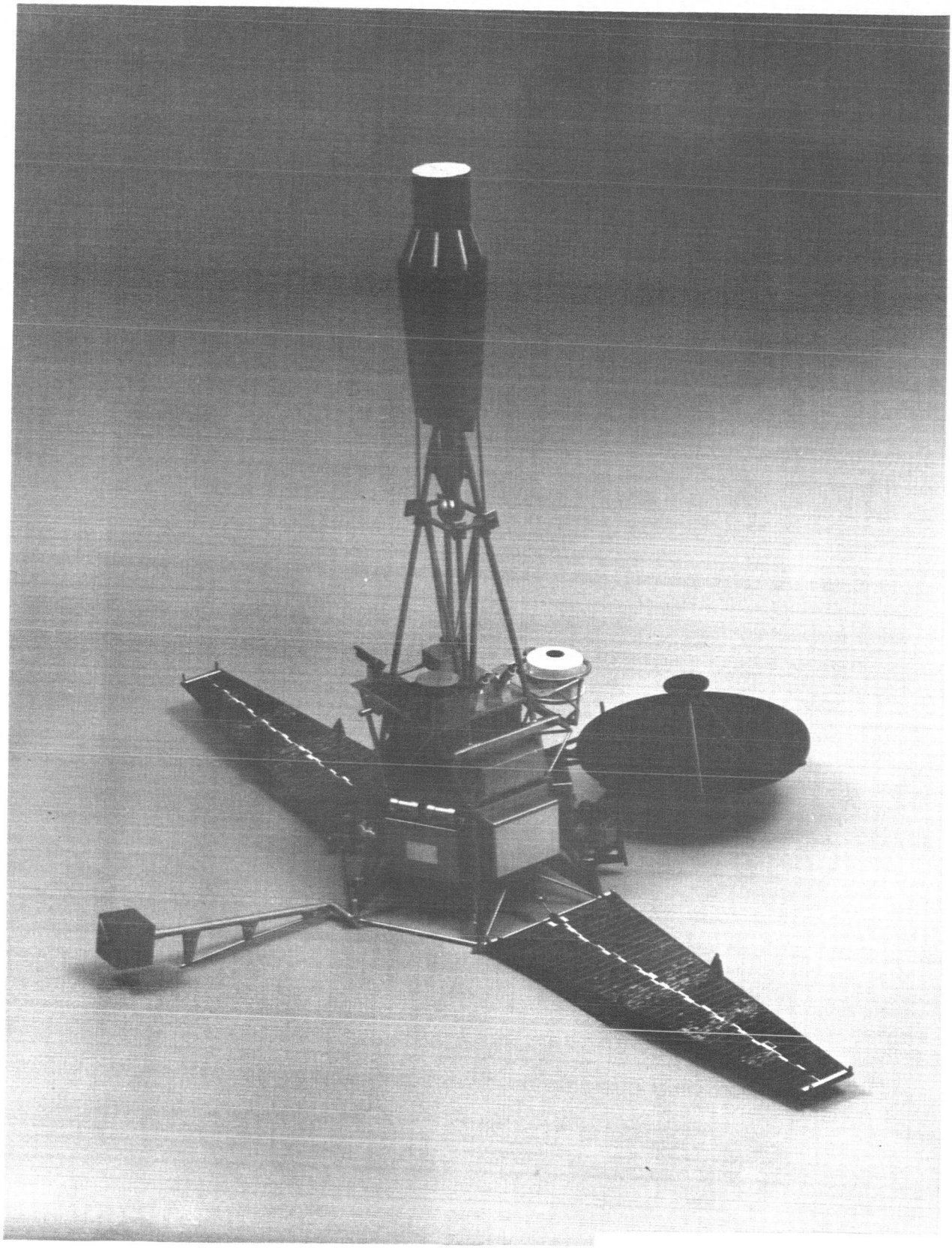

Figure 1. Model of Rangers 1 and 2

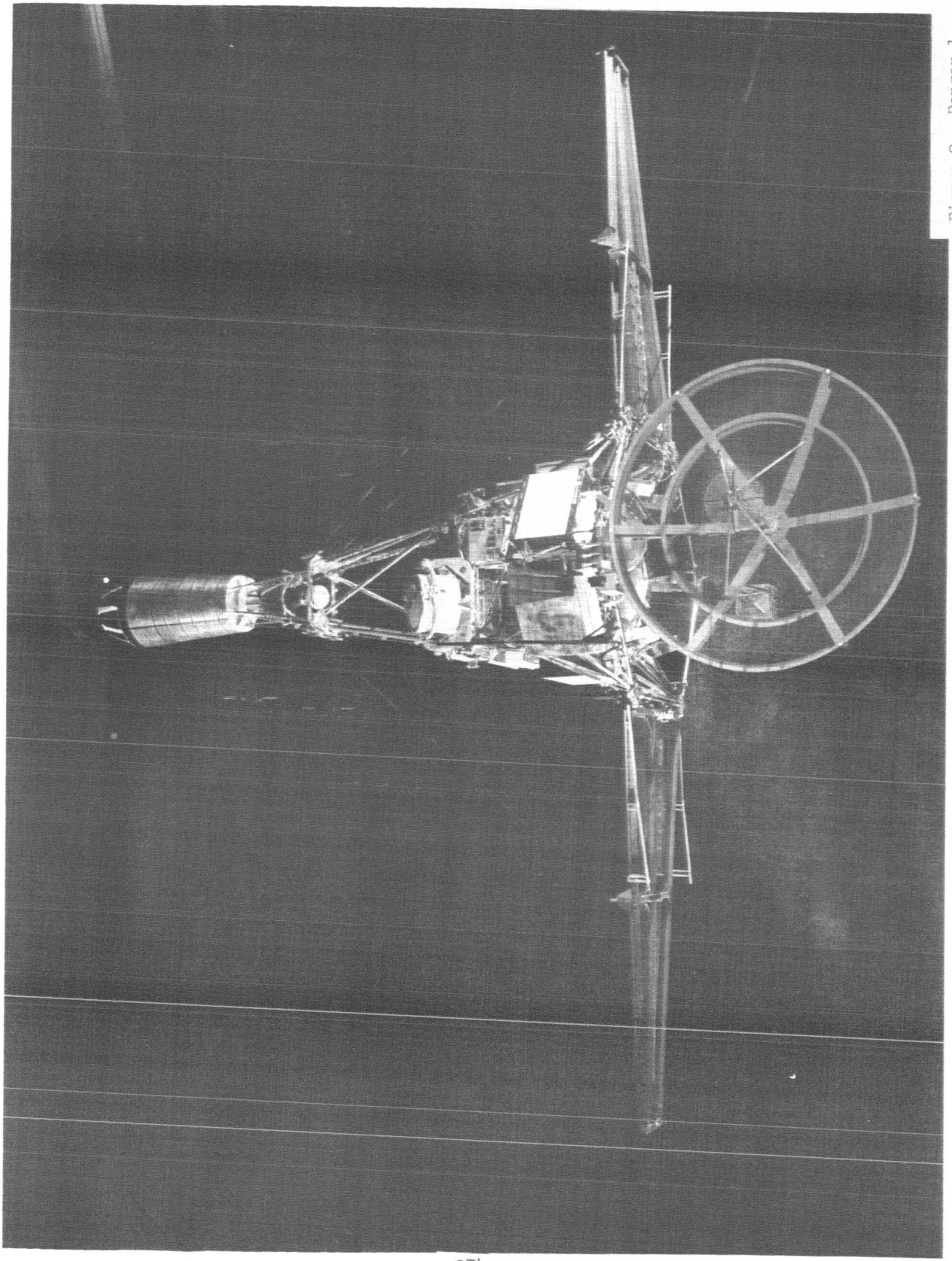

Figure 2. Ranger 1

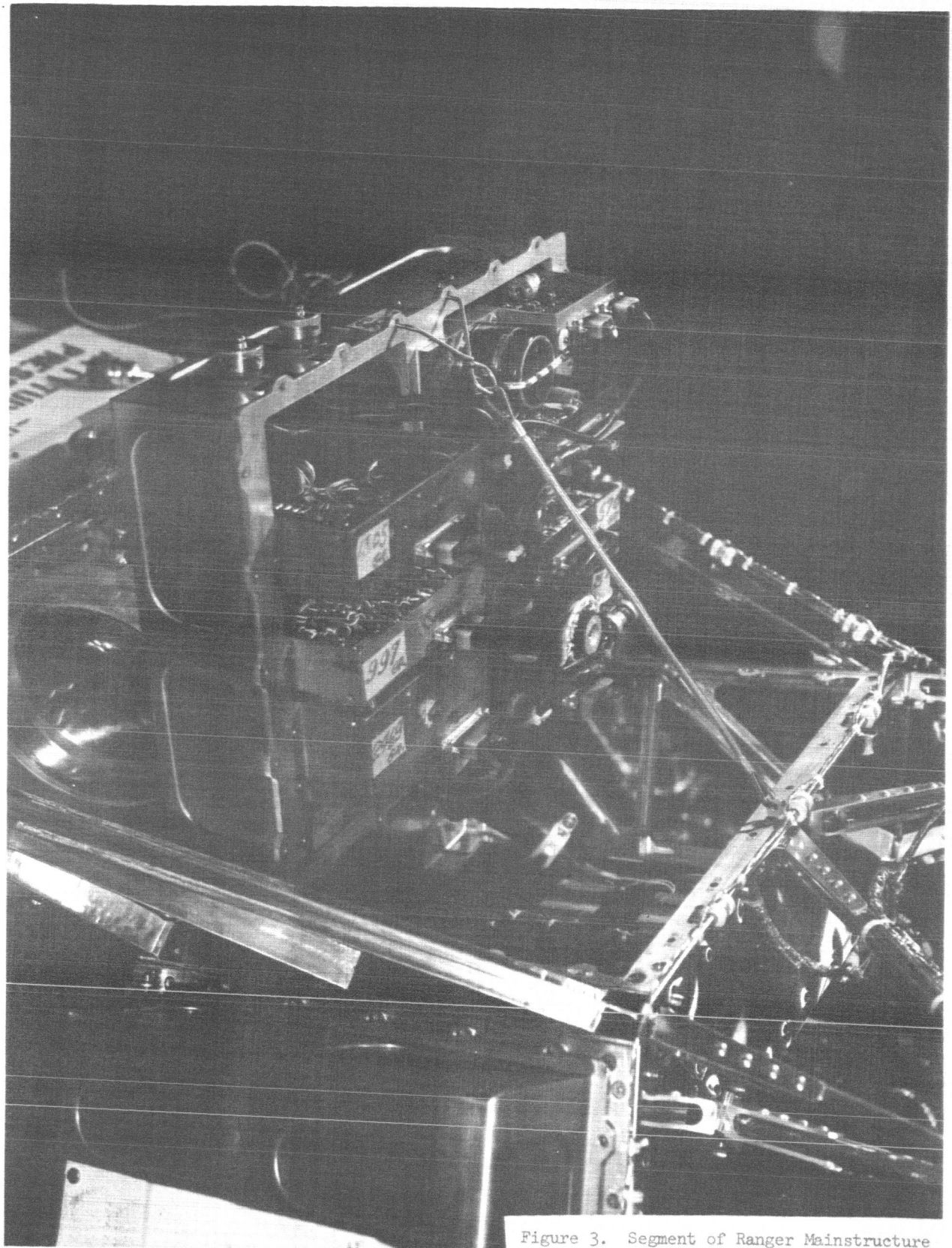

Figure 3. Segment of Ranger Mainstructure and Electronic Chassis Assemblies

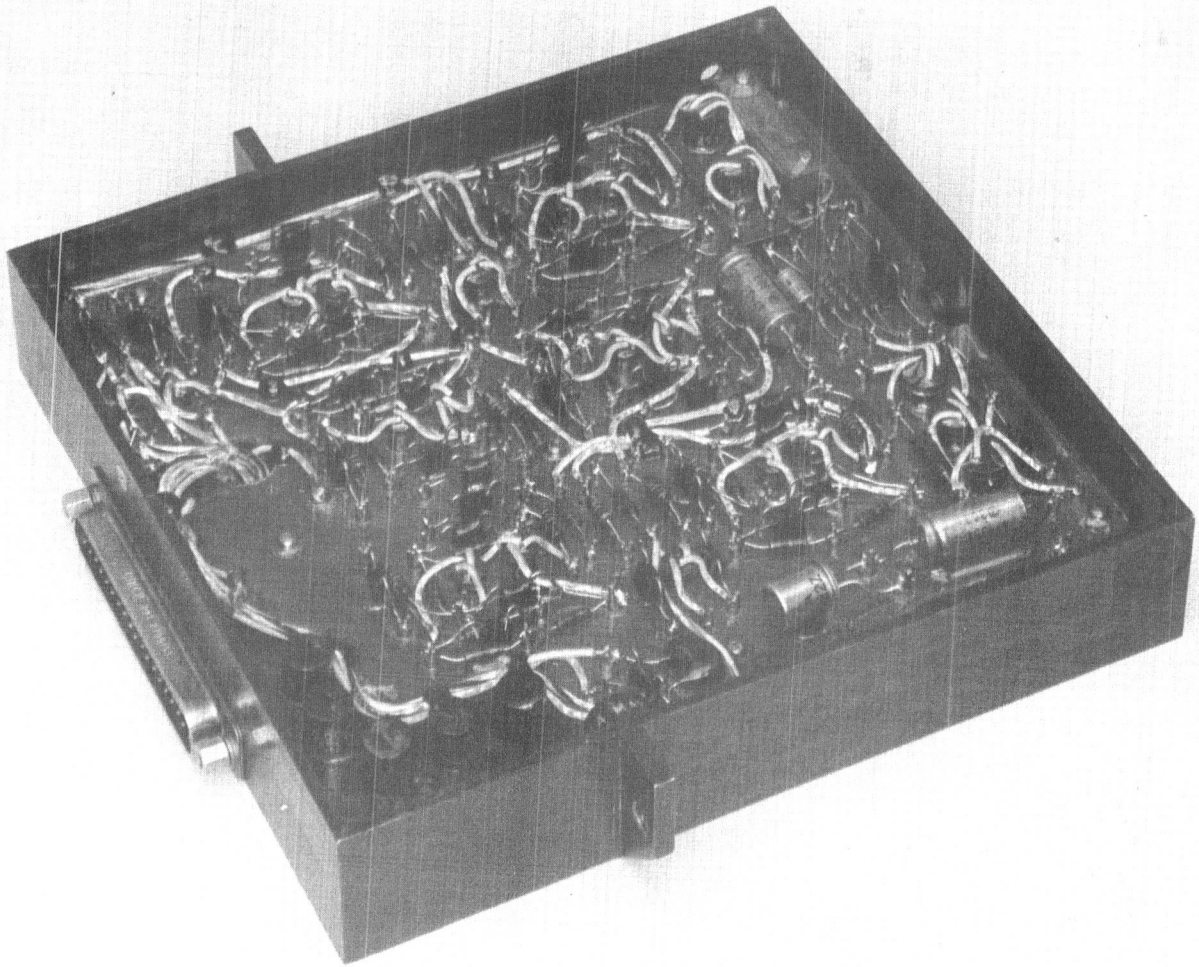

Figure 4. Typical Electronic Module

Figure 5. Light Sources for Six-Foot Vacuum Facility

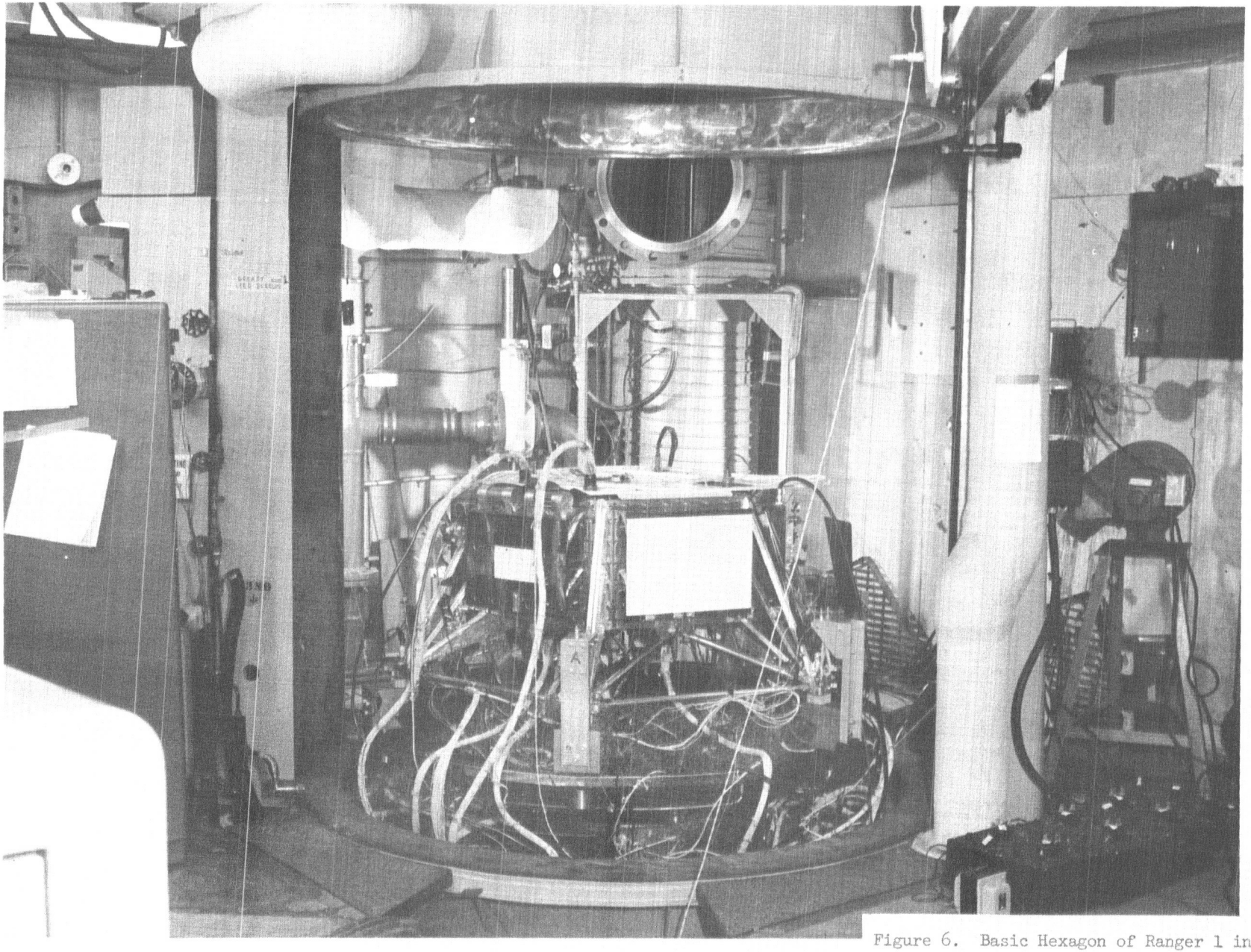

Figure 6. Basic Hexagon of Ranger 1 in Six-Foot Facility

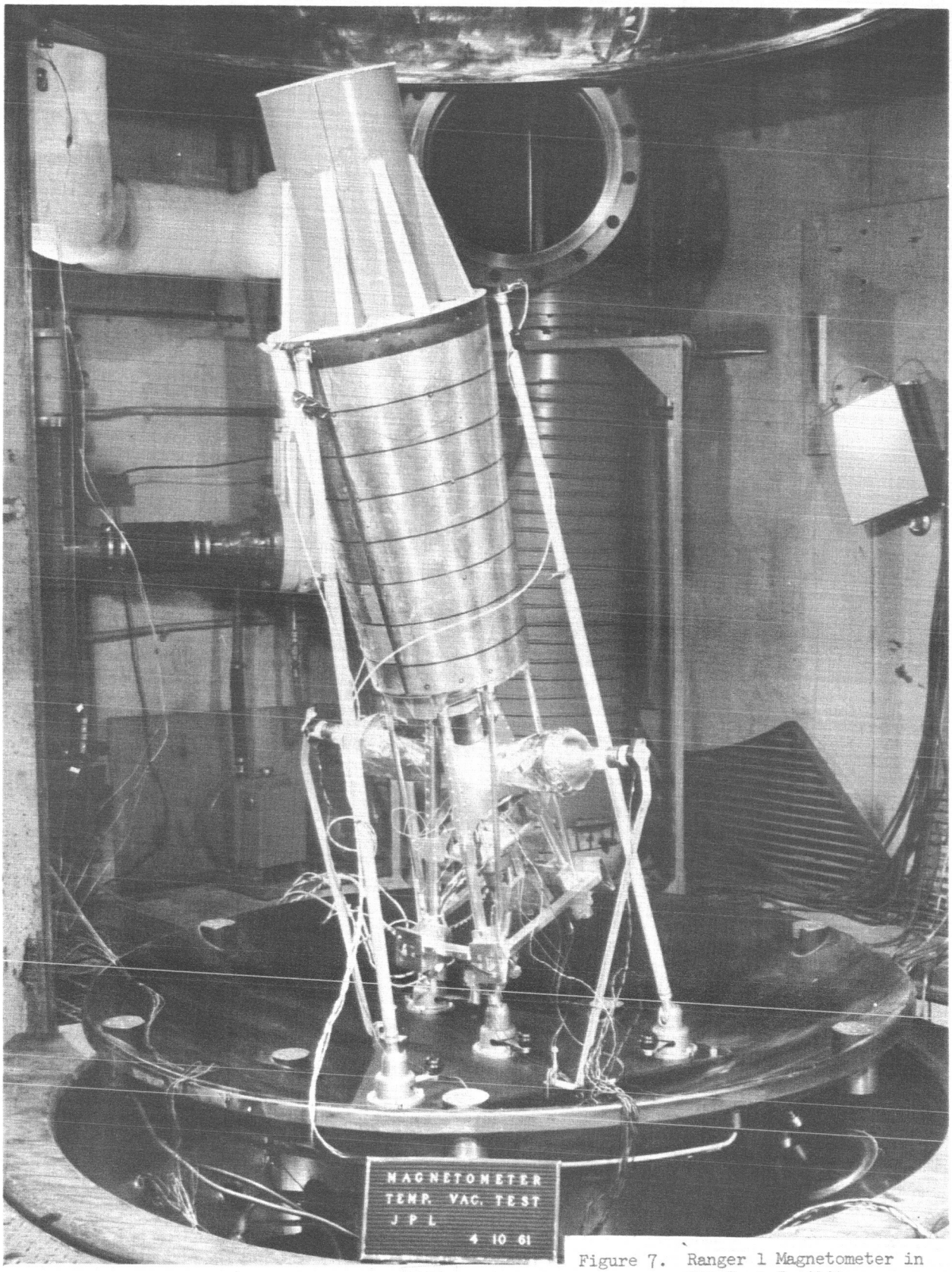

Figure 7. Ranger 1 Magnetometer in Six-Foot Facility

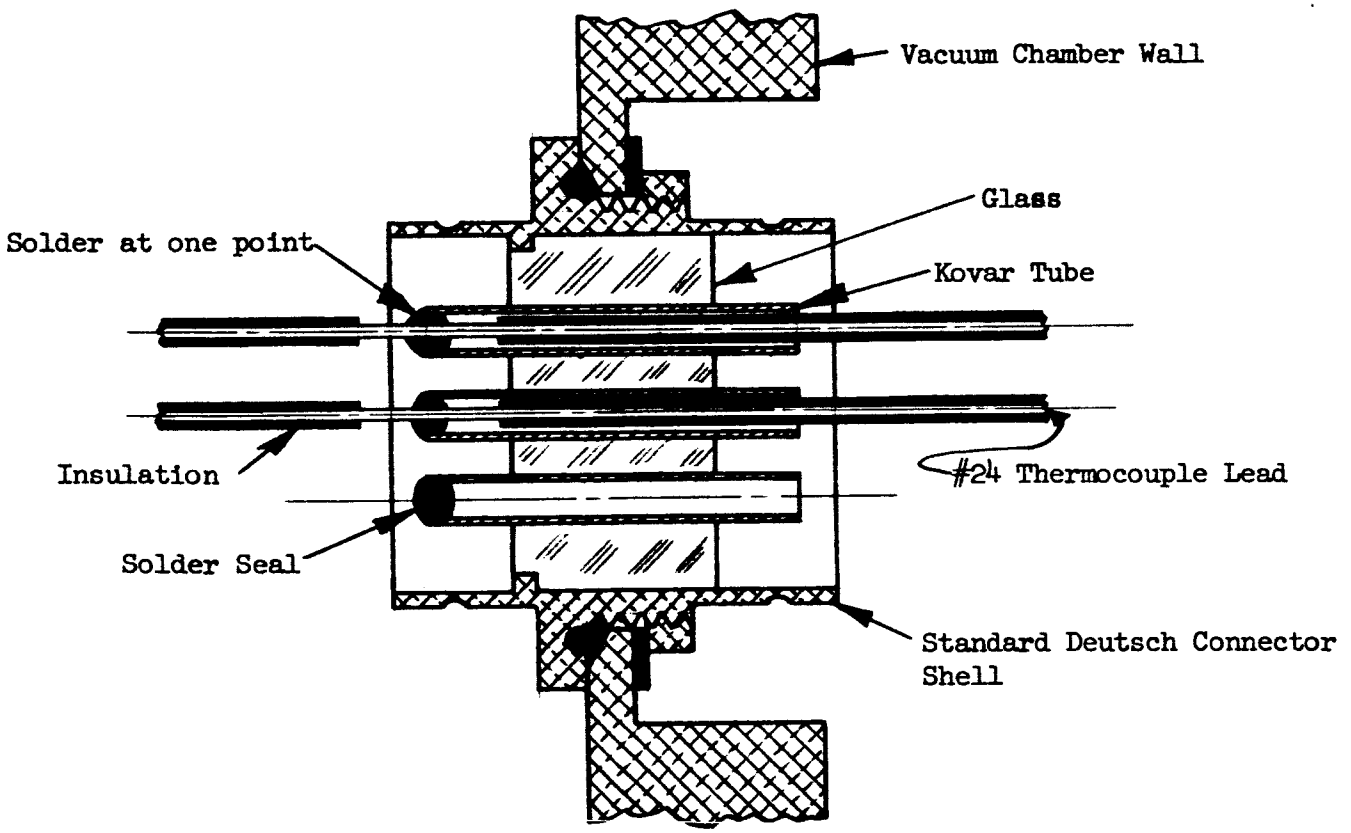

Figure 8. Thermocouple Lead Through Vacuum Tank Wall

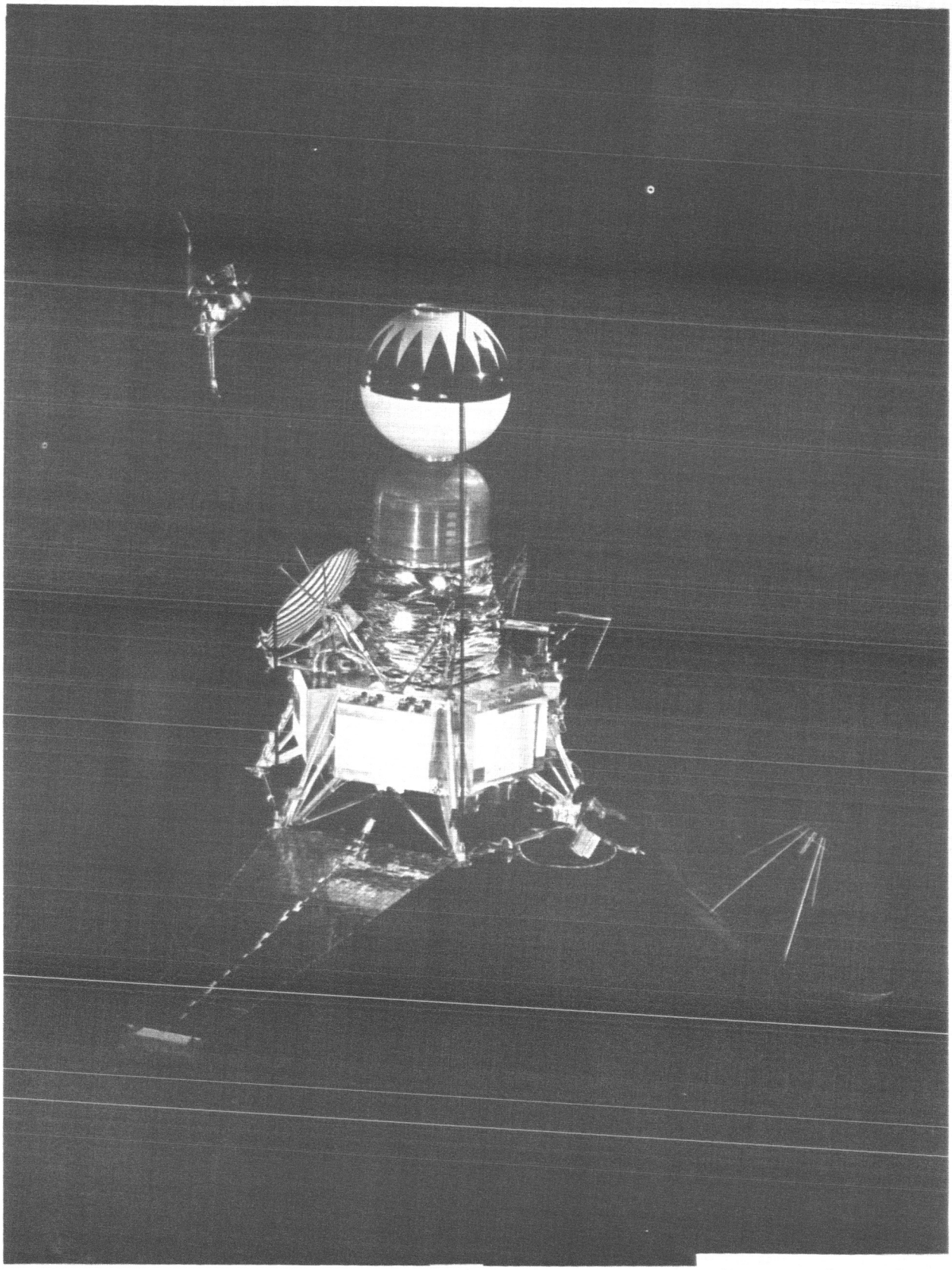

Figure 9. Ranger 3

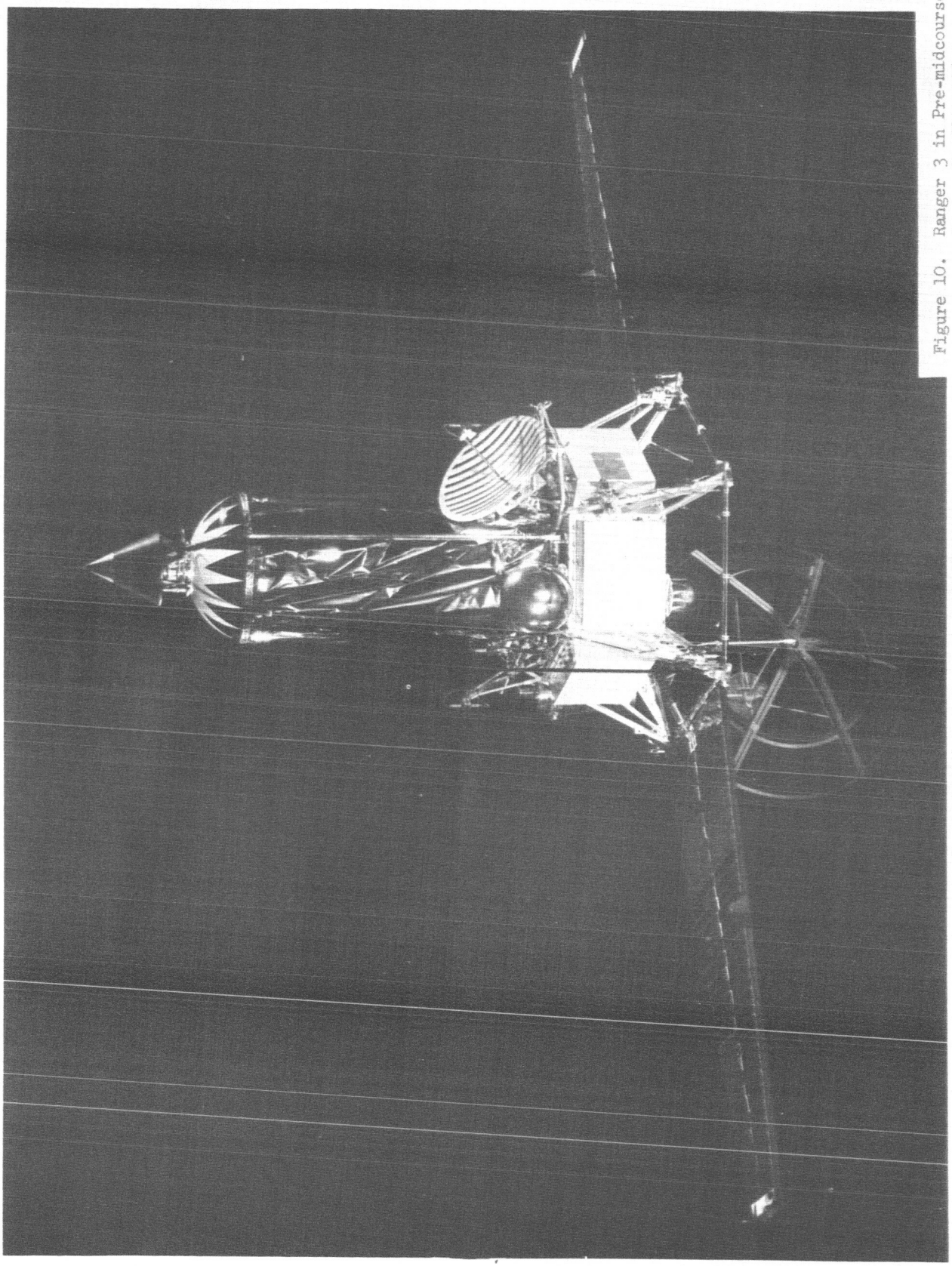

Figure 10. Ranger 3 in Pre-midcourse Cruise Configuration

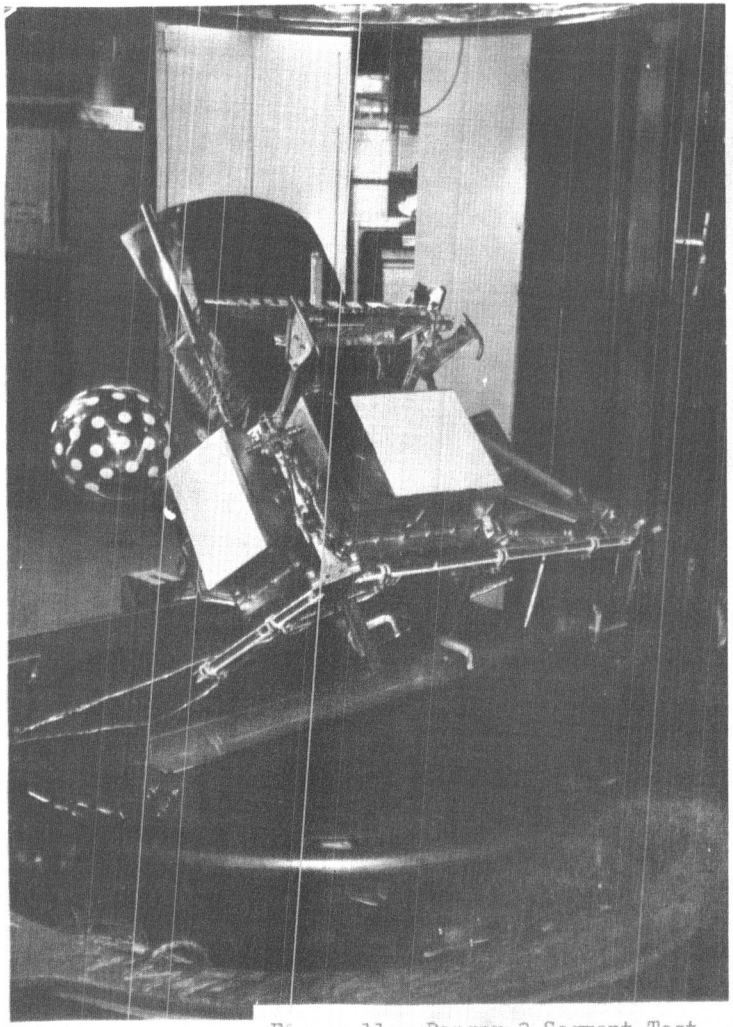

Figure 11. Ranger 3 Segment Test

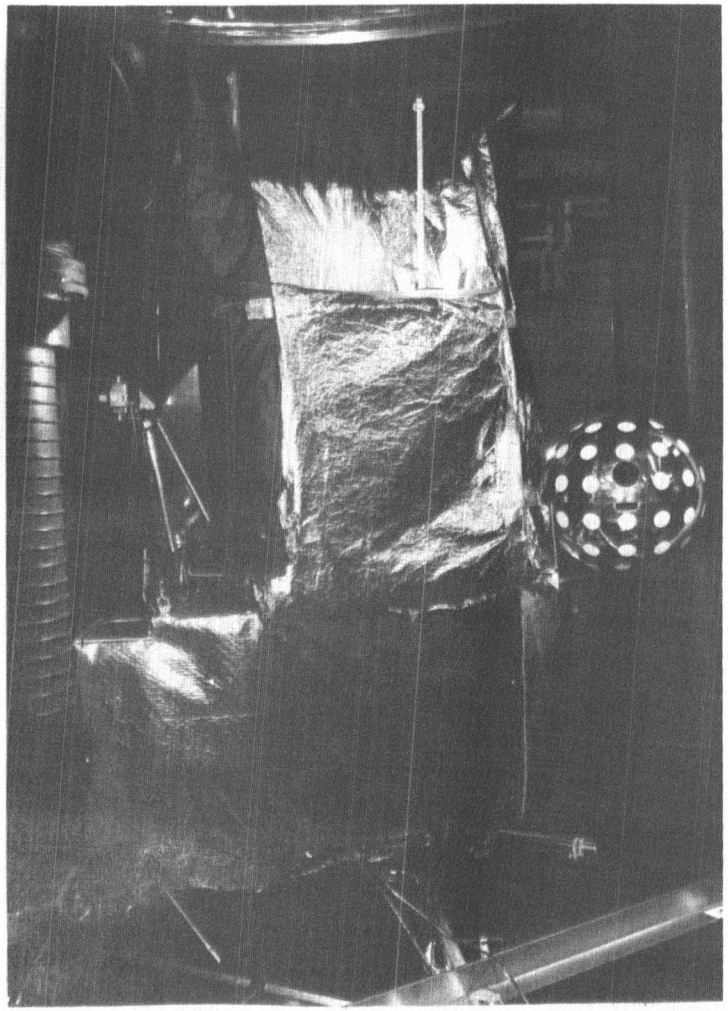

Figure 12. Ranger 4 Segment with Thermal Shield Attached

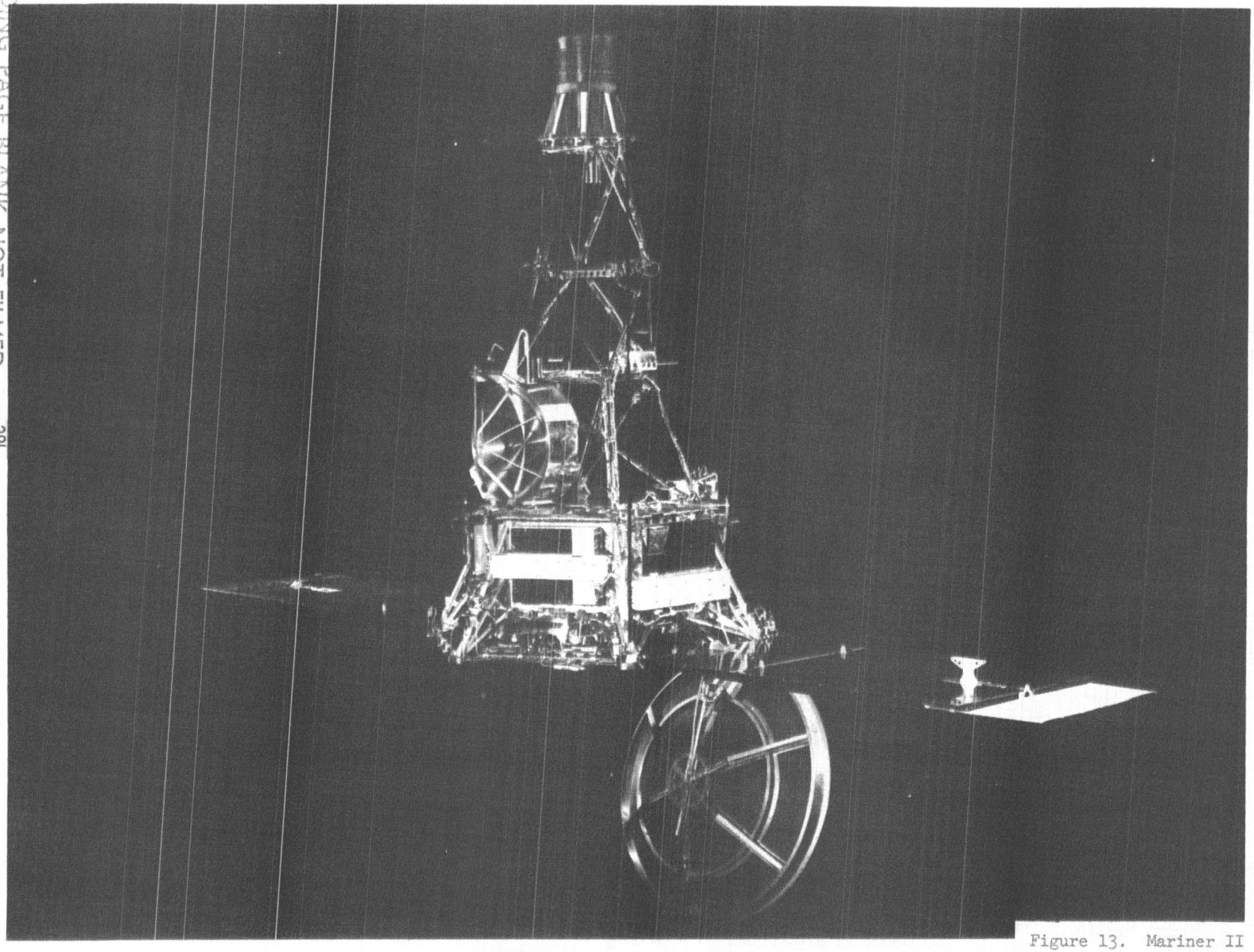

Figure 13. Mariner II

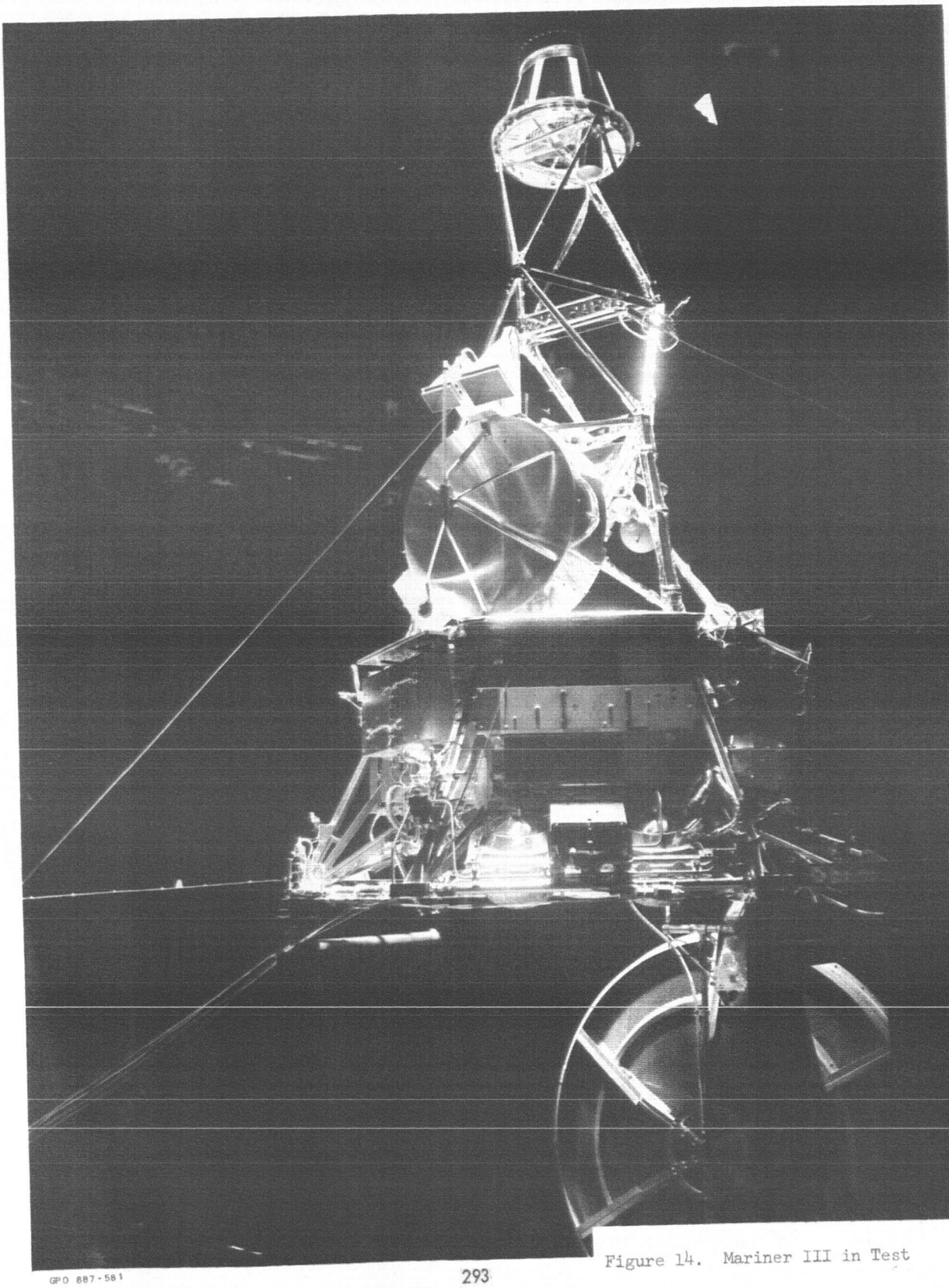

Figure 14. Mariner III in Test

GPO 887-581